

Electronic Thesis and Dissertation Repository

---

8-12-2011 12:00 AM

## Strategies for the Thermal and Photochemical Modification of Gold Nanoparticles (AuNPs) and the Fabrication of AuNP Hybrid Materials

Hossein Ismaili, *The University of Western Ontario*

Supervisor: Mark S. Workentin, *The University of Western Ontario*

A thesis submitted in partial fulfillment of the requirements for the Doctor of Philosophy degree in Chemistry

© Hossein Ismaili 2011

Follow this and additional works at: <https://ir.lib.uwo.ca/etd>

 Part of the [Organic Chemistry Commons](#)

---

### Recommended Citation

Ismaili, Hossein, "Strategies for the Thermal and Photochemical Modification of Gold Nanoparticles (AuNPs) and the Fabrication of AuNP Hybrid Materials" (2011). *Electronic Thesis and Dissertation Repository*. 214.

<https://ir.lib.uwo.ca/etd/214>

This Dissertation/Thesis is brought to you for free and open access by Scholarship@Western. It has been accepted for inclusion in Electronic Thesis and Dissertation Repository by an authorized administrator of Scholarship@Western. For more information, please contact [wlsadmin@uwo.ca](mailto:wlsadmin@uwo.ca).

# **Strategies for the Thermal and Photochemical Modification of Gold Nanoparticles (AuNPs) and the Fabrication of AuNP Hybrid Materials**

(Spine title: Gold Nanoparticles: Modification and Fabrication of Hybrids)

(Thesis format: Integrated-Article)

by

Hossein Ismaili

Graduate Program in Chemistry

A thesis submitted in partial fulfillment  
of the requirements for the degree of  
Doctor of Philosophy

The School of Graduate and Postdoctoral Studies  
The University of Western Ontario  
London, Ontario, Canada

© Hossein Ismaili 2011

THE UNIVERSITY OF WESTERN ONTARIO  
SCHOOL OF GRADUATE AND POSTDOCTORAL STUDIES

**CERTIFICATE OF EXAMINATION**

Supervisor

\_\_\_\_\_  
Dr. Mark S. Workentin

Examiners

\_\_\_\_\_  
Dr. Robert H. E. Hudson

\_\_\_\_\_  
Dr. Brian L. Pagenkopf

\_\_\_\_\_  
Dr. Giovanni Fanchini

\_\_\_\_\_  
Dr. Alex Adronov

The thesis by

**Hossein Ismaili**

entitled:

**Strategies for the Thermal and Photochemical Modification of Gold Nanoparticles (AuNPs) and the Fabrication of AuNP Hybrid Materials**

is accepted in partial fulfillment of the  
requirements for the degree of  
Doctor of Philosophy

Date \_\_\_\_\_

\_\_\_\_\_  
Chair of the Thesis Examination Board

## Abstract

Among the existing approaches for the functionalization of the gold nanoparticle (AuNP), a direct interfacial organic reaction of terminal functional groups exposed on the surface of template nanoparticles with various reactants has been shown as a promising strategy to incorporate desired functionality onto the AuNP monolayer. In our own attempts to extend the types of reactions that can be utilized for efficient interfacial modifications of AuNPs, we examined uncatalyzed Huisgen 1,3-dipolar click-type cycloaddition of azide-modified AuNPs to terminal alkynes. These particular reactions were found to be generally too slow to be useful at ambient temperatures but it was shown that high pressure conditions (11 000 atm) can be used as an efficient tool to facilitate these reactions on the AuNPs with high yields and with no detrimental effects on the gold core.

Photochemical reactions of suitably functionalized gold nanoparticles (AuNPs) can also be utilized to chemically modify AuNPs under mild conditions, given that photoinitiated reactions don't require high temperature or catalysis. Diazirine readily generates the reactive carbene intermediate by photoinitiated nitrogen extrusion. In chapter three, the synthesis and characterization of diazirine-modified AuNPs are described and it is demonstrated that upon irradiation, intermediate carbene-modified AuNPs are formed and that their subsequent insertion reactions with trapping reagents lead to interfacial modification of the diazirine-modified AuNPs.

Furthermore, I show that photo-generation of a carbene on the monolayer of AuNPs in the presence of host materials drives the formation of covalently assembled AuNP-based hybrid materials via carbene insertion/addition reactions. Diazirine-modified



AuNPs with different sizes were prepared and irradiated in the presence of a series of substrates including CNTs, diamond, graphene, and glass slide. Upon UV irradiation of diazirines attached onto the AuNPs, intermediate carbenes were generated and the following carbene insertion/addition reactions could occur with the surface functionality of substrates. Using this method, we prepared hybrids including AuNP-CNT, AuNP-Diamond, AuNP-Graphene, and AuNP-Glass.

In total, this thesis work reviews my efforts toward chemical modification of AuNPs via thermal and photothermal interfacial reactions. Moreover, it provides an efficient strategy for the synthesis of covalently assembled AuNP-based hybrid materials employing carbene insertion/addition reactions.

**Keywords:** Gold Nanoparticles, Chemical Modification, Click Reaction, High Pressure Conditions, Carbene Reactions, Hybrid Materials.

## **Acknowledgments**

I would like to take this opportunity to express my gratitude and appreciation for Mark Workentin, for his patience, supervision, encouragement, and support through these years. I would like to thank him for his continued guidance and insightful comments that have helped me in getting my thesis in the present form. It has been a great pleasure working with and learning from him.

I wish to express my thank to my fellow labmates in Dr. Workentin's group for providing invaluable support, friendship, and help during my time at UWO; in particular I would like to thank Kurtis Hartlen, Brandon Lines, Kristen Snell, and Jun Zhu. I enjoyed working with you and learning from all of you.

I would particularly like to acknowledge Prof. Hudson and Prof. Corrigan for writing reference letters for me. Special acknowledgements are also given to my examiners for taking the time out of their busy schedules to be on my thesis defence committee.

I would also like to express my special thanks to my family for all their support. I never would have made it through my graduate studies without their support and constant encouragement over the last six years. Thank you for helping in all the ways that you did. Finally, I would like to give special thanks to Kiana Lahring. Your love and encouragement have been great motivation in my life, in particular in my Ph.D. studies. I appreciate everything you have done for me and thank you for making my life so enjoyable.

## Table of Contents

<b>Certificate of Examination</b>	ii
<b>Abstract</b>	iii
<b>Acknowledgements</b>	v
<b>Table of Contents</b>	vi
<b>List of Schemes</b>	ix
<b>List of Figures</b>	xi
<b>List of Tables</b>	xvii
<b>List of Abbreviations</b>	xvii
<b>Chapter One: Introduction</b>	
<b>1.1 Monolayer-Protected Gold Nanoparticles (AuNPs)</b>	1
<b>1.1.1 Background</b>	1
<b>1.1.2 Physical and Chemical Properties</b>	3
<b>1.1.3 Synthesis of AuNPs</b>	7
<b>1.1.4 Characterization of AuNPs</b>	11
<b>1.1.5 Applications of AuNPs</b>	13
<b>1.2 Approaches to Synthesis of Functionalized AuNPs (1 – 5 nm)</b>	19
<b>1.2.1 Direct synthesis</b>	19
<b>1.2.2 Ligand Exchange Reactions</b>	20
<b>1.2.3 Interfacial Reactions</b>	22
<b>1.3 Thermal and Photochemical Interfacial Reactions on AuNPs</b>	24
<b>1.3.1 Thermal Interfacial Reactions</b>	24
<b>1.3.1.1 High Pressure Induced Interfacial Reactions</b>	27
<b>1.3.2 Photochemical Interfacial Reactions</b>	30
<b>1.4 AuNP-based Nanohybrid Materials</b>	33

1.4.1 Direct Formation of AuNPs onto a Surface	34
1.4.2 Non-covalent Approach	39
1.4.3 Covalent Attachment of AuNPs onto the Surface	43
1.5 Thesis Objectives	45
1.5.1 Modification of AuNPs Using Click-type Cycloaddition and Under High Pressure Conditions (Chapter 2)	45
1.5.2 Photochemically Generated Carbenes for the Modification of AuNPs via a Carbene Insertion Reaction (Chapter 3)	49
1.5.3 Fabrication of AuNP-based Hybrid Materials (Chapters 4 – 6)	52
1.6 References	53

**Chapter Two: Remarkable High-yielding Chemical Modification of Gold Nanoparticles Using Uncatalyzed Click-type 1, 3-Dipolar Cycloaddition Chemistry and Hyperbaric Conditions**

2.1 Introduction	65
2.2 Results and Discussion	67
2.3 Conclusion	74
2.4 Experimental	75
2.5 Supplementary Information	89

**Chapter Three: Diazirine-modified Gold Nanoparticle: Template for Efficient Photoinduced Interfacial Carbene Insertion Reactions**

3.1 Introduction	116
3.2 Results and Discussion	119
3.3 Conclusion	130
3.4 Experimental	131
3.5 Supplementary Information	150

**Chapter Four: Covalently Assembled Gold Nanoparticle-Carbon Nanotube Hybrids (AuNP-CNT) via a Photoinitiated Carbene Addition Reaction**

4.1 Introduction	159
4.2 Results and Discussion	163
4.3 Conclusion	171
4.4 Experimental	173
4.5 Supplementary Information	182

**Chapter Five: Covalent Diamond-Gold Nanoparticles Hybrids via Photochemically Generated Carbenes**

5.1 Introduction	186
5.2 Results and Discussion	188
5.3 Conclusion	195
5.4 Experimental	196
5.5 Supplementary Information	202

**Chapter Six: Covalent Immobilization of Gold Nanoparticles onto Graphene and Glass Surfaces**

6.1 Introduction	206
6.2 Results and Discussion	210
6.3 Conclusion	220
6.4 Experimental	221
6.5 Supplementary Information	229

<b>Chapter Seven: Contributions of the Studies</b>	232
--	-----

<b>Appendix: Copyright &amp; Permission</b>	238
---	-----

<b>Curriculum Vitae</b>	250
-------------------------	-----

### **List of Schemes**

<b>1.1</b>	N-diazeniumdiolate-modified AuNP as nitric oxide carrier.	15
<b>1.2</b>	Release of the fluorescein dye from the AuNP using photothermal induced the retro-Diels–Alder reaction.	16
<b>1.3</b>	DNA-conjugated AuNP sensor for detecting free DNA in solution.	17
<b>1.4</b>	A sensing strategy using the quenching properties of AuNP.	18
<b>1.5</b>	Functionalization of AuNP by a ligand exchange reaction (resulting AuNP contains both alkanethiol and functionalized (incoming) thiol).	21
<b>1.6</b>	Functionalization of AuNP via an interfacial reaction.	23
<b>1.7</b>	Examples of thermal interfacial reactions on AuNPs: a) esterification, b) S <sub>N</sub> 2 substitution, c) amine nucleophilic addition to an aldehyde, d) amination reaction of C <sub>60</sub> , e) Michael addition, f) coupling reaction of aliphatic hydroxyl, g) Grignard functionalization of Weinreb amide-modified AuNPs, and h) cross olefin metathesis.	26
<b>1.8</b>	Modification of maleimide-modified AuNP under high pressure conditions (11 000 atm); a) Diels–Alder cycloaddition, b) 1,3-dipolar nitrene cycloaddition, d) Michael addition reaction.	28
<b>1.9</b>	Photoenolization of <i>ortho</i> -methylbenzophenone-modified AuNP and subsequent Diels–Alder reaction.	30
<b>1.10</b>	Norrish type II photoreaction of aryl ketone-functionalized AuNP.	32
<b>1.11</b>	Immobilization of metal nanoparticles onto material surface.	33
<b>1.12</b>	Preparation of AuNP/graphene hybrid via direct formation of AuNPs on graphene oxide.	37
<b>1.13</b>	Synthesis of perylene-coated reduced graphene oxide decorated with AuNPs.	38

<b>1.14</b>	Schematic illustrations of decoration of CNTs with AuNPs using hydrogen bonding and hydrophobic interactions.	40
<b>1.15</b>	Non-covalent decoration of cation-modified MWNTs with crown-modified AuNPs.	41
<b>1.16</b>	Illustration of the non-covalent ( $\pi$ - $\pi$ stacking) loading of AuNP on CNT through a linker molecule.	42
<b>1.17</b>	Attachment of amine-modified AuNPs onto the graphene oxide surface using covalent approach.	44
<b>1.18</b>	Cycloadditions of alkynes with azides. The uncatalyzed reaction leads to a mixture of 1,4- and 1,5-regioisomers.	46
<b>1.19</b>	Proposed mechanistic steps in an alkyne-azide click reaction.	47
<b>1.20</b>	Modification of azide-functionalized AuNPs via click-type reaction.	48
<b>1.21</b>	Interfacial photoinduced carbene formation from a diazirine-functionalized AuNP and, subsequent carbene insertion/addition into a selection of model trapping agents.	50
<b>1.22</b>	Photoinduced reaction pathways of diazirine in carbene formation.	51
<b>2.1</b>	The 1,3-dipolar cycloaddition of <b>1</b> -C <sub>12</sub> AuNP with a variety of terminal acyl-alkynes ( <b>4a-j</b> ) at 11,000 atm.	69
<b>2.2</b>	Model reaction of 1-azidododecane ( <b>3</b> ) with alkenes <b>4a-j</b> to yield 1,2,3-triazoles <b>5a-j</b> .	69
<b>3.1</b>	Interfacial photoinduced carbene formation from a diazirine-functionalized AuNP and, subsequent carbene insertions into a selection of model trapping agents.	119
<b>3.2</b>	Synthesis of 3-aryl-3-(trifluoromethyl) diazirine-modified AuNPs ( <b>2</b> -C <sub>12</sub> AuNP) using a ligand exchange reaction.	119
<b>3.3</b>	Synthesis of 3-aryl-3-(trifluoromethyl)diazirine dodecanethiol ( <b>9</b> ).	121
<b>3.4</b>	Photoinduced reaction pathways of diazirine in carbene formation.	124
<b>3.5</b>	Model reaction of <b>6</b> with trapping reagents to yield model <b>11a-g</b> .	128
<b>4.1</b>	Illustration of the reaction protocol utilized for the functionalization of CNT with diazirine-modified AuNPs (Diaz-AuNPs).	163
<b>4.2</b>	Synthetic procedure used in the preparation of Lg-Diaz-AuNPs.	163

<b>5.1</b>	Cartoon representation showing the photoreaction of the Diaz-AuNP with the OH functionality on the micro-diamond surface via a carbene insertion reaction.	188
<b>6.1</b>	Illustration of carbene insertion/addition approach utilized for the covalent attachment of AuNPs onto graphene and glass.	211

## List of Figures

<b>1.1</b>	A, B) Cartoon representations of a thiolate-stabilized AuNP, C) HRTEM of a single AuNP (reprint with permission from Ref. 2), D) TEM of multiple AuNPs ( $3.9 \pm 0.9$ nm).	3
<b>1.2</b>	Surface plasmon resonances of AuNPs with average size of 9, 22, 4, and 99 nm.	5
<b>1.3</b>	A schematic representation of AuNP conjugated with a wide range of functionalities.	6
<b>1.4</b>	Cartoon representation of Brust-Schiffrin two-phase synthesis of AuNPs.	9
<b>1.5</b>	<sup>1</sup> H NMR spectra of A) acetophenone-modified AuNPs B) model compound, and C) acetophenone-modified AuNPs with impurities (Im = impurity, free thiols) (*solvent peak).	13
<b>1.6</b>	A) A schematic representation of the direct formation of AuNPs onto the surface to fabricate AuNP/CNT hybrid B) TEM images of synthesized AuNP/MWCNT hybrid (white dots are AuNPs).	35
<b>1.7</b>	A) Illustration of the in situ synthesis and assembly of AuNPs (red circles) on rGO, B) TEM image of AuNP/graphene hybrid (inset is HRTEM of AuNP on rGO surface).	38
<b>2.1</b>	<sup>1</sup> H NMR spectra of A) 1-C <sub>12</sub> AuNP and representative product 1,2,3-triazoles 2-C <sub>12</sub> AuNP formed in click reactions of 1-C <sub>12</sub> AuNP with acyl alkynes 4h, 4d and 4c: B) 2h-C <sub>12</sub> AuNP C) 2d-C <sub>12</sub> AuNP D) 2c-C <sub>12</sub> AuNP. Solvent CD <sub>2</sub> Cl <sub>2</sub> , residual proton signal is indicated by *.	68



<b>2.2</b>	<sup>1</sup> H NMR spectra of A) 2g-C <sub>12</sub> AuNP in CD <sub>2</sub> Cl <sub>2</sub> <sup>*</sup> , B) Compound 5g, in CDCl <sub>3</sub> .	74
<b>S2.1</b>	<sup>1</sup> H NMR spectra of 11-bromoundecanethiolate/dodecanethiolate AuNP in CD <sub>2</sub> Cl <sub>2</sub> .	90
<b>S2.2</b>	<sup>1</sup> H NMR spectra of 11-azidoundecanethiolate/11-bromo-1-undecanethiolate/ dodecanethiolate AuNP (1-C <sub>12</sub> AuNP), in CD <sub>2</sub> Cl <sub>2</sub> .	91
<b>S2.3</b>	<sup>1</sup> H NMR spectra of A)1,2,3-triazole 2a-C <sub>12</sub> AuNP formed in click reaction of 1-C <sub>12</sub> AuNP with 4a, in CD <sub>2</sub> Cl <sub>2</sub> . B) 1,2,3-triazole 5a formed in click reaction of 1-Azidododecane with 4a, in CDCl <sub>3</sub> .	92
<b>S2.4</b>	<sup>1</sup> H NMR spectra of A)1,2,3-triazole 2b-C <sub>12</sub> AuNP formed in click reaction of 1-C <sub>12</sub> AuNP with 4b, in CD <sub>2</sub> Cl <sub>2</sub> . B) 1,2,3-triazole 5b formed in click reaction of 1-Azidododecane with 4b, in CDCl <sub>3</sub> . <i>* Signals due to other regioisomer.</i>	93
<b>S2.5</b>	<sup>1</sup> H NMR spectra of A) 1,2,3-triazole 2c-C <sub>12</sub> AuNP formed in click reaction of 1-C <sub>12</sub> AuNP with 4c, in CD <sub>2</sub> Cl <sub>2</sub> . B) 1,2,3-triazole 5c formed in click reaction of 1-Azidododecane with 4c, in CDCl <sub>3</sub> .	94
<b>S2.6</b>	<sup>1</sup> H NMR spectra of A) 1,2,3-triazole 2d-C <sub>12</sub> AuNP formed in click reaction of 1-C <sub>12</sub> AuNP with 4d, in CD <sub>2</sub> Cl <sub>2</sub> B) 1,2,3-triazole 5d formed in click reaction of 1-Azidododecane with 4d, in CDCl <sub>3</sub> .	95
<b>S2.7</b>	<sup>1</sup> H NMR spectra of A)1,2,3-triazole 2e-C <sub>12</sub> AuNP formed in click reaction of 1-C <sub>12</sub> AuNP with 4e, in CD <sub>2</sub> Cl <sub>2</sub> . B) 1,2,3-triazole 5e formed in click reaction of 1-Azidododecane with 4e, in CDCl <sub>3</sub> .	96
<b>S2.8</b>	<sup>1</sup> H NMR spectra of A)1,2,3-triazole 2f-C <sub>12</sub> AuNP formed in click reaction of 1-C <sub>12</sub> AuNP with 4f, in CD <sub>2</sub> Cl <sub>2</sub> . B) 1,2,3-triazole 5f formed in click reaction of 1-Azidododecane with 4f, in CDCl <sub>3</sub> . <i>* Second regioisomer .</i>	97
<b>S2.9</b>	<sup>1</sup> H NMR spectra of A) 1,2,3-triazole 2g-C <sub>12</sub> AuNP formed in click reaction of 1-C <sub>12</sub> AuNP with 4g, in CD <sub>2</sub> Cl <sub>2</sub> , B) 1,2,3-triazole 5g formed in click reaction of 1-Azidododecane with 4g, in CDCl <sub>3</sub> .	98
<b>S2.10</b>	<sup>1</sup> H NMR spectra of A) 1,2,3-triazole 2h-C <sub>12</sub> AuNP formed in click reaction of 1-C <sub>12</sub> AuNP with 4h, in CD <sub>2</sub> Cl <sub>2</sub> , B) 1,2,3-triazole 5h formed in click reaction of 1-Azidododecane with 4h, in CDCl <sub>3</sub> .	99

<b>S2.11</b>	<sup>1</sup> H NMR spectra of A) 1,2,3-triazole 2i-C <sub>12</sub> AuNP formed in click reaction of 1-C <sub>12</sub> AuNP with 4i, in CD <sub>2</sub> Cl <sub>2</sub> . B) 1,2,3-triazole 5i formed in click reaction of 1-Azidododecane with 4i, in CDCl <sub>3</sub> . <i>*indicated peaks from the other regioisomer.</i>	100
<b>S2.12</b>	<sup>1</sup> H NMR spectra of A) 1,2,3-triazole 2j-C <sub>12</sub> AuNP formed in click reaction of 1-C <sub>12</sub> AuNP with 4j, in CD <sub>2</sub> Cl <sub>2</sub> . B) 1,2,3-triazole 5j formed in click reaction of 1-Azidododecane with 4j, in CDCl <sub>3</sub> .	101
<b>S2.13</b>	IR Spectrum of 1-C <sub>12</sub> AuNP (thin film).	102
<b>S2.14</b>	IR spectra of 2a-C <sub>12</sub> AuNP after 15 h of reaction under hyperbaric conditions.	103
<b>S2.15</b>	IR spectra of 2b-C <sub>12</sub> AuNP after 15 h of reaction under hyperbaric conditions.	104
<b>S2.16</b>	IR spectra of 2c-C <sub>12</sub> AuNP after 15 h of reaction under hyperbaric conditions.	105
<b>S2.17</b>	IR spectra of 2d-C <sub>12</sub> AuNP after 15 h of reaction under hyperbaric conditions.	106
<b>S2.18</b>	IR spectra of 2e-C <sub>12</sub> AuNP after 15 h of reaction under hyperbaric conditions.	107
<b>S2.19</b>	IR spectra of 2f-C <sub>12</sub> AuNP after 15 h of reaction under hyperbaric conditions.	108
<b>S2.20</b>	IR spectra of 2g-C <sub>12</sub> AuNP after 15 h of reaction under hyperbaric conditions.	109
<b>S2.21</b>	IR spectra of 2h-C <sub>12</sub> AuNP after 15 h of reaction under hyperbaric conditions.	110
<b>S2.22</b>	IR spectra of 2i-C <sub>12</sub> AuNP after 24 h of reaction under hyperbaric conditions.	111
<b>S2.23</b>	IR spectra of 2j-C <sub>12</sub> AuNP after 15 h of reaction under hyperbaric conditions.	112
<b>S2.24</b>	UV-vis spectra of 1-C <sub>12</sub> AuNP and 2a-j-C <sub>12</sub> AuNP (normalized). There is no change in the spectra in the area of the plasmon band (530 nm) indicating no significant change in size of the particle core before and after reaction.	113

This was confirmed by TEM.

<b>S2.25</b>	High resolution TEM images of 1-C <sub>12</sub> AuNP before (left) and 2h-C <sub>12</sub> AuNP after applying 11 000 atm for 24 h (right), as a representative example.	114
<b>3.1</b>	<sup>1</sup> H NMR spectra of A) 2-C <sub>12</sub> AuNP and B) thiol 9, * denotes the signal due to residual protons in the solvent, which are CD <sub>2</sub> Cl <sub>2</sub> in A and CDCl <sub>3</sub> in B.	122
<b>3.2</b>	<sup>19</sup> F NMR of A) 2-C <sub>12</sub> AuNP; B) 3 h and C) 7 h after irradiation of 2-C <sub>12</sub> AuNP in the presence of CH <sub>3</sub> COOH, D) product 3a-2-C <sub>12</sub> AuNP.	125
<b>3.3</b>	<sup>1</sup> H and <sup>19</sup> F NMR spectra of A) 3a-C <sub>12</sub> AuNP and B) compound 11a, * denotes the signal due to residual protons in the solvent CD <sub>2</sub> Cl <sub>2</sub> . Key assignments are indicated.	126
<b>3.4</b>	<sup>1</sup> H NMR spectra of A) 3b-C <sub>12</sub> AuNP B) 3c-C <sub>12</sub> AuNP C) 3e-C <sub>12</sub> AuNP D) 3f-C <sub>12</sub> AuNP, * denotes the signal due to residual protons CD <sub>2</sub> Cl <sub>2</sub> . Key assignments are indicated.	129
<b>S3.1</b>	<sup>1</sup> H NMR spectra of A) 11b in CDCl <sub>3</sub> , B) 3b-C <sub>12</sub> AuNP in CD <sub>2</sub> Cl <sub>2</sub> .	151
<b>S3.2</b>	<sup>19</sup> F NMR spectra of A) 11b in CDCl <sub>3</sub> , B) 3b-C <sub>12</sub> AuNP in CD <sub>2</sub> Cl <sub>2</sub> .	151
<b>S3.3</b>	<sup>1</sup> H NMR spectra of A) 11c in CDCl <sub>3</sub> , B) 3c-C <sub>12</sub> AuNP in CD <sub>2</sub> Cl <sub>2</sub> .	152
<b>S3.4</b>	<sup>19</sup> F NMR spectra of A) 11c in CDCl <sub>3</sub> , B) 3c-C <sub>12</sub> AuNP in CD <sub>2</sub> Cl <sub>2</sub> .	152
<b>S3.5</b>	<sup>1</sup> H NMR spectra of A) 11d in CDCl <sub>3</sub> , B) 3d-C <sub>12</sub> AuNP in CD <sub>2</sub> Cl <sub>2</sub> .	153
<b>S3.6</b>	<sup>19</sup> F NMR spectra of A) 11d in CDCl <sub>3</sub> , B) 3d-C <sub>12</sub> AuNP in CD <sub>2</sub> Cl <sub>2</sub> .	153
<b>S3.7</b>	<sup>1</sup> H NMR spectra of A) 11e in CDCl <sub>3</sub> , B) 3e-C <sub>12</sub> AuNP in CD <sub>2</sub> Cl <sub>2</sub> .	154
<b>S3.8</b>	<sup>19</sup> F NMR spectra of A) 11e in CDCl <sub>3</sub> , B) 3e-C <sub>12</sub> AuNP in CD <sub>2</sub> Cl <sub>2</sub> .	154
<b>S3.9</b>	<sup>1</sup> H NMR spectra of A) 11f in CDCl <sub>3</sub> , B) 3f-C <sub>12</sub> AuNP in CD <sub>2</sub> Cl <sub>2</sub> .	155
<b>S3.10</b>	<sup>19</sup> F NMR spectra of A) 11f in CDCl <sub>3</sub> , B) 3f-C <sub>12</sub> AuNP in CD <sub>2</sub> Cl <sub>2</sub> .	155
<b>S3.11</b>	<sup>1</sup> H NMR spectra of A) 11g in CDCl <sub>3</sub> , B) 3g-C <sub>12</sub> AuNP in CD <sub>2</sub> Cl <sub>2</sub> .	156
<b>S3.12</b>	<sup>19</sup> F NMR spectra of A) 11g in CDCl <sub>3</sub> , B) 3g-C <sub>12</sub> AuNP in CD <sub>2</sub> Cl <sub>2</sub> .	156
<b>S3.13</b>	IR spectra of 2-C <sub>12</sub> AuNP (black), 2-C <sub>12</sub> AuNP + CH <sub>3</sub> COOH after 1 h irradiation (blue), and 3a-C <sub>12</sub> AuNP (red) after the completion of reaction.	157
<b>S3.14</b>	TEM of 2-C <sub>12</sub> AuNPs before and after irradiation.	157
<b>4.1</b>	<sup>1</sup> H and <sup>19</sup> F NMR spectra of A) Lg-Diaz-AuNPs; B) Sm-Diaz-AuNPs and C) diazirinethiol 1.	164
<b>4.2</b>	TEM images of CNTs after photoreaction and washing/purification	167

protocol A, B) photoreaction with Lg-Diaz-AuNPs (Lg-Diaz-AuNP-CNT);  
 C, D) photoreaction of Sm-Diaz-AuNPs (Sm-Diaz-AuNP-CNT); E, F)  
 CNTs exposed to the same solutions as A/B but in the absence of UV  
 irradiation and after the washing/purification protocol.

<b>4.3</b>	XRD patterns of A) Lg-Diaz-AuNP-CNT; B) Sm-Diaz-AuNP-CNT and C) pure CNT.	169
<b>4.4</b>	Raman spectra of Lg-Diaz-AuNP-CNT (dashed line) and unmodified CNT (solid line).	170
<b>4.5</b>	UV-vis absorption spectra of unmodified CNTs, Sm-Diaz-AuNP-CNT and Lg-Diaz-AuNP-CNT, The latter clearly exhibits the Plasmon absorption band.	171
<b>S4.1</b>	TEM image of Lg-Diaz-AuNPs (inset: statistical size distribution).	183
<b>S4.2</b>	Absorption spectra of Model-AuNP, Sm-Diaz-AuNP, Lg-Diaz-AuNP and Diazirinethiol 1 in THF.	183
<b>S4.3</b>	Raman spectra for as received, unmodified multi walled CNT. Top: laser wavelength is 514 nm, D/G ratio is 0.9. Bottom: Laser wavelength is 638 nm, D/G ratio is 1.19.	184
<b>5.1</b>	DRIFT-IR spectra of the micro-diamond powder before (blue) and after (red) the Fenton treatment. The green is the IR spectrum of the Fenton-treated diamond-AuNP hybrid material isolated after irradiation.	190
<b>5.2</b>	XPS spectra of A) as-received micro-diamond powder B) Fenton-treated micro-diamond powder, C) Fenton-treated diamond-AuNP hybrid pressed on an indium foil, and D) Fenton-treated micro-diamond powder subjected to the dark control experiment. Note: the indium foil is necessary as the sample with the AuNP incorporation is not a powder but greasier due to the ligands on the AuNP.	190
<b>5.3</b>	XRD of A) diamond-AuNP hybrid prepared using Fenton-treated micro-diamond, B) diamond-AuNP hybrid prepared using as-received micro-diamond, and C) Fenton-treated micro-diamond.	192
<b>5.4</b>	Absorption spectra of Diaz-AuNP, Fenton-treated diamond and Fenton-treated diamond-AuNP hybrid in THF.	194

<b>5.5</b>	Photograph of the following suspensions in THF; A) Fenton- treated micro-diamond B) Fenton-treated micro-diamond after dark/control reaction C) Diamond-AuNP hybrid prepared using as-received micro-diamond post-photolysis and D) Diamond-AuNP hybrid prepared using Fenton-treated micro-diamond post-photolysis.	195
<b>S5.1</b>	TEM image of Lg-Diaz-AuNPs (inset: statistical size distribution).	203
<b>S5.2</b>	<sup>1</sup> H and <sup>19</sup> F NMR spectra of A) Diaz-AuNPs and B) Diazirinethiol.	203
<b>S5.3</b>	SEM of Diamond-AuNP hybrid.	204
<b>6.1</b>	TEM images of A, B) graphene-AuNP hybrid after washing/purification protocol, C) graphene after dark/control experiment (in the absence of UV irradiation and after the washing/ purification protocol), and D) unmodified graphene.	213
<b>6.2</b>	XRD patterns of graphene-AuNP.	214
<b>6.3</b>	UV-vis absorption spectra of Diaz-AuNPs, graphene-AuNP hybrid (SPR peak growing at ~ 500 nm), unmodified graphene, and Diazirinethiol ( $\lambda$ max at 275 nm).	215
<b>6.4</b>	UV-vis absorption spectra of Diaz-AuNPs (SPR peak at 535 nm), untreated glass-AuNP (SPR peak at 545 nm) and piranha-treated glass-AuNP (SPR peak at 550 nm).	217
<b>6.5</b>	XPS spectrum of piranha-treated glass-AuNP (The inset is Au 4f and Mg 4s peaks).	218
<b>6.6</b>	A) Tapping mode AFM image showing AuNPs covalently deposited onto piranha-treated glass surface, B) cross section analysis of AuNPs attached onto the surface, c) AFM image of piranha-treated glass slide, and D) cross section analysis of piranha-treated glass slide.	219
<b>6.7</b>	AuNPs patterned on a piranha-treated glass slide utilizing photoinitiated carbene insertion method.	220
<b>S6.1</b>	SEM image of graphene.	230
<b>S6.2</b>	TEM image of graphene.	230
<b>S6.3</b>	XRD patterns of natural graphite powder (NG), graphite oxide (GO), and graphene (G).	231

<b>S6.4</b>	FT-IR of natural graphite powder (NG), graphite oxide (GO), and graphene (G).	231
-------------	---	-----

## List of Tables

<b>1.1</b>	Conversion % of the Diels–Alder reaction at selective populated sites	31
<b>2.1</b>	Extent of reaction of 1-C <sub>12</sub> AuNP with alkynes 4a-j via uncatalyzed 1,3-dipolar cycloaddition reaction at atmospheric and hyperbaric pressure conditions	70
<b>3.1</b>	Products of reaction of photolysis of the diazirines 2-C <sub>12</sub> AuNP and 6 with a variety of carbene trapping agents to yield 3-C <sub>12</sub> AuNP and 11, respectively, and the <sup>19</sup> F NMR chemical shifts of the products 3-C <sub>12</sub> AuNP	127

## List of Abbreviations

AFM	Atomic force microscopy
AgNP	Silver nanoparticle
atm	Atmosphere
AuNP	Gold nanoparticle
BDD	Boron-doped diamond
BINOL	1,1'-Binaphthalene-2,2'-diol
BODIPY	4,4-difluoro-4-bora-3a,4a-diaza-s-indacene
DCM	Dichloromethane
DMAP	4-Dimethylaminopyridine
DMSO	Dimethyl sulfoxide
DNA	Deoxyribonucleic acid
DRIFT	Diffuse reflectance Fourier transform infrared
EWG	Electron withdrawing group
fcc	Face centered cubic

FT-IR	Fourier transform infrared
GC	Glassy electrode
GO	Graphite oxide
GSH	Glutathione
HRMS	High resolution mass spectrometry
HRTEM	High resolution transmission electron microscopy
MHz	Megahertz
MWCNT	Multi-walled carbon nanotubes
NG	Natural graphite powder
nm	Nanometer
NMR	Nuclear magnetic resonance
NO	Nitric oxide
NP	Nanoparticle
ODT	Octadecanethiol
P	Pressure
PDDA	Poly(diallyldimethylammonium) chloride
PEG	Polyethylene glycol
ppm	Parts per million
PTCA	Perylene tetracarboxylate
PtNP	Platinum nanoparticle
PVP	Polyvinylpyrrolidone
rGO	Reduced graphene oxide
RNA	Ribonucleic acid
ROMP	Ring-opening metathesis polymerization
SAM	Self-assembled monolayer
SEM	Scanning electron microscopy
S <sub>N</sub> 2	Bimolecular nucleophilic substitution
SPR	Surface plasmon resonance
SWCNT	Single-walled carbon nanotubes
TEM	Transmission electron microscopy
TGA	Thermogravimetric analysis

THF	Tetrahydrofuran
TLC	Thin-layer chromatography
TMS	Tetramethylsilane
TOAB	Tetraoctylammonium bromide
XPS	X-ray Photoelectron Spectroscopy
XRD	X-ray diffraction
$\Delta G$	Gibbs energy
$\Delta V^\ddagger$	Activation volume



# Chapter 1

## Introduction

### 1.1 Monolayer-Protected Gold Nanoparticles (AuNPs)

#### 1.1.1 Background

Gold, since its discovery, has fascinated human beings with its attractive luster and noble characteristics. It has been used in many works of art and jewelry as a luxury component to raise the value of the object. Moreover, gold was the main motive for alchemists to establish and explore proto-chemistry, the precursor to modern chemistry. With the aim of turning copper or other metals into the gold, alchemists established many procedures and tools, some of which are still in use today. The alluring character of the gold motivated the ancients to discover valid, or in some cases mystical, uses for it. For example, the Egyptians and the Chinese used colored colloidal gold to make ruby-colored glasses and the Indians prepared colloidal gold containing ashes, “swarna bhasma”, and used it for medical purposes.<sup>1-3</sup>

Due to the inertness and high cost of gold, not much was done to develop the chemistry of gold until the 19<sup>th</sup> century. Faraday was the first to demonstrate detailed experiments with gold colloids and thin films.<sup>2,3</sup> In 1857, he published a paper entitled “The Experimental Relation of Gold (and other Metals) to Light” wherein he reported the

synthesis of gold colloids and stated that the gold was dispersed in a ruby color solution in a “finely divided metallic state”.<sup>4</sup> He prepared his colloidal gold by reducing an aqueous solution of gold salt,  $\text{AuCl}_4$ , with phosphorus in carbon disulfide. About 150 years later, transmission electron microscopy (TEM) images taken of Faraday’s gold solution revealed that he had actually synthesized gold nanoparticles with an average size of  $6 \pm 2$  nm.<sup>2</sup> Faraday’s method of metallic colloidal preparation (aqueous reduction of a metal salt) was a breakthrough, although the significance of gold colloids was not comprehended at the time. Initiated by Faraday’s revolutionary discovery, the field of colloidal science experienced slow growth during the first half of the 20<sup>th</sup> century due to a lack of adequate imaging and material surface analysis techniques. However, advances in optical microscopy in the last 60 years have provided the opportunity for visualizing metal colloids, and amplified the development in the colloid and nanoparticle field.<sup>1, 5</sup> Using TEM, Turkevich investigated for the first time the size and shape of gold nanoparticles (AuNPs) prepared by reduction of  $\text{AuCl}_4$  with sodium citrate.<sup>6</sup> He found that the size of nanoparticles can be controlled simply by the variation of the sodium citrate concentration. His preparation procedure of AuNPs was popular until 1994 when Brust and Schiffrin introduced their unique preparation method.<sup>7</sup> They reported the synthesis of AuNPs protected with a monolayer of thiolate ligands. In their procedure,  $\text{AuCl}_4$  is reduced by a reducing agent (such as sodium borohydride ( $\text{NaBH}_4$ )) in the presence of a thiol as a protecting ligand. The AuNPs obtained using the Brust-Schiffrin method are stable, due to the strong affinity of sulfur toward gold, and control over the size of nanoparticles is feasible. More importantly, functionalized nanoparticles can be readily obtained by using functionalized thiols. Thus, the real renaissance of the AuNP

began with the Brust-Schiffrin thiol-protected AuNPs. Following their report, a rapid growth in the AuNP field has taken place, given that twenty years ago there were few reports published about AuNPs, and in 2010 more than 3600 papers exist on this topic.

### 1.1.2 Physical and Chemical Properties

The AuNPs (1-100 nm in diameter) are comprised of a metal core and an organic ligand shell (protecting group, e. g. thiolate ligand) that stabilizes the metal core and prevents aggregation of nanoparticles. Figure 1.1A and B show a typical cartoon representation of a thiolate stabilized AuNP. A high resolution TEM (HRTEM) image of a AuNP ( $\sim 2$  nm in diameter) is provided in Figure 1.1C, where individual gold atoms can be seen, making up the metal core. The oxidation state of the gold atoms in the core is 0. However, similar to bulk gold, the AuNP gold core doesn't oxidize at ambient conditions, making the AuNPs the most stable metal nanoparticles.<sup>8</sup> The AuNP core is characterized by a face-centered cubic (fcc) gold lattice, where gold atoms occupy terrace, edge and vertex sites (Figure 1.1B).

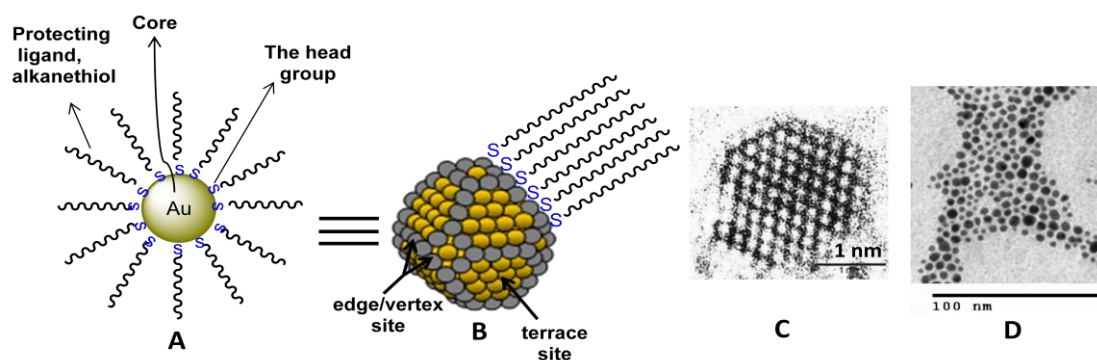


Figure 1.1 A, B) Cartoon representations of a thiolate-stabilized AuNP, C) HRTEM of a single AuNP (reprint with permission from Ref. 2), D) TEM of multiple AuNPs ( $3.9 \pm 0.9$  nm).

Various protecting group with sulfur, nitrogen, phosphorous, or oxygen containing head groups can be utilized to prepare AuNPs, although protection of the metal core is greater when thiolate ligands are utilized.<sup>3, 5, 8</sup> The AuNPs prepared using the Brust-Schiffrin method with alkanethiol ligands are usually soluble in non-polar organic solvents including toluene, benzene, hexanes, chloroform, dichloromethane, and tetrahydrofuran. However, the solubility can sometimes be tuned by altering the polarity of the thiol ligands. For example, AuNPs passivated by polar polyethylene glycol-thiol (PEG-SH) are water-soluble.<sup>9</sup>

While AuNPs can be stored for several months without consequence, some conditions including high temperature ( $>100\text{ }^{\circ}\text{C}$ ) and strong acid or base can affect their stability and cause irreversible aggregation. Most likely, in harsh conditions the protecting thiolate ligands are detached from the AuNP cores, leaving exposed regions. In this case, partially naked cores coalesce, giving aggregated and insoluble structures.<sup>10</sup> Moreover, chemical decomposition of AuNPs can be induced by molecular iodine ( $\text{I}_2$ ) or the cyanide ion ( $\text{CN}^-$ ), as examples. Iodine quantitatively liberates the thiol ligands as dialkyl disulfide compounds and addition of cyanide to a solution of AuNPs leads to dissociation of the thiol ligands along with etching of the AuNP core.<sup>11</sup>

The response of AuNPs toward light is one of their most significant physical properties. While the UV-vis absorption spectrum of AuNPs smaller than 3 nm in diameter exhibits a very broad peak with a large absorption coefficient at shorter wavelengths and sloping decrease in the intensity at higher wavelengths, the UV-vis of absorption for AuNPs larger than 3 nm exhibits a detectable peak at  $\sim 530 - 570\text{ nm}$ , the so-called surface plasmon resonance (SPR) band (Figure 1.2). The AuNPs with  $>3\text{ nm}$

size interact with light (electromagnetic waves) and exhibit a SPR band as a result of collective oscillation of their conduction band electrons. The ruby color of Faraday's colloidal gold and ancient glasses reflects the SPR band of AuNP.<sup>12-14</sup>

The position of the SPR band strongly depends on the nanoparticles' morphology, interparticle interactions, and medium dielectric constant. It has been shown that when the size of AuNPs gets larger and the distance between them is reduced, the SPR band shifts to higher wavelengths. The protecting ligands of AuNPs can also alter the SPR band position and cause a blue or red shift.<sup>12, 13</sup> It is noteworthy that the SPR band shift is the origin of many of AuNP applications and has been studied extensively (Section 1.1.5).<sup>14</sup>

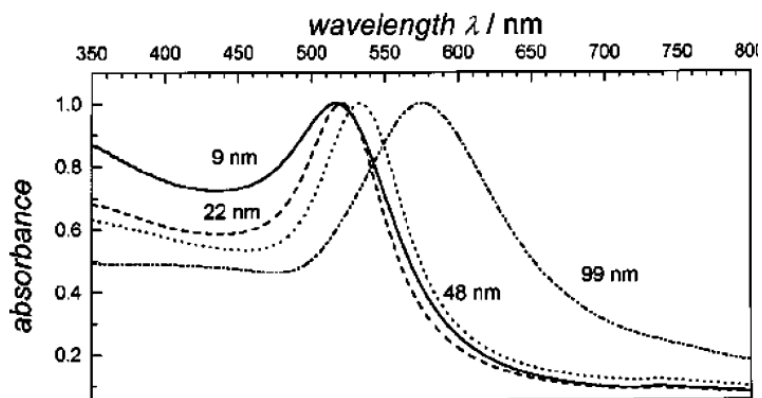


Figure 1.2 Surface plasmon resonances of AuNPs with average size of 9, 22, 4, and 99 nm, reprint with permission from Ref.12.

In addition, an important attribute of AuNPs is their low cytotoxicity and biocompatibility.<sup>15, 16</sup> Many biological molecules including polynucleotide and proteins with a thiol functional group have been attached to AuNPs and their *in vitro* and *in vivo* applications have been widely investigated.<sup>17</sup> Furthermore, AuNPs with a well-defined

interface can interact with target cells to carry out a specific function, such as drug delivery.<sup>18, 19</sup>

Many AuNP applications in biomedical, chemical, and technological fields are due to their unique morphology and protecting ligand properties.<sup>3, 14–19</sup> Use of a thiol ligand as a protecting group not only gives rise to stabilized nanoparticles but also provides a powerful tool for synthesizing functionalized AuNPs designed for specific applications. Furthermore, the mild conditions used in the Brust-Schiffrin method is compatible with a wide variety of chemical functionalities and employing this method allows preparation of AuNPs with a wide range of functional moieties (Figure 1.3).

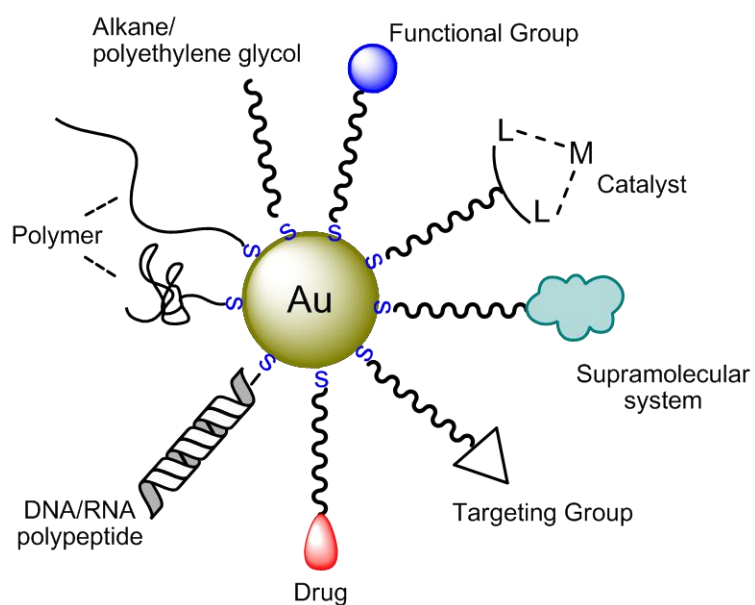


Figure 1.3 A schematic representation of AuNP conjugated with a wide range of functionalities.

### 1.1.3 Synthesis of AuNPs

One of the key reasons behind the exploitation of AuNPs in various applications is their ease of synthesis. A typical “bottom up” procedure of AuNP synthesis involves reduction of a gold salt, usually tetrachloroaurate,  $\text{AuCl}_4$ , in the presence of protecting ligands.<sup>8</sup> The formation of AuNPs in the solution follows a two-step process: nucleation and successive growth.<sup>5, 20, 21</sup> Reduction of the gold salt initiates nucleation and the following collisions between gold ions, atoms and small clusters carry on the nucleation step. The clusters formed at this stage experience fluctuation in size and shape due to the competition between incorporation and detachment of gold atoms. However, the incorporation of atoms often overcomes the detachment, giving rise to clusters which are large enough to become stable as a result of energy released by creation of a new volume. The collision of stable clusters leads to cessation of the nucleation step accompanied by the formation of irreversible seeds. The growth of the seeds in the successive growth step takes place by reduction of more gold salt upon them. The rate of growth and morphology of the seeds dictate the final size and shape of the resultant AuNPs.

In addition, because the two-step process of formation of AuNPs occurs in the presence of protecting ligands, the interactions between the gold ions/atoms/clusters and the protecting ligands play an important role in the size and morphology of the product AuNPs as well. This is because of the physical barrier provided by the ligands attached to the gold clusters during nucleation. Where the interaction between gold atom and ligand is stronger, the amount of ligands on the clusters or seeds is greater; in other words, the physical barrier is greater. Therefore, the stronger interactions (such as that between thiol and gold) cause formation of smaller clusters in the nucleation step – due to less effective

collisions between gold ions/atoms/clusters – as well as slow growth rate in successive growth step. Besides the nature of utilized ligands, various factors including temperature, rate of reduction of gold ions, and molar ratio of ligand to gold influence the nucleation and growth steps, thus affecting the size and shape of AuNPs.<sup>5, 8, 20, 21</sup>

The existing procedures for the preparation of AuNPs can be classified into two major methods: the Turkevich method and the Brust-Schiffrin synthesis. In both synthetic approaches AuCl<sub>4</sub> is reduced in the presence of a protecting ligand, which is citrate in Turkevich method<sup>6</sup> and thiol in the Brust-Schiffrin synthesis.<sup>7</sup> In the Turkevich method, an aqueous solution of AuCl<sub>4</sub> is brought to a boil, followed by addition of sodium citrate. The citrate anion acts as both a reducing agent and a protecting ligand. Upon addition of citrate, the gold (III) ions are reduced to gold (0) atoms, and modestly monodisperse citrate-protected AuNPs are formed following the rapid nucleation and successive growth. The size of AuNPs, varying from ~10 nm to ~150 nm in diameter, can be controlled by altering the reaction conditions, including the molar ratio of gold to citrate, the temperature, and the order of addition of the reagents.<sup>3, 6, 22</sup> Due to the polarity of physisorbed citrate ions, the AuNPs obtained are water-soluble. However, the weak ionic interactions between AuNP core and citrate allow replacement of the latter with hydrophobic ligands containing thiol groups, which interact with the AuNP core through stronger roughly covalent interactions, resulting in AuNPs soluble in organic solvents.<sup>23</sup> In spite of the low stability and poor solubility in organic solvents, many still utilize the Turkevich method to prepare large AuNPs, particularly where a loose protecting shell is required.



To overcome the issues associated with the Turkevich method, Brust and Schiffrin introduced their own unique method.<sup>7</sup> In the Brust-Schiffrin two-phase synthesis (Figure 1.4), aqueous  $\text{AuCl}_4^-$  is first transferred into the organic phase (toluene) by the phase transfer agent (tetraoctylammonium bromide, TOAB). Upon addition of a thiol to the organic phase, the gold (III) salt is reduced to the gold (I)-thiol polymeric form,  $[(\text{Au(I)SR})_n]$ , accompanied by a decolorization of the organic phase. The disappearance of the gold (III) orange color after addition of thiol indicates the occurrence of the reaction between gold (III) and thiol in accordance with the formation of the polymeric structure. It is noteworthy that the gold(I)-thiol polymeric structures are known and the synthesis and characterization of them have been reported.<sup>24, 25</sup> Lastly, addition of a reducing agent ( $\text{NaBH}_4$ ) converts the gold(I)-thiol polymer to the AuNPs where the oxidation state of gold is (0). The resulting AuNPs are in the size range of  $\sim 1 - 4$  nm, depending on the reaction conditions.<sup>7</sup>

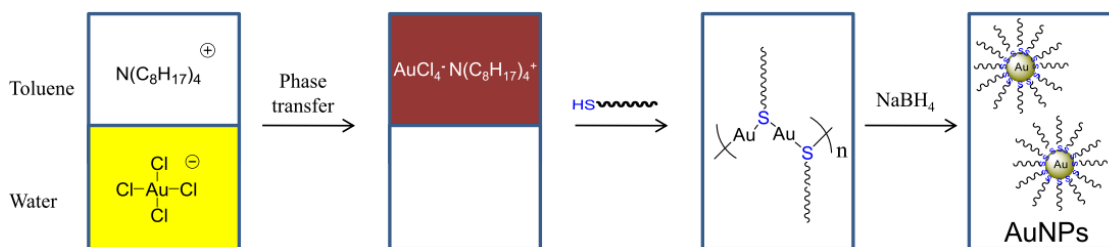


Figure 1.4 Cartoon representation of Brust-Schiffrin two-phase synthesis of AuNPs.

The core size of the AuNPs can be tuned by varying the preparation conditions; adjusting the molar ratio of thiol to gold, the temperature, and the rate of reductant addition can all have effects on the core size.<sup>26 - 28</sup> A larger molar ratio of thiol to gold results in smaller nanoparticles. For example, using 3:1 and 1:1 molar ratios of thiol to gold leads to the synthesis of AuNPs with the average size of 1.7 and 2.2 nm,

respectively.<sup>26</sup> Additionally, decreasing the temperature of reaction<sup>27</sup> and increasing the rate of reductant addition, NaBH<sub>4</sub>,<sup>28</sup> result in nanoparticles with smaller size.

The Brust-Schiffrin two-phase synthesis is the most popular synthetic scheme in the field, giving extremely robust AuNPs which can be isolated, redissolved in commonly used organic solvents, and stored for months. However, broad size distribution and limitation to the synthesis of AuNPs < 4 nm are drawbacks of the Brust-Schiffrin synthesis approach.<sup>7, 26–28</sup> A number of modifications have been made to this approach in order to obtain AuNPs with larger size and narrower size distribution. Knol reported a modified Brust-Schiffrin synthesis by which large AuNPs with an average size of ~5 nm can be prepared.<sup>29</sup> In this modified method, the gold (III) salt is slowly reduced only in the presence of TOAB. In this case the AuNPs obtained are capped by TOABs. However, due to weak interaction between TOABs and the AuNP core, the TOABs can be place-exchanged with the thiols to obtain thiol-protected AuNPs.

The synthesis of monodisperse AuNPs was demonstrated by Peng and co-workers.<sup>30</sup> When aliphatic amines were utilized as protecting ligands, in place of thiols, monodispersed amine-capped AuNPs (3.2 nm) were produced. Afterward, the thiols could replace the amines to give monodispersed thiol-protected AuNPs. It has been suggested that the strong ligands like thiols typically cause slow activity of the clusters present in the nucleation step, leading to the formation of polydisperse AuNPs. In contrast, weak ligands such as amines are desirable for the formation of monodisperse nanoparticles.<sup>30</sup> In addition to AuNPs bearing organic functionalities, water-soluble,<sup>31</sup> biomolecule-nanoparticle conjugate systems,<sup>32, 33</sup> and polymer-supported AuNPs<sup>34, 35</sup> have all been synthesized by using the original and/or modified Brust-Schiffrin synthesis.

Recently, photochemical approaches have been developed for the synthesis of AuNPs.<sup>36–40</sup> In these approaches, light-induced reduction of gold (III) is employed to obtain AuNPs with a desired size. One of the significant advantages of photochemical strategies includes controlled reduction of gold ions without need for use of excess reducing agents.<sup>36</sup> Photoreduction of gold (III) can be carried out by direct excitation of AuCl<sub>4</sub> using hard UV light below 300 nm in the presence of an additive (such as acetone or polyvinylpyrrolidone (PVP)).<sup>37, 38</sup> In addition, photolysis of aromatic ketones in the solution gives electron donor ketyl radicals which can act as a reducing agent. The redox potentials of ketyl radicals are such that the reduction of gold (III) by ketyl radicals is thermodynamically favored.<sup>39, 40</sup>

#### **1.1.4 Characterization of AuNPs**

The gold core of AuNPs can be analyzed using material surface analysis and imaging techniques. Transmission electron microscopy (TEM) provides structural information on AuNPs as well as their size distribution. More detailed analysis of the nanoparticles' morphology, including lattice structure and even the number of gold atoms in the AuNP core can be studied using images taken with high resolution transmission electron microscopy (HRTEM).<sup>2</sup> Atomic force microscopy (AFM) and scanning electron microscopy (SEM) are also useful techniques for determining the size and morphology of AuNPs, especially when taking TEM images is not feasible. In addition, the X-ray diffraction (XRD) technique is extensively applied to verify the formation and presence of AuNPs in hybrid materials. The planes of a face-centered cubic (fcc) AuNP including (111), (200), (220), (311), (222), (331), and (420) planes can usually be seen in the XRD spectrum of AuNPs.<sup>41</sup> X-ray photoelectron spectroscopy (XPS) has also been utilized to

characterize AuNPs. A typical XPS spectrum of AuNPs shows peaks corresponding to Au (4f), (4d) and (4p), and S (2s).<sup>42</sup> As stated prior, the UV-vis absorption of AuNPs larger than 3 nm exhibits a SPR peak at ~530 – 570 nm; therefore, UV-vis spectroscopy is often required to verify the synthesis of AuNPs larger than 3 nm.

The solubility of AuNPs prepared via the Brust-Schiffrin method in a variety of organic solvents provides the opportunity to employ traditional techniques to characterize the protecting ligands of nanoparticles. Nuclear magnetic resonance (NMR) spectroscopy is the most important characterization technique that offers significant information about the composition and structure of the ligands attached onto the AuNPs. Figure 1.5A shows an example (from our own work) of a typical <sup>1</sup>H NMR spectrum of 2.2 nm functionalized AuNPs (acetophenone-modified AuNPs). As can be seen, the signals in the <sup>1</sup>H NMR spectrum of functionalized AuNPs are broad; therefore assignment of these peaks is usually a difficult task. However, we overcome this hurdle by comparing the <sup>1</sup>H NMR peaks of functionalized AuNPs with those of the model compound for a more confident assignment (Figure 1.5B). The broadness of the peaks corresponding to ligands attached onto the AuNPs is due to the inhomogeneous AuNP surfaces and Au-S bonding sites, leading to more diverse chemical shifts. Furthermore, slow rotation of thiolates bound to the AuNP core causes a very fast spin-spin relaxation ( $T_2$ ), which is another factor contributing to this broadening.<sup>43</sup> The <sup>1</sup>H NMR spectroscopy is also used to investigate the purity of AuNPs. The presence of the free non-bound ligands appears as sharp <sup>1</sup>H NMR signals, while bound ligands (on AuNPs) will appear at the same chemical shift as their non-bound counterparts, however the signals will become much broader (Figure 1.5C, sharp signals are due to the free acetophenone thiols, labeled Im). As a result, the

purity of AuNPs free from non-bound ligands (or other impurities) can be verified by the lack of sharp signals in the  $^1\text{H}$  NMR spectrum.

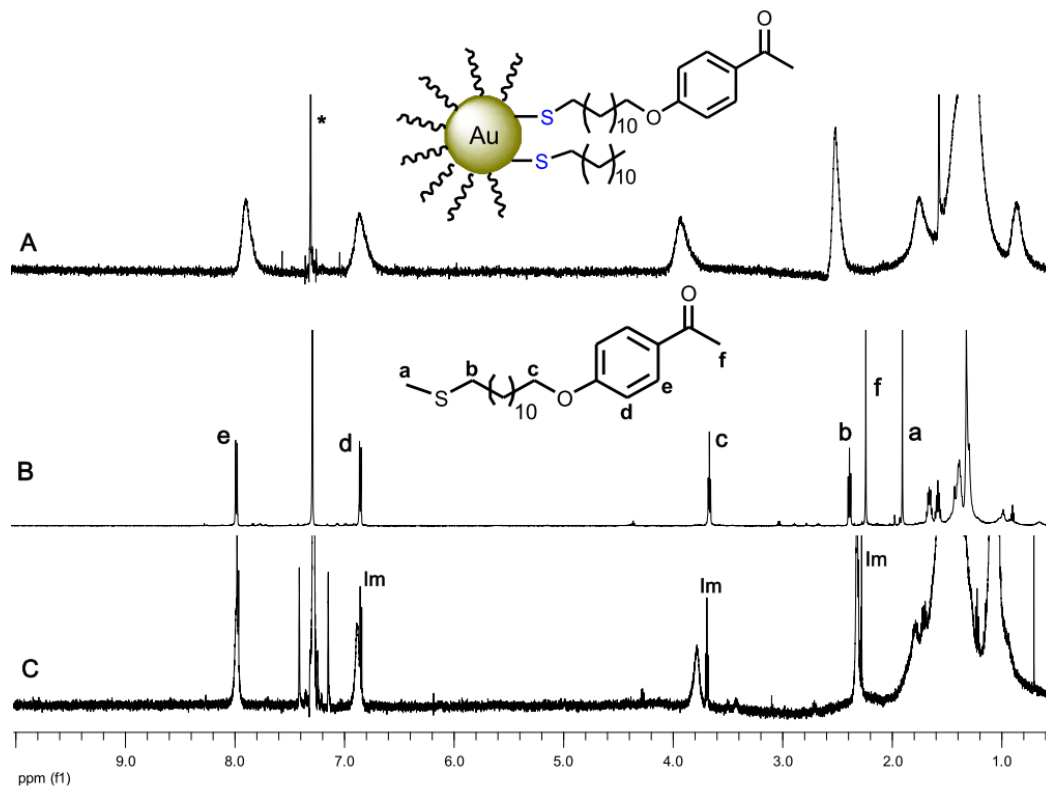


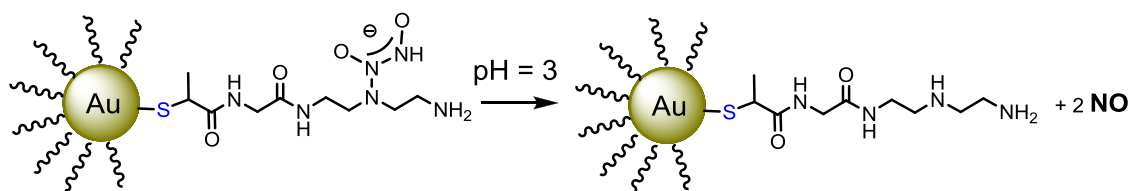
Figure 1.5  $^1\text{H}$  NMR spectra of A) acetophenone-modified AuNPs B) model compound, and C) acetophenone-modified AuNPs with impurities (Im = impurity, free thiols) (\*solvent peak).

### 1.1.5 Applications of AuNPs

Over the last decade, the potential use of AuNPs in a wide variety of applications has been a key reason for significant attention being drawn toward their active research.<sup>1–3, 14–19</sup> Here, a number of AuNP applications in biology, medicine, sensors, solar cells, and catalysis will be highlighted.

AuNPs possess two incredibly important features that make them special in biology and medicine: first is their size range which aligns with that of biomolecules such as proteins and polynucleic acids (3-10 nm), and the next feature arises from the gold-thiol chemistry, allowing incorporation of various functionality onto AuNPs (Figure 1.3).<sup>44, 45</sup> AuNPs provide a unique platform for targeted delivery of therapeutic agents, including small drug molecules and large biomolecules like proteins, DNA, or RNA. An important advantage of using AuNPs as a therapeutic agent carrier is their high loading capacity of pharmaceuticals onto their surface. For example, ~100 functionalized thiols can be found attached onto a AuNP with a 2 nm core diameter, therefore it can serve as platform that allows controlled and sustained liberation of a drug.<sup>46</sup>

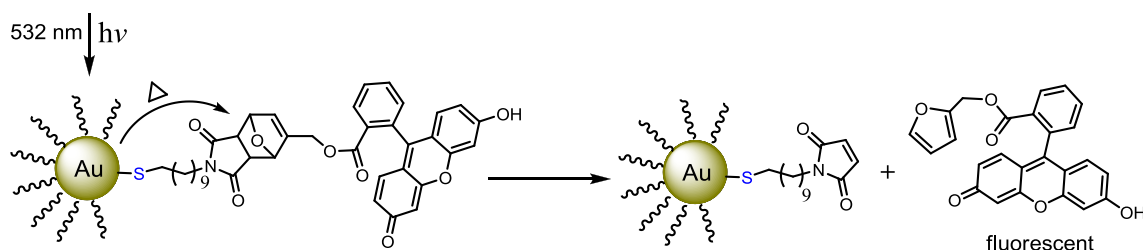
A successful approach to drug delivery involves place-exchange of the drug attached onto AuNPs (via Au-S bond) with intracellular thiols such as glutathione (GSH), leading to release of the drug in a cell (i.e. bound thiols to the AuNPs can be displaced by new incoming thiols). Rotello and co-workers demonstrated glutathione (GSH)-mediated release of small molecules by utilizing hydrophobic dye (BODIPY)-modified AuNPs with 2 nm in diameter (BODIPY was used as a model of hydrophobic drug). They showed that the AuNPs can penetrate into the cell and following place-exchange of intracellular GSH, BODIPY thiol incorporated onto AuNPs is released into the cell.<sup>47</sup> An alternative approach for drug delivery involves decoration of AuNPs with pH-<sup>48</sup> or light-responsive<sup>49</sup> drug molecules. For example, using a pH-responsive approach, Schoenfish *et al.* could release nitric oxide (NO) (an effective drug for hypoxic respiratory failure) in a controlled way. They prepared water-soluble N-diazeniumdiolate-modified AuNPs and showed the releasing of nitric oxide in acidic conditions (Scheme 1.1).<sup>48</sup>



Scheme 1.1 N-diazeniumdiolate-modified AuNP as nitric oxide carrier.

Currently, AuNP-mediated hyperthermia is a hot topic in AuNP applications in cancer treatment and photothermal drug release.<sup>50–52</sup> As previously stated, AuNPs with a core size >3 nm in size interact with light and exhibit a surface plasmon resonance (SPR) band as a result of collective oscillations (excitation) of their conduction electrons. Upon relaxation of the excited electrons thermal energy is generated, causing an increase in the temperature of the AuNP core. Following heat dissipation from the core, the temperature of surrounding environment rises. Therefore, exposing AuNPs that are positioned nearby a cell to the SPR excitation source can raise the local temperature of the cell. It is well-known that cells are very susceptible to heat and a small increase in temperature can result in cell death.<sup>50</sup> El-Sayed *et al.* reported the first AuNP use in *in vitro* hyperthermia therapy of cancer cells. They observed that oral cancerous cells targeted with AuNPs were destroyed upon illumination with a laser (514 nm). The utilized laser was 2-3 times less powerful than that normally need to destroy cells without AuNPs.<sup>51</sup> The ability of AuNPs to convert light to heat has also been recently used in photothermal release that can potentially be used for drug delivery. Branda's group showed that thermally activated bond-breaking reactions can be carried out in the vicinity of nanoparticle surfaces via stimulation with visible light (Scheme 1.2) The photothermally induced retro-Diels–Alder reaction, that can proceed at above 60 °C, released a furan (7-oxa-bicyclo-[2.2.1] hept-5-ene-2,3-dicarboxylic imide, fluorescent)

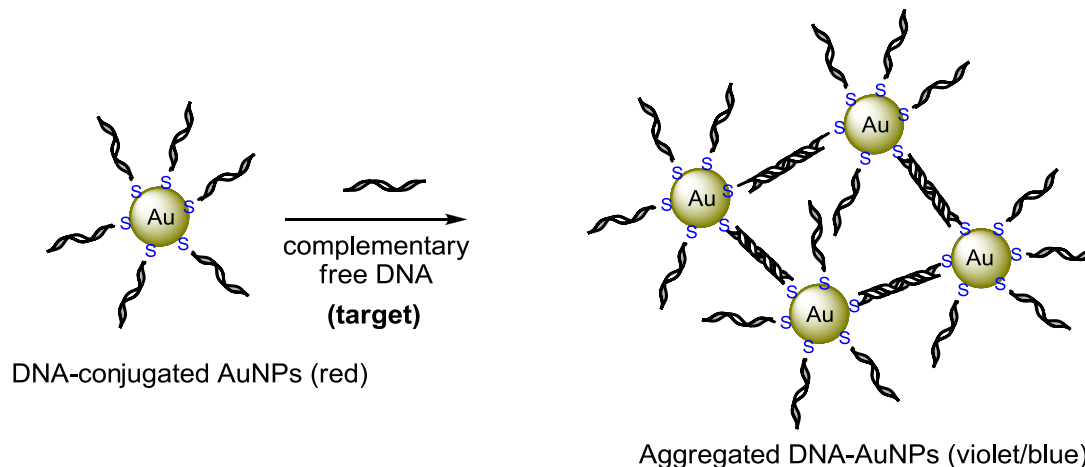
and a maleimide component ( $16 \pm 3$  nm maleimide-modified AuNP) upon irradiation with 532 nm light (the heat thus generated by the AuNP core could trigger the retro-Diels–Alder reaction).<sup>52</sup>



Scheme 1.2 Release of the fluorescein dye from the AuNP using photothermal induced the retro-Diels–Alder reaction, reproduced with permission from ref. 52.

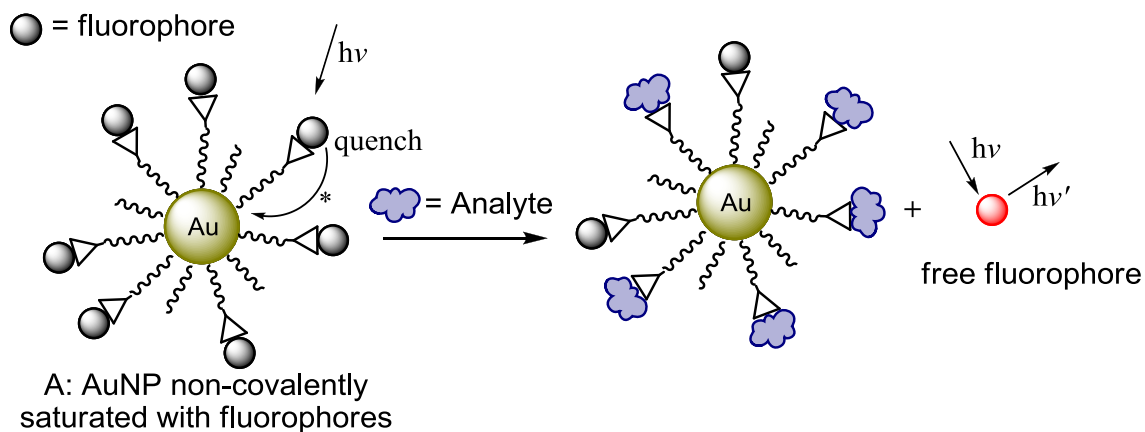
Biosensing is another important biological application of AuNPs. The tunable SPR band of AuNPs has been the main focus of active research in this field because the wavelength and intensity of the SPR band can be tuned by varying the distance between nanoparticles.<sup>11–14</sup> In 1996 Mirkin and coworkers prepared the first DNA-conjugated AuNP (DNA-AuNP) sensor, capable of detecting free DNA in solution. In their sensor, AuNPs are capped by sequence-specific DNA which is complementary to the free DNA in the solution that is to be detected. Upon hybridization of DNA strands attached onto AuNPs with the complementary free DNA, the DNA-AuNPs aggregate (Scheme 1.3). This is accompanied by an intense color change of solution, from light red (DNA-AuNPs) to violet/blue color (aggregated DNA-AuNPs). The color change which acts as an indicator is due to particle-particle SPR coupling that occurs when AuNPs are aggregated and the distance between nanoparticles is reduced.<sup>53</sup> Since Mirkin's pioneering work, DNA-AuNPs have been utilized extensively in ultrasensitive DNA detection.<sup>17</sup>





Scheme 1.3 DNA-conjugated AuNP sensor for detecting free DNA in solution.

AuNPs are also well-known as strong quenchers; generally, a photo-excited fluorophore located in the vicinity of AuNPs undergoes quenching via energy or electron transfer to the nanoparticle's core.<sup>54 - 56</sup> Scheme 1.4 illustrates the sensing strategy of using the quenching properties of AuNPs. Nanoparticle (A) represents an AuNP non-covalently saturated with fluorophores (e.g. via hydrogen and/or ionic bonds between the fluorophore (circles) and the outermost functional group of the AuNP (triangles)). The fluorophores are quenched by the AuNP core and no fluorescence can be measured. When analyte is added to a solution of (A), the fluorophores attached onto the AuNP will be displaced by analyte molecules through a dynamic equilibrium. Upon release, fluorescence of the fluorophores can be detected as it is no longer quenched by the AuNP core. Higher concentrations of the analyte lead to the release of more fluorophores and consequently, more intense fluorescence. Therefore, the concentration of analyte can be found by plotting a calibration curve.<sup>55, 56</sup>



Scheme 1.4 A sensing strategy using the quenching properties of AuNP.

Another very useful application of AuNPs involves improvement in the conversion efficiency of organic hybrid solar cells. The most effective method of increasing the conversion efficiency of organic hybrid solar cells is to increase light harvesting by organic semiconductors in the active layer.<sup>57, 58</sup> A novel method to enlarge the photon absorption of organic semiconductors is to trap incident light by plasmonic metal nanoparticles such as AuNPs. Because of the SPR properties, nanoparticles can act as antennas for light and refocus incident light into neighboring regions.<sup>59</sup> Therefore, the light harvesting capability of organic semiconductors can be enhanced if they are located nearby AuNPs. Employing this principle, enhancement in the conversion efficiency of a variety of organic solar cells due to incorporation of AuNPs has been demonstrated.<sup>60</sup> For example, polymer bulk-heterojunction solar cells show an improvement in conversion efficiency following incorporation of AuNPs into active layer.<sup>61</sup>

Catalysis with the use of AuNPs has also been an active research area of AuNP applications.<sup>62 - 67</sup> Soluble catalysts exposed on a AuNP surface via Au-S bonding can give rise to a heterogeneous AuNP-supported catalyst. The ease of separation and the

possibility of reuse are significant benefits of AuNP-supported catalysts.<sup>62, 63</sup> Tremel et al. reported the AuNPs bearing a Ru complex as the first AuNP-supported catalyst.<sup>64</sup> It has been found that these types of AuNPs can catalyze ring-opening metathesis polymerization. Several soluble catalysts such as 1,1'-bi-2-naphthol (BINOL),<sup>65</sup> chiral bis-(oxazoline),<sup>66</sup> and cinchona alkaloid<sup>67</sup> have also been incorporated onto AuNPs so that their catalytic reactivity could be studied.

An essential conclusion from the very useful AuNP applications demonstrated is that the majority of these applications rely on the characteristics of the monolayer and functionality of the organic protecting ligands attached onto the AuNP core. Therefore, developing techniques to prepare nanoparticles with specific moieties or functionalities, directly or by carrying out specific and reproducible chemical reactions on these protecting shells, is a critical aspect of AuNP applications.

## **1.2 Approaches to Synthesis of Functionalized AuNPs (1 – 5 nm)**

### **1.2.1 Direct synthesis**

In the Brust-Schiffrin synthesis (Figure 1.4) the reduction of AuCl<sub>4</sub> in the presence of a thiol ligand, usually a non-functionalized alkanethiol, such as dodecanethiol, is employed to prepare non-functionalized alkanethiol-protected AuNP (we refer to these as base-AuNP).<sup>7, 3</sup> Of course, the thiol utilized can contain additional functionality; then this functionality can also be introduced directly onto the AuNP, as long as the functionality is compatible with the Brust-Schiffrin synthesis conditions. Using this approach, so-called direct synthesis, a variety of functionalized AuNPs such as hydroxyl-

,<sup>68</sup> amine-,<sup>69</sup> alkene-,<sup>70</sup> ester-,<sup>71</sup> imidazolium-based ionic liquid-,<sup>72</sup> and phthalocyanine-functionalized AuNPs<sup>73</sup> have been prepared.

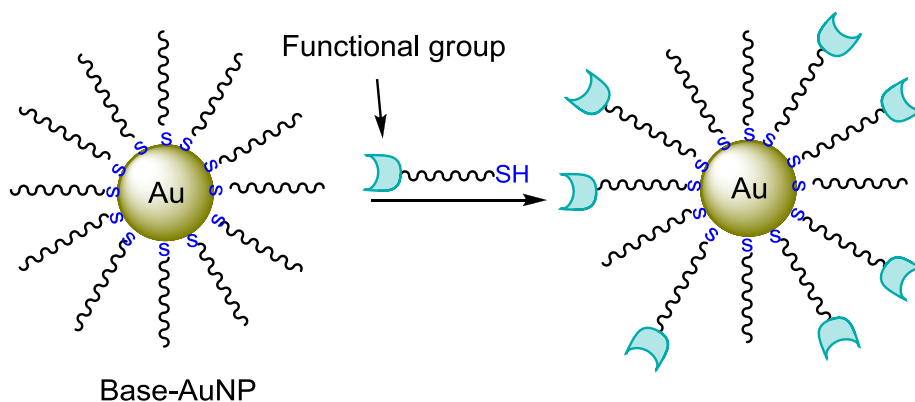
It is noteworthy that the direct synthesis works when the functional group of the thiol ligands remains intact during the synthesis of nanoparticles. More specifically, strong reducing conditions accompanying the use of NaBH<sub>4</sub> can unintentionally reduce the functional group of thiols and limit the possible utility of this method. Another drawback is that, in contrast to the non-functionalized alkanethiols, a broader size distribution of AuNPs results when functionalized thiols are utilized.<sup>7,26–28</sup>

### 1.2.2 Ligand Exchange Reactions

The ligand exchange reaction is the most important method for the controlled functionalization of AuNPs; particularly, when the precursor thiols are sensitive to the reducing conditions of the direct AuNP synthesis. This method involves replacement of alkanethiols on the surface of the base-AuNP with functionalized thiol ligands. The resulting AuNP usually contain a mixture of both alkanethiol and functionalized thiol (Scheme 1.5).<sup>74–79</sup>

Mechanistic studies suggest that the ligand exchange reaction follows a second order-associative (S<sub>N</sub>2-type) pathway in which the rate-determining step depends on the concentration of both the incoming ligand and AuNPs.<sup>75,76</sup> However, the overall rate and extent of the exchange reaction are affected most by the core size,<sup>76</sup> the electronic charge of the AuNP,<sup>77</sup> and the nature of the incoming ligands, in particular the steric effects.<sup>78,79</sup> In general, the rate of the place exchange reaction is initially fast but slows down with time due to the packing structure of AuNPs. It should be noted that unlike a gold self-

assembled monolayer (Au-SAM), which is flat with ordered ligand packing, the surface of AuNPs is not uniform, and defect sites including vertex and edge sites are sterically more accessible than Au (111) terrace sites where organic monolayer packing is denser (Figure 1.1B). Therefore the rate of the exchange reaction is more rapid at the defect sites.<sup>27</sup> The ratio of defect sites to terrace sites in a AuNP core increases as the core size decreases, thus the smaller the core, the faster the rate and the greater the extent of exchange reaction.<sup>76</sup>



Scheme 1.5 Functionalization of AuNP by a ligand exchange reaction (resulting AuNP contains both alkanethiol and functionalized (incoming) thiol).

Due to the difference in the rate of ligand exchange at terrace versus edge/vertex sites, adding the incoming ligand onto the base-AuNPs can be done in a controlled manner. To this end, displacement by the incoming ligand at the edge/vertex sites is most prominent when the exchange reaction is performed via the use of a dilute solution of incoming ligand and short reaction time.<sup>75, 79, 80</sup> Additionally, thiol ligands on AuNPs migrate from edge/vertex sites onto terrace sites and vice versa over time. Therefore a longer exchange time with a more concentrated reaction mixture allows for a more uniform place exchange at edge/vertex and terraces sites.<sup>76</sup>

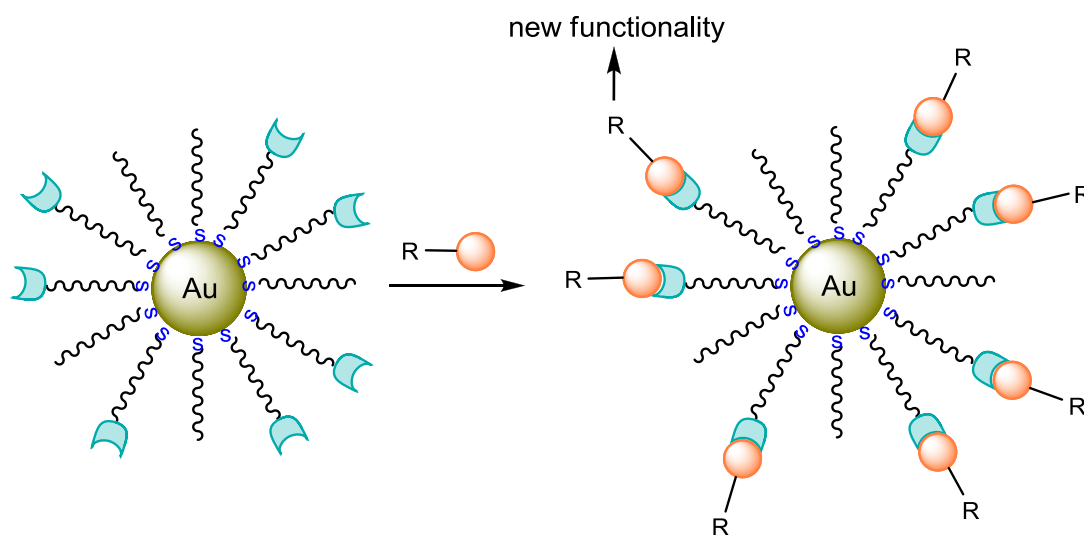
The structural properties of the incoming ligand are another important factor affecting the exchange reaction. A primary thiol in comparison with a secondary or a tertiary thiol shows more reactivity in an exchange reaction due to the lesser degree of steric hindrance.<sup>75</sup> Surprisingly, however, branched thiols are more reactive than linear ones and AuNPs obtained after an exchange reaction with branched thiols are more stable, evidenced by thermogravimetric analysis (TGA). It has been suggested that branched thiols can be packed more efficiently onto AuNP, resulting in more stable AuNPs.<sup>78</sup>

### 1.2.3 Interfacial Reactions

The synthesis of thiol derivatives is usually tedious or in some cases ineffective, therefore functionalization of AuNPs cannot always be achieved by using the direct synthesis method or the place exchange reaction which requires synthesized functionalized thiols. However, an elegant alternative approach for the functionalization of AuNP can include a direct organic reaction of terminal functional groups exposed on the surface of template nanoparticles with various reactants. Using AuNP as a macromolecular-type reagent and carrying out organic reactions on the surface monolayer containing suitable functionality has been shown as a promising strategy to introduce new functionality onto AuNP (Scheme 1.6).<sup>81–87</sup>

In the self-assembled structure of AuNPs, the mobility of functional thiols is limited, causing a pseudo-solid phase environment. Therefore the interfacial reactions taking place between outermost functional groups on the nanoparticle and reactants can be substantially different from those taking place in a homogeneous solution phase.<sup>82, 83</sup> In spite of the aforementioned usefulness of interfacial reactions, the low stability of AuNPs

to common reaction conditions such as high temperature, aggregation in the presence of some reactants (e.g. interparticular aggregation induced by cross-linking), and decomposition of nanoparticles in the case of using some catalysts, limit the utility of this approach.<sup>84, 85</sup> In addition, reactions of the monolayer moieties on the AuNPs are slowed or impeded relative to similar reactions in the solution phase.<sup>86</sup> Therefore, finding and employing reactions which work efficiently under mild conditions is an important challenge in the modification of AuNPs and in their desired applications.



Scheme 1.6 Functionalization of AuNP via an interfacial reaction.

## 1.3 Thermal and Photochemical Interfacial Reactions on AuNPs

The chemical modification of AuNPs by interfacial reactions has been the subject of numerous studies and it was, in fact, pursued immediately after the synthesis of the first thiol-protected AuNPs. As a pioneer, Brust *et al.* demonstrated the reactivity of *p*-mercaptophenol-protected AuNPs toward esterification of the surface bound phenolic hydroxyl group (Scheme 1.7 **a**). The esterification was carried out using propionic anhydride in aqueous sodium acetate and verified by elemental analysis and infrared spectroscopy.<sup>7</sup> Since Brust's report, many efforts have been made to perform thermal and photochemical interfacial reactions to chemically modify AuNPs and investigate the reactivity of the protecting monolayer.<sup>87–93</sup>

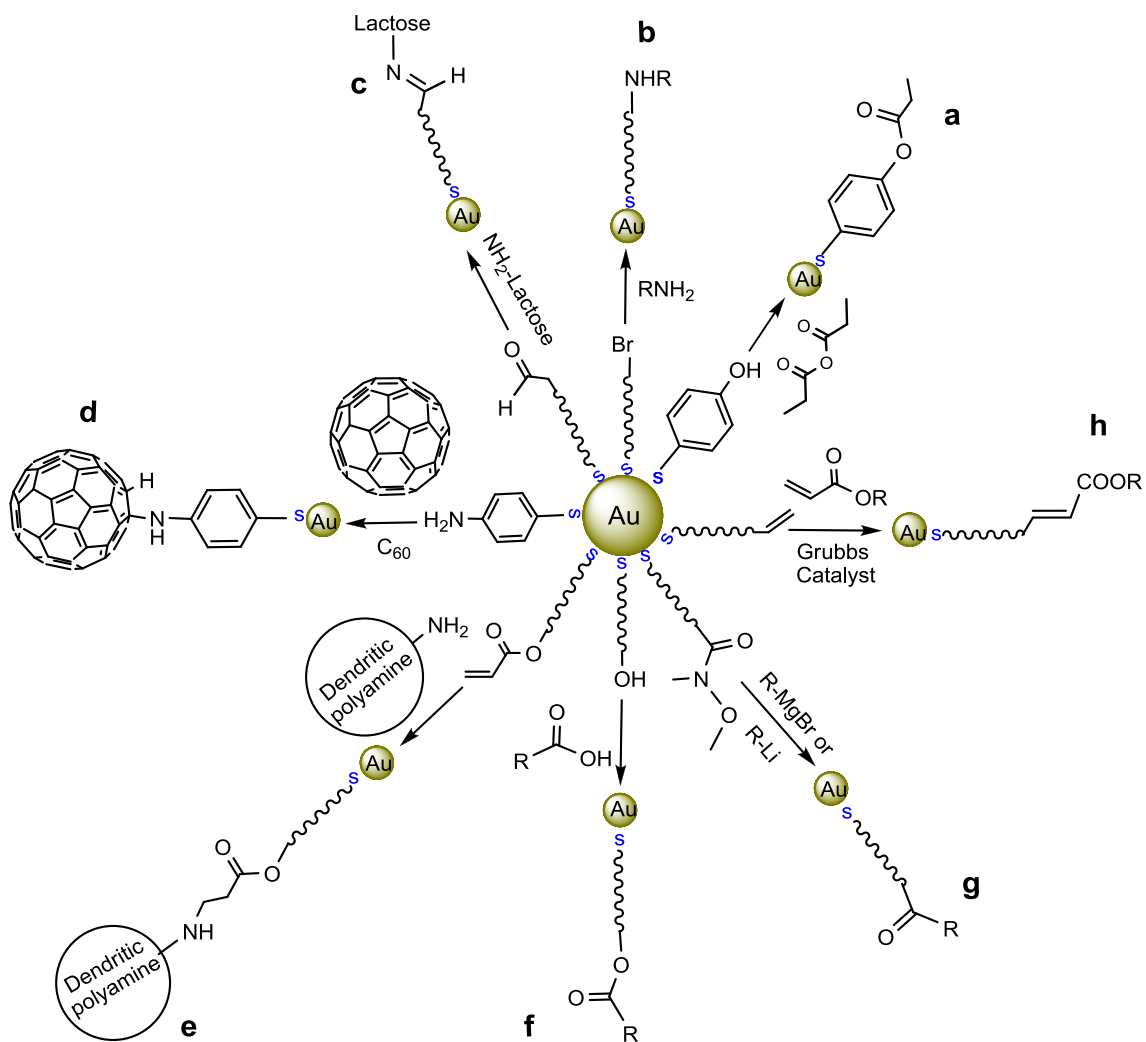
### 1.3.1 Thermal Interfacial Reactions

The S<sub>N</sub>2 reaction was one of the first employed to incorporate new functionality onto AuNPs (Scheme 1.7 **b**).<sup>87</sup> Murray *et al.* synthesized bromoalkanethiol-functionalized AuNPs utilizing a place exchange reaction and investigated their S<sub>N</sub>2 reactivity toward alkyl amines. The functionalized AuNP cores after the exchange reaction were surrounded by a mixture of both alkanethiol (dodecanethiol C<sub>12</sub>) and bromoalkanethiol (C<sub>n</sub>Br, n = 12, 8, or 3). It was found that the selectivity and rate of the S<sub>N</sub>2 reactions are dependent upon the steric bulk of the amines, as well as on the relative chain length of bromoalkanethiol (C<sub>n</sub>Br) and alkanethiol (C<sub>12</sub>). Similar to the S<sub>N</sub>2 reaction of bromoalkane in solution phase, the less bulky amines reacted faster. Moreover, AuNPs containing shorter bromoalkanethiol (e. g. C<sub>3</sub>Br), in comparison with the longer bromoalkanethiol, underwent reaction with the primary amine at a slower rate (rates of



reactions:  $C_{12}:C_{12}Br-AuNP > C_{12}:C_8Br-AuNP > C_{12}:C_3Br-AuNP$ ). This finding implies that interfacial reactions on AuNPs occur faster if the functional group is sterically accessible.

Nucleophilic addition reactions are among the most popular reactions utilized for the modification of AuNPs. For example, Otsuka and co-workers reported the incorporation of AuNPs with lactose through amine addition reaction.<sup>88</sup> AuNPs (1-10 nm size range) protected with 1-acetal-poly(ethylene glycol) were prepared, followed by conversion of the terminal acetal group to an aldehyde by gentle acid treatment. Next, an amine addition reaction between the terminal aldehyde group anchored to the AuNPs and the amine group of lactose was performed to afford lactose-modified AuNPs (Scheme 1.7 c).<sup>88</sup> Another successful nucleophilic addition reaction includes an amination between  $C_{60}$  and 4-aminothiophenol/hexanethiolate-protected AuNP (AH-AuNP) to obtain  $C_{60}$ -linked AuNP (Scheme 1.7 d). In this example, 4-aminothiophenoxide/hexanethiolate-protected AuNPs (~ 2 nm) were synthesized using the modified Brust-Schiffrin synthesis followed by ligand place exchange reaction of hexanethiolate-protected AuNPs with 4-aminothiophenoxide.  $C_{60}$  was added to a solution of AH-AuNPs in toluene and stirred for 3 days at room temperature to couple  $C_{60}$  to the AH-AuNPs.<sup>89</sup> Michael addition, as one of the most powerful and useful bond-forming reactions, is simple and high yielding, making it an ideal reaction candidate for the AuNP modification. Chechik *et al.* investigated Michael addition reactions on AuNPs (Scheme 1.7 e). They prepared acrylate-modified AuNPs and exposed them to dendritic polyamine and studied the reactions kinetics.<sup>90</sup> They found that the Michael addition reactions between the dendritic polyamine and acrylate-modified AuNPs were slightly retarded compared to a similar



Scheme 1.7 Examples of thermal interfacial reactions on AuNPs: a) esterification, b) S<sub>N</sub>2 substitution, c) amine nucleophilic addition to an aldehyde, d) amination reaction of C<sub>60</sub>, e) Michael addition, f) coupling reaction of aliphatic hydroxyl, g) Grignard functionalization of Weinreb amide-modified AuNPs, and h) cross olefin metathesis.

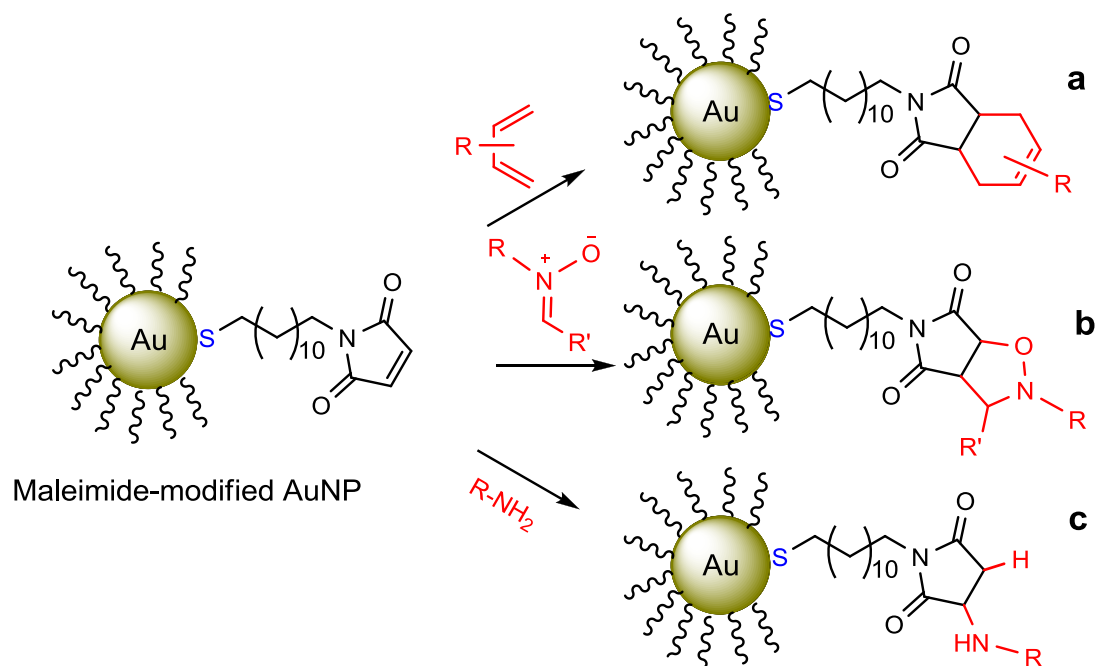
solution phase Michael addition between a model acrylate and polyamine. Coupling reaction of aliphatic hydroxyl to benzoic acid derivatives was also performed to synthesize AuNPs bearing phosphine moieties which were later deposited on a SAM containing Pd<sup>II</sup> pincer molecules (Scheme 1.7 f).<sup>91</sup>

Carbon–carbon bond-forming reactions have also been carried out on AuNPs to prepare functionalized AuNPs via interfacial reactions. For example, Thode *et al.* demonstrated Grignard functionalization of Weinreb amide-modified AuNPs (Scheme 1.7 g). To prepare the Weinreb amide-modified AuNPs, the  $\omega$ -N-methoxy-N-methyl amide alkylthiol was exchanged onto octanethiol-stabilized AuNPs (~ 1.5 nm) by stirring latter in a solution of amide alkylthiol. Nine organometallic reagents were selected and reacted with Weinreb amide groups on the AuNPs to covalently modify nanoparticles.<sup>92</sup> Additionally, Astruc and co-workers showed that cross olefin metathesis using a second-generation Grubbs catalyst can be performed to further functionalize alkene-functionalized AuNPs (Scheme 1.7 h).<sup>93</sup>

### 1.3.1.1 High Pressure Induced Interfacial Reactions

In many cases, reactions at the interface of the monolayer moieties on the AuNPs are slowed (less efficient) when compared to similar reactions carried out in the solution phase because of factors associated with the unique environments of the AuNPs (e.g. steric hindrance of adjacent ligands).<sup>86</sup> Slow or impeded reactions in solution phase can be accelerated by heat or utilizing catalysts; however, exposing AuNPs to these conditions leads to aggregation or their decomposition. To remedy this, our group demonstrated that high pressure conditions can be used as an efficient tool for the high

yielding modification of AuNPs via interfacial reactions.<sup>86, 94, 95</sup> Maleimide-modified AuNPs were synthesized and their interfacial reactions were studied. At ambient conditions, Diels–Alder cycloaddition reactions of maleimide-modified AuNPs with dienes require a long period of time (days to weeks).<sup>86</sup> However, the identical reactions proceeded in high pressure conditions (11 000 atm) in only a few minutes without affecting the nanoparticles core size or other physical properties (Scheme 1.8 a). More recently, the reactivity of maleimide-modified AuNPs toward nitron 1,3-dipolar cycloaddition<sup>94</sup> and Michael addition reactions<sup>95</sup> under ambient and high pressure conditions was investigated (Scheme 1.8 b, c). Again, the use of high pressure conditions was found to significantly accelerate these interfacial reactions and turned them into practical reactions to incorporate new functionality onto AuNPs.



Scheme 1.8 Modification of maleimide-modified AuNP under high pressure conditions (11 000 atm); a) Diels–Alder cycloaddition, b) 1,3-dipolar nitron cycloaddition, d) Michael addition reaction.

The use of high pressure is a well-established tool in organic synthesis, due to the increased reaction rate and avoidance of catalyst use, and has been applied in most cycloaddition reactions.<sup>96–99</sup> The equilibrium constant ( $K$ ) of a chemical reaction can be described as (Eq. 1):

$$\left(\frac{\partial \ln K}{\partial P}\right)_T = -\frac{\Delta V^\ddagger}{RT} \quad \text{Eq. 1}$$

where  $P$  is pressure and  $\Delta V^\ddagger$  is activation volume. When the volume of activation is negative,  $K$  of the reaction increases exponentially with pressure at constant temperature.

The basic thermodynamic relation can be obtained by

$$\Delta G = -RT \ln K$$

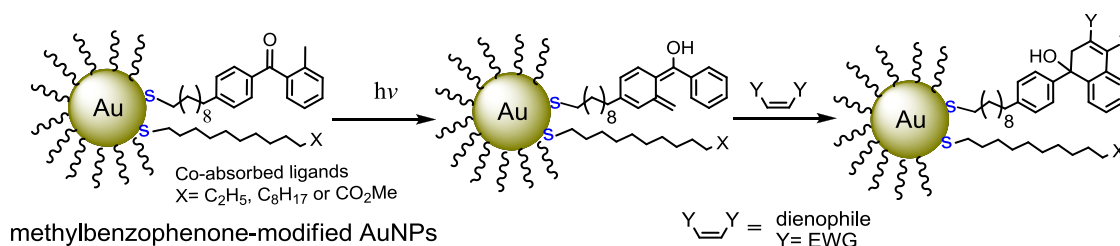
Therefore any increase in  $K$  gives a more negative Gibbs free energy ( $\Delta G$ ) which is thermodynamically favored.<sup>96</sup>

The activation volume ( $\Delta V^\ddagger$ ) is the difference between the volume of the transition state and the initial state, which is approximately equal to the difference in the molar volumes of reactant and product. Reactions involving bond formation and concentration of charge in the transition state show a negative activation volume. In contrast, bond cleavage and charge dispersal in the transition state of a reaction lead to a positive activation volume.<sup>97</sup> As an example, Diels–Alder reactions, in which bond forming takes place, contain an activation volume ( $\Delta V^\ddagger$ ) of -30 to -50 cm<sup>3</sup>/mol; therefore these reactions can be accelerated by applying high pressure.<sup>98,99</sup> The physical properties of the solvent, including the freezing point, density, and viscosity are also influenced by the high pressure conditions. Hence, the role of the medium in the mechanism of a reaction

occurring at hyperbaric conditions can be different from that taking place at ambient conditions. It has been suggested that the most important effect of the pressure arises from changes in the viscosity of the solvent.<sup>97</sup>

### 1.3.2 Photochemical Interfacial Reactions

Workentin *et al.* have done extensive research on photo-initiated chemical reactions to probe interfacial reactivity of organic substrates anchored to AuNPs.<sup>100 - 103</sup> They reported the Diels–Alder reaction between a dienophile and photogenerated dienol-modified AuNPs (Scheme 1.9). *Ortho*-methylbenzophenone-modified AuNPs with a variety of co-absorbed ligands, synthesized using the Brust-Schiffrin method and the exchange reaction, were irradiated in the presence of a series of dienophiles.<sup>100</sup> Upon irradiation, photogenerated dienols were formed (via  $\gamma$ -hydrogen abstraction) on the AuNPs, followed by a Diels–Alder reaction between the attached dienol and the dienophile.



Scheme 1.9 Photoenolization of *ortho*-methylbenzophenone-modified AuNP and subsequent Diels–Alder reaction.

It was found that the nature of the co-absorbed ligands and the concentration of the dienophile have no effect on the extent of the Diels–Alder reaction. However, the yield of

the conversion (Diels–Alder reaction) was influenced by the selective population of three distinct AuNP sites with thiols bearing *ortho*-methylbenzophenone (Table 1.1).

Table 1.1 Conversion % of the Diels–Alder reaction at selective populated sites

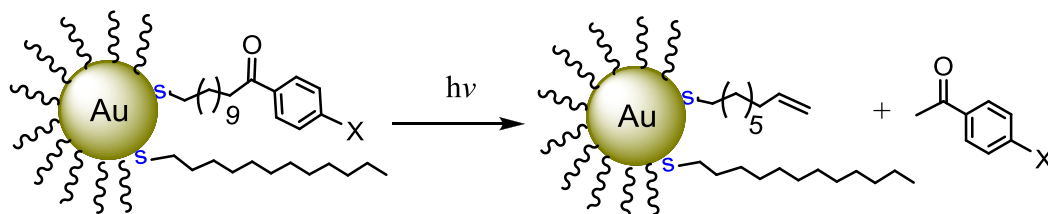
Functionalized site(s)	Conversion %
edge, vertex and terrace	< 60
edge and vertex	85 ± 3
terrace	36 ± 2

These results together show that the Diels–Alder reaction of *ortho*-methylbenzophenone thiols incorporated to the AuNPs is site-dependent and the photogenerated dienols placed at the edge and vertex sites more readily participate in the Diels–Alder reaction. In general the accessibility and orientation of terminal functional groups at the edge, vertex, and terrace sites is the key factor affecting the interfacial reactivity of AuNPs.<sup>100, 101</sup>

The selective population of edge/vertex and terrace sites was achieved by varying the time period of the exchange reaction and the concentration of incoming ligand. To selectively position *ortho*-methylbenzophenone thiols (incoming thiols) at edge/vertex sites, a low concentration of the incoming thiol and a short exchange reaction time (1 hour) were used. In contrast, using a high concentration of incoming ligand and a longer exchange reaction time (5 days) resulted in population of all possible exchangeable sites (edge, vertex and terrace). The selective population of terrace sites with *ortho*-methylbenzophenone thiols required two successive place exchange reactions. First, all edge, vertex and terrace sites underwent the exchange reaction with methylbenzophenone thiols in 5 days. Next, *ortho*-methylbenzophenone thiols positioned at edge/vertex sites

were place exchanged with dodecanethiols in a short exchange reaction, affording AuNPs with *ortho*-methylbenzophenone thiols positioned at only terrace sites.

As stated, the functional groups located at edge/vertex sites relative to those at terrace sites show higher reactivity toward the interfacial reactions, and because the ratio of edge/vertex sites to terrace sites increases as the AuNP gets smaller, it is expected that the reactivity of functionalized AuNPs increases as the core size decreases. Workentin's group investigated this concept by probing the Norrish type II photoreaction of aryl ketone-functionalized AuNPs (Scheme 1.10).<sup>102</sup> They prepared  $1.7 \pm 0.4$  nm,  $2.2 \pm 0.4$  nm, and  $4.5 \pm 0.7$  nm aryl ketones-modified AuNPs and irradiated to yield their alkene-modified counterpart via a Norrish Type II reaction. It was found that the smallest AuNPs ( $1.7 \pm 0.4$  nm), with the highest ratio of edge/vertex sites to terrace sites, underwent Norrish Type II transformation quantitatively, while only  $65 \pm 6$  % of aryl ketones anchored to the large AuNPs ( $4.5 \pm 0.7$  nm) were converted to alkenes. The conversion percentage for medium size AuNPs ( $2.2 \pm 0.4$  nm) was  $85 \pm 5$  %. The small nanoparticles, with a larger ratio of edge/vertex sites and an environment with greater curvature, provide more free space at the termini of the AuNP ligand monolayer and a more favorable orientation for interfacial reactions.



aryl ketone-functionalized AuNPs

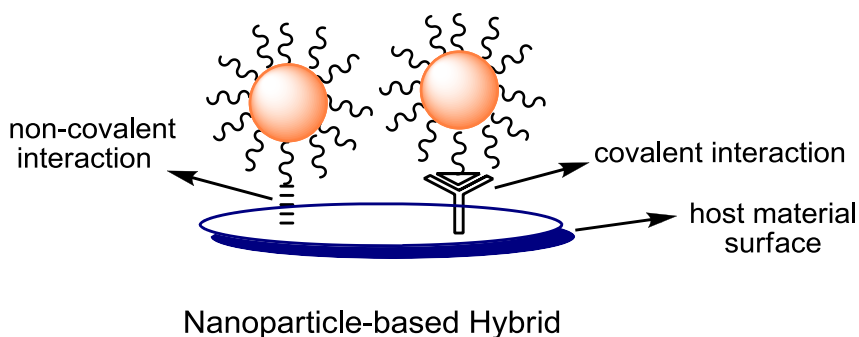
Scheme 1.10 Norrish type II photoreaction of aryl ketone-functionalized AuNP.



To put it briefly, photochemical reactions of suitably functionalized AuNPs can be used to chemically modify nanoparticles. Utilizing photochemical methods simply eliminates the need for the destructive reaction conditions for AuNPs (high temperature and catalyst) and AuNPs can be chemically modified under mild photoreaction conditions at ambient (or lower) temperatures.

## 1.4 AuNP-based Nanohybrid Materials

The assembly and immobilization of metal nanoparticles onto material surfaces is a primary step in the engineering of interparticle properties and the development of new hybrid materials. It has been shown that the physical and optical properties of individual nanoparticles can be modified by interaction with other nanoparticles and/or with the substrate.<sup>104–106</sup>



Scheme 1.11 Immobilization of metal nanoparticles onto material surface.

The immobilization of metal nanoparticles onto a surface to fabricate hybrid materials can be done via non-covalent or covalent interactions between nanoparticles and the host material surface (Scheme 1.11).<sup>107, 108</sup> Lately, the deposition of AuNPs onto

material surfaces to fabricate AuNP-based hybrid materials has gained much attention for the following reasons: 1) incorporation of AuNPs can improve the physical and mechanical properties of the host materials; 2) interparticle properties which have potential applications in catalysis, sensing, as well as electronic and optoelectronic devices, can be directed by assembling AuNPs onto a surface; 3) the combination of AuNPs with a host nanomaterial extends the possible uses of both AuNPs and the host nanomaterial by prosperous integration of the properties of the two components; 4) defined patterned structures can be obtained by depositing AuNPs on a surface; and 5) AuNPs are an ideal candidate to study the interaction of material and biomaterial surfaces with metallic nanoparticles because there are conventional procedures to synthesize AuNPs with a monolayer bearing functional groups.<sup>104, 105, 109 – 111</sup> Because a key aspect of this thesis is the development of reaction protocols for the fabrication of robust AuNP-based hybrids, a basis for these types of materials, including preparative procedures and applications is provided next.

Decoration of materials such as silicon oxide,<sup>112</sup> carbon nanotubes (CNTs),<sup>113</sup> graphene,<sup>114</sup> and diamond<sup>115</sup> with AuNPs can be achieved by three main strategies, including: direct formation of AuNPs onto the surface, non-covalent approaches, and covalent approaches. In the next section, some successful examples of hybrids fabricated using these methods will be described.

#### **1.4.1 Direct Formation of AuNPs onto a Surface**

In this approach reduction process of a gold (III) salt to produce nanoparticles takes place at the surface of the host material. If the interactions (mostly van der Waals

interactions) between synthesized AuNPs and the surface (or functionalities at the surface) are sufficient, the hybrid materials composed of AuNPs and host materials can be fashioned. Wang and co-workers adopted the Turkevich citrate reduction method and prepared multi-walled carbon nanotubes (MWCNTs) coated with AuNPs (Figure 1.6). The MWCNTs were suspended in an aqueous solution of  $\text{AuCl}_4$  by sonication, followed by the addition of sodium citrate as a reducing and protecting reagent. Roughly, all of the synthesized AuNPs in the range of 12 to 21 nm were attached to the wall of the MWCNTs and little of the free AuNPs could be observed in solution, evident by TEM analysis. Furthermore, they showed that the modification of glassy carbon (GC) electrodes with AuNP/MWCNT hybrids enhances the respective electrochemical response of an analyte, suggesting that sensitive electrochemical sensors can be made using these types of hybrids.<sup>116</sup>

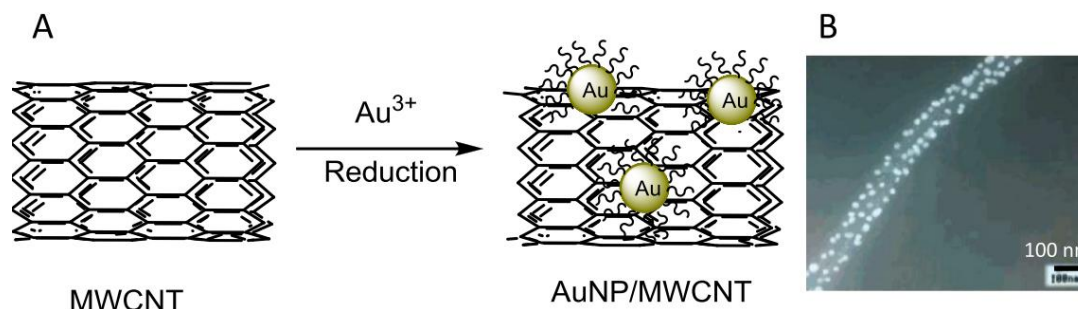
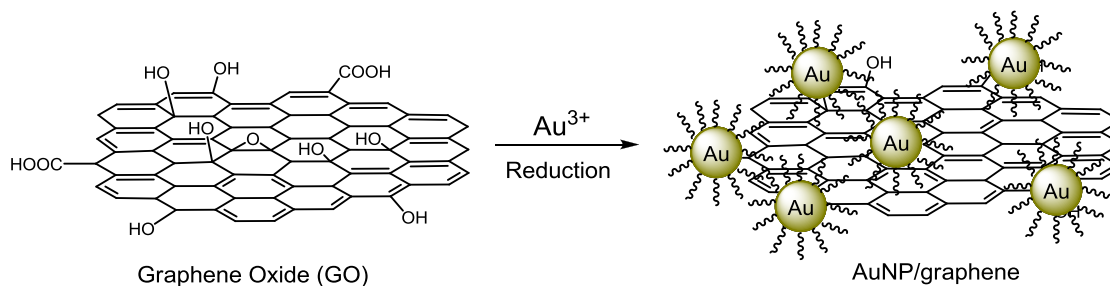


Figure 1.6 A) A schematic representation of the direct formation of AuNPs onto the surface to fabricate AuNP/CNT hybrid B) TEM images of synthesized AuNP/MWCNT hybrid (white dots are AuNPs), reprint with permission from ref. 116.

Interestingly, Dai *et al.* observed that when single-walled carbon nanotubes (SWCNTs) are immersed in gold (III) solution, AuNPs are formed spontaneously on the SWCNT sidewalls.<sup>117</sup> The average size of the AuNPs was estimated at  $\sim 7$  nm. They suggested that the direct redox reaction between SWCNTs and gold salt leads to the

formation of AuNPs on SWCNT sidewalls. The Fermi level of a SWCNT is well above the reduction potential of gold (III), which rationalizes the spontaneous electron transfer from the nanotube to the gold ions and their subsequent reduction.

More recently, graphene (a closely packed 2D nanomaterial composed of  $sp^2$ -bonded carbon atoms) has been served as the host substrates for deposition of AuNPs. In 2008, Kamat's group reported the first AuNP/graphene hybrid fabricated by the reduction of  $AuCl_4$  by  $NaBH_4$  in the presence of graphene oxide (Scheme 1.12).<sup>118</sup> In the obtained hybrids, AuNPs were physisorbed onto the graphene oxide surface. The average size of AuNPs could be tuned from  $\sim 6$  nm to  $\sim 12$  nm by using a more dilute solution of graphene oxide or higher concentration of  $AuCl_4$ . Graphene oxide surface contains oxygen functionalities such as hydroxyls, carbonyls, and acidic groups. A study showed that these functionalities play an important role in the formation of AuNPs at the surface of graphene oxide.<sup>119</sup> When the gold (III) salt was reduced by citrate in the presence of graphene oxide, the formation of AuNPs at the surface was evident by TEM and SEM images. However, reduction of gold (III) salt in the presence of reduced graphene oxide (rGO) with no oxygen functionalities at the surface, prepared by reduction of graphene oxide with hydrazine, showed no AuNPs deposited onto the graphene. These results revealed that the oxygen functionalities govern the nucleation and growth of AuNPs at the graphene oxide surface.



Scheme 1.12 Preparation of AuNP/graphene hybrid via direct formation of AuNPs on graphene oxide.

More efficient decoration of graphene with nanoparticles can be achieved by modification of graphene surface with pre-adsorbed entities. For this reason, Zhang *et al.* first coated the reduced graphene oxide surface (rGO, synthesized by reduction of graphene oxide with hydrazine) with 1-octadecanethiol (ODT) which can hold AuNPs on the surface via S-Au bond formation and then deposited octadecanethiol-protected AuNPs synthesized in situ using photoreduction of gold (III) method (Figure 1.7). The synthesized AuNPs, with sizes of  $1.2 \pm 0.3$  nm, were situated in ordered patterns, as dictated by the graphene lattice. Figure 1.7B shows TEM of AuNPs assembled on the rGO surface.<sup>120</sup> In another effort, perylene tetracarboxylate (PTCA) was deposited onto the rGO prior to the reduction of gold ions (Scheme 1.13). In this case, PTCA could interact with the  $\pi$ -conjugated carbon skeleton of graphene through  $\pi$ - $\pi$  stacking and on the other hand, due to carboxylate groups of PTCA, more active sites were provided for the growth of AuNPs at the surface of rGO (Scheme 1.13, PTCA/rGO composite). An amino-terminated ionic liquid was additionally used to protect the AuNPs after loading them onto the rGO surface. The obtained AuNP/PTCA/rGO hybrids were examined for electrocatalytic oxygen reduction. It was found that electrodes modified with the above hybrids reduce oxygen very effectively, in comparison with the unmodified electrode.<sup>121</sup>

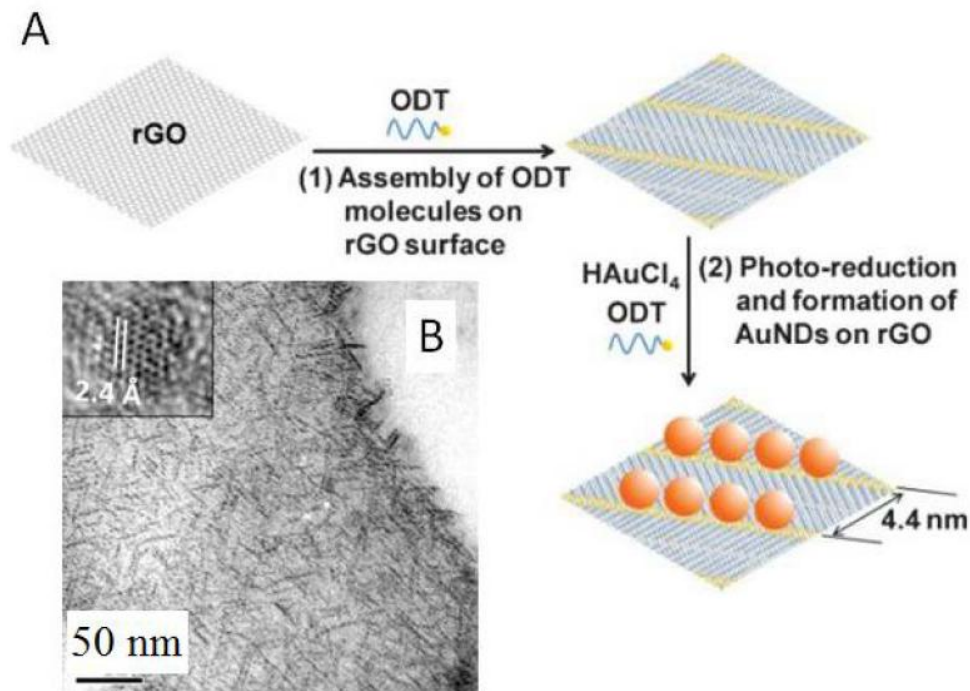
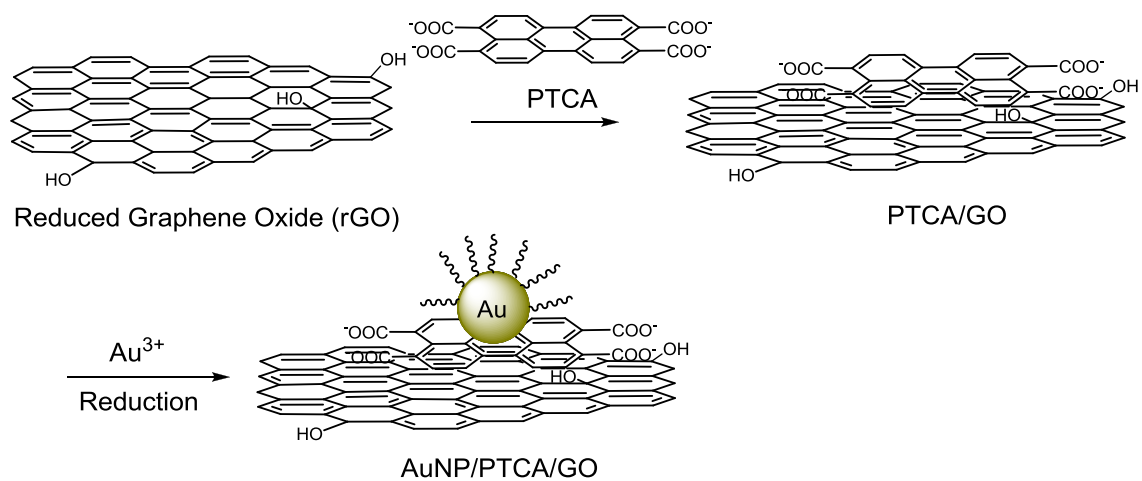


Figure 1.7 A) Illustration of the in situ synthesis and assembly of AuNPs (red circles) on rGO, B) TEM image of AuNP/graphene hybrid (inset is HRTEM of AuNP on rGO surface), reprint with permission from ref 120.



Scheme 1.13 Synthesis of perylene-coated reduced graphene oxide decorated with AuNPs, reprint with permission from ref. 121.

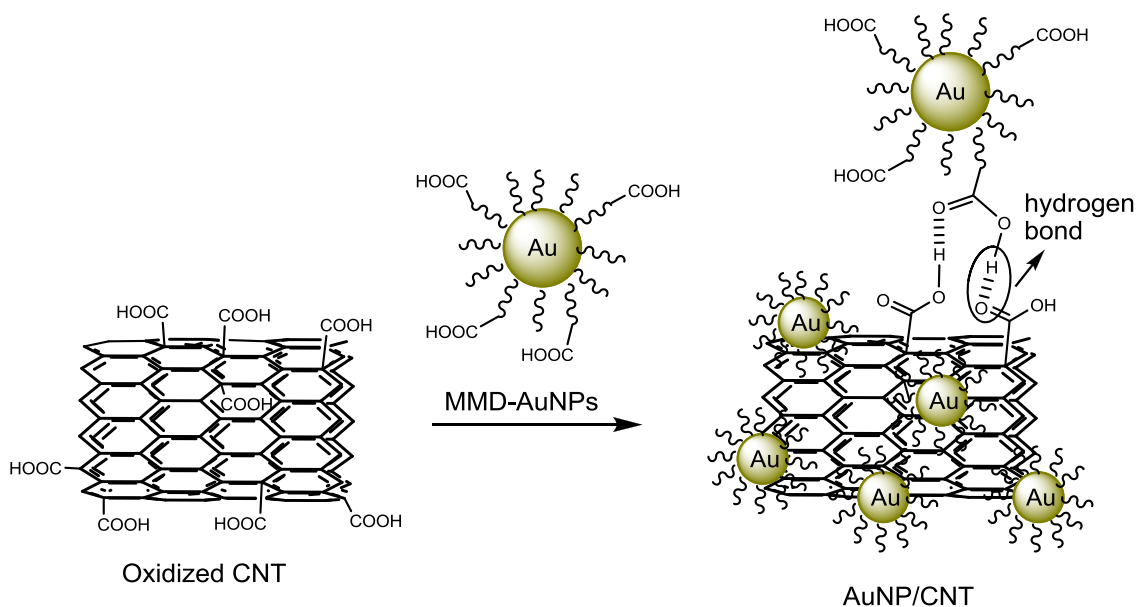
Boron-doped diamond (BDD) electrodes are other substrates that the deposition of AuNPs has been done upon, with the aim of effectively enhancing the sensitivity and analytical capability of BDD electrodes.<sup>122, 123</sup> For example, AuNPs were electrochemically deposited onto a BDD electrode by scanning the potential from 0.7 V to 0.0 V in a solution of AuCl<sub>4</sub>. The SEM images revealed that the AuNPs formed at BDD electrode surface had a size distribution between 20 to 400 nm. The AuNP-modified BDD was utilized for the detection of dopamine and showed excellent sensitivity toward the analyte.<sup>123</sup>

In spite of their extensive use, direct formation of AuNPs onto the surface suffers from slow deposition rate, weak non-covalent interactions between AuNPs and the host material surface, and more importantly a lack of control over AuNP size. Therefore, this approach is useful when a specific size of nanoparticles is not required to prepare a hybrid.

#### **1.4.2 Non-covalent Approach**

To assemble AuNP-based hybrids with the use of non-covalent approach, AuNPs bearing suitable functionality need to be prepared in advance. Furthermore, functionalization of the host material surface is often required. When the non-covalent interactions between functionalized AuNPs and functional groups at the surface of the host are able to hold the nanoparticles at the surface, the hybrid can be formed. Hydrophobic interactions, hydrogen bonding, electrostatic forces, van der Waals interactions, along with  $\pi$ - $\pi$  stacking are frequently used to immobilize nanoparticles at a surface.<sup>104, 105, 109 – 111, 124</sup>

CNTs are among the first nanomaterials with which non-covalent deposition of AuNPs has been utilized to prepare AuNP-base hybrids. Han and co-workers synthesized mixed-monolayer (mercaptoundecanoic and decanethiol)-protected AuNPs (MMD-AuNPs) with a size of 2 nm and 5 nm, and immobilized them on oxidized CNTs (Scheme 1.14).<sup>125</sup> The oxidized CNTs contain carboxylic acid groups, capable of forming head-to-head hydrogen bonds with the carboxylic acid groups of the AuNP monolayer. In addition, the hydrophobic interactions between the alkyl chains of the AuNPs and the CNT surface facilitated the assembly of AuNP/CNT hybrids. The loading of the nanoparticles on CNTs was tailored by varying the relative concentrations of AuNPs, CNTs, and mediating agents.

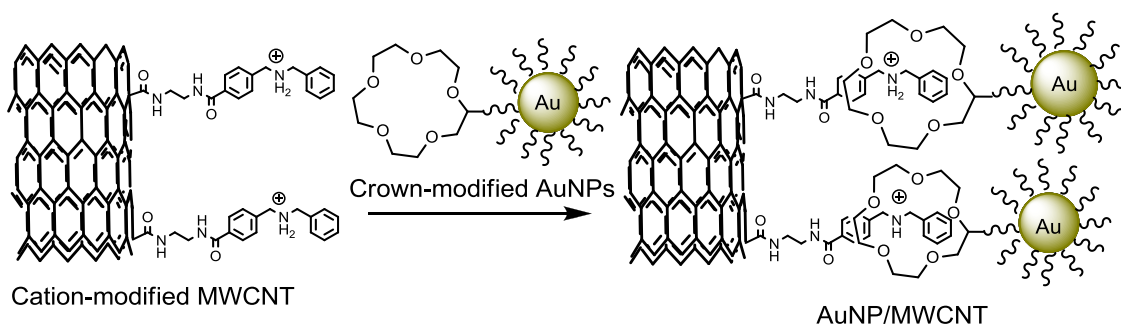


Scheme 1.14 Schematic illustrations of decoration of CNTs with AuNPs using hydrogen bonding and hydrophobic interactions.

Sainsbury's group demonstrated a high-density assembly of AuNPs on CNT sidewalls using non-covalent approach. They prepared dibenzylammonium-cation-



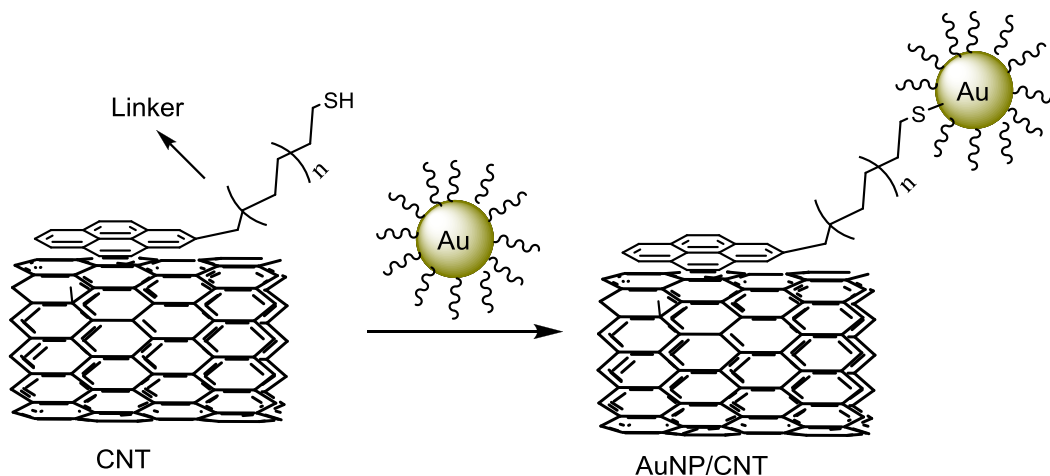
modified MWCNTs on which to deposit crown-modified (dibenzo[24]crown) AuNPs (Scheme 1.15).<sup>126</sup> The crown moiety in the crown-modified AuNPs coordinates to the dibenzylammonium cation on MWCNT and the formation of a surface-combined pseudorotaxane leads to non-covalent incorporation of AuNPs. This was evident by a control test in which the dibenzylammonium cation of MWCNTs and crown ether of AuNPs were pre-complexed and in this case, no AuNP/MWCNT hybrid was observed.



Scheme 1.15 Non-covalent decoration of cation-modified MWNTs with crown-modified AuNPs.

$\pi$ - $\pi$  stacking has been also shown to be an effective and simple method in the fabrication of AuNP/CNT hybrids. Using this strategy, AuNPs were self-assembled onto the CNT surface through a bi-functionalized linker (terminated with a pyrenyl unit at one end and a thiol group at the other end). As shown in Scheme 1.16, the pyrene end of the linker stacks onto the CNT surface by  $\pi$ - $\pi$  interactions, and the thiol end connects to the AuNP, affording AuNP/CNT hybrids.<sup>127</sup>

Very recently, non-covalent decoration of graphene with AuNPs has been reported and it has been shown that the obtained hybrids have potential applications in biosensors,<sup>128</sup> catalysis,<sup>129</sup> and memory devices.<sup>130</sup> To fabricate non-covalently assembled AuNP/



Scheme 1.16 Illustration of the non-covalent ( $\pi$ - $\pi$  stacking) loading of AuNP on CNT through a linker molecule.

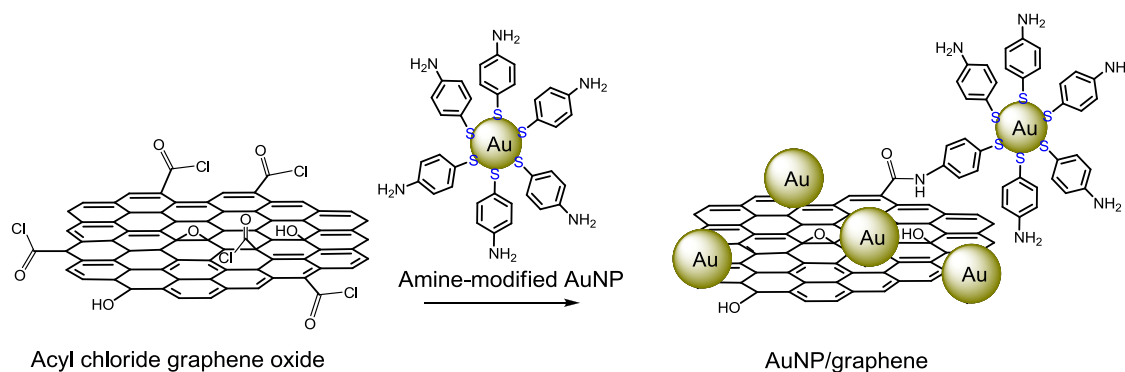
graphene hybrid, often the functionalization of graphene is necessary. Wang and co-workers functionalized graphene with cationic polyelectrolyte poly(diallyldimethyl ammonium chloride) (PDDA) prior to the deposition of citrate-protected AuNPs on the graphene surface (PDDA was physisorbed onto the graphene surface). Electrostatic interactions between PDDA and the AuNPs were suggested as a driving force for the formation of hybrids.<sup>131</sup> In another report, Shi *et al.* demonstrated the functionalization of graphene with 1-pyrenebutyric acid which, afterward served to immobilize positively charged 4-dimethylaminopyridine (DMAP)-protected AuNPs with diameters of 2 – 6 nm. It was observed that AuNPs can self-assemble onto the graphene surface via non-covalent interactions between DMAP and the pyrene functionality of graphene, resulting in AuNP/graphene hybrids with uniform morphology. The hybrids obtained were then utilized to modify a GC electrode to electrochemically detect uric acid. The modified electrode showed strong electrocatalytic activity and high sensitivity with a rapid response time in comparison with unmodified electrode.<sup>132</sup>

In conclusion, the non-covalent approach is a simple and practical procedure for the fabrication of AuNP-based hybrid materials. However, because relatively weak non-covalent interactions are involved in the hybrid fabrication, the nanoparticles are not usually assembled on the host surface in a robust manner, thus nanoparticles may easily be removed from the surface often by simple washing of the hybrids.

### 1.4.3 Covalent Attachment of AuNPs onto the Surface

To covalently bond the AuNPs onto the surface, the host material should have desirable groups at the surface or the monolayer of AuNPs should contain a suitable functionality that can undergo a direct reaction with the functional groups accessible at the surface. Due to difficulties associated with the functionalization of the host material surface, this approach is less employed.<sup>104, 105, 109 - 111</sup> Daasbjerg and co-workers synthesized CNTs with a single layer of thiophenols (or closely related derivatives) on the nanotube surface. These thiol-functionalized CNTs were further loaded with 3.5 nm AuNPs via the formation of Au-S bonds to achieve covalently assembled AuNP/CNT hybrids.<sup>133</sup> Graphene oxide is another substrate that AuNPs have been covalently deposited upon. Amino-modified AuNPs (5 nm) were synthesized and underwent an amidation reaction with acyl chloride functionalized graphene oxide (Scheme 1.17).<sup>134</sup> Kawai *et al.* reported the immobilization of ~ 12 nm AuNPs on amine- and thiol-terminated boron-doped diamond prepared with the silane coupling method. It was found that AuNPs cannot be adsorbed by hydrogen- or oxygen-terminated diamond surfaces and the presence of amine or thiol groups at the surface of diamond is a key in preparation of AuNP/diamond hybrid.<sup>135</sup>

Covalent attachment of AuNPs onto surfaces is the most promising approach in the preparation of robust AuNP-based hybrid materials. With the use of covalent strategy three important goals can be achieved: 1) control over the size of nanoparticles will be possible because the AuNPs are synthesized prior to deposition; 2) hybrids assembled through covalent bonds are robust and the AuNPs cannot be easily removed from the surface; 3) the amount of nanoparticles loading onto the surface can be tailored via variation of the AuNP concentration.



Scheme 1.17 Attachment of amine-modified AuNPs onto the graphene oxide surface using covalent approach.

## 1.5 Thesis Objectives

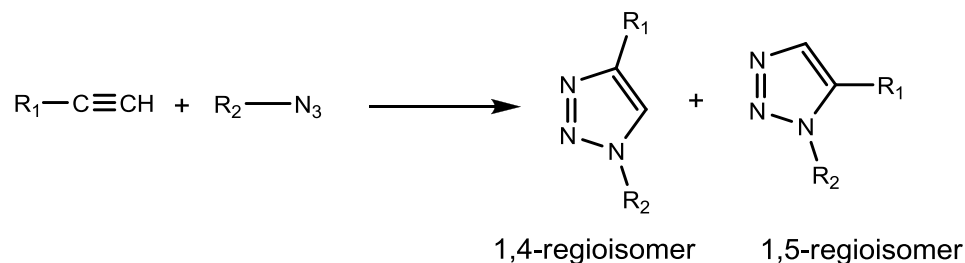
AuNP applications in biomedical, chemical, and technological fields require task specific functionalization at the AuNP monolayer surface. Thus, the ability to modify nanoparticles by interfacial reactions is a critical aspect of all AuNP applications. Our group was first to demonstrate that sluggish or impractical interfacial cycloaddition reactions of functionalized AuNPs at ambient pressure can proceed efficiently under hyperbaric conditions without altering the gold core of the nanoparticles or its inherent physical properties.<sup>86, 94</sup> Furthermore, as a pioneer, our group utilized photochemical interfacial reactions to chemically modify AuNPs.<sup>100 - 103</sup> Extending these methodologies, this thesis will describe modification of AuNPs using a) Huisgen click-type 1,3-dipolar cycloaddition under high pressure conditions and b) photoinitiated carbene insertion reactions. Next, we show that photochemically generated carbenes at the monolayer of AuNPs undergo addition/insertion reactions with functional groups at various material surfaces, leading to formation of AuNP-based hybrids. In Chapters 4 – 6 the preparation and characterization of AuNP-Carbon nanotube, AuNP-Diamond, AuNP-Graphene, and AuNP-Glass hybrids will be described.

### 1.5.1 Modification of AuNPs Using Click-type Cycloaddition and Under High Pressure Conditions (Chapter 2)

The Huisgen 1,3-dipolar cycloaddition of alkynes with azides provides a versatile tool for the synthesis of complex substances by the irreversible connection of smaller substrates, especially when the reaction is catalyzed by copper (I) (better known as a “click” reaction). High yields, inertness of azides and alkynes toward most organic

reagents and biological conditions, a stable heteroatom linkage resulting from reaction, readily available reagents, and insensitivity to atmospheric conditions led to considerable interest in alkyne-azide “click” 1,3-dipolar cycloaddition.<sup>136–139</sup>

The first uncatalyzed cycloaddition of azides with alkynes was reported by Huisgen. The reaction is slow and takes place at high temperature, and the resulting product is a mixture of both 1,4- and 1,5-regioisomers (Scheme 1.18).<sup>140</sup> However, the rate and the yield of the reaction can be increased using alkynes activated by electron-withdrawing substituents,<sup>141</sup> cycloalkynes with ring strain,<sup>142</sup> and high pressure conditions.<sup>143</sup>

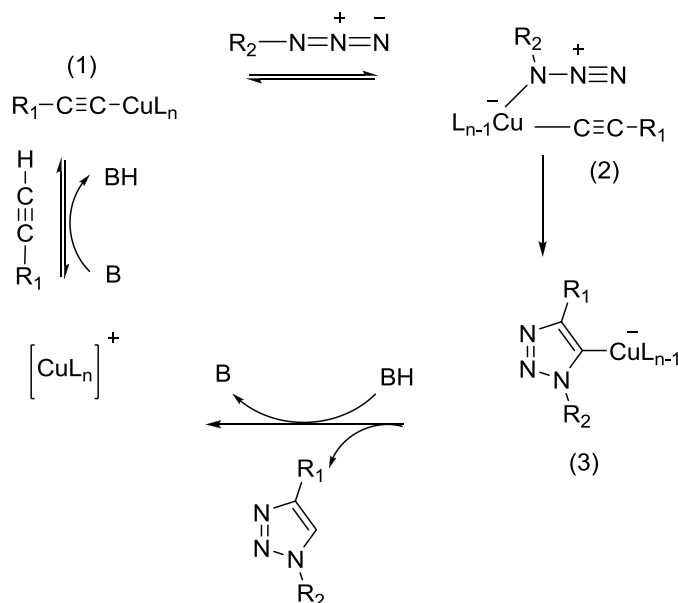


Scheme 1.18 Cycloadditions of alkynes with azides. The uncatalyzed reaction leads to a mixture of 1,4- and 1,5-regioisomers.

Sharpless discovered that in the presence of copper (I), the rate of the alkyne-azide 1,3-cycloaddition reaction dramatically increases (up to  $10^7$  times) and the 1,4-regioisomer is exclusively formed.<sup>136</sup> Copper (I) can be used directly as a copper (I) complex<sup>144</sup> or a copper (I) salt,<sup>145</sup> however, mostly it is generated in situ by reduction of copper (II) sulfate using sodium ascorbate.<sup>136</sup> Both experimental and theoretical studies reveal that the formation of a  $\pi$ -complex between a terminal alkyne and  $[CuL_n]^+$  is the beginning of the catalytic cycle. This coordination lowers the  $pK_a$  value of the alkyne C–H to 9.8 and deprotonation occurs in the aqueous medium, resulting in copper (I) acetylide (1). At the next step an organic azide replaces one of the L ligands in the copper

(I) acetylide. Following the formation of (2), intramolecular cyclization gives a copper (I) triazolide intermediate (3) that readily protonates in the presence of water (Scheme 1.19).

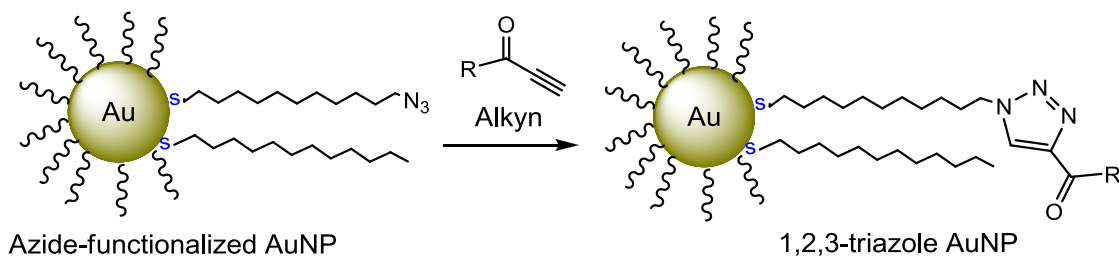
146, 147



Scheme 1.19 Proposed mechanistic steps in an alkyne-azide click reaction.

The copper (I)-catalyzed “click” 1,3-cycloaddition has been used as an efficient reaction for the modification and functionalization of a wide variety of nanomaterial structures and surfaces such as CdSe,<sup>148</sup> iron oxide nanoparticles,<sup>149</sup> silica<sup>150</sup> and gold<sup>151</sup> self-assembled monolayer (SAM), as well as carbon nanotubes.<sup>152</sup> Moreover, this reaction has been employed for the immobilization of biological molecules,<sup>139</sup> the synthesis and modification of polymers,<sup>153</sup> the synthesis of dendrimers<sup>154</sup> and the design of pharmaceutical drugs.<sup>155</sup> Despite the extensive use, there are certain drawbacks to the copper-catalyzed click reaction, including the toxicity of copper to biological systems, the difficulty in separation of the catalyst after the click reaction, and most importantly, the decomposition of the AuNPs in the presence of copper (I).<sup>84, 142, 146</sup>

Williams and co-workers investigated the modification of AuNPs via a click-type reaction for the first time.<sup>84</sup> Azide-functionalized AuNPs were synthesized and click-type reactions with a variety of activated alkynes without a catalyst were performed (Scheme 1.20). It was found that the yields (based on the extent of conversion of the azide groups) were extremely low (13% and less in 60h in dioxane, depending on the alkyne) and could only be improved slightly by changing the solvent. The use of copper catalyst also failed to give greater yields because of decomposition of the azide-functionalized AuNPs. Following Williams' results, Weck *et al.* reported microwave-assisted copper-catalyzed 1,3-dipolar cycloaddition of azide-functionalized AuNPs with alkynes.<sup>156</sup> Although the yields of these reactions were high, this methodology was limited to the use of copper (I) as a catalyst, high temperature (100 °C), and a maximum reaction time of 10 minutes, after which the nanoparticles would decompose. To this end, the development of a catalyst-free click-type reaction which works under mild conditions has definite value for the chemical modification of AuNPs via 1,3-cycloaddition.



Scheme 1.20 Modification of azide-functionalized AuNPs via click-type reaction.

Recently our group reported that the inefficient modification of maleimide-modified AuNPs by the Diels–Alder reaction and 1,3-nitrone dipolar cycloaddition at ambient conditions could be improved dramatically using hyperbaric conditions (11 000 atm) without affecting the nanoparticle core size nor the physical properties of the AuNPs

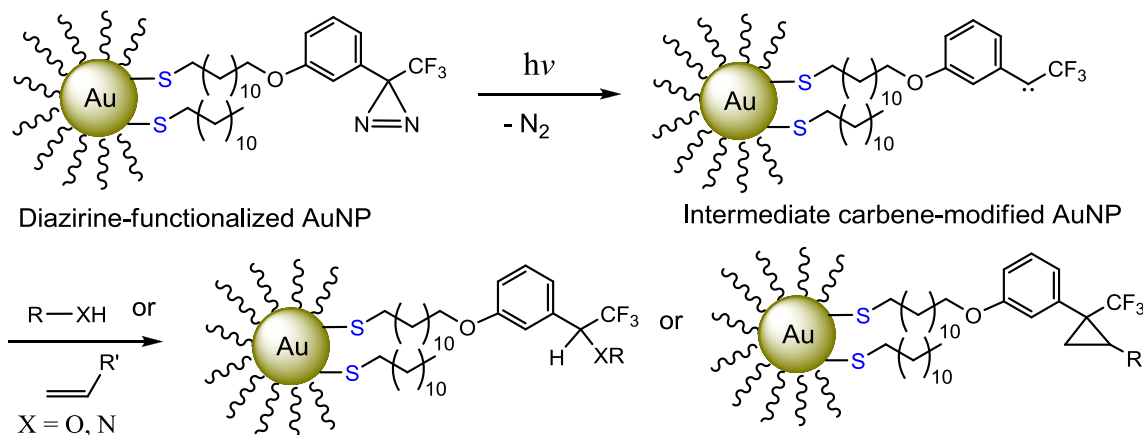


(Scheme 1.8).<sup>86, 94</sup> The reaction of maleimide-modified AuNPs with dienes and nitrones went to completion in less than 30 min at hyperbaric conditions, while the identical reactions under ambient conditions needed, in some cases, days to weeks to proceed. In this thesis, I describe the synthesis of azide-functionalized AuNPs and the catalyst-free click-type reaction of these nanoparticles with a series of terminal alkynes under high pressure conditions resulting in 1,2,3-triazole-functionalized AuNPs. We show that the reactions proceed to high yield under hyperbaric conditions. The product AuNPs were characterized by IR, <sup>1</sup>H NMR and UV-vis spectroscopy. In addition, model 1,2,3-triazole compounds were synthesized and their <sup>1</sup>H NMR spectra were compared with those of 1,2,3-triazole-functionalized AuNPs to verify the occurrence of the click-type reaction on the AuNPs.

### **1.5.2 Photochemically Generated Carbenes for the Modification of AuNPs via a Carbene Insertion Reaction (Chapter 3)**

Photochemical methods open an outstanding opportunity for AuNP modification, given that photoreactions usually take place without need for neither high temperature nor catalyst and, as mentioned previously, AuNPs are sensitive to these conditions. Therefore, utilizing photochemical methods simply eliminates the need for these destructive reaction conditions and suitably functionalized AuNPs can therefore be chemically modified under mild photoreaction conditions. In continuation of our investigations on AuNP modification, this thesis reports on photochemical interfacial reactions of diazirine-functionalized AuNPs that upon irradiation yield reactive carbenes at the AuNP monolayer. The subsequent insertion reactions of the photogenerated

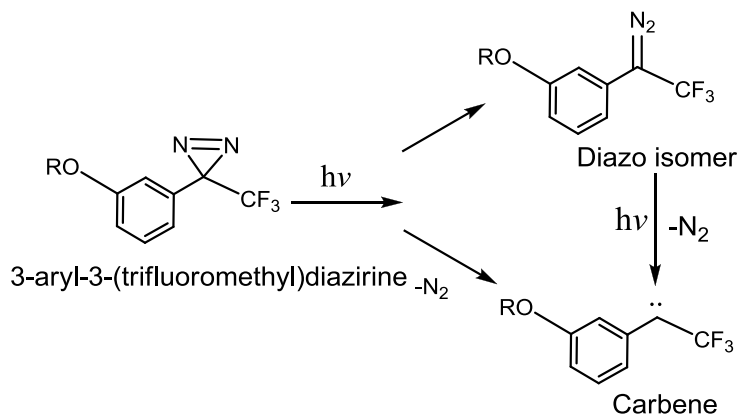
carbenes with trapping reagents afford AuNPs modified with desired functionality (Scheme 1.21).



Scheme 1.21 Interfacial photoinduced carbene formation from a diazirine-functionalized AuNP and, subsequent carbene insertion/addition into a selection of model trapping agents.

Diazirines as excellent carbene precursors are well known photophores for photoaffinity labeling and photo-cross-linking probes.<sup>157–160</sup> Photolysis of the diazirine with wavelengths above 300 nm results reactive carbene via photochemical nitrogen extrusion. Usually, diazo isomerization via intramolecular rearrangement is a side reaction of diazirine photolysis; however, longer irradiation of the diazo isomer can generate carbene as well (Scheme 1.22). Among the diazirine derivatives, 3-aryl-3-(trifluoromethyl)diazirine is used most because of its high thermal stability, less diazo isomerization, along with useful characterization by <sup>19</sup>F NMR spectroscopy. Above all, due to the strong bond between carbon and fluorine in the CF<sub>3</sub> group, rearrangement resulting from fluoride migration to the sp<sup>2</sup> carbene carbon doesn't occur and all of the generated carbene would be involved in the insertion reaction.<sup>161</sup> The ground state of a trifluorophenyl carbene is triplet, which is in equilibrium with its higher energy singlet

state. It is from the latter state that this carbene becomes involved in insertion reactions.<sup>162, 163</sup>



Scheme 1.22 Photoinduced reaction pathways of diazirine in carbene formation.

Diazirine-modified AuNPs ( $1.8 \pm 0.3$  nm) were synthesized using the Brust-Schiffrin method followed by a ligand exchange reaction and characterized by  $^1\text{H}$  NMR,  $^{19}\text{F}$  NMR and IR spectroscopies, as well as TEM. The obtained AuNPs were then irradiated in the presence of trapping reagents such as alcohols, amines or alkenes. Upon irradiation, intermediate carbene-modified AuNPs were formed and their subsequent insertion reaction with trapping reagents led to interfacial modification of the diazirine-modified AuNPs. Depending on the reagent, the reactions went to completion in 13- 26 h. The product AuNPs after the insertion reactions were verified by comparison with model compounds that were prepared via solution insertion reactions carried out under the same conditions as those used for AuNP modification.

### 1.5.3 Fabrication of AuNP-based Hybrid Materials (Chapters 4 – 6)

Nanostructured hybrid materials based on AuNPs represent an intriguing opportunity for the exploration of novel electronic, magnetic, and optical properties. As described in section 1.4, covalent attachment of AuNPs onto the host material surface is a complementary means of fabrication of robust hybrid materials. To this end, synthesis of AuNP with reactive functional groups would allow such a covalent connection of the AuNPs with a variety of nanomaterial structures to obtain hybrid materials.

Carbenes have been known as a very reactive intermediate for over a century and its versatility has been the topic of many studies.<sup>164–166</sup> Insertion of carbene into O–H, N–H and C–H bonds along with the addition to the carbon double bond are among the possible reactions that can be observed if a carbene is created in close proximity to these type of bonds. Therefore, a carbene carrier can covalently couple to a material which has the aforementioned bonds at the surface. In this thesis we show that photogeneration of a carbene on the monolayer of AuNPs in the presence of host materials leads to the formation of covalently assembled AuNP-based hybrid materials via carbene insertion or addition reactions. Diazirine-modified AuNPs with different sizes were prepared and irradiated in the presence of a series of substrates including MWCNTs, micro-diamond, graphene, and glass slide. Upon UV irradiation of diazirines attached onto the AuNPs, intermediate carbenes were generated and the following carbene insertion or addition reactions could occur with the surface functionality of substrates. Utilizing this method, we prepared hybrids including AuNP-CNT, AuNP-Diamond, AuNP-Graphene, and AuNP-Glass. The hybrids were characterized using TEM, SEM, XRD, XPS, Raman, and UV-vis spectroscopy.

## 1.6 References

- 1) Hutchings, G. J.; Brust, M.; Schmidbaur, H. *Chem. Soc. Rev.* **2008**, *37*, 1759.
- 2) Edwards, P. P.; Thomas, J. M. *Angew. Chem. Int. Ed.* **2007**, *46*, 5480.
- 3) Daniel, M. C.; Astruc, D. *Chem. Rev.* **2004**, *104*, 293.
- 4) Faraday, M. *Philos. Trans. R. Soc. London* **1857**, *147*, 145.
- 5) Wilcoxon, J. P.; Abrams, B. L. *Chem. Soc. Rev.* **2006**, *35*, 1162.
- 6) Turkevich, J.; Stevenson, P. C.; Hillier, J. *Discuss. Faraday Soc.* **1951**, *11*, 55.
- 7) Brust, M.; Walker, M.; Bethell, D.; Schiffrin, D. J.; Whyman, R. J. *Chem. Soc., Chem. Commun.* **1994**, *7*, 801.
- 8) Jin, R. *Nanoscale* **2010**, *2*, 343.
- 9) Wuelfmg, W. P.; Gross, S. M.; Miles, D. T.; Murray, R. W. *J. Am. Chem. Soc.* **1998**, *120*, 12696.
- 10) Schlenoff, J. B.; Li, M.; Ly, H. *J. Am. Chem. Soc.* **1995**, *117*, 12528
- 11) Templeton, A. C.; Hostetler, M. J.; Kraft, C. T.; Murray, R. W. *J. Am. Chem. Soc.* **1998**, *120*, 1906.
- 12) Link, S.; El-Sayed, M. A. *J. Phys. Chem. B* **1999**, *103*, 8410.
- 13) Moores, A.; Goettman, F. *New J. Chem.* **2006**, *30*, 1121.
- 14) Stewart, M. E.; Anderton, C. R.; Thompson, L. B.; Maria, J.; Gray, S. K.; Rogers, J. A.; Nuzzo, R. G. *Chem. Rev.* **2008**, *108*, 494.
- 15) Thanh, N. T. K.; Green, L. A. W. *Nano Today* **2010**, *5*, 213.
- 16) De, M.; Chosh, P. S.; Rotello, V. M. *Adv. Mater.* **2008**, *20*, 4225.
- 17) Giljohann, D. A.; Seferos, D. S.; Daniel, W. L.; Massich, M. D.; Patel, P. C.; Mirkin, C. A. *Angew. Chem. Int. Ed.* **2010**, *49*, 3280.

- 18) Patra, C. R.; Bhattacharya, R.; Mukhopadhyay, D.; Mukherjee, P. *Adv. Drug Deliv. Rev.* **2010**, *62*, 346.
- 19) Xie, J.; Lee, S.; Chen, X. *Adv. Drug Deliv. Rev.* **2010**, *62*, 1064.
- 20) Sau, T. K.; Rogach, A. L. *Adv. Mater.* **2010**, *22*, 1781.
- 21) Crzelczak, M.; Perez-Juste, J.; Mulvaney, P.; Liz-Marzan, L. *Chem. Soc. Rev.* **2008**, *37*, 1783.
- 22) Keating, C. D.; Musick, M. D.; Keefe, M. H.; Natan, M. J. *J. Chem. Ed.* **1999**, *76*, 949.
- 23) Baranov, D.; Kadnikova, E. N. *J. Mater. Chem.* **2011**, *21*, 6152.
- 24) Brinas, R. P.; Hu, M.; Qian, L.; Lyman, E. S.; Hainfeld, J. F. *J. Am. Chem. Soc.* **2008**, *130*, 975.
- 25) Bachtman, R. E.; Bodolosky-Bettis, S. A.; Glennon, S. C.; Sirchio, S. A. *J. Am. Chem. Soc.* **2000**, *122*, 7146.
- 26) Hostetler, M. J.; Wingate, J. E.; Zhong, C. Z.; Harris, J. E.; Vachet, R. W.; Clark, M. R.; Londono, J. D.; Green, S. J.; Stokes, J. J.; Wignall, G. D.; Glish, G. L.; Porter, M. D.; Evans, N. D.; Murray, R. W. *Langmuir* **1998**, *14*, 17.
- 27) Whetten, R. L.; Khoury, J. T.; Alvarez, M. M.; Murthy, S.; Vezmar, I.; Wang, Z. L.; Stephen, P. W.; Cleveland, C. L.; Luedtke, W. D.; Landman, U. *Adv. Mater.* **1996**, *5*, 428.
- 28) Schaaff, T. G.; Shafigullin, M. N.; Khoury, J. T.; Vezmar, I.; Whetten, R. L.; Cullen, W.; First, P. N.; Gutierrez-Wing, C.; Ascensio, J.; Jose-Yacamán, M. J. *J. Phys. Chem. B* **1997**, *101*, 7885.

- 29) Manna, A.; Chen, P. L.; Akiyama, H.; Wei, T. X.; Tamada, K.; Knol, W. *Chem. Mater.* **2003**, *15*, 20.
- 30) Jana, N. R.; Peng, X. *J. Am. Chem. Soc.* **2003**, *125*, 14280.
- 31) Huang, T.; Murray, R. W. *J. Chem. Phys. B* **2001**, *105*, 12498.
- 32) Katz, E.; Willner, I. *Angew. Chem. Int. Ed.* **2004**, *43*, 6042.
- 33) Wang, Z.; Ma, L. *Coord. Chem. Rev.* **2009**, *253*, 1607.
- 34) Ohno, K.; Hoh, K. m.; Tsuji, Y.; Fukuda, T. *Macromolecules* **2002**, *35*, 8989.
- 35) Alexandridis, P. *Chem. Eng. Technol.* **2011**, *34*, 15.
- 36) Yagci, Y.; Sangermano, M.; Rizza, G. *Chem. Commun.* **2008**, 2771.
- 37) Dong, S. A.; Zhou, S. P. *Mater. Sci. Eng. B* **2007**, *140*, 153.
- 38) Wang, L.; Wei, G.; Guo, C.; Sun, L.; Sun, Y.; Song, Y.; Yang, T.; Li, Z. *Colloids Surf. A* **2008**, *312*, 148.
- 39) Marin, A. L.; McGilvray, K. L. Scaiano, J. C. *J. Am. Chem. Soc.* **2008**, *130*, 16572.
- 40) Housni, A.; Ahmed, M.; Liu, S.; Narain, R. *J. Phys. Chem. C* **2008**, *112*, 12282.
- 41) Ismaili, H.; Lagugne-Labarthe, F.; Workentin, M. S. *Chem. Mater.* **2011**, *23*, 1519.
- 42) Ismaili, H.; Workentin, M. S. *Chem. Commun.* **2011**, accepted.
- 43) Song, Y.; Harper, A. S.; Murray, R. W. *Langmuir* **2005**, *21*, 5492.
- 44) Sperling, R. A.; Rivera Gil, P.; Zhang, F.; Zanella, M.; Parak, W. J. *Chem. Soc. Rev.* **2008**, *37*, 1896.
- 45) Biosselier, E.; Astruc, D. *Chem. Soc. Rev.* **2009**, *38*, 1759.
- 46) Ghosh, P.; Han, G.; De, M.; Kim, C. K.; Rotello, V. M. *Adv. Drug Deliv. Rev.* **2008**, *60*, 1307.

- 47) Hong, R.; Han, G.; Fernandez, J. M.; Kim, B. J.; Forbes, N. S.; Rotello, V. M. *J. Am. Chem. Soc.* **2006**, *128*, 1078.
- 48) Polizzi, M. A.; Stasko, N. A.; Schoenfisch, M. H. *Langmuir* **2007**, *23*, 4938.
- 49) Nakanishi, J.; Nakayama, H.; Shimizu, T.; Ishida, H.; Kikuchi, Y.; Yamaguchi, K.; Horiike, Y. *J. Am. Chem. Soc.* **2009**, *131*, 3822.
- 50) Kennedy, L. C.; Bickford, L. R.; Lewinski, N. A.; Coughlin, A. J.; Hu, Y.; Day, E. S.; West, J. L.; Drezek, R. A. *Small* **2011**, *7*, 169.
- 51) El-Sayed, I. H.; Huang, X.; El-Sayed, M. A. *Cancer Lett.* **2006**, *239*, 129.
- 52) Bakhtiari, A. B. S.; Hsiao, D.; Jin, G.; Gates, B. D.; Branda, N. R. *Angew. Chem. Int. Ed.* **2009**, *48*, 4166.
- 53) Elghanian, R.; Storhoff, J. J.; Mucic, R. C.; Letsinger, R. L.; Mirkin, C. A. *Science* **1997**, *277*, 1078.
- 54) Thomas, K. G.; Kamat, P. V. *Acc. Chem. Res.* **2003**, *36*, 888.
- 55) Ghosh, S. K.; Pal, T. *Phys. Chem. Chem. Phys.* **2009**, *11*, 3831.
- 56) Oh, E.; Hong, M. Y.; Lee, D.; Nam, S. H.; Yoon, H. C.; Kim, H. S. *J. Am. Chem. Soc.* **2005**, *127*, 3270.
- 57) Peumans, P.; Yakimov, A.; Forrest, S. R. *J. Appl. Phys.* **2003**, *93*, 3693.
- 58) Cai, W.; Gong, X.; Cao, Y. *Sol. Energy Mater. Sol. Cells* **2010**, *94*, 114.
- 59) Atwater, H. A.; Polman, A. *Nature Mater.* **2010**, *9*, 205.
- 60) Morfa, A. J.; Rowlen, K. L.; Reilly II, T. H.; Romero, M. J.; Van De Lagemaat, J. *Appl. Phys. Lett.* **2008**, *92*, 013504.
- 61) Wu, J. L.; Chen, F. C.; Hsiao, Y. S.; Chien, F. C.; Chen, P.; Kuo, C. H.; Huang, M. H.; Hsu, C. S. *ACS Nano* **2011**, *5*, 959.



- 62) Schatz, A.; Reiser, O.; Stark, W. J. *Chem.–Eur. J.* **2010**, *16*, 8950.
- 63) Trindade, A. F.; Gois, P. M. P.; Afonso, C. A. M. *Chem. Rev.* **2009**, *109*, 418.
- 64) Bartz, M.; Küther, J.; Seshadri, R.; Tremel, W. *Angew. Chem. Int. Ed.* **1998**, *37*, 2466.
- 65) Marubayashi, K.; Takizawa, S.; Kawakusu, T.; Arai, T.; Sasai, H. *Org. Lett.* **2003**, *5*, 4409.
- 66) Oila, M. J.; Koskinen, A. M. P. *ARKIVOK* **2006**, 76.
- 67) Li, H.; Luk, Y. Y.; Mrksich, M. *Langmuir* **1999**, *15*, 4957.
- 68) Choo, H.; Cutler, E.; Shon, Y. S. *Langmuir* **2003**, *19*, 8555.
- 69) Niidome, T.; Nakashima, K.; Takahashi, H.; Niidome, Y. *Chem. Commun.* **2004**, 1978.
- 70) Watson, k. J.; Zhu, J.; Nguyen, S. T.; Mirkin, C. A. *J. Am. Chem. Soc.* **1999**, *121*, 462.
- 71) Paulini, R.; Frankamp, B. L.; Rotello, V. M. *Langmuir* **2002**, *18*, 2368.
- 72) Itoh, H.; Naka, K.; Chujo, Y. *J. Am. Chem. Soc.* **2004**, *126*, 3026.
- 73) Kotiaho, A.; Lahtinen, R.; Efimov, A.; Metsberg, H. K.; Sariola, E.; Lehtivuori, H.; Tkachenko, N. V.; Lemmetyinen, H. *J. Phys. Chem. C* **2010**, *114*, 162.
- 74) Hostetler, M. J.; Green, S. J.; Stokes, J. J.; Murray, R. W. *J. Am. Chem. Soc.* **1996**, *118*, 4212.
- 75) Hostetler, M. J.; Templeton, A. C.; Murray, R. W. *Langmuir* **1999**, *15*, 3782.
- 76) Caragheorghopol, A.; Chechik, V. *Phys. Chem. Chem. Phys.* **2008**, *10*, 5029.
- 77) Song, Y.; Murray, R. W. *J. Am. Chem. Soc.* **2002**, *124*, 7096.

- 78) Hong, R.; Fernandez, J. M.; Nakade, H.; Arvizo, R.; Emrick, T.; Rotello, V. M. *Chem. Commun.* **2006**, 2347.
- 79) Donkers, R. L.; Song, Y.; Murray, R. W. *Langmuir* **2004**, *20*, 4703.
- 80) Ionita, P.; Caragheorgheopol, A.; Gilbert, B. C.; Chechik, V., *Langmuir* **2004**, *20* 11536.
- 81) Templeton, A. C.; Wuelfing, W. P.; Murray, R. W. *Acc. Chem. Res.* **2000**, *33*, 27.
- 82) Sardar, R.; Funston, A. M.; Mulvaney, P.; Murray, R. W. *Langmuir* **2009**, *25*, 13840.
- 83) Chechik, V. *Annu. Rep. Prog. Chem. Sect. B* **2006**, *102*, 357.
- 84) Fleming, D. A.; Thode, C. J.; Williams, M. E. *Chem. Mater.* **2006**, *18*, 2327.
- 85) Shon, Y. S.; Choo, H. *C. R. Chimie* **2003**, *6*, 1009.
- 86) Zhu, J.; Ganton, M.; Kerr, M. A.; Workentin, M. S. *J. Am. Chem. Soc.* **2007**, *129*, 4904.
- 87) Templeton, A. C.; Hostetler, M. J.; Kraft, C. T.; Murray, R. W. *J. Am. Chem. Soc.* **1998**, *120*, 1906.
- 88) Otsuka, H.; Akiyama, Y.; Nagasaki, Y.; Kataoka, K. *J. Am. Chem. Soc.* **2001**, *123*, 8226.
- 89) Shon, Y. S.; Choo, H. *Chem. Commun.* **2002**, 2560.
- 90) Koenig, S.; Chechik, V. *Langmuir* **2003**, *19*, 9511.
- 91) Friggeri, A.; Van Manen, H. J.; Auletta, T.; Li, X. M.; Zapotoczny, S.; Schönherr, H.; Vancso, G. J.; Huskens, J.; Van Veggel, F. C. J. M.; Reinhoudt, D. N. *J. Am. Chem. Soc.* **2001**, *123*, 6388.
- 92) Thode, C. J.; Williams, M. E. *Langmuir* **2008**, *24*, 5988.
- 93) Ornelas, C.; Mery, D.; Cloutet, E.; Aranzaes, J. R.; Astruc, D. *J. Am. Chem. Soc.*

- 2008**, *130*, 1495.
- 94) Zhu, J.; Lines, B. M.; Ganton, M. D.; Kerr, M. A.; Workentin, M. S. *J. Org. Chem.* **2008**, *73*, 1099.
- 95) Hartlen, K. D.; Ismaili, H.; Zhu, J.; Workentin, M. S. **2011**, (to be submitted).
- 96) Schettino, V.; Bini, R. *Chem. Soc. Rev.* **2007**, *36*, 869.
- 97) Matsumoto, K.; Hamana, H.; Iida, H. *Helv. Chim. Acta* **2005**, *88*, 2033.
- 98) McCabe, J. R.; Eckert, C. A. *Acc. Chem. Res.* **1974**, *7*, 251.
- 99) Diedrich, M. K.; Klarner, F.G. *J. Am. Chem. Soc.* **1998**, *120*, 6212.
- 100) Kell, A. J.; Montcalm, C. C.; Workentin, M. S. *Can. J. Chem.* **2003**, *81*, 484.
- 101) Kell, A. J.; Workentin, M. S. *Langmuir* **2001**, *17*, 7355.
- 102) Kell, A. J.; Donkers, R. L.; Workentin, M. S. *Langmuir* **2005**, *21*, 735.
- 103) Kell, A. J.; Stringle, D. L. B.; Workentin, M. S. *Org. Lett.* **2000**, *2*, 3381.
- 104) Nie, Z.; Petukhova, A.; Kumacheva, E. *Nature Nanotech.* **2010**, *5*, 15.
- 105) Sau, T. K.; Rogach, A. L.; Jackel, F.; Klar, T. A.; Feldmann, J. *Adv. Mater.* **2010**, *22*, 1825.
- 106) Lim, S. I.; Zhong, C. J. *Acc. Chem. Res.* **2009**, *42*, 798.
- 107) Curri, M. L.; Comparelli, R.; Striccoli, M.; Agostiano, A. *Phys. Chem. Chem. Phys.* **2010**, *12*, 11197.
- 108) Kinge, S.; Crego-Calama, M.; Reinhoudt, D. N. *Chem. Phys. Chem.* **2008**, *9*, 20.
- 109) Singh, R.; Premkumar, T.; Shin, J. Y.; Geckeler, K. E. *Chem. Eur. J.* **2010**, *16*, 1728.
- 110) Navalon, S.; Martin, R.; Alvaro, M.; Garcia, H. *Angew. Chem. Int. Ed.* **2010**, *49*, 8403.

- 111) Cobley, C. M.; Chen, J.; Cho, E. C.; Wang, L. V.; Xia, Y. *Chem. Soc. Rev.* **2011**, *40*, 44.
- 112) Aureau, D.; Varin, Y.; Roodenko, K.; Seitz, O.; Pluchery, O.; Chabal, Y. J. *J. Phys. Chem. C* **2010**, *114*, 14180.
- 113) Rance, G. A.; Marsh, D. H.; Bourne, S. J.; Reade, T. J.; Khlobystov, A. N. *ACS Nano* **2010**, *4*, 4920.
- 114) Liu, Z.; Jiang, L.; Galli, F.; Nederlof, I.; Olsthoorn, R. C. L.; Lamers, G. E. M.; Oosterkamp, T. H.; Abrahams, J. P. *Adv. Funct. Mater.* **2010**, *20*, 2857.
- 115) Kondo, T.; Aoshima, S.; Hirata, K.; Honda, K.; Einaga, Y.; Fujishima, A.; Kawai, T. *Langmuir* **2008**, *24*, 7545.
- 116) Zhang, R.; Wang, X. *Chem. Mater.* **2007**, *19*, 976.
- 117) Choi, H. C.; Shim, M.; Bangsaruntip, S.; Dai, H. *J. Am. Chem. Soc.* **2002**, *124*, 9058.
- 118) Muszynski, R.; Seger, B.; Kamat, P. V. *J. Phys. Chem. C* **2008**, *112*, 5263.
- 119) Goncalves, G.; Marques, P. A. A. P.; Granadeiro, C. M.; Nogueira, H. I. S.; Singh, M. K.; Grácio, J. *Chem. Mater.* **2009**, *21*, 4796.
- 120) Huang, X.; Zhou, X.; Wu, S.; Wei, Y.; Qi, X.; Zhang, J.; Boey, F.; Zhang, H. *Small* **2010**, *6*, 513.
- 121) Li, F.; Yang, H.; Shan, C.; Zhang, Q.; Han, D.; Ivaska, A.; Niu, L. *J. Mater. Chem.* **2009**, *19*, 4022.
- 122) Toghill, K. E.; Compton, R. G. *Electroanalysis* **2010**, *22*, 1947.
- 123) Weng, J.; Xue, J.; Wang, J.; Ye, J. S.; Cui, H.; Sheu, F. S.; Zhang, Q. *Adv. Funct. Mater.* **2005**, *15*, 639.

- 124) Peng, X.; Chen, J.; Misewich, J. A.; Wong, S. S. *Chem. Soc. Rev.* **2009**, *38*, 1076.
- 125) Han, L.; Wu, W.; Kirk, F. L.; Luo, J.; Maye, M. M.; Kariuki, N. N.; Lin, Y.; Wang, C.; Zhong, C. J. *Langmuir* **2004**, *20*, 6019.
- 126) Sainsbury, T.; Fitzmaurice, D. *Chem. Mater.* **2004**, *16*, 2174.
- 127) Liu, L.; Wang, T.; Li, J.; Guo, Z. X.; Dai, L.; Zhang, D.; Zhu, D. *Chem. Phys. Lett.* **2003**, *367*, 747.
- 128) Jung, J. H.; Cheon, D. S.; Liu, F.; Lee, K. B.; Seo, T. S. *Angew. Chem. Int. Ed.* **2010**, *49*, 5708.
- 129) Huang, J.; Zhang, L.; Chen, B.; Ji, N.; Chen, F.; Zhang, Y.; Zhang, Z. *Nanoscale* **2010**, *2*, 2733.
- 130) Myung, S.; Park, J.; Lee, H.; Kim, K. S.; Hong, S. *Adv. Mater.* **2010**, *22*, 2045.
- 131) Fang, Y.; Guo, S.; Zhu, C.; Zhai, Y.; Wang, E. *Langmuir* **2010**, *26*, 11277.
- 132) Hong, W.; Bai, H.; Xu, Y.; Gu, Z.; Shi, G. *J. Phys. Chem. C* **2010**, *114*, 1822.
- 133) Peng, Z.; Holm, A. H.; Nielsen, L. T.; Pedersen, S. U.; Daasbjerg, K. *Chem. Mater.* **2008**, *20*, 6068.
- 134) Pham, T. A.; Choi, B. C.; Lim, K. T.; Jeong, Y. T. *Appl. Surf. Sci.* **2011**, *257*, 3350.
- 135) Kondo, T.; Aoshima, S.; Honda, K.; Einaga, Y.; Fujishima, A.; Kawai, T. *J. Phys. Chem. C* **2007**, *111*, 12650.
- 136) Rostovtsev, V. V.; Green, L. G.; Fokin, V.; Sharpless, K. B. *Angew. Chem. Int. Ed.* **2001**, *40*, 2004.
- 137) Wu, P.; Feldman, A. K.; Nugent, A. K.; Scheel, A.; Voit, B.; Pyun, J.; Fréchet, M. J.; Sharpless, K. B.; Fokin, V. V. *Angew. Chem. Int. Ed.* **2004**, *43*, 3928.
- 138) Lutz, J. F. *Angew. Chem. Int. Ed.* **2007**, *46*, 1018.

- 139) Nandivanda, H.; Jiang, X.; Lahann, J. *Adv. Mater.* **2007**, *19*, 2197.
- 140) Huisgen, R. *Angew. Chem. Int. Ed.* **1963**, *2*, 633.
- 141) Li, Z.; Seo, T. S.; Ju J. *Tetrahedron Lett.* **2004**, *45*, 3143.
- 142) Agard, N. J.; Prescher, J. A.; Bertozzi, C. R. *J. Am. Chem. Soc.* **2004**, *126*, 15046.
- 143) Melai, V.; Brillante, A.; Zanirato, P. *J. Chem. Soc., Perkin Trans. 2* **1998**, 2447.
- 144) Lewis, W. G.; Magallon, F. G.; Fokin, V. V.; Finn, M. G. *J. Am. Chem. Soc.* **2004**, *126*, 9152.
- 145) Tornøe, C. W.; Christensen, C.; Meldal, M. *J. Org. Chem.* **2001**, *67*, 3057.
- 146) Himo, F.; Lovell, T.; Hilgraf, R.; Rostovtsev, V. V.; Noodleman, L.; Sharpless, K. B.; Fokin, V. V. *J. Am. Chem. Soc.* **2005**, *127*, 210.
- 147) Nolte, C.; Mayer, P.; Straub, B. F. *Angew. Chem. Int. Ed.* **2007**, *46*, 2101.
- 148) Binder, W. H.; Sachsenhofer, R.; Zirbs, R. *J. Mater. Chem.* **2007**, *17*, 2125.
- 149) White, M. A.; Johnson, J. A.; Koberstein, J. T.; Turro, N. J. *J. Am. Chem. Soc.* **2006**, *128*, 11356.
- 150) Rozkiewicz, D. I.; Janczewski, W. V.; Ravoo, B. J.; Reinhoudt, D. N. *Angew. Chem. Int. Ed.* **2006**, *45*, 5292.
- 151) Collmann, J. P.; Devarj, N. K.; Eberspacher, T. P. A.; Chidsey, C. D. E. *Langmuir* **2006**, *22*, 2457.
- 152) Li, H.; Cheng, F.; Duft, A. M.; Adronov, A. *J. Am. Chem. Soc.* **2005**, *127*, 14518.
- 153) Binder, W. H.; Sachsenhofer, R. *Macromol. Rapid Commun.* **2007**, *28*, 15.
- 154) Helms, B.; Mynar, J. L.; Hawker, C. J.; Frechet, J. M. J. *J. Am. Chem. Soc.* **2004**, *126*, 15020.

- 155) Mocharla, V. P.; Colasson, B.; Lee, L. V.; Roper, S.; Sharpless, K. B.; Wong, C. H.; Kolb, H. C. *Angew. Chem. Int. Ed.* **2005**, *44*, 116.
- 156) Sommer, W. J.; Weck, M. *Langmuir* **2007**, *23*, 11991.
- 157) Qiu, Z.; Lu, L.; Jian, X.; He, C. *J. Am. Chem. Soc.* **2008**, *130*, 14398.
- 158) Hashimoto, M.; Hatanaka, Y. *Eur. J. Org. Chem.* **2008**, 2513.
- 159) Hatanaka, T.; Hatanaka, Y.; Setou, M. *J. Am. Chem. Soc.* **2006**, *128*, 15092.
- 160) Vila-Perello, M.; Pratt, M. R.; Tulin, F.; Muir, T. W. *J. Am. Chem. Soc.* **2007**, *129*, 8086.
- 161) Blencowe, A.; Hayes, W. *Soft Matter* **2005**, *1*, 178
- 162) Admasu, A.; Gudmundsdottir, A. D.; Platz, M. S.; Watt, D. S.; Kwiatkowski, S.; Crocker, P. J. *J. Chem. Soc., Perkin Trans. 2* **1998**, 1093.
- 163) Platz, M.; Admasu, A. S.; Kwiatkowski, S.; Crocker, P. J.; Imai, N.; Watt, D. S. *Bioconjugate Chem.* **1991**, *2*, 337.
- 164) Kirmse, W. *Eur. J. Org. Chem.* **2005**, 237, 260.
- 165) Sander, W.; Kotting, C.; Hubert, R. *J. Phys. Org. Chem.* **2000**, *13*, 561.
- 166) Bourissou, D.; Guerret, O.; Gabbai, F. P.; Bertrand, G. *Chem. Rev.* **2000**, *100*, 39.

## Chapter 2

# Remarkable High-yielding Chemical Modification of Gold Nanoparticles Using Uncatalyzed Click-type 1, 3-Dipolar Cycloaddition Chemistry and Hyperbaric Conditions

- Chapter 2 has been published as a full paper. The corresponding reference is: Hossein Ismaili, Abdolhamid Alizadeh, Kristen E. Snell, Mark. S. Workentin\*, *Can. J. Chem.* **2009**, *87*, 1708.
- Abdolhamid Alizadeh (visiting scientist) synthesized compound 4d and was involved in the initiation of the project. Kristen Snell helped in the preparation and editing of the manuscript. Hossein Ismaili carried out the remainder of work reported in Chapter 2.
- All of the schemes, figures, and text in Chapter 2 reproduced with permission, © 2009 Canadian Science Publishing or its licensors.



## 2.1 Introduction

The Cu(I)-catalyzed Huisgen 1,3-dipolar cycloaddition of azides to terminal alkynes to produce a triazole ring, the “click” reaction, is a popular and powerful tool in organic synthesis and combinatorial chemistry.<sup>1</sup> This reaction is also being exploited in material science applications for the modification of metal and silica surfaces,<sup>2</sup> dendrimers,<sup>3</sup> and polymers.<sup>4</sup> Recently, the reaction was extended to monolayer protected CdSe,<sup>5</sup> iron oxide,<sup>6</sup> and monolayer-protected gold nanoparticles (AuNPs).<sup>7-12</sup> Because the 1,3-dipolar cycloaddition reaction of an alkyne and azide is slow, this type of reaction is typically done in the presence of a Cu(I) catalyst because it facilitates the rapid, high reaction conversions with little or no by-products under mild conditions. The latter is of key importance for the functionalization of AuNPs. While the catalyzed reaction is effective for the modification of the CdSe and iron oxide nanoparticles, this approach is not considered as feasible with gold nanoparticles. AuNPs in the presence of the Cu catalyst have been suggested to be unstable, and lead to aggregation or decomposition likely due to the reaction of the Cu catalyst with the gold surface. In another case, Brennan et al. reported using the Cu-catalyzed route to modify azide-functionalized 12 nm AuNPs with alkyne-appended lipases but a million-fold excess of Cu was required and the yield was less than 1% conversion.<sup>7</sup> More recently, and while this work was in progress, Astruc and co-workers reported specific reaction conditions to circumvent the difficulties of the Cu(I) click reaction on azide-terminated AuNPs.<sup>13</sup>

Williams and co-workers reported a thorough study showing that the Huisgen dipolar cycloaddition reaction can be used to modify azide-terminated AuNPs with a variety of activated alkynes without a catalyst.<sup>8</sup> However, the yields (extent of conversion of the

azide groups) were extremely low (13% and less after 60 h in dioxane, depending on the alkyne) and could only be marginally improved by altering the solvent. In a latter study where they reported on the kinetics of this reaction on the AuNP, they stated that these yields were slightly underestimated because of the method used to follow reaction conversion.<sup>9</sup> However, the yields were still relatively low (22%, or 54% in one specific case) and did not allow the product AuNPs to be completely characterized by NMR spectroscopy. Because of the potential of this type of reaction as a general approach to surface modification and to allow the introduction of a variety of functionalities from common starting AuNPs, an important goal is to improve the efficiency of this type of reaction on AuNP. To this end, and while this work was in progress, Sommer and Weck reported on the microwave-assisted catalyzed 1,3-dipolar cycloaddition of azide-terminated AuNPs.<sup>10</sup> The method proved successful and allowed a large variety of terminal alkynes to form triazole-functionalized AuNP with near-quantitative yields, but still required very careful control of the microwave conditions because excess heating of the AuNP lead to nanoparticle decomposition ascribed to particle aggregation.

Recently, we reported that the inefficient modification of a maleimide-modified AuNP by the Diels–Alder reaction at ambient conditions with a series of dienes was improved remarkably using hyperbaric conditions without affecting the particle core.<sup>14</sup> The hyperbaric method for modification of AuNPs was more general and was further used to accelerate the 1,3-cycloadditions of a large variety of nitrones with the maleimide-modified AuNPs in quantitative yields.<sup>15</sup> In both of these studies, we showed that the reactions carried out on the AuNPs at ambient temperature and pressure were significantly slower than the corresponding reactions on model compounds under the

same conditions. We attributed this difference in reactivity to the unique steric effects of the environment at the interfacial site of reactivity on the AuNP. In the present report, we extend this methodology to study the Huisgen 1,3-dipolar cycloaddition of azide-terminated AuNP to terminal alkynes to improve the efficiency of this reaction and to expand the scope of reactions that can be utilized for modification of nanoparticles using hyperbaric conditions. The Huisgen 1,3-dipolar cycloaddition of azides to terminal alkynes is also subject to rate acceleration at elevated pressure, although as far as we are aware, this has only been the subject of one report.<sup>16</sup> Specifically, we report herein that azide-terminated, 1.8 nm core size AuNPs prepared to be essentially identical to the original report of Williams and co-workers,<sup>8</sup> will react with activated acyl-alkynes efficiently under high pressure conditions at ambient temperature to form the 1,2,3-triazoles essentially quantitatively in the absence of a Cu catalyst. This approach eliminates the complications due to the presence of catalysts or higher temperatures.

## 2.2 Results and Discussion

The azide-terminated AuNPs were prepared similarly to that recently reported.<sup>8</sup> Starting with  $1.8 \pm 0.2$  nm dodecanethiol-stabilized AuNP ( $C_{12}$ AuNP), 11-bromoundecanethiol was introduced onto the AuNP using the place exchange method to yield a mixed monolayer containing Br-terminated undecanethiol ligands. Reaction of this AuNP with  $NaN_3$  in DMSO introduced the azide functionality onto the AuNP. Figure 2.1A shows the  $^1H$  NMR spectrum of azide-terminated AuNPs (**1**- $C_{12}$ AuNPs). The key diagnostic signals are the characteristically broad signals due to the methylene protons

alpha to the azide and bromide functionality at 3.24 and 3.41 ppm, respectively. The ratio of terminal azide : bromide : methyl in the newly made mixed AuNP was estimated to be roughly 3.5:1:5 by  $^1\text{H}$  NMR spectroscopy of  $\text{I}_2$  reduced particles. This mixed monolayer particle ( $\mathbf{1-C}_{12}\text{AuNP}$ ) was further characterized by IR and UV-vis spectroscopy and TEM. The IR spectrum of  $\mathbf{1-C}_{12}\text{AuNP}$  shows a strong absorbance at  $2096\text{ cm}^{-1}$  due to the anti-symmetric  $\text{N}=\text{N}=\text{N}$  stretch in addition to the  $\text{CH}_2/\text{CH}_3$  stretches at  $2959$ ,  $2921$  and  $2852\text{ cm}^{-1}$ .

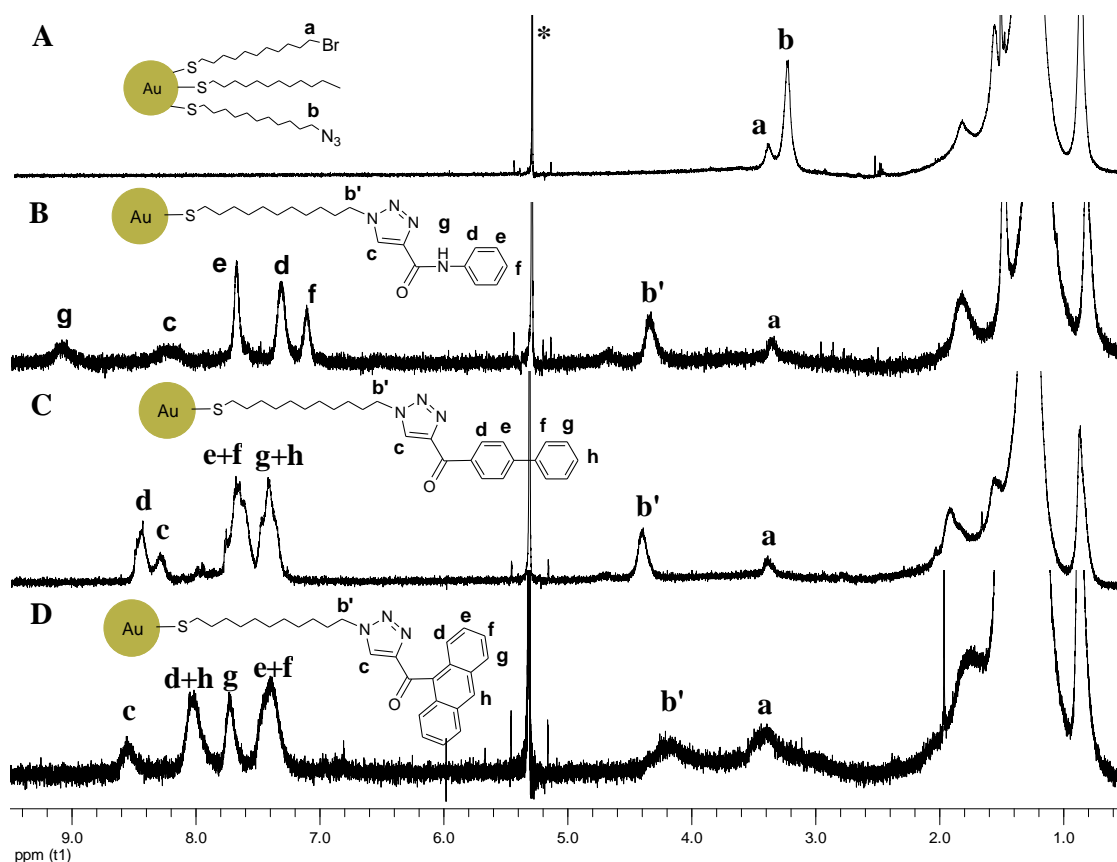
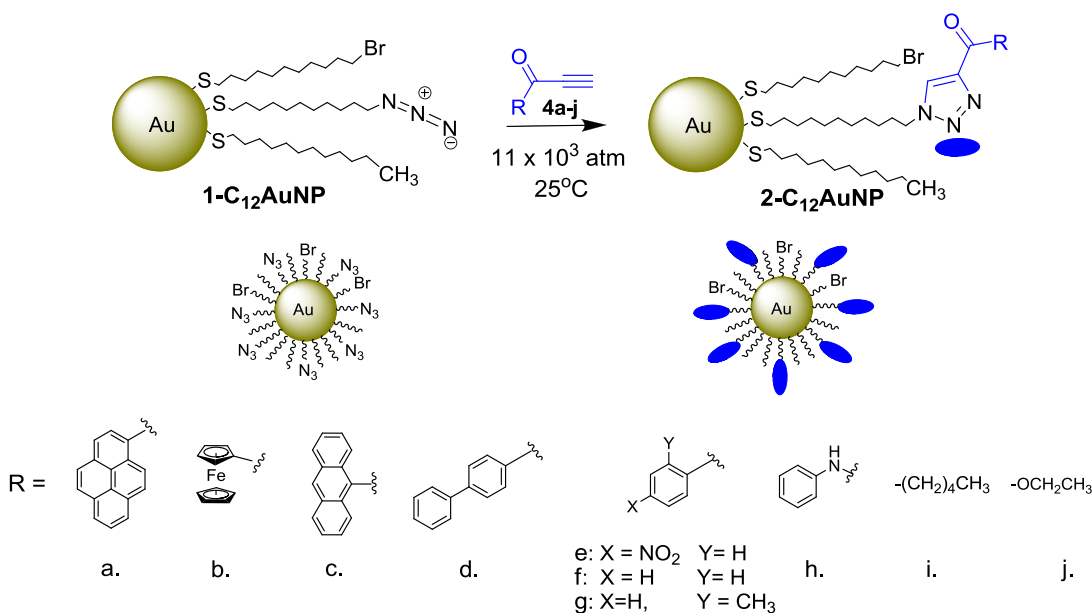
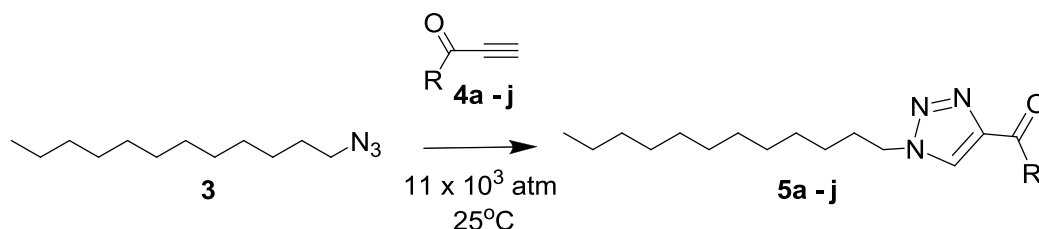


Figure 2.1  $^1\text{H}$  NMR spectra of A)  $\mathbf{1-C}_{12}\text{AuNP}$  and representative product 1,2,3-triazoles  $\mathbf{2-C}_{12}\text{AuNP}$  formed in click reactions of  $\mathbf{1-C}_{12}\text{AuNP}$  with acyl alkynes  $\mathbf{4h}$ ,  $\mathbf{4d}$  and  $\mathbf{4c}$ : B)  $\mathbf{2h-C}_{12}\text{AuNP}$  C)  $\mathbf{2d-C}_{12}\text{AuNP}$  D)  $\mathbf{2c-C}_{12}\text{AuNP}$ . Solvent  $\text{CD}_2\text{Cl}_2$ , residual proton signal is indicated by \*.

Compound **1-C<sub>12</sub>AuNP** (ca. 10 mg) was then mixed with each of the activated acyl-alkynes **4a-j**, shown in Scheme 2.1, in a ratio of 1:15-20, azide : alkyne, in 2 mL of CH<sub>2</sub>Cl<sub>2</sub> and placed in a high pressure reactor at 11 000 atm at room temperature. Model reactions of 1-azidododecane (**3**) with each alkyne were also performed under high pressure conditions to aid in monitoring the extent of reaction and to provide analogous 1,2,3-triazole products (**5a-j**) to allow for characterization of the reactions on **1-C<sub>12</sub>AuNP** (Scheme 2.2).



Scheme 2.1 The 1,3-dipolar cycloaddition of **1-C<sub>12</sub>AuNP** with a variety of terminal acyl-alkynes (**4a-j**) at 11,000 atm.



Scheme 2.2 Model reaction of 1-azidododecane (**3**) with alkenes **4a-j** to yield 1,2,3-triazoles **5a-j**.

The extent of reaction of **1-C<sub>12</sub>AuNP** was followed by <sup>1</sup>H NMR and IR spectroscopy. The reaction was considered complete when there was no evidence of the protons alpha to the azide in the <sup>1</sup>H NMR spectrum and by the disappearance of the azide peak in the IR spectrum. For most cases this occurred after 15 – 24 h, depending on the alkyne (Table 2.1). We note that high temperatures cannot be employed to decrease reaction times for **1-C<sub>12</sub>AuNP** because AuNP are not thermally stable for extended periods. The reaction of **1-C<sub>12</sub>AuNP** with alkynes **4a**, **4c**, **4d**, **4e**, **4f** resulting in the corresponding **2-C<sub>12</sub>AuNP**, was quantitative after 15 h.

Table 2.1 Extent of reaction of **1-C<sub>12</sub>AuNP** with alkynes **4a-j** via uncatalyzed 1,3-dipolar cycloaddition reaction at atmospheric and hyperbaric pressure conditions.

Alkyne	% Conversion atmospheric Pressure <sup>a</sup> (Ref. 8)	% Conversion, 11 000 atm
<b>4a</b>	13	>95 <sup>b</sup>
<b>4b</b>	12	>80 <sup>c</sup>
<b>4c</b>	6	>95 <sup>b</sup>
<b>4d</b>	6	>95 <sup>b</sup>
<b>4e</b>	6	>95 <sup>b</sup>
<b>4f</b>	d	>95 <sup>b</sup>
<b>4g</b>	d	>95 <sup>c</sup>
<b>4h</b>	d	>95 <sup>c</sup>
<b>4i</b>	d	>80 <sup>c</sup>
<b>4j</b>	d	>95 <sup>c</sup>

a. 60 h in dioxane.

b. As determined by <sup>1</sup>H NMR after 15 hr

c. As determined by <sup>1</sup>H NMR after 24 hr

d. not reported

Alkynes **4b**, **4g**, **4h**, **4i** and **4j** had slightly lower 1,3-dipolar cycloaddition reactivity and their reactions with **1-C<sub>12</sub>AuNP** was carried out for 24 h. After which time, the azide peak in the IR spectra was completely absent for mixtures containing **4g**, **4h** and **4j**, indicating near complete conversion, but only around 80 % conversion was observed for the reaction of the **1-C<sub>12</sub>AuNP** with **4b** and **4i** (Table 2.1). Presumably, extending the reaction times further would lead to more complete conversion for these two less activated alkynes.

After completion of the reaction and removal of the reaction mixture from the high pressure reactor, the mixtures were washed several times to remove excess alkyne from the AuNP and a <sup>1</sup>H NMR spectrum was recorded. These spectra show that **1-C<sub>12</sub>AuNPs** had reacted to form the corresponding 1,2,3-triazole product **2-C<sub>12</sub>AuNPs**. Figure 2.1B – D shows representative <sup>1</sup>H NMR spectra of the product **2-C<sub>12</sub>AuNP** formed by reaction of **1-C<sub>12</sub>AuNP** with alkynes **4h**, **4d**, and **4c**. Evidence for the reaction include the downfield chemical shift of the protons alpha to the nitrogen atom from 3.24 ppm in the azide (labeled b) to ~4.2 ppm (labeled b'), alpha to the triazole ring (Figure 2.1). The disappearance of the signal at 3.24 ppm on the **1-C<sub>12</sub>AuNP** was considered as a sign of complete conversion of the azide. IR spectra of **2a-j-C<sub>12</sub>AuNP** also show loss of the N<sub>3</sub> stretch at 2096 cm<sup>-1</sup>, verifying completion of the reaction, and a new stretch at ca. 1639-1670 cm<sup>-1</sup> due to the C=O (1734 cm<sup>-1</sup> for ester **2j-C<sub>12</sub>AuNP**). Common to all spectra is the absence of the signal at 3.24 due to the CH<sub>2</sub> alpha to the azide and a new signal between 7.8 – 8.6 ppm (chemical shift varies slightly with structure) due to the triazole C–H proton (labeled c in the spectra, Figure 2.1). Of course, other signals in the <sup>1</sup>H NMR

spectra due to the functionality introduced with the cycloaddition with the alkyne are assignable easily by comparison to the spectra of the products of the model reactions, **5a-j**. These are provided in the supporting information. For example, The  $^1\text{H}$  NMR spectra of **2h**- $\text{C}_{12}\text{AuNPs}$  (Figure 2.1B) shows new peaks in the aromatic region attributed to the aromatic ring as well as the triazole C–H proton at 8.25 ppm and the amide proton at 9.15 ppm verifying the formation of the triazole ring. It is noticeable that the  $^1\text{H}$  NMR of the **2a**- and **2c**- $\text{C}_{12}\text{AuNPs}$  with a relatively bulky R group (pyrene and anthracene) shows broadened peaks, especially for the peak assigned to the methylene group (b') adjacent to the triazole ring, in comparison to the **2**- $\text{C}_{12}\text{AuNPs}$  with less-bulky R groups. This broadness suggests that the bulky group limits the mobility of these groups on the AuNPs more than that of the less-bulky R groups.

UV-vis spectra and TEM of the nanoparticles after reaction verify that there is no measureable change to the AuNP core size and that the only effect of the high pressure conditions is the acceleration of the 1,3-dipolar cycloaddition. Although these reactions were only carried out at relatively small scale, they are easily scalable to the higher scales, making the use of the hyperbaric reactor practical for synthetic preparations on AuNPs.

As mentioned above, in order to facilitate the assignment of the protons of the  $^1\text{H}$  NMR spectra of **2**- $\text{C}_{12}\text{AuNPs}$ , the reactions were also carried out using the solution phase reaction of 1-azidododecane (**3**) with the same alkynes at high pressure conditions as a model reaction to yield compounds **5a-j** (Scheme 2.2). Compounds **5a-j** could be characterized more completely via  $^1\text{H}$  NMR,  $^{13}\text{C}$  NMR and IR spectroscopy, as well as



mass spectrometry (see experimental). Because the  $^1\text{H}$  NMR spectra of **5a-j** are not broad as are those of **2-C<sub>12</sub>AuNPs**, they are more easily assignable and hence they provide the confidence in the assignments of the spectra for **2-C<sub>12</sub>AuNPs**. For example, Figure 2.2 shows the  $^1\text{H}$  NMR spectra of **2g-C<sub>12</sub>AuNP** and the model compound **5g**, respectively. The signals at 4.4 ppm (b') and 8.18 ppm (c), attributed to the C–H proton of triazole ring, verify the formation of the cycloaddition product on the AuNP. The other signals observed for **2g-C<sub>12</sub>AuNP** are also readily assignable because the intensity and chemical shift are comparable to **5g** except the expected broadening of the  $^1\text{H}$  NMR signals on the AuNP. The labeled  $^1\text{H}$  NMR spectra of **2a-j-C<sub>12</sub>AuNP** and the corresponding model compounds **5a-j** are provided in the supporting information. In general, the reaction of the 1-azidododecane with the less electron deficient dipolarophiles (**4d**, **4f** and **4h**) provided a higher yield in the same reaction time compare to the more electron deficient (**4e**, **4j**) and sterically hindered (**4a-c**) alkynes; a result mirrored in the reactivity of **1-C<sub>12</sub>AuNP** with the same alkynes (Table 2.1).

The Huisgen uncatalyzed 1,3-dipolar cycloaddition of an azide with an alkyne can lead to two possible regioisomers: the 1,4- and 1,5-isomers (only the 1,4-isomer is shown as a major product in Schemes 2.1 and 2.2). In cases where the alkyne is electron-deficient<sup>25</sup> or when a sterically bulky azide<sup>26</sup> is used, the 1,4-isomer is usually the major product (e.g. 1,3-dipolar cycloadditions of bulky 1-azidoadamantane with ethyl propionates form only 1,4 isomers). The formation and ratio of the 1,4- and 1,5-isomers can be determined by  $^1\text{H}$  NMR spectroscopy because the C–H triazole protons of the 1,4- and 1,5-isomers are different, the latter usually downfield of the former. In this study the

$^1\text{H}$  NMR spectra of **2a-j**- $\text{C}_{12}\text{AuNPs}$  show only one peak that can be assigned as a C–H proton of triazole ring; this indicates that there is one major isomer formed. Because the alkynes used in this study are electron deficient and the environment around the azide moiety in **1**- $\text{C}_{12}\text{AuNP}$  is sterically hindered the formation of 1,4-isomer is the regioisomer that is most likely preferred.

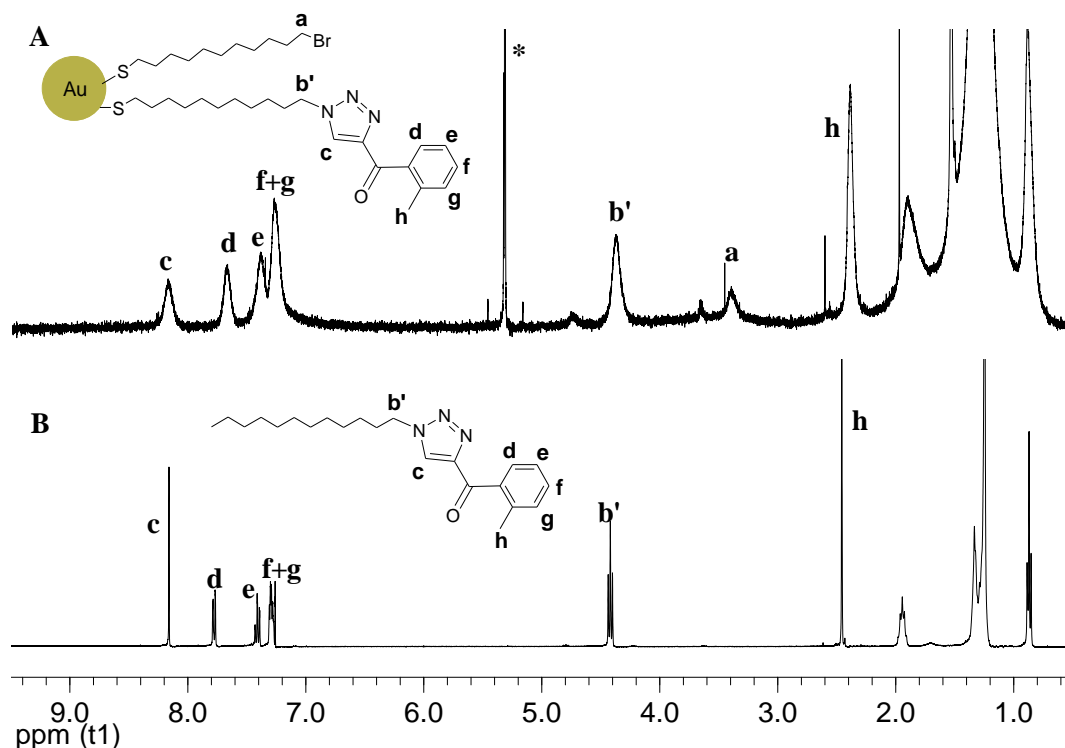


Figure 2.2  $^1\text{H}$  NMR spectra of A) **2g**- $\text{C}_{12}\text{AuNP}$  in  $\text{CD}_2\text{Cl}_2^*$ , B) Compound **5g**, in  $\text{CDCl}_3$ .

### 2.3 Conclusion

The NMR and IR data together indicate the essentially quantitative conversion of the azide-terminated AuNPs (**1**- $\text{C}_{12}\text{AuNPs}$ ) to the corresponding 1,2,3-triazole **2a-j**-

C<sub>12</sub>AuNPs under hyperbaric conditions. This can be compared to those of the reaction of the similarly azide-terminated AuNPs with a number of the same alkynes in the absence of a catalyst in dioxane for 60 h: **a** (13 %), **b** (12 %), **c** (6 %), **e** (6 %) and **h** (6 %).<sup>8</sup> The use of high pressure leads to efficient and high yielding chemical modification of monolayer protected gold nanoparticles for this reaction system. We believe that the hyperbaric reaction method described here is general for performing this reaction with activated alkynes in the absence of catalyst. As such, it can be used as a preparative tool in performing these azide-alkyne 1,3-dipolar cycloadditions for the preparation of novel materials where high chemical conversion is desirable, where the use of the copper-based catalysts is problematic, or in applications where the toxicity of the Cu complicates purification.

Supplementary Information: <sup>1</sup>H NMR spectra of the bromine terminated-AuNP, **1**-C<sub>12</sub>AuNP, <sup>1</sup>H NMR and IR spectra **2a-j**-C<sub>12</sub>AuNP and <sup>1</sup>H NMR spectra of **5a-j** are provided.

## 2.4 Experimental

### Commercial Solvents and Reagents Used

The compounds dodecanethiol, hydrogen tetrachloroaurate(III), tetraoctylammonium bromide, 1,12-dibromododecane, 11-bromo-1-undecene, azobisisobutyronitrile (AIBN), 1-bromododecane, sodium azide, ethynyl magnesium bromide, 1-octyn-3-ol and ethyl propiolate were all purchased from Aldrich and used as received. Deuterated Benzene

(C<sub>6</sub>D<sub>6</sub>), deuterated chloroform (CDCl<sub>3</sub>) and deuterated dichloromethane (CD<sub>2</sub>Cl<sub>2</sub>) (Cambridge Isotope Laboratories) were also used as received.

### **General Instrumentation**

High pressure reactions were carried out utilizing a LECO Tempres High-Pressure chemical reactor, which operates at 11 000 atm. <sup>1</sup>H and <sup>13</sup>C NMR spectra were recorded, as indicated, on either a Varian Inova 600 (<sup>1</sup>H: 600 MHz, <sup>13</sup>C: 150 MHz ) or 400 (<sup>1</sup>H: 400 MHz, <sup>13</sup>C: 100 MHz) spectrometers and were referenced to the residual protons in the solvent relative to (CH<sub>3</sub>)<sub>4</sub>Si (δ/ppm: chloroform-d 7.26, dichloromethane-d<sub>2</sub> 5.32, or benzene-d<sub>6</sub> 7.15). Mass spectra and exact mass were recorded on a MAT 8200 Finnigan High resolution Mass Spectrometer. Infrared spectra were recorded on a Bruker Vector 33 FTIR spectrometer and are reported in wavenumbers (cm<sup>-1</sup>). Melting points were measured using the Electrothermal 9100 melting point instrument and are uncorrected. High resolution transmission electron microscopy images were collected on a JEOL 2010F HRTEM.

### **Synthetic Details**

#### **Dodecanethiolate AuNP (C<sub>12</sub>AuNP)**

Following the procedures of Brust-Shiffrin and Murray<sup>17, 18</sup>, hydrogen tetrachloroaurate (III) trihydrate (0.30 g, 0.77 mmol) was dissolved in 28 mL distilled water (resulting in a bright yellow solution) and then mixed with tetraoctylammonium bromide (2.30 g, 4.2 mmol) in 70 mL toluene. The contents were stirred for 30 minutes at room temperature in order to facilitate the phase transfer of the hydrogen

tetrachloroaurate (III) trihydrate into the toluene layer, which resulted in the organic layer turning to a dark orange colour and the aqueous layer becoming clear and colourless. After phase transfer, the aqueous layer was removed and the organic layer was cooled to 0 °C in ice bath. Dodecanethiol (0.468 g, 0.57 mL, 2.31 mmol) was added to the solution via a volumetric pipette and allowed to stir for ten minutes. The addition of dodecanethiol resulted in a colour change from brownish-orange to clear and colorless. A fresh solution of sodium borohydride (0.33 g, 8.7 mmol) in 28 mL water was then added to the rapidly stirring toluene solution over 5 seconds. The solution darkened instantly, eventually becoming dark brown. The mixture was allowed to stir overnight (~18 h) as it warmed to room temperature, after which time the aqueous layer was removed and the toluene layer was washed with 3 x 20 mL distilled water and dried over MgSO<sub>4</sub>. The toluene layer was then isolated by gravity filtration and evaporated to dryness. The resulting mixture of C<sub>12</sub>AuNP and tetraoctylammonium bromide was suspended in 200 mL of 95 % ethanol and placed in the freezer overnight during which time the C<sub>12</sub>AuNP precipitated from solution. When the AuNP had precipitated, the supernatant was decanted and the precipitate was dissolved in benzene and concentrated, resulting in the formation of a film in the round bottom flask. This film was washed repeatedly with 10 x 15 mL of 95 % ethanol, resulting in pure C<sub>12</sub>AuNP as judged by <sup>1</sup>H NMR spectroscopy, which showed no signs of free dodecanethiol, dodecyl disulfide or tetraoctylammonium bromide. The resulting C<sub>12</sub>AuNP was dark brown in color.

### Synthesis of Br-terminated C<sub>12</sub>AuNP

Approximately 200 mg of C<sub>12</sub>AuNP was dissolved in 60 mL of benzene and degassed with nitrogen. 290 mg (1.54 mmol) of 11-bromo-1-undecanethiol was added to the solution and stirred for 2 days at room temperature. The mixture was then concentrated and the resulting film was washed with 95 % ethanol and dried. The <sup>1</sup>H NMR spectrum of this AuNP is shown in Figure S2.1. (<sup>1</sup>H NMR 600 MHz, CD<sub>2</sub>Cl<sub>2</sub>) δ: 3.4, 1.9, 1.8-1.0, 0.9). The integrated areas of methylene protons alpha to the bromide and terminal methyl group of dodecanethiolate in the <sup>1</sup>H NMR spectrum reveals that the ratio of ligands on the bromoundecane thiolate-modified C<sub>12</sub>AuNP was 1 : 1.2 , terminal bromide to terminal methyl.

The required 11-bromo-1-undecanethiol was synthesized by the reported method.<sup>19</sup> Compound 11-bromo-1-undecene (1.5 g, 6.43 mmol), AIBN (0.6 g, 3.65 mmol) and thioacetic acid (3 mL) were dissolved in toluene and refluxed for 2 h. The reaction mixture was washed with water and then concentrated. The crude product was purified by column chromatography (eluting with 5:1 hexanes/ethyl acetate) to separate. A solution of 11-bromo-1-undecanethioacetate in dry methanol was cooled in the ice bath, then acetyl chloride was added drop-wise and the solution was stirred for 6 h at room temperature. The reaction was quenched by adding water and extracted with CH<sub>2</sub>Cl<sub>2</sub>, and then combined extracts were washed with water. The organic layer was dried over MgSO<sub>4</sub> and evaporated to get the pure product: Yellow oil, <sup>1</sup>H NMR (600 MHz, CDCl<sub>3</sub>) δ: 3.40 (t, J = 6.8, 2H), 2.51 (q, J = 7.3, 2H), 1.84 (m, 2H), 1.60 (m, 2H), 1.44-1.27 (m, 15H).

### Synthesis of Azide-terminated AuNP (**1-C<sub>12</sub>AuNP**)

**1-C<sub>12</sub>AuNP** was prepared according to the procedure of Fleming *et al.*<sup>8</sup> A 60 mL solution of 0.25 M NaN<sub>3</sub> in DMSO was added to the mixture of the bromo-terminated AuNP (prepared as above) in benzene (~200 mg of bromo-terminated-C<sub>12</sub>AuNP in 60 mL of benzene) and the mixture was stirred for 48 h. After which time, the reaction was quenched with water and organic layer was separated and washed with water for 3 times, dried over MgSO<sub>4</sub> and then concentrated. The resulting film was rinsed with 95 % ethanol and dried. <sup>1</sup>H NMR (600 MHz, CD<sub>2</sub>Cl<sub>2</sub>) δ: 3.4, 3.25, 1.9, 1.85-1.0, 0.9. The <sup>1</sup>H NMR spectrum of this **1-C<sub>12</sub>AuNP** is shown in Figure S2.2. The integrated areas of the three types of ligands, determined by decomposition of 10 mg of **1-C<sub>12</sub>AuNP** with ~2 mg of iodine, showed that the ratio of terminal azide : bromide : methyl was 3.5 : 1 : 5. Additionally, **1-C<sub>12</sub>AuNP** was characterized using IR spectroscopy and TEM. IR (cm<sup>-1</sup>): 2959, 2921, 2853, 2096, 1467, 1366, 1282, 1089, 1040, 801. The average particle size was determined by analysis of TEM images of numerous samples: 1.8 ± 0.2 nm.

### Synthesis of 1-Azidododecane (**3**)

A solution of 1-bromododecane (2 g, 8 mmol) and NaN<sub>3</sub> (0.57 g, 8.8 mmol) in DMSO (30 mL) was stirred over night at room temperature. The reaction mixture was diluted with diethyl ether and washed with water 5 times to remove DMSO. The ethereal layer was dried over MgSO<sub>4</sub> and concentrated. The spectral data are in accord with the literature.<sup>20</sup> Colourless oil, <sup>1</sup>H NMR (400 MHz, CDCl<sub>3</sub>) δ: 3.25 (t, J = 6.9, 2H), 1.59 (m, 2H), 1.37-1.26 (broad, 18H), 0.88 (t, J = 6.8, 3H). <sup>13</sup>C NMR (100 MHz, CDCl<sub>3</sub>) δ: 51.7,

32.1, 29.8, 29.77, 29.71, 29.5, 29.4, 29.0, 26.9, 22.9, 14.3. IR (cm<sup>-1</sup>): 2955, 2924, 2854, 2095, 1467, 1366, 1258.

### Synthesis of Alkynes (4a-i)

Compounds 1-Pyren-1-yl-propyn-1-one (**4a**), 1-anthracen-9-yl-propyn-1-one (**4c**), propynoic acid phenylamide (**4h**),<sup>8</sup> 1-ferrocenyl-2-propyn-1-one (**4b**),<sup>21</sup> 1-(4-nitrophenyl)-2-propyn-1-one (**4e**)<sup>22</sup> were prepared by their literature method and their <sup>1</sup>H NMR spectra are in accord with those reported. Compounds 1-phenyl-2-propyn-1-one (**4f**), 1-(4-biphenyl)-2-propyn-1-one (**4d**) and 1-octyn-3-one (**4i**),<sup>23</sup> as well as 1-(2-methylphenyl)-2-propyn-1-one (**4g**),<sup>24</sup> were synthesized by the following procedure (except for **4i** which commercial alcohol was oxidized by magnesium (IV) oxide), and their <sup>1</sup>H NMR spectra are in accord with those reported: 5 mmol of corresponding aldehyde was dissolved in 10 mL of THF and cooled in the ice bath. 10 mL of ethynyl magnesium bromide (0.5 M in THF) was added dropwise in 15 minutes. The mixture was allowed to stir for 3 h as it warmed to room temperature, after which time the reaction was quenched with saturated NH<sub>4</sub>Cl and extracted with ether. Organic layer was dried over MgSO<sub>4</sub> and then concentrated. The crude product was purified by column chromatography (eluting with 3:1 hexanes/ethyl acetate). The corresponding alcohol was dissolved in 10 mL CH<sub>2</sub>Cl<sub>2</sub> and 5.2 g (60 mmol) of magnesium (IV) oxide was added and the mixture was stirred at room temperature for 1 h. The oxidized reagent was removed by filtration through celite and organic layer was washed with water (3 times) and solvent was evaporated.



## General Procedures for Azide–alkyne Huisgen 1,3-Dipolar Cycloaddition Reactions at High Pressure Conditions

### Preparation of 2-C<sub>12</sub>AuNP

Approximately 10 mg of 1-C<sub>12</sub>AuNP was dissolved in ~2.0 mL of CH<sub>2</sub>Cl<sub>2</sub> then mixed with 15 – 20 equivalents of the appropriate activated acyl-alkynes (**4a-j**). The mixture was transferred into a brass-clamp sealed PTFE tube and placed in the LECO Tempres High-Pressure reactor at 11 000 atm for 15 – 24 h. The products **2a-j**-C<sub>12</sub>AuNPs were purified by washing with 95 % ethanol and then CH<sub>3</sub>CN, to remove any unreacted alkyne. IR and <sup>1</sup>H NMR spectroscopies were utilized to check the completion of the reaction, as described below, and purity of the resulting **2a-j**-C<sub>12</sub>AuNPs. The <sup>1</sup>H NMR spectra obtained were compared to those of the products of the model reaction, **5a-j**. These are provided, along with IR spectra in the Supporting Information.

**2a-C<sub>12</sub>AuNP**: <sup>1</sup>H NMR (Inova 600 MHz, CD<sub>2</sub>Cl<sub>2</sub>) δ: 8.63-7.73, 4.28, 3.40. IR (cm<sup>-1</sup>, dropcast on NaCl): 2921, 2851, 1643, 1467, 1225, 923, 849, 805, 716.

**2b-C<sub>12</sub>AuNP**: <sup>1</sup>H NMR (Inova 600 MHz, CD<sub>2</sub>Cl<sub>2</sub>) δ: 8.23, 5.49, 4.95, 4.63, 4.42, 4.14, 3.66, 3.41, 3.25, 1.9-0.88. IR (cm<sup>-1</sup>, dropcast on NaCl): 2925, 2853, 2096, 1631, 1530, 1453, 1260, 1039, 825, 721.

**2c-C<sub>12</sub>AuNP**: <sup>1</sup>H NMR (Inova 600 MHz, CD<sub>2</sub>Cl<sub>2</sub>) δ: 8.58, 8.04, 7.73, 7.39, 4.16, 3.40, 1.70-0.86. IR (cm<sup>-1</sup>, dropcast on NaCl): 2962, 2921, 2851, 1678, 1467, 1261, 1095, 1019, 805.

**2d-C<sub>12</sub>AuNP:** <sup>1</sup>H NMR (Inova 600 MHz, CD<sub>2</sub>Cl<sub>2</sub>) δ: 8.45-8.30, 7.67-7.42, 4.41, 3.40, 1.94-0.87. IR (cm<sup>-1</sup>, dropcast on NaCl): 2961, 2922, 2851, 1652, 1603, 1458, 1261, 1092, 1056, 906, 801, 749.

**2e-C<sub>12</sub>AuNP:** <sup>1</sup>H NMR (Inova 600 MHz, CD<sub>2</sub>Cl<sub>2</sub>) δ: 8.58, 8.33, 4.45, 3.40, 1.97-0.87. IR (cm<sup>-1</sup>, dropcast on NaCl): 2960, 2920, 2851, 1653, 1525, 1343, 1261, 1093, 1041, 848, 798.

**2f-C<sub>12</sub>AuNP:** <sup>1</sup>H NMR (Inova 600 MHz, CD<sub>2</sub>Cl<sub>2</sub>) δ: 8.34, 7.59-7.46, 4.40, 3.40, 1.90-0.87. IR (cm<sup>-1</sup>, dropcast on NaCl): 2964, 2924, 2854, 1653, 1603, 1457, 1261, 1115, 1019, 904, 815, 698.

**2g-C<sub>12</sub>AuNP:** <sup>1</sup>H NMR (Inova 600 MHz, CD<sub>2</sub>Cl<sub>2</sub>) δ: 8.18, 7.67, 7.38-7.26, 4.36, 3.38, 2.38, 1.89-0.87. IR (cm<sup>-1</sup>, dropcast on NaCl): 2918, 2849, 2075, 1657, 1524, 1457, 1228, 1015, 904, 798, 742.

**2h-C<sub>12</sub>AuNP:** <sup>1</sup>H NMR (Inova 600 MHz, CD<sub>2</sub>Cl<sub>2</sub>) δ: 9.09, 8.24, 7.71, 7.33, 7.13, 4.36, 3.41, 1.86-0.87. IR (cm<sup>-1</sup>, dropcast on NaCl): 2961, 2921, 2851, 2094, 1678, 1599, 1467, 1260, 1087, 1036, 797.

**2i-C<sub>12</sub>AuNP:** <sup>1</sup>H NMR (Inova 600 MHz, CD<sub>2</sub>Cl<sub>2</sub>) δ: 8.18, 4.33, 3.37, 1.87-0.87. IR (cm<sup>-1</sup>, dropcast on NaCl): 2955, 2921, 2852, 1739, 1437, 1260, 1224, 1199, 1108, 1039, 800, 721.

**2j-C<sub>12</sub>AuNP:** <sup>1</sup>H NMR (Inova 600 MHz, CD<sub>2</sub>Cl<sub>2</sub>) δ: 8.15, 4.39, 3.40, 3.25, 3.06, 1.92-0.89. IR (cm<sup>-1</sup>, dropcast on NaCl): 2922, 2852, 2091, 1691, 1468, 1261, 1224, 798, 723.

### Preparation of 5a-j

Alkynes (**4a-j**) (0.15 mmol) and 1-azidododecane (**3**) (0.16 mmol) were dissolved in ~2 mL of CH<sub>2</sub>Cl<sub>2</sub> then transferred into a brass-clamp sealed PTFE tube and placed in the LECO Tempres High-Pressure reactor at 11 000 atm and room temperature for 10 h. The product was removed from unreacted alkyne by preparative TLC plate (3:1 hexanes : ethyl acetate). The resulting products, **5a-j**, were characterized as summarized below.

**5a:** Yellow Solid: mp 81-84 °C. <sup>1</sup>H NMR (Inova 600 MHz, CDCl<sub>3</sub>) δ: 8.61 (d, J = 9.3, 1H), 8.32-8.30(m, 2H), 8.25-8.20 (m, 4H), 8.15-8.10 (m, 2H), 7.81 (s, 1H), 4.93 (t, J = 7.4, 2H), 2.10-2.04 (m, 2H), 1.49-1.37 (m, 4H), 1.32-1.25 (broad, 14 H), 0.87 (t, J = 7.0, 3H). <sup>13</sup>C NMR (CDCl<sub>3</sub>) δ: 14.1, 22.7, 26.6, 29.1, 29.3, 29.4, 29.5, 29.6, 30.5, 31.9, 50.9, 123.8, 123.9, 124.1, 124.8, 126.5, 126.6, 126.7, 126.9, 127.1, 127.2, 127.3, 130.0, 130.2, 130.9, 131.1, 132.1, 134.3, 140.4, 186.0 IR (cm<sup>-1</sup>, dropcast on NaCl): 3240, 2923, 2853, 1650, 1510, 1221, 999, 926, 849, 708. MS (EI): Exact mass (C<sub>31</sub>H<sub>35</sub>N<sub>3</sub>O) calc: 465.2780; found: 465.2777.

**5b:** Maroon oil. <sup>1</sup>H NMR (Inova 400 MHz, CDCl<sub>3</sub>) δ: 8.16 (s, 1H), 5.52-5.51 (m, 2H), 4.65-4.64 (m, 2H), 4.42 (t, J = 7.2, 2H), 4.17 (s, 5H), 2.00-1.93 (m, 2H), 1.35-1.25 (broad, 18H), 0.87 (t, J = 6.7, 3H). <sup>13</sup>C NMR (CDCl<sub>3</sub>) δ: 14.1, 22.7, 26.4, 28.9, 29.3, 29.4, 29.5, 29.6, 30.1, 31.9, 50.5, 70.2, 71.6, 73.0, 126.3, 149.1, 189.2. IR (cm<sup>-1</sup>, dropcast on NaCl): 3117, 2925, 2853, 1629, 1528, 1444, 1377, 1260, 1107, 1041, 826, 771. MS (EI): Exact mass (C<sub>25</sub>H<sub>35</sub>N<sub>3</sub>FeO) calc: 449.2129; found: 449.2139.

**5c:** Yellow Solid: mp 84-86 °C.  $^1\text{H}$  NMR (Inova 600 MHz,  $\text{CDCl}_3$ )  $\delta$ : 8.57 (s, 1H), 8.05 (d,  $J = 8.2$ , 2H), 7.97 (s, 1H), 7.80 (d,  $J = 8.6$ , 2H), 7.47 (t, 2H), 7.42 (t, 2H), 4.35 (t,  $J = 7.3$ , 2H), 1.92-1.87 (m, 2H), 1.31-1.24 (broad, 18H), 0.88 (t,  $J = 7.0$ , 3H).  $^{13}\text{C}$  NMR ( $\text{CDCl}_3$ )  $\delta$ : 14.1, 22.7, 26.4, 28.9, 29.3, 29.4, 29.5, 29.6, 30.1, 31.9, 50.7, 125.0, 125.4, 126.6, 127.4, 128.5, 128.7, 129.1, 131.1, 133.4, 149.0, 192.0. IR ( $\text{cm}^{-1}$ , dropcast on NaCl): 3132, 3056, 2920, 2852, 1653, 1525, 1470, 1180, 884, 841, 729. MS (EI): Exact mass ( $\text{C}_{29}\text{H}_{35}\text{N}_3\text{O}$ ) calc: 441.2780; found: 441.2783.

**5d:** Yellow Solid: mp 94-98 °C.  $^1\text{H}$  NMR (Inova 600 MHz,  $\text{CDCl}_3$ )  $\delta$ : 8.55 (d,  $J = 8.2$ , 2H), 8.27 (s, 1H), 7.75 (d,  $J = 8.2$ , 2H), 7.66 (d,  $J = 7.4$ , 2H), 7.48 (t, 2H), 7.40 (t,  $J = 7.3$ , 1H), 4.45 (t,  $J = 7.2$ , 2H), 2.00-1.95 (m, 2H), 1.37-1.25 (broad, 18H), 0.88 (t,  $J = 6.9$ , 3H).  $^{13}\text{C}$  NMR ( $\text{CDCl}_3$ )  $\delta$ : 14.1, 22.6, 26.4, 28.9, 29.2, 29.3, 29.4, 29.5, 30.1, 31.9, 50.8, 127.0, 127.3, 128.1, 128.2, 128.9, 131.2, 135.3, 140.0, 145.8, 148.2, 185.2. IR ( $\text{cm}^{-1}$ , dropcast on NaCl): 3126, 2918, 2848, 1633, 1602, 1523, 1467, 1344, 1255, 909, 876, 851, 746, 692. MS (EI): Exact mass ( $\text{C}_{27}\text{H}_{35}\text{N}_3\text{O}$ ) calc: 417.2780; found: 417.2787.

**5e:** Yellow Solid: mp 74-76 °C.  $^1\text{H}$  NMR (Inova 400 MHz,  $\text{CDCl}_3$ )  $\delta$ : 8.64 (d,  $J = 9.0$ , 2H), 8.35 (d,  $J = 9.0$ , 2H), 8.32 (s, 1H), 4.46 (t,  $J = 7.2$ , 2H), 2.01-1.94 (m, 2H), 1.35-1.24 (broad, 18H), 0.86 (t,  $J = 6.8$ , 3H).  $^{13}\text{C}$  NMR ( $\text{CDCl}_3$ )  $\delta$ : 14.0, 22.6, 26.4, 28.9, 29.2, 29.3, 29.4, 29.5, 30.1, 31.8, 50.8, 123.4, 128.5, 131.6, 141.2, 147.4, 150.3, 183.8. IR ( $\text{cm}^{-1}$ , dropcast on NaCl): 3129, 2915, 2849, 1643, 1599, 1518, 1331, 1237, 1047, 1016, 911, 881, 847, 785, 725, 694. MS (EI): Exact mass ( $\text{C}_{21}\text{H}_{30}\text{N}_4\text{O}_3$ ) calc: 384.2317; found: 386.2320.

**5f:** Yellow Solid: mp 49-51 °C.  $^1\text{H}$  NMR (Inova 400 MHz,  $\text{CDCl}_3$ )  $\delta$ : 8.43 (d,  $J = 8.7$ , 2H), 8.25(s, 1H), 7.61 (t, 1H), 7.51 (t, 2H), 4.44 (t,  $J = 7.2$ , 2H), 1.99-1.92 (m, 2H), 1.34-1.24 (broad, 18H), 0.86 (t,  $J = 6.8$ , 3H).  $^{13}\text{C}$  NMR ( $\text{CDCl}_3$ )  $\delta$ : 14.0, 22.6, 26.4, 28.9, 29.2, 29.3, 29.4, 29.5, 30.1, 31.8, 50.6, 128.1, 128.4, 130.6, 133.2, 136.5, 148.0, 185.7. IR ( $\text{cm}^{-1}$ , dropcast on NaCl): 3137, 2957, 2853, 1653, 1577, 1260, 1234, 1181, 1045, 1018, 904, 798, 725, 696. MS (EI): Exact mass ( $\text{C}_{21}\text{H}_{31}\text{N}_3\text{O}$ ) calc: 341.2467; found: 341.2477.

**5g:** Yellow oil.  $^1\text{H}$  NMR (Inova 400 MHz,  $\text{CDCl}_3$ )  $\delta$ : 8.15 (s, 1H), 7.77 (d,  $J = 7.7$ , 1H), 7.41 (t,  $J = 7.5$ , 1H), 7.31-7.28 (m, 2H), 4.42 (t,  $J = 7.2$ , 2H), 2.45(s, 3H), 1.98-1.91 (m, 2H), 1.33-1.25 (broad, 18H), 0.87 (t,  $J = 6.8$ , 3H).  $^{13}\text{C}$  NMR ( $\text{CDCl}_3$ )  $\delta$ : 14.1, 20.3, 22.6, 26.4, 28.9, 29.2, 29.3, 29.4, 29.5, 30.1, 31.8, 50.6, 125.2, 127.5, 130.1, 131.2, 131.3, 137.1, 137.9, 148.3, 189.5. IR ( $\text{cm}^{-1}$ , dropcast on NaCl): 3135, 2925, 2855, 1658, 1524, 1460, 1440, 1233, 1042, 905, 742. MS (EI): Exact mass ( $\text{C}_{22}\text{H}_{33}\text{N}_3\text{O}$ ) calc: 355.2623; found: 355.2614.

**5h:** Yellow Solid: mp 128-130°C.  $^1\text{H}$  NMR (Inova 400 MHz,  $\text{CDCl}_3$ )  $\delta$ : 8.94 (s, 1H), 8.13 (s, 1H), 7.69 ( $J = 7.6$ , 2H), 7.38 (t, 2H), 7.15 (t,  $J = 7.4$ , 1H), 4.42 (t,  $J = 7.2$ , 2H), 1.98-1.92 (m, 2H), 1.33-1.25 (broad, 18H), 0.87 (t,  $J = 6.9$ , 3H).  $^{13}\text{C}$  NMR ( $\text{CDCl}_3$ )  $\delta$ : 14.1, 22.7, 26.4, 28.9, 29.3, 29.34, 29.5, 29.6, 30.1, 31.9, 50.9, 119.8, 124.5, 125.5, 129.1, 137.5, 143.4, 163.9. IR ( $\text{cm}^{-1}$ , dropcast on NaCl): 3317, 3139, 2920, 2851, 1664, 1558, 1437, 1047, 800, 749, 689. MS (EI): Exact mass ( $\text{C}_{21}\text{H}_{32}\text{N}_4\text{O}$ ) calc: 356.2576; found: 356.2589.

**5i:** Colourless solid: mp 80-82 °C. <sup>1</sup>H NMR (Inova 400 MHz, CDCl<sub>3</sub>) δ: 8.02 (s, 1H), 4.39 (t, J = 7.2, 2H), 3.11 (t, J = 7.5, 2H), 1.95-1.88 (m, 2H), 1.78-1.71 (m 2H), 1.40-1.24(broad, 22H), 0.92-0.86 (m, 6H). <sup>13</sup>C NMR (CDCl<sub>3</sub>) δ: 13.9, 14.1, 22.5, 22.7, 23.7, 26.4, 28.9, 29.31, 29.33, 29.5, 29.6, 30.1, 31.5, 31.9, 39.5, 50.6, 125.1, 148.1, 195.7. IR (cm<sup>-1</sup>, dropcast on NaCl): 3102, 2915, 2847, 1687, 1469, 1241, 1159, 1055, 970, 887, 719. MS (EI): Exact mass (C<sub>20</sub>H<sub>37</sub>N<sub>3</sub>O) calc: 335.2936; found: 335.3001.

**5j:** Colourless oil. <sup>1</sup>H NMR (Inova 400 MHz, CDCl<sub>3</sub>) δ: 8.11 (s, 1H), 4.70 (t, J = 7.4, 2H), 4.38 (q, J = 7.1, 2H), 1.94-1.84 (m, 2H), 1.39 (t, J = 7.1, 2H), 1.31-1.24 (broad, 18H), 0.87 (t, J = 6.5, 3H). <sup>13</sup>C NMR (CDCl<sub>3</sub>) δ: 14.1, 14.14, 22.7, 26.4, 29.0, 29.3, 29.4, 29.5, 29.6, 30.3, 31.9, 50.4, 61.7, 127.7, 137.9, 158.5. IR (cm<sup>-1</sup>, dropcast on NaCl): 2956, 2855, 1731, 1528, 1457, 1311, 1255, 1092, 772. MS (EI): Exact mass (C<sub>17</sub>H<sub>32</sub>N<sub>3</sub>O<sub>2</sub>) (M+H<sup>+</sup>) calc: 310.2494; found: 310.2482.

## References

- 1) (a) W. G. Lewis, L. G. Green, F. Grynszpan, Z. Radic, P. R. Carlier, P. Taylor, M. G. Finn, K. B. Sharpless, *Angew. Chem., Int. Ed.* **2002**, *41*, 1053. (b) J. E. Moses, A. D. Moorhouse, *Chem. Soc. Rev.* **2007**, *36*, 1249.
- 2) See as examples: (a) S. Ciampi, T. Bocking, K. A. Kilian, M. James, J. B. Harper, J. J. Gooding, *Langmuir* **2007**, *23*, 9320. (b) T. Lummerstorfer, H. Hoffmann, *J. Phys. Chem. B.* **2004**, *108*, 3963. (c) J. P. Collman, N. K. Devaraj, C. E. D. Chidsey, *Langmuir* **2004**, *20*, 1051 and references therein.

- 3) M. R. Whittaker, C. N. Urbani, M. J. Monteiro, *J. Am. Chem. Soc.* **2006**, *128*, 11360.
- 4) J. F. Lutz, *Angew. Chem. Int. Ed.* **2007**, *46*, 1018 and references therein.
- 5) W. H. Binder, R. Sachsenhofer, C. J. Straif, R. Zirbs, *J. Mater. Chem.* **2007**, *17*, 2125.
- 6) M. A. White, J. A. Johnson, J. T. Koberstein, N. J. Turro, *J. Am. Chem. Soc.* **2006**, *128*, 11356.
- 7) J. L. Brennan, N. S. Hatzakis, T. R. Tshikhudo, N. Dirvianskyte, V. Razumas, S. Patkar, J. Vind, A. Svendsen, R. J. M. Nolte, A. E. Rowan, M. Brust, *Bioconjugate Chem.* **2006**, *17*, 1373.
- 8) D.A. Fleming, C. J. Thode, M. E. Williams, *Chem. Mater.* **2006**, *18*, 2327.
- 9) C. J. Thode, M. E. Williams, *J. Colloid Interface Sci.* **2008**, *320*, 346.
- 10) W. J. Sommer, M. Weck, *Langmuir* **2007**, *23*, 11991.
- 11) W. Limapichat, A. Bsu, *J. Colloid and Interface Sci.* **2008**, *318*, 140.
- 12) Y. Zhou, S. Wang, K. Zhang, X. Jiang, *Angew. Chem. Int. Ed.* **2008**, *47*, 1.
- 13) E. Boisselier, L. Salmon, J. Ruiz, D. Astruc, *Chem. Commun.* **2008**, 5788.
- 14) J. Zhu, M. Ganton, M. A. Kerr, and M. S. Workentin, *J. Am. Chem. Soc.* **2007**, *129*, 4904.
- 15) J. Zhu, B. Lines, M. Ganton, M. A. Kerr, M. S. Workentin, *J. Org. Chem.* **2008**, *73*, 1099.
- 16) V. Melai, A. Brillante, P. Zanirato, *J. Chem. Soc., Perkins Trans. 2* **1998**, 2447.
- 17) M. Brust, M. Walker, D. Bethell, D. J. Schiffrin, R. J. J. Whyman, *Chem. Soc. Chem. Commun.* **1994**, 801.

- 18) M. H. Hostetler, J. E. Wingate, C. J. Zhong, J. E. Harris, R. W. Vachet, M. R. Clark, J. D. Londono, S. J. Green, J. J. Stokes, G. D. Wignall, G. L. Glish, M. D. Porter, N. D. Evans, R. W. Murray, *Langmuir* **1998**, *14*, 17.
- 19) A. R. Rothrock, R. L. Donkers, M. H. Schoenfisch, *J. Am. Chem. Soc.* **2005**, *127*, 9362.
- 20) D. S. Hays, G. C. Fu, *J. Org. Chem.* **1998**, *63*, 2796.
- 21) S. Barriga, C. F. Marcos, O. Riant, T. Torroba, *Tetrahedron* **2002**, *58*, 9785.
- 22) F. C. Pigge, F. Ghasedi, Z. Zheng, N. P. Rath, G. Nichol, J. S. Chickos, *J. Chem. Soc., Perkin Trans. 2* **2000**, 2458.
- 23) N. Kumar, M. Kiuchi, J. A. Tallarico, S. L. Schreiber, *Org. Lett.* **2005**, *7*, 2535.
- 24) Y. Maeda, Y. Washitake, T. Nishimura, K. Iwai, T. Yamauchib, S. Uemuraa, *Tetrahedron* **2004**, *60*, 9031.
- 25) K. N. Houk, J. Sims, C. R. Watts, L. J. Luskus, *J. Am. Chem. Soc.* **1973**, *95*, 7301.
- 26) T. Sasaki, S. Eguchi, M. Yamaguchi, T. Esaki, *J. Org. Chem.* **1981**, *46*, 180.



**2.5 Supplementary Information For:**

**Chapter 2,**

**Remarkable High-yielding Chemical Modification of  
Gold Nanoparticles Using Uncatalyzed Click-type 1,3-  
Dipolar Cycloaddition Chemistry and Hyperbaric  
Conditions**

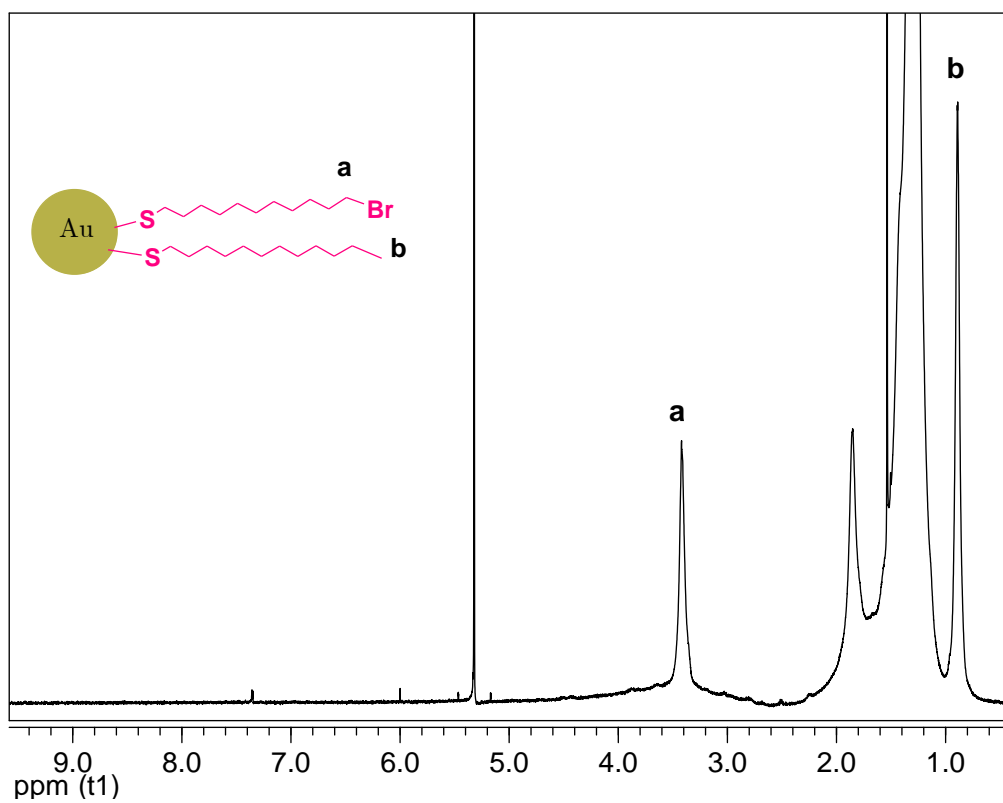


Figure S2.1 <sup>1</sup>H NMR spectra of 11-bromoundecanethiolate/dodecanethiolate AuNP in CD<sub>2</sub>Cl<sub>2</sub>.

<sup>1</sup>H NMR (600 MHz, CDCl<sub>3</sub>) δ: 3.4, 1.9, 1.8-1.0, 0.9.

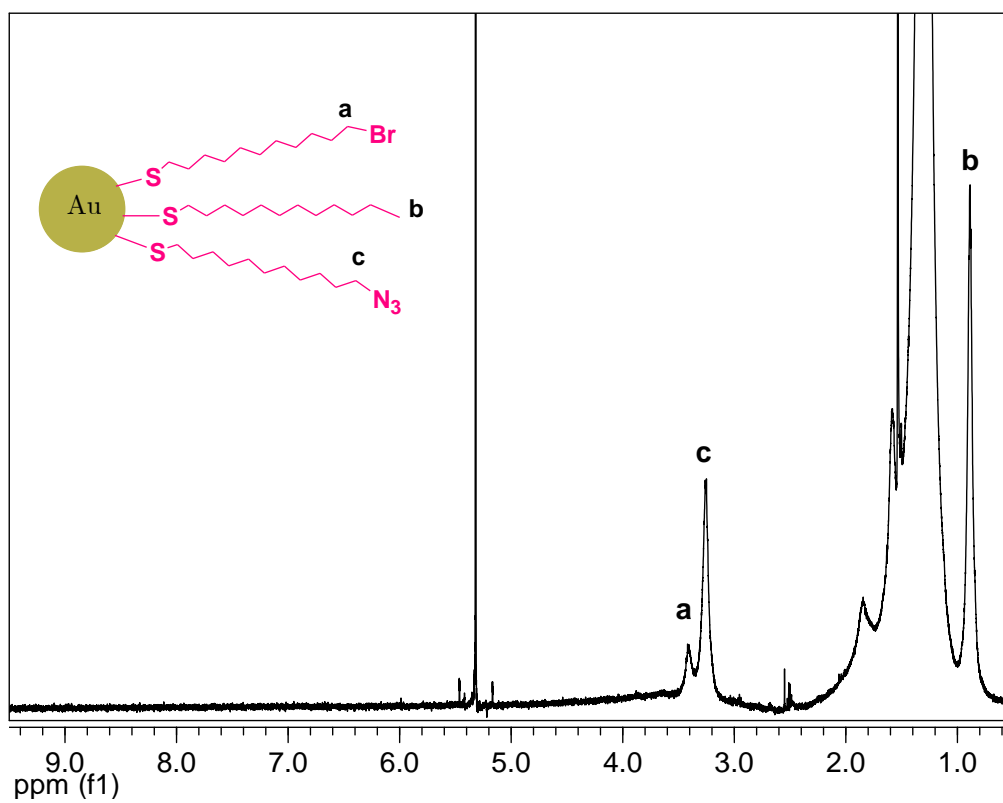


Figure S2.2  $^1\text{H}$  NMR spectra of 11-azidoundecanethiolate/11-bromo-1-undecanethiolate/dodecanethiolate AuNP ( $1\text{-C}_{12}\text{AuNP}$ ), in  $\text{CD}_2\text{Cl}_2$ .

$^1\text{H}$  NMR (600 MHz,  $\text{CDCl}_3$ )  $\delta$ : 3.4, 3.25, 1.9, 1.85-1.0, 0.9.

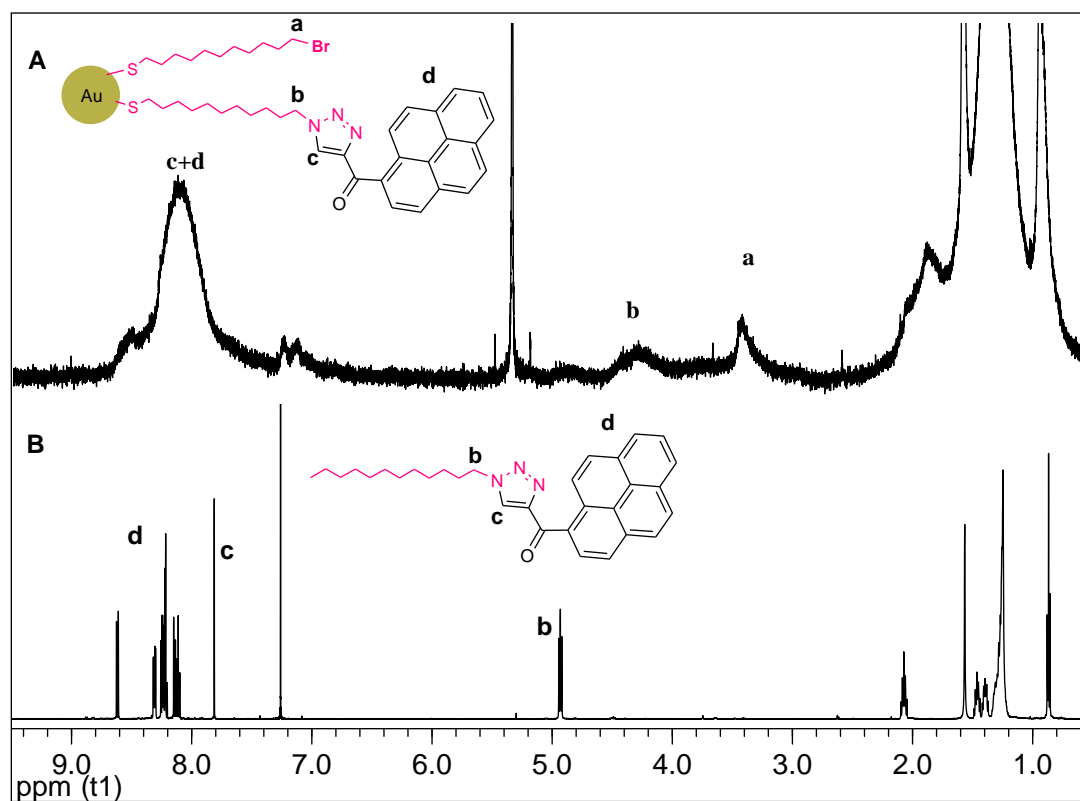


Figure S2.3  $^1\text{H}$  NMR spectra of A) 1,2,3-triazole **2a**- $\text{C}_{12}\text{AuNP}$  formed in click reaction of **1**- $\text{C}_{12}\text{AuNP}$  with **4a**, in  $\text{CD}_2\text{Cl}_2$ . B) 1,2,3-triazole **5a** formed in click reaction of 1-Azidododecane with **4a**, in  $\text{CDCl}_3$ .

A:  $^1\text{H}$  NMR (600 MHz,  $\text{CH}_2\text{Cl}_2$ )  $\delta$ : 8.63 (1H), 8.18 (very br., 9H), 4.28 (2H), 3.40, 1.9, 1.8-1.0. 0.9.

B:  $^1\text{H}$  NMR (600 MHz,  $\text{CDCl}_3$ )  $\delta$ : 8.61 (d,  $J = 9.3$ , 1H), 8.32-8.30(m, 2H), 8.25-8.20 (m, 4H), 8.15-8.10 (m, 2H), 7.81 (s, 1H), 4.93 (t,  $J = 7.4$ , 2H), 2.10-2.04 (m, 2H), 1.49-1.37 (m, 4H), 1.32-1.25 (broad, 14 H), 0.87 (t,  $J = 7.0$ , 3H).

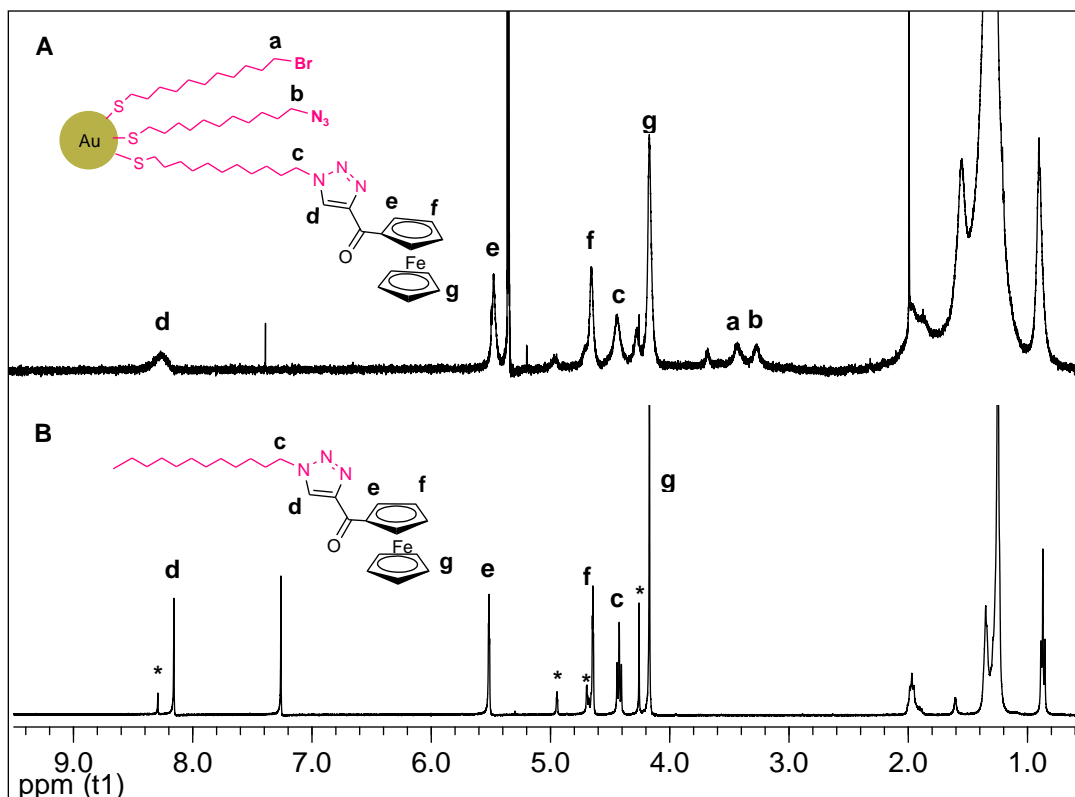


Figure S2.4  $^1\text{H}$  NMR spectra of A) 1,2,3-triazole **2b**- $\text{C}_{12}\text{AuNP}$  formed in click reaction of **1**- $\text{C}_{12}\text{AuNP}$  with **4b**, in  $\text{CD}_2\text{Cl}_2$ . B) 1,2,3-triazole **5b** formed in click reaction of 1-Azidododecane with **4b**, in  $\text{CDCl}_3$ . \* Signals due to other regioisomer.

A:  $^1\text{H}$  NMR (600 MHz,  $\text{CH}_2\text{Cl}_2$ )  $\delta$ : 8.23 (1H), 5.49 (2H), 4.63 (2H), 4.42 (2H), 4.14 (5H), 3.66 (2H), 3.41, 3.25, 1.96, 1.8, 1.7-1.0, 0.88.

B:  $^1\text{H}$  NMR (400 MHz,  $\text{CDCl}_3$ )  $\delta$ : 8.16 (s, 1H), 5.52-5.51 (m, 2H), 4.65-4.64 (m, 2H), 4.42 (t,  $J = 7.2$ , 2H), 4.17 (s, 5H), 2.00-1.93 (m, 2H), 1.35-1.25 (broad, 18H), 0.87 (t,  $J = 6.7$ , 3H).

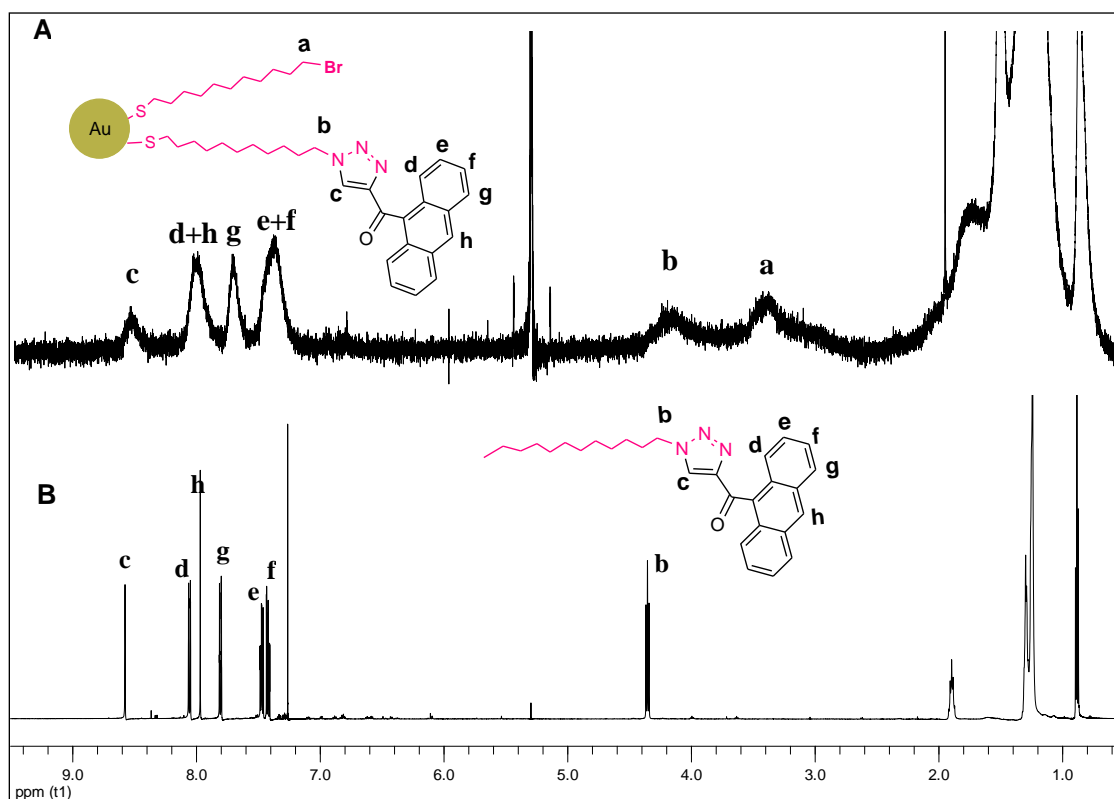


Figure S2.5  $^1\text{H}$  NMR spectra of A) 1,2,3-triazole **2c**-C<sub>12</sub>AuNP formed in click reaction of **1**-C<sub>12</sub> AuNP with **4c**, in CD<sub>2</sub>Cl<sub>2</sub>. B) 1,2,3-triazole **5c** formed in click reaction of 1-Azidododecane with **4c**, in CDCl<sub>3</sub>.

A:  $^1\text{H}$  NMR (600 MHz, CH<sub>2</sub>Cl<sub>2</sub>)  $\delta$ : 8.58 (1H), 8.04 (3H), 7.73 (2H), 7.39 (4H), 4.16 (2H), 3.40, 1.78, 1.7-1.0, 0.86.

B:  $^1\text{H}$  NMR (Inova 600 MHz, CDCl<sub>3</sub>)  $\delta$ : 8.57 (s, 1H), 8.05 (d, J = 8.2, 2H), 7.97 (s, 1H), 7.80 (d, J = 8.6, 2H), 7.47 (t, 2H), 7.42 (t, 1H), 4.35 (t, J = 7.3, 2H), 1.92-1.87 (m, 2H), 1.31-1.24 (broad, 18H), 0.88 (t, J = 7.0, 3H).

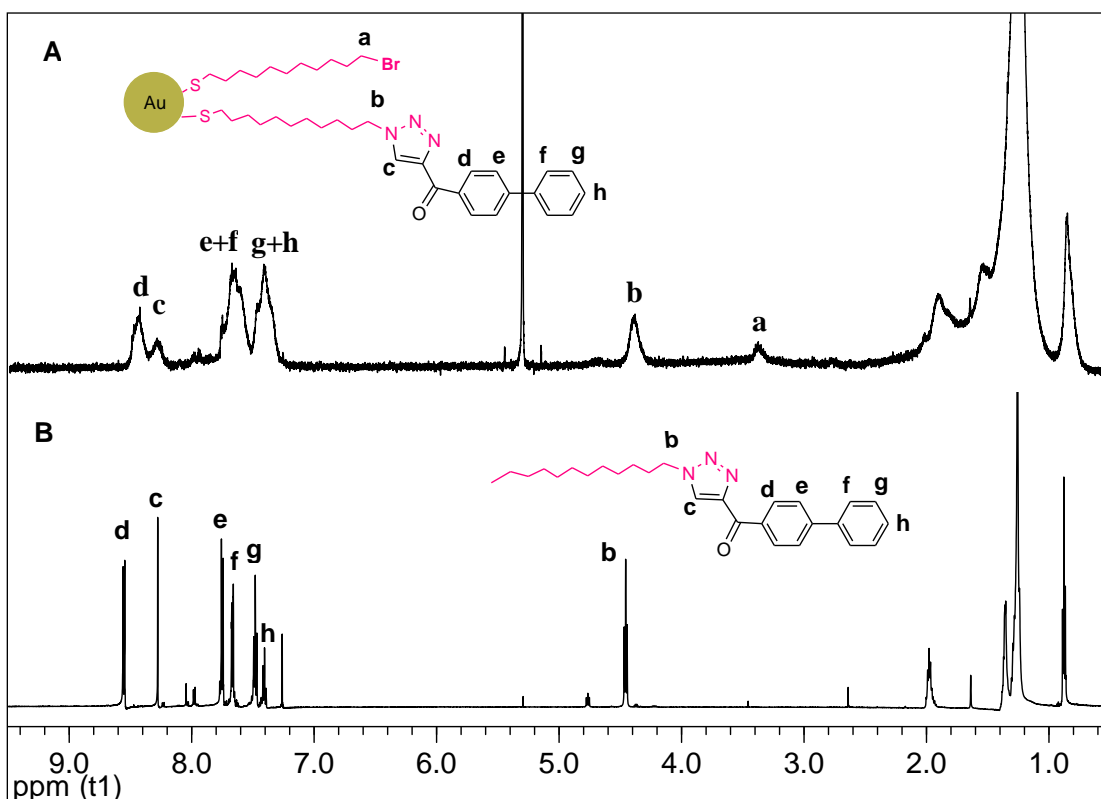


Figure S2.6  $^1\text{H}$  NMR spectra of A) 1,2,3-triazole **2d**-C<sub>12</sub>AuNP formed in click reaction of **1**-C<sub>12</sub> AuNP with **4d**, in CD<sub>2</sub>Cl<sub>2</sub> B) 1,2,3-triazole **5d** formed in click reaction of 1-Azidododecane with **4d**, in CDCl<sub>3</sub>.

A:  $^1\text{H}$  NMR (600 MHz, CH<sub>2</sub>Cl<sub>2</sub>)  $\delta$ : 8.45(2H), 8.30 (1H), 7.67 (4H), 7.42 (3H), 4.41 (2H), 3.40, 1.94, 1.75-1.0, 0.87.

B:  $^1\text{H}$  NMR (600 MHz, CDCl<sub>3</sub>)  $\delta$ : 8.55 (d,  $J = 8.2$ , 2H), 8.27 (s, 1H), 7.75 (d,  $J = 8.2$ , 2H), 7.66 (d,  $J = 7.4$ , 2H), 7.48 (t, 2H), 7.40 (t,  $J = 7.3$ , 1H), 4.45(t,  $J = 7.2$ , 2H), 2.00-1.95 (m, 2H), 1.37-1.25 (broad, 18H), 0.88 (t,  $J = 6.9$ , 3H).

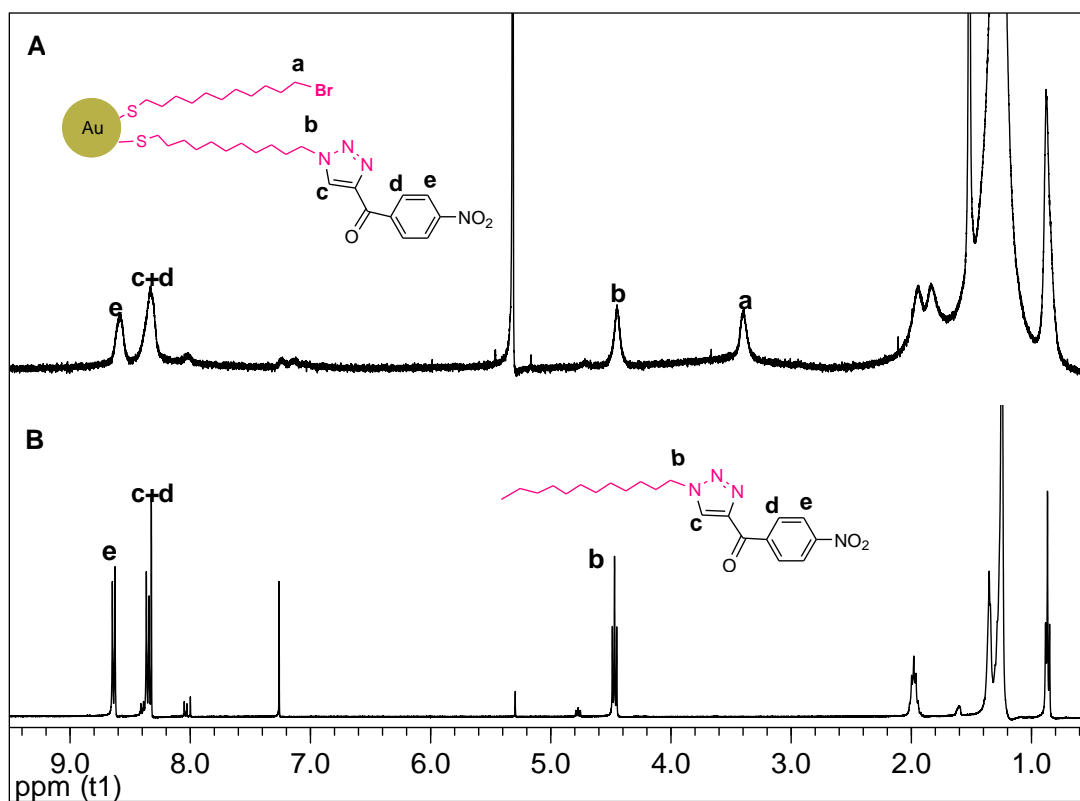


Figure S2.7  $^1\text{H}$  NMR spectra of A) 1,2,3-triazole **2e**-C<sub>12</sub>AuNP formed in click reaction of **1**-C<sub>12</sub>AuNP with **4e**, in CD<sub>2</sub>Cl<sub>2</sub>. B) 1,2,3-triazole **5e** formed in click reaction of 1-Azidododecane with **4e**, in CDCl<sub>3</sub>.

A:  $^1\text{H}$  NMR (600 MHz, CH<sub>2</sub>Cl<sub>2</sub>)  $\delta$ : 8.58 (2H), 8.33 (3H), 4.45 (2H), 3.40, 1.97, 1.81, 1.7-1.0, 0.87.

B:  $^1\text{H}$  NMR (400 MHz, CDCl<sub>3</sub>)  $\delta$ : 8.64(d,  $J = 9.0$ , 2H), 8.35 (d,  $J = 9.0$ , 2H), 8.32 (s, 1H), 4.46 (t,  $J = 7.2$ , 2H), 2.01-1.94 (m, 2H), 1.35-1.24 (broad, 18H), 0.86 (t,  $J = 6.8$ , 3H).



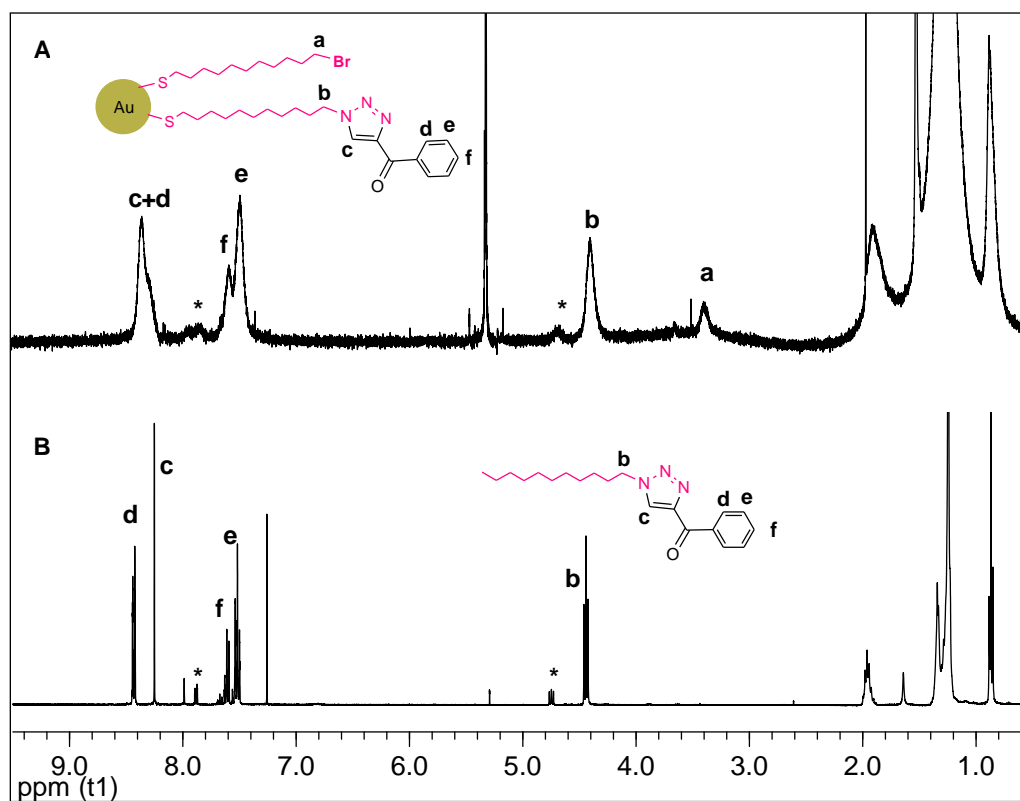


Figure S2.8  $^1\text{H}$  NMR spectra of A) 1,2,3-triazole **2f**- $\text{C}_{12}\text{AuNP}$  formed in click reaction of **1**- $\text{C}_{12}\text{AuNP}$  with **4f**, in  $\text{CD}_2\text{Cl}_2$ . B) 1,2,3-triazole **5f** formed in click reaction of 1-Azidododecane with **4f**, in  $\text{CDCl}_3$ . \* *Second regioisomer*.

A:  $^1\text{H}$  NMR (600 MHz,  $\text{CH}_2\text{Cl}_2$ )  $\delta$ : 8.34 (3H), 7.59 (1H), 7.46 (2H), 4.40 (2H), 3.40, 1.90, 1.8-1.0, 0.88.

B:  $^1\text{H}$  NMR (400 MHz,  $\text{CDCl}_3$ )  $\delta$ : 8.43 (d,  $J = 8.7$ , 2H), 8.25 (s, 1H), 7.61 (t, 1H), 7.51 (t, 2H), 4.44 (t,  $J = 7.2$ , 2H), 1.99-1.92 (m, 2H), 1.34-1.24 (broad, 18H), 0.86 (t,  $J = 6.8$ , 3H).

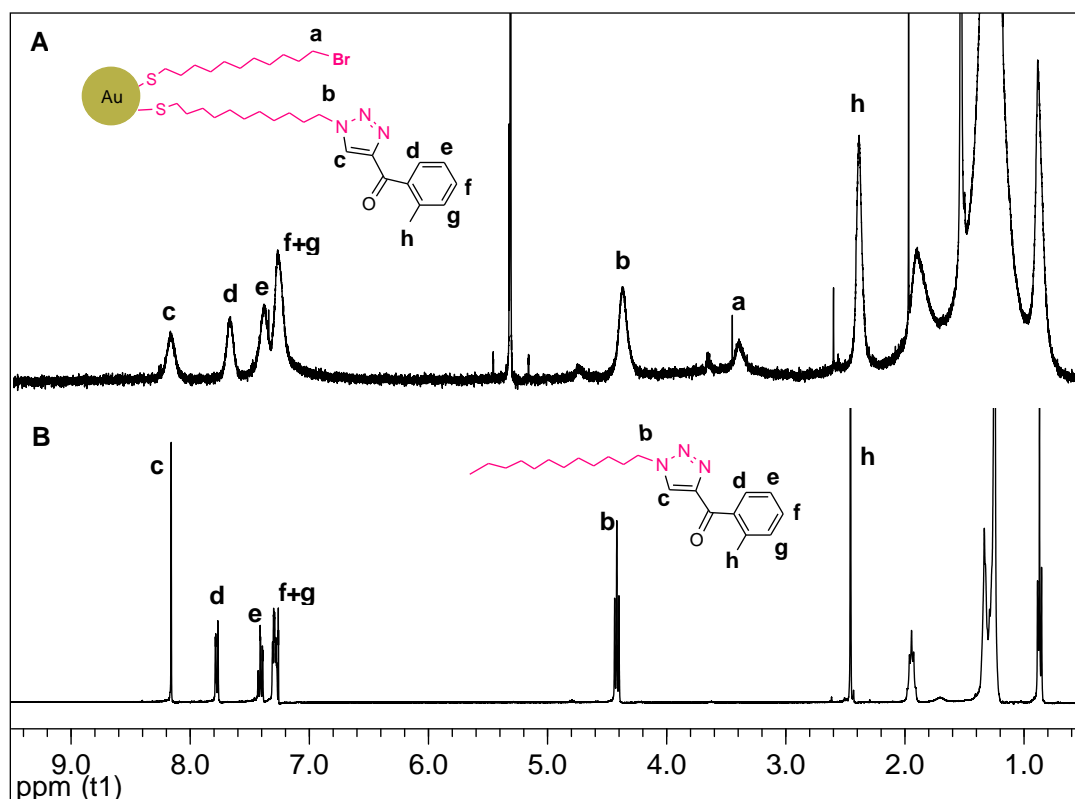


Figure S2.9  $^1\text{H}$  NMR spectra of A) 1,2,3-triazole **2g**-C<sub>12</sub>AuNP formed in click reaction of **1**-C<sub>12</sub>AuNP with **4g**, in CD<sub>2</sub>Cl<sub>2</sub>, B) 1,2,3-triazole **5g** formed in click reaction of 1-Azidododecane with **4g**, in CDCl<sub>3</sub>.

A:  $^1\text{H}$  NMR (600 MHz, CH<sub>2</sub>Cl<sub>2</sub>)  $\delta$ : 8.18 (1H), 7.67 (1H), 7.38 (1H), 7.26 (2H), 4.36 (2H), 3.38, 2.38 (3H), 1.89, 1.7-1.0, 0.87.

B:  $^1\text{H}$  NMR (400 MHz, CDCl<sub>3</sub>)  $\delta$ : 8.15(s, 1H), 7.77 (d,  $J = 7.7$ , 1H), 7.41 (t,  $J = 7.5$ , 1H), 7.31-7.28 (m, 2H), 4.42 (t,  $J = 7.2$ , 2H), 2.45(s, 3H), 1.98-1.91 (m, 2H), 1.33-1.25 (broad, 18H), 0.87 (t,  $J = 6.8$ , 3H).

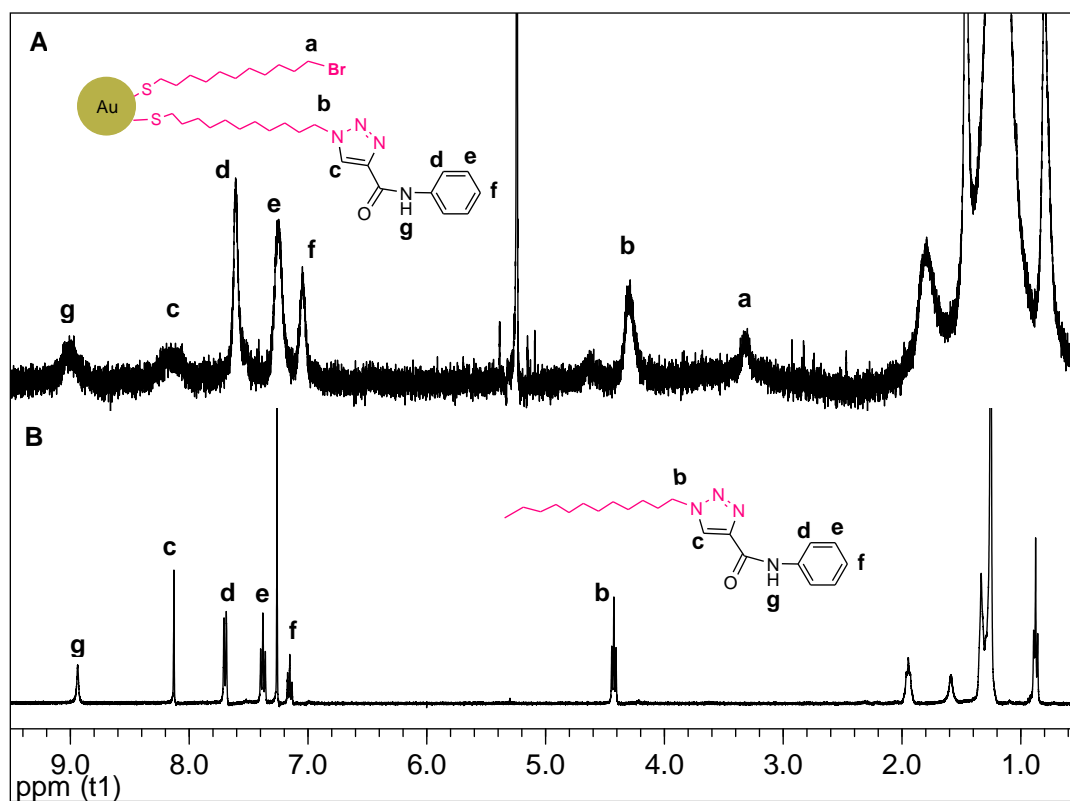


Figure S2.10  $^1\text{H}$  NMR spectra of A) 1,2,3-triazole **2h**-C<sub>12</sub>AuNP formed in click reaction of **1**-C<sub>12</sub>AuNP with **4h**, in CD<sub>2</sub>Cl<sub>2</sub>, B) 1,2,3-triazole **5h** formed in click reaction of 1-Azidododecane with **4h**, in CDCl<sub>3</sub>.

A:  $^1\text{H}$  NMR (600 MHz, CH<sub>2</sub>Cl<sub>2</sub>)  $\delta$ : 9.09 (1H), 8.24 (1H), 7.71 (2H), 7.33 (2H), 7.13 (1H), 4.36 (2H), 3.41, 1.86, 1.7-1.0, 0.87.

B:  $^1\text{H}$  NMR (400 MHz, CDCl<sub>3</sub>)  $\delta$ : 8.94 (s, 1H), 8.13 (s, 1H), 7.69 ( $J = 7.6$ , 2H), 7.38 (t, 2H), 7.15 (t,  $J = 7.4$ , 1H), 4.42 (t,  $J = 7.2$ , 2H), 1.98-1.92 (m, 2H), 1.33-1.25 (broad, 18H), 0.87 (t,  $J = 6.9$ , 3H).

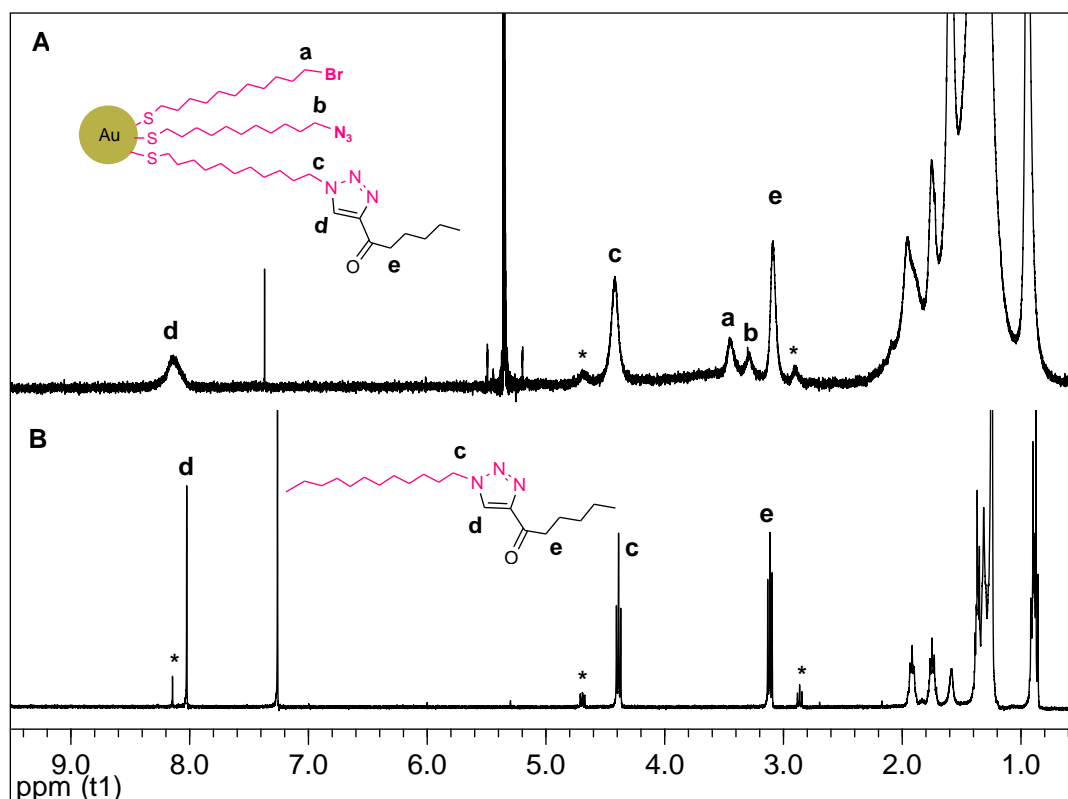


Figure S2.11  $^1\text{H}$  NMR spectra of A) 1,2,3-triazole **2i**-C<sub>12</sub>AuNP formed in click reaction of **1**-C<sub>12</sub>AuNP with **4i**, in CD<sub>2</sub>Cl<sub>2</sub>. B) 1,2,3-triazole **5i** formed in click reaction of 1-Azidododecane with **4i**, in CDCl<sub>3</sub>. \*indicated peaks from the other regioisomer.

A:  $^1\text{H}$  NMR (600 MHz, CH<sub>2</sub>Cl<sub>2</sub>)  $\delta$ : 8.15 (1H), 4.39 (2H), 3.40, 3.25, 3.06 (2H), 1.92 (2H), 1.85, 1.8-1.0, 0.89.

B:  $^1\text{H}$  NMR (400 MHz, CDCl<sub>3</sub>)  $\delta$ : 8.02 (s, 1H), 4.39 (t,  $J = 7.2$ , 2H), 3.11 (t,  $J = 7.5$ , 2H), 1.95-1.88 (m, 2H), 1.78-1.71 (m 2H), 1.40-1.24(broad, 22H), 0.92-0.86 (m, 6H).

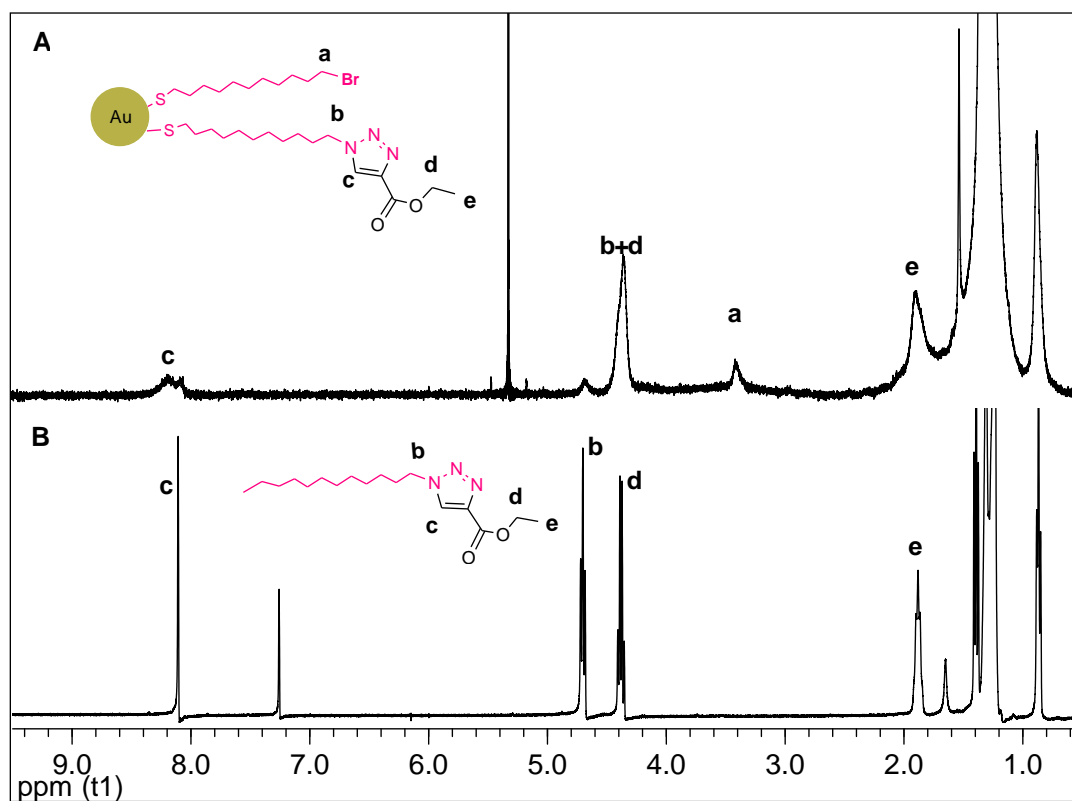


Figure S2.12  $^1\text{H}$  NMR spectra of A) 1,2,3-triazole **2j**- $\text{C}_{12}\text{AuNP}$  formed in click reaction of **1**- $\text{C}_{12}\text{AuNP}$  with **4j**, in  $\text{CD}_2\text{Cl}_2$ . B) 1,2,3-triazole **5j** formed in click reaction of 1-Azidododecane with **4j**, in  $\text{CDCl}_3$ .

A:  $^1\text{H}$  NMR (600 MHz,  $\text{CH}_2\text{Cl}_2$ )  $\delta$ : 8.18 (1H), 4.33 (4H), 3.37, 1.87(3H), 1.7-1.0, 0.87.

B:  $^1\text{H}$  NMR (400 MHz,  $\text{CDCl}_3$ )  $\delta$ : 8.11 (s, 1H), 4.70 (t,  $J = 7.4$ , 2H), 4.38 (q,  $J = 7.1$ , 2H), 1.94-1.84 (m, 2H), 1.39 (t,  $J = 7.1$ , 2H), 1.31-1.24 (broad, 18H), 0.87 (t,  $J = 6.5$ , 3H).

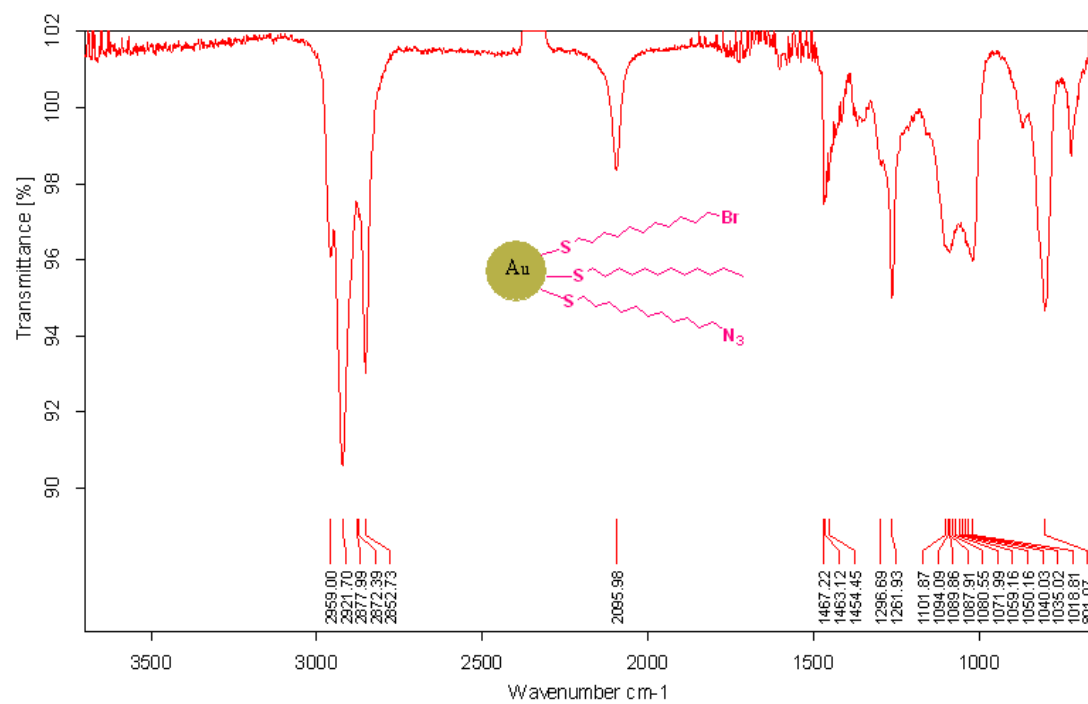


Figure S2.13 IR Spectrum of 1-C<sub>12</sub>AuNP (thin film).

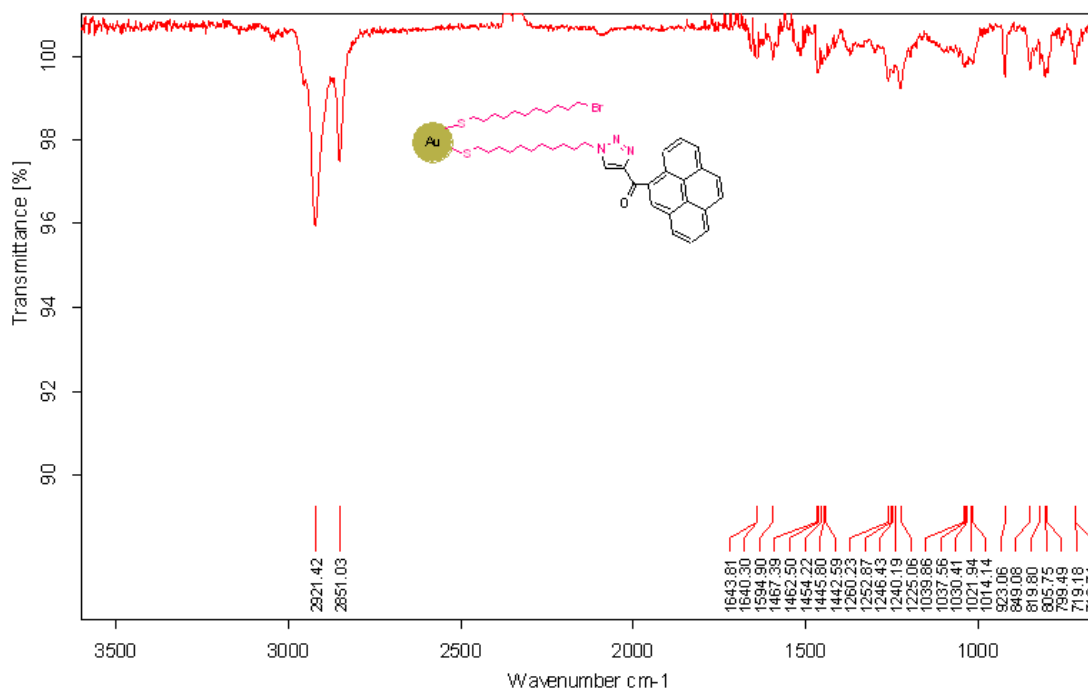


Figure S2.14 IR spectra of **2a**-C<sub>12</sub>AuNP after 15 h of reaction under hyperbaric conditions.

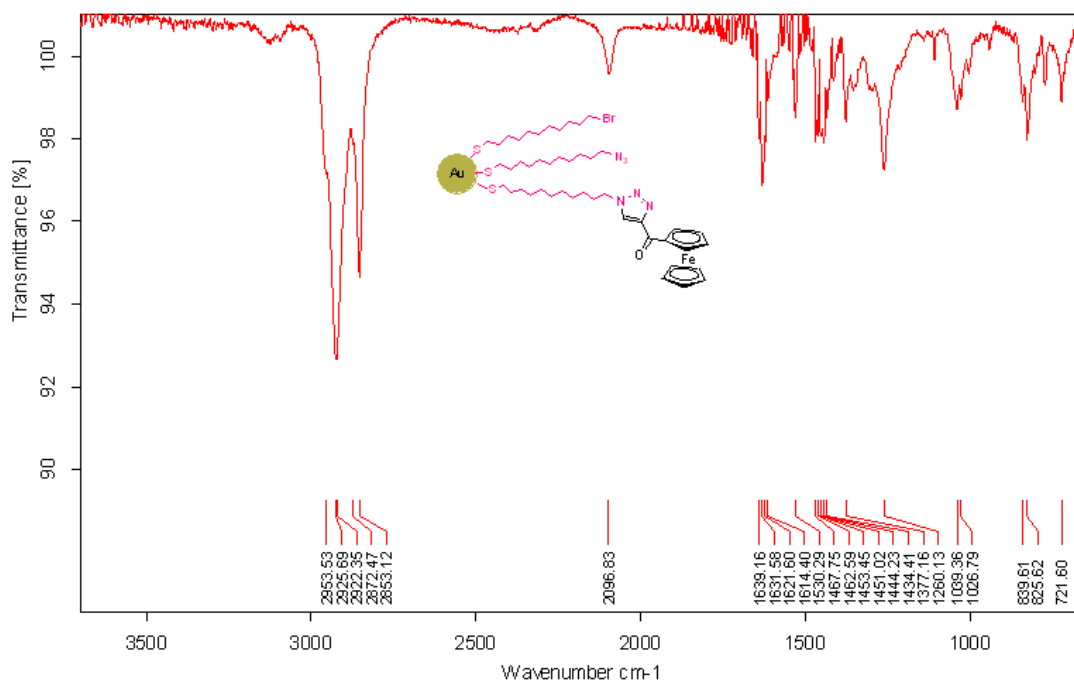


Figure S2.15 IR spectra of **2b**-C<sub>12</sub>AuNP after 15 h of reaction under hyperbaric conditions.



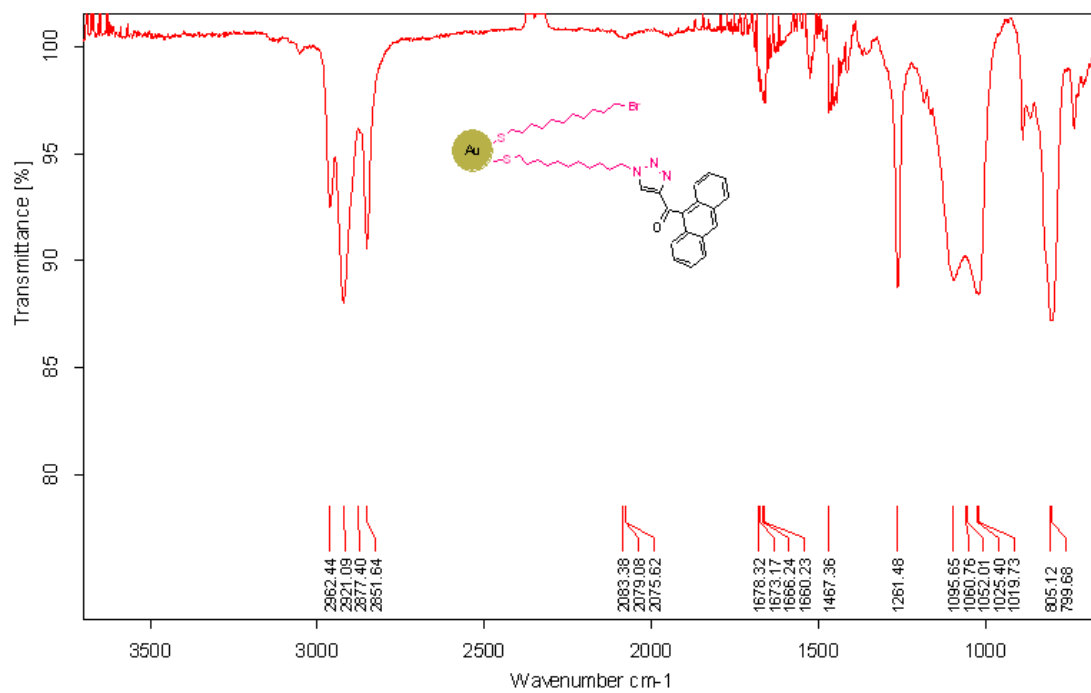


Figure S2.16 IR spectra of **2c**- $\text{C}_{12}\text{AuNP}$  after 15 h of reaction under hyperbaric conditions.

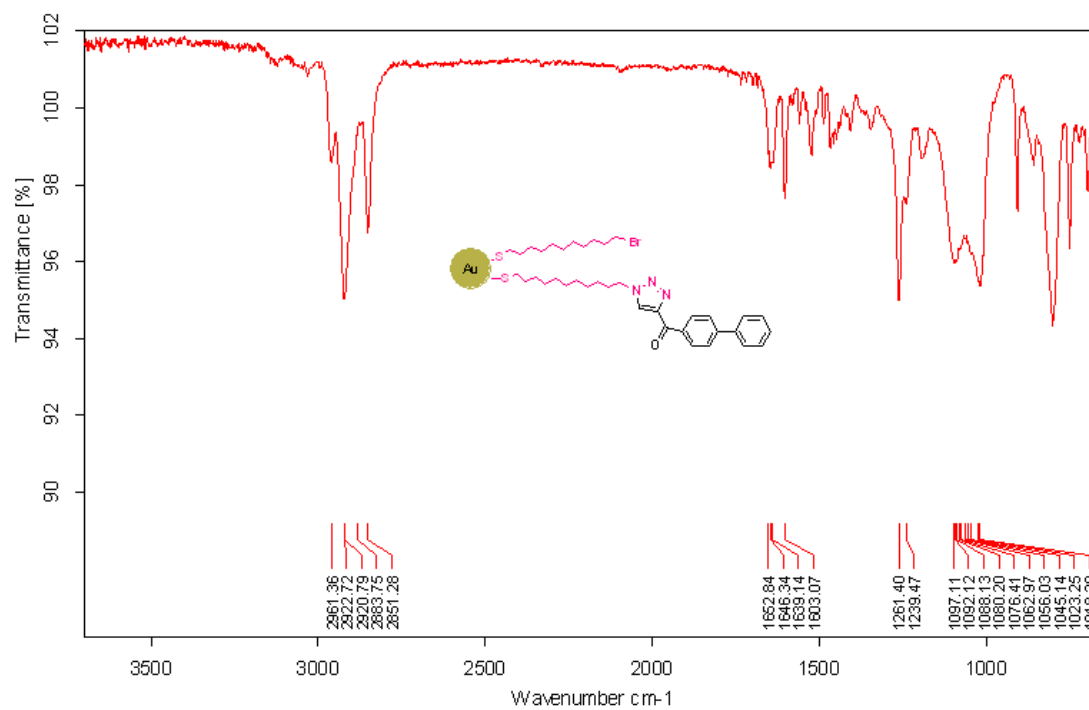


Figure S2.17 IR spectra of **2d**-C<sub>12</sub>AuNP after 15 h of reaction under hyperbaric conditions.

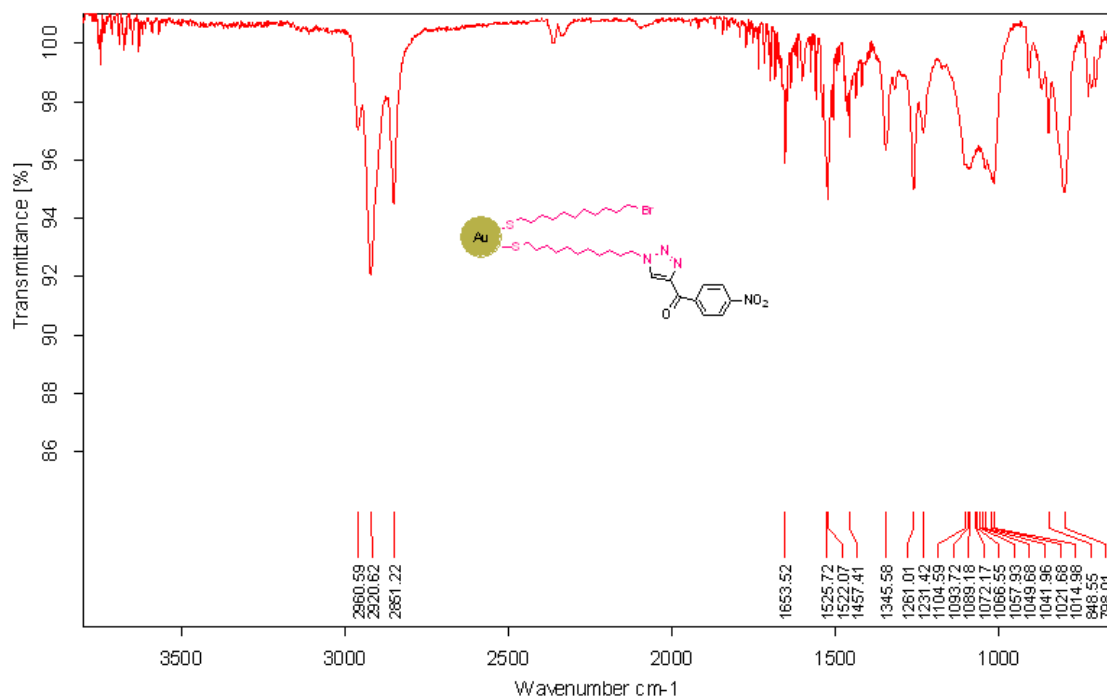


Figure S2.18 IR spectra of **2e**-C<sub>12</sub>AuNP after 15 h of reaction under hyperbaric conditions.

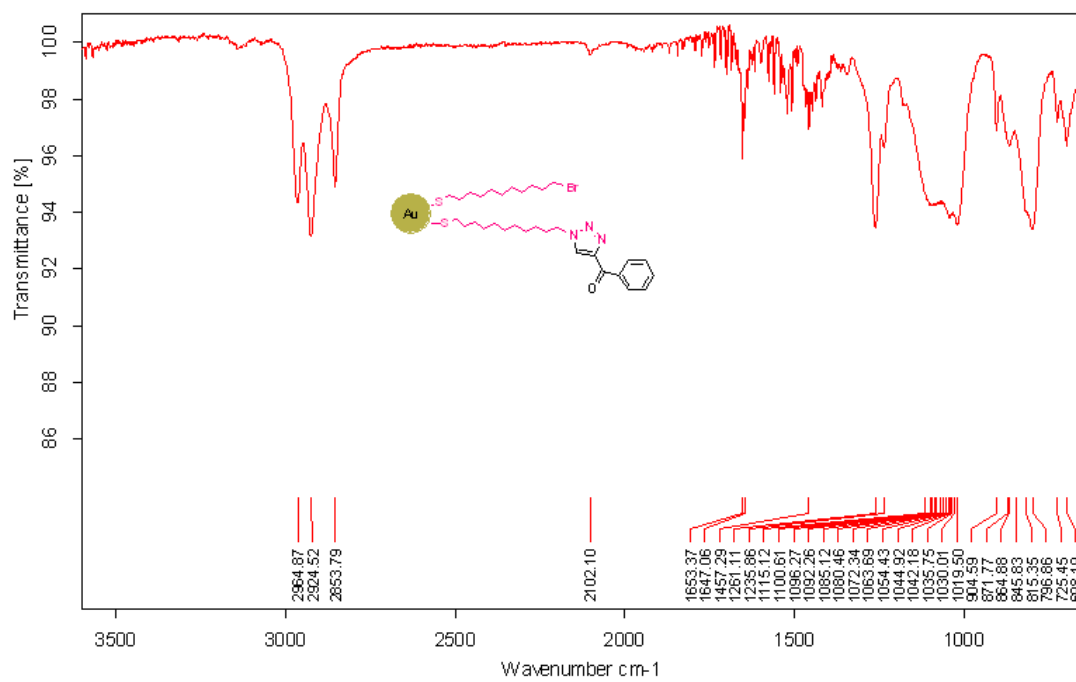


Figure S2.19 IR spectra of **2f**-C<sub>12</sub>AuNP after 15 h of reaction under hyperbaric conditions.

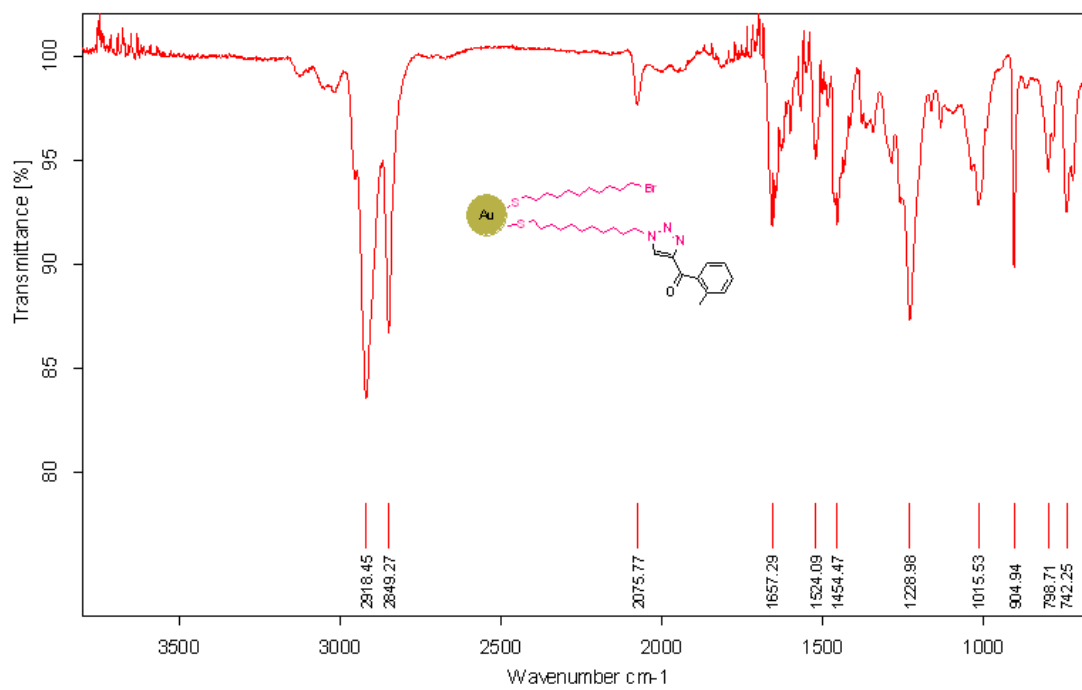


Figure S2.20 IR spectra of **2g**-C<sub>12</sub>AuNP after 15 h of reaction under hyperbaric conditions.

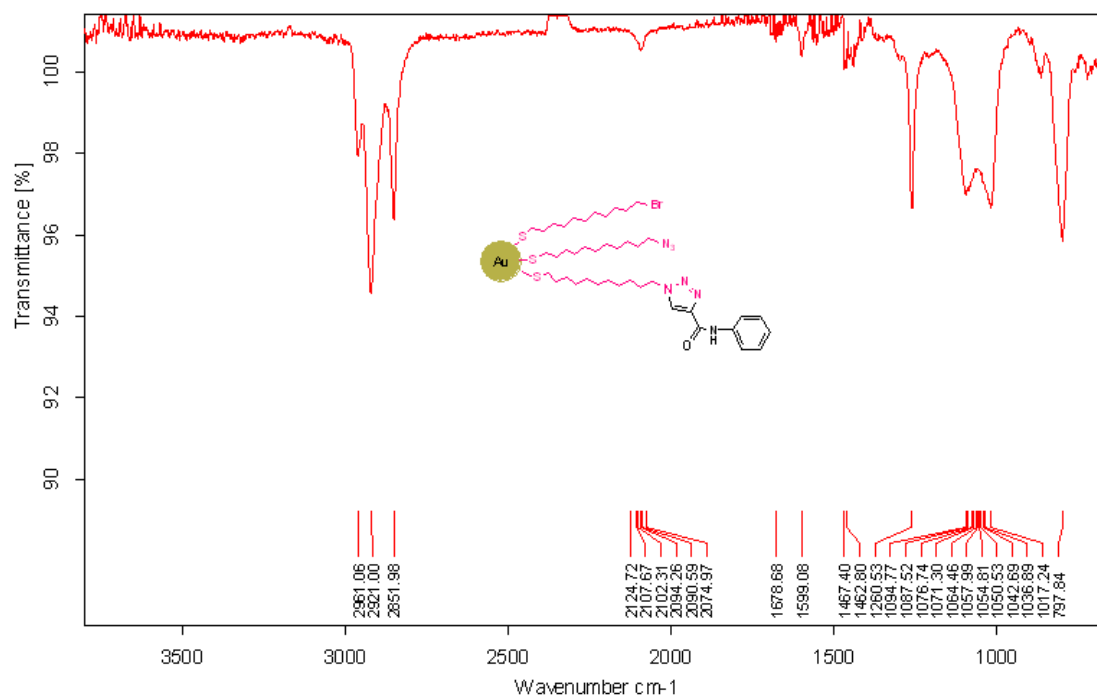


Figure S2.21 IR spectra of **2h**-C<sub>12</sub>AuNP after 15 h of reaction under hyperbaric conditions.

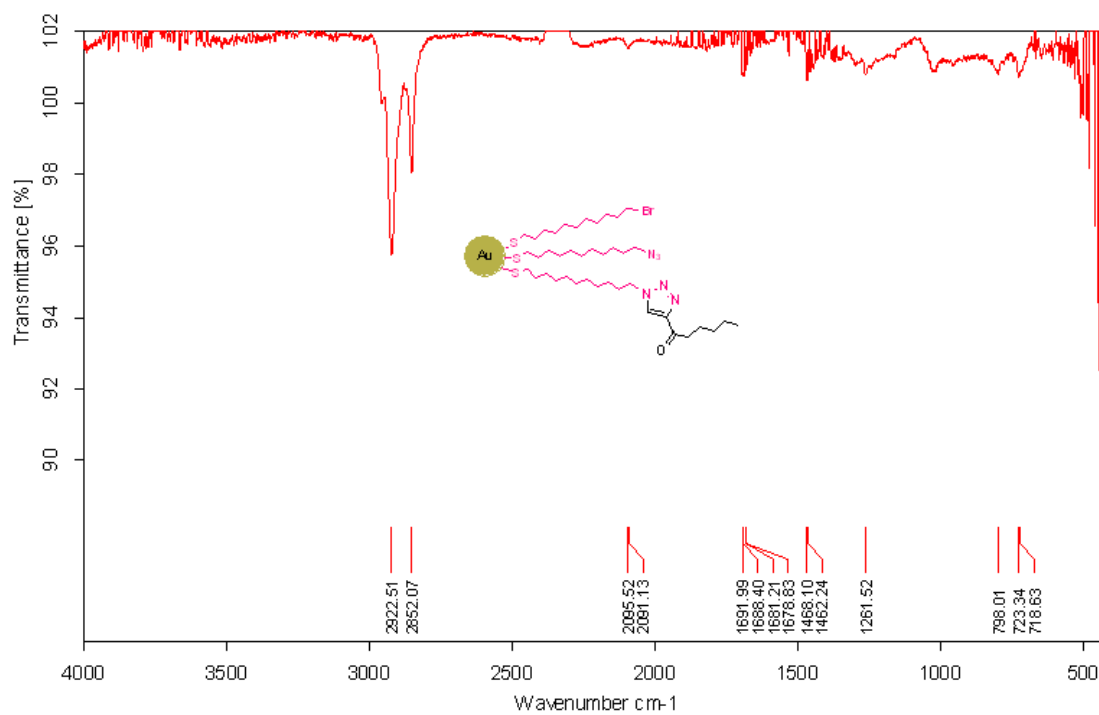


Figure S2.22 IR spectra of **2i**-C<sub>12</sub>AuNP after 24 h of reaction under hyperbaric conditions.

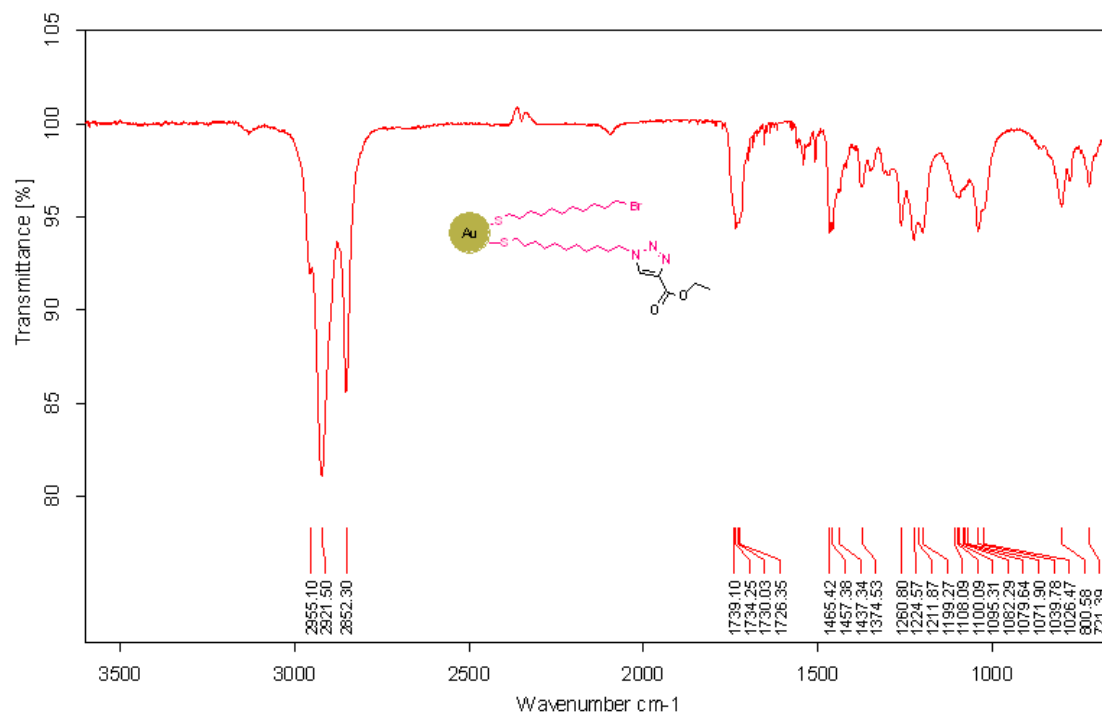


Figure S2.23 IR spectra of **2j**-C<sub>12</sub>AuNP after 15 h of reaction under hyperbaric conditions.



## UV-vis Spectra of MPN modified via Click Chemistry Reaction

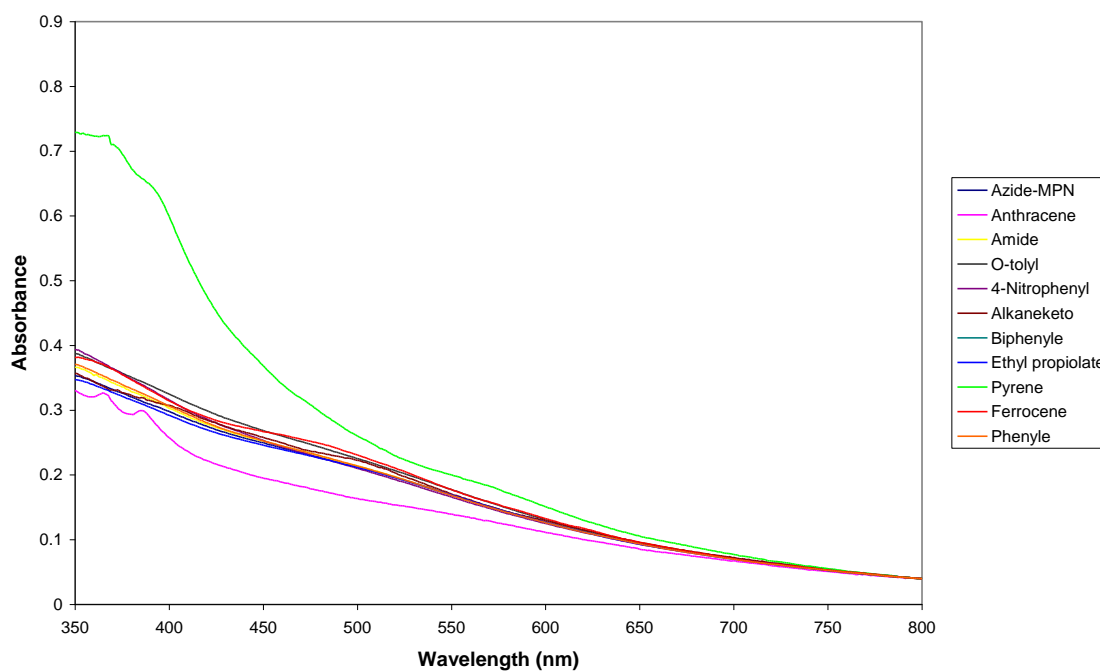


Figure S2.24 UV-vis spectra of **1**-C<sub>12</sub>AuNP and **2a-j**-C<sub>12</sub>AuNP (normalized). There is no change in the spectra in the area of the plasmon band (530 nm) indicating no significant change in size of the particle core before and after reaction. This was confirmed by TEM (figure S2.25).

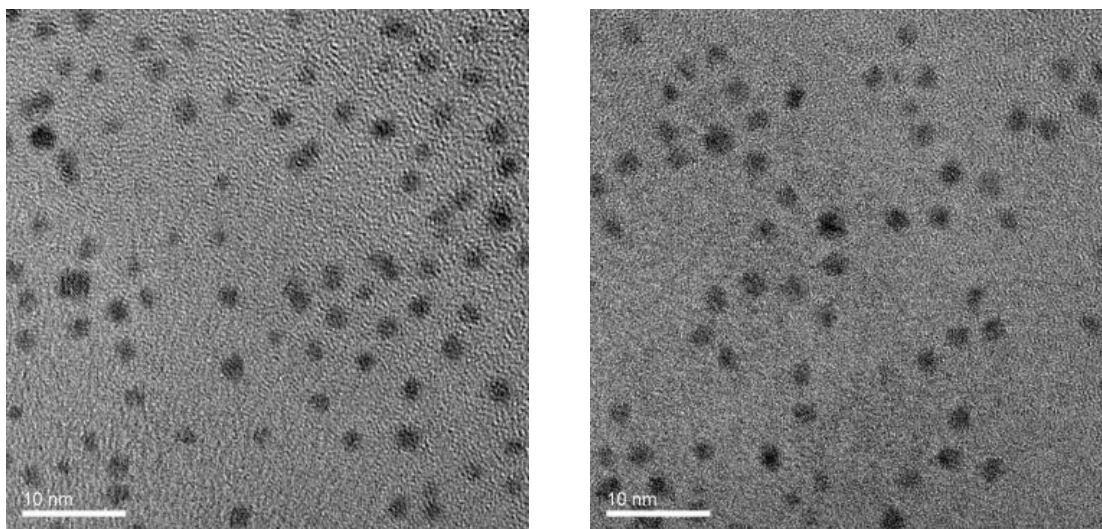


Figure S2.25 High resolution TEM images of **1**-C<sub>12</sub>AuNP before (left) and **2h**-C<sub>12</sub>AuNP after applying 11 000 atm for 24 h (right), as a representative example.

## Chapter 3

# **Diazirine-Modified Gold Nanoparticle: Template for Efficient Photoinduced Interfacial Carbene Insertion Reactions**

- Chapter 3 has been published as a full paper. The corresponding reference is: Hossein Ismaili, Soo Lee, Mark S. Workentin\*, *Langmuir* **2010**, 26, 14958.
- Soo Lee was a summer undergraduate student and involved in the synthesis of 2-C<sub>12</sub>AuNP. Hossein Ismaili carried out all of the work reported in Chapter 3.
- All of the schemes, figures, and text in Chapter 3 reprinted with permission from *Langmuir*, 2010, 26, 14958, Copyright 2010 American Chemical Society.

### 3.1 Introduction

Monolayer protected gold nanoparticles (AuNPs) continue to be an active area of discovery because of their unique chemical and physical properties as well as potential applications in catalysis,<sup>1</sup> sensors,<sup>2</sup> drug delivery,<sup>3</sup> and nanomedicine.<sup>4</sup> The key to their use in any application is the ability to prepare AuNPs with a specific chemical functionality for the interaction or reaction required. The ability to chemically modify nanoparticles by a direct interfacial reaction of terminal functional groups, exposed on the surface of AuNPs, with various reactants is a critical and important goal.<sup>5</sup> Because of this, the chemical modification of AuNPs has been the subject of numerous studies and a host of reaction types have been explored at the interface, including esterifications,<sup>6</sup> siloxane formation reaction,<sup>7</sup> nucleophilic substitutions,<sup>8</sup> transition-metal catalyzed ring-opening metathesis polymerization (ROMP),<sup>9</sup> coupling reaction of aliphatic hydroxyl group,<sup>10</sup> reductive amination reaction,<sup>11</sup> Michael additions,<sup>12</sup> 1,3-dipolar cycloadditions,<sup>13</sup> Diels – Alder reactions,<sup>14</sup> Grignard reactions,<sup>15</sup> and olefin cross metathesis.<sup>16</sup> While some reactions are efficient at ambient temperatures many reaction types require refluxing conditions or catalysts and the low stability of the AuNPs in the 1 – 5 nm in diameter size regime to higher temperatures (>100 °C) and some catalysts limits the efficacy.

The need to perform reactions on AuNPs under relatively mild and low temperature conditions limits the types of reactions that can be done efficiently and quantitatively in these systems. In addition, reactions of the monolayer moieties on the AuNPs are typically slower (less efficient) relative to similar reactions in the solution phase because

of the reaction environment provided at the interface.<sup>12 – 15</sup> Therefore, finding efficient interfacial reactions that work under mild reaction conditions is an important challenge in AuNPs applications. In our own attempts to extend the types of reactions that can be utilized for efficient interfacial modifications of AuNPs, we examined some Diels – Alder and 1,3-dipolar cycloadditions. These particular reactions were found to be generally too slow to be useful at ambient temperatures but showed that high pressure conditions can be used as an efficient tool to facilitate these reactions on the AuNPs with high yields and with no detrimental effects on the gold core.<sup>13c, d, 14</sup>

Photochemical reactions of suitably functionalized AuNPs can also be utilized to perform chemical modifications under ambient (or lower) temperature conditions.<sup>17</sup> In the continuation of our studies on exploring new methods for the modification of AuNPs through interfacial reactions, we report here the interfacial photoinduced carbene formation from a diazirine-modified AuNPs and, as proof of concept, show that the subsequent carbene insertions into a selection of model trapping agents such as alcohols, amines, and alkenes is quantitative (Scheme 3.1).

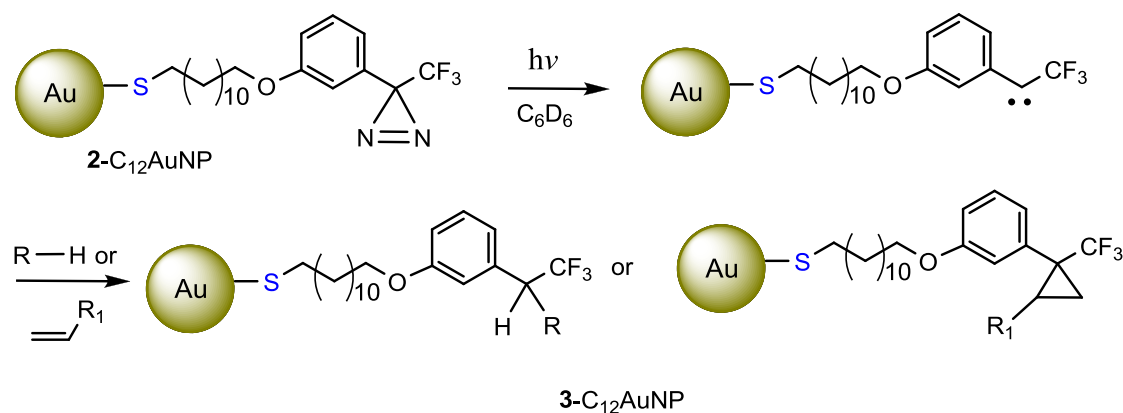
Carbene and nitrene insertion reaction approaches have been considered as feasible strategies to chemically modify surfaces or immobilize biological molecules on the functionalized surfaces.<sup>18</sup> Early in the advent of the use of gold monolayers, Wrighton and coworkers developed a gold self-assembled monolayer (Au-SAM) with aryl azide terminal groups that upon irradiation generated a reactive nitrene that then reacted with amines.<sup>19</sup> Surface modification with nylon 6,6,<sup>20</sup> protein immobilization on Fischer carbene-derivatized SAM,<sup>21</sup> and immobilization of small natural products on a glass

slide<sup>22</sup> are other examples of employing carbene insertion approaches on surfaces, but to date we are not aware of any reports of generating and utilizing a reactive carbene moiety on AuNPs.

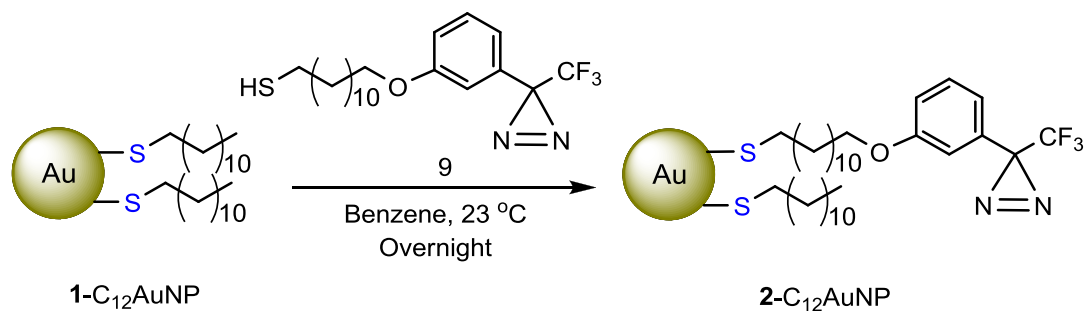
Diazirines are excellent carbene precursors and are well known photophores for photoaffinity labeling and photo-cross-linking probes.<sup>23</sup> Diazirines readily generate reactive carbene intermediates by photoinitiated nitrogen extrusion and as importantly, are relatively stable (chemically and thermally) prior to photolysis, hence do not undergo undesired reactions prior to photolysis or thermal activation.<sup>23a, 24</sup> Among the diazirine derivatives, 3-aryl-3-(trifluoromethyl)diazirine has received the most widespread use because of its high thermal stability. Because of the nature of the strong C–F bonds in the CF<sub>3</sub> group, fluorine migrations to the carbene carbon do not occur leaving a stable carbene available for quantitative insertion or addition reactions.<sup>23a</sup>

In this paper we report the synthesis and characterization of a 3-aryl-3-(trifluoromethyl)diazirine-modified AuNPs (**2**-C<sub>12</sub>AuNPs) (Scheme 3.2). We demonstrate that photolysis leads to a carbene-modified AuNP either directly and/or via the diazo-derivative resulting from photo-rearrangement of the diazirine. The carbene-AuNP intermediate is reactive towards X–H (X: O, N) bond insertion and alkene addition and this can be used as a template surface to introduce new functionality at the interface to obtain **3**-C<sub>12</sub>AuNPs (Scheme 3.1). A further benefit of utilizing the 3-aryl-3-(trifluoromethyl)diazirine as the carbene precursor is that it allows for the use of <sup>19</sup>F NMR spectroscopy to follow the course of the reactions and to further characterize the resulting product **3**-C<sub>12</sub>AuNP. In fact, the use of <sup>19</sup>F NMR has some advantages over <sup>1</sup>H

NMR characterization where the signals due to ligands on the AuNP are generally very broad.



Scheme 3.1 Interfacial photoinduced carbene formation from a diazirine-functionalized AuNP and, subsequent carbene insertions into a selection of model trapping agents.



Scheme 3.2 Synthesis of 3-aryl-3-(trifluoromethyl) diazirine-modified AuNPs (2-C<sub>12</sub>AuNP) using a ligand exchange reaction.

## 3.2 Results and Discussion

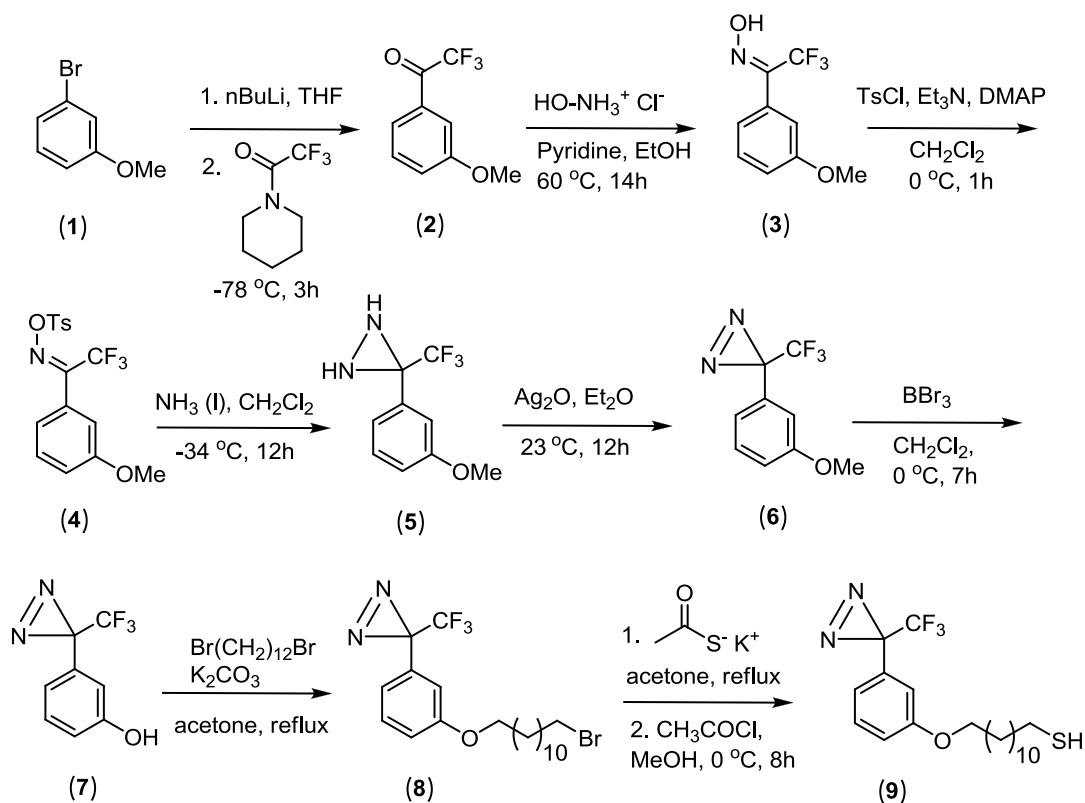
To prepare the desired 3-aryl-3-(trifluoromethyl)diazirine modified AuNP (2-C<sub>12</sub>AuNP), we utilized a place exchange reaction incorporating 3-aryl-3-

(trifluoromethyl)diazirine dodecanethiol (**9**) onto  $1.8 \pm 0.3$  nm dodecanethiolate-modified gold nanoparticles (**1-C<sub>12</sub>AuNP**) as illustrated in Scheme 3.2. The synthetic route to **9** is shown in Scheme 3.3. Briefly, *ortho*-lithiation of 3-bromoanisole **1** with *n*-butyllithium followed by trifluoroacetylation of aryllithium intermediate provided ketone **2** in 54% yield. Reaction of **2** with hydroxylamine hydrochloride gave corresponding the oxime **3** (90%) which in turn, was treated with tosyl chloride to afford *p*-tolylsulfonyloxime **4** in quantitative yield. Exposure of **4** to liquid ammonia and the subsequent oxidation of diaziridine **5** using freshly prepared silver oxide gave diazirine **6** in 52% overall yield for two steps.<sup>25, 26</sup> Compound **6** was converted to the corresponding phenol **7** (62%) using BBr<sub>3</sub>.<sup>27</sup> Alkylation of **7** using 1,12-dibromododecane followed by conversion of the bromide to the thioacetate and then hydrolysis in acidic conditions afforded the desired 3-aryl-3-(trifluoromethyl)diazirine dodecanethiol (**9**) in 73% yield.<sup>28</sup>

The **1-C<sub>12</sub>AuNPs** were prepared utilizing the Brust-Schiffrin two-phase method using a protocol we have previously reported.<sup>29, 13d</sup> This protocol results in AuNPs with the average core diameter of  $1.8 \pm 0.3$  nm as shown by TEM analysis (Supporting Information). The desired **2-C<sub>12</sub>AuNPs** were prepared using a ligand exchange reaction (Scheme 3.2).<sup>30</sup> Stirring a solution of **1-C<sub>12</sub>AuNP** (200 mg) and thiol **9** (206 mg, 0.51 mmol) in benzene for 20 h gave **2-C<sub>12</sub>AuNP**. The <sup>1</sup>H NMR spectrum of the **2-C<sub>12</sub>AuNP** show broad peaks at 0.87, 0.95 – 1.74 and 3.89 ppm attributed to the methyl group of the CH<sub>3</sub>-terminated dodecanethiolate ligands, the methylene groups of both ligands (CH<sub>3</sub>-terminated dodecanethiolate and **9**) and the methylene alpha to oxygen (labeled proton e, Figure 3.1A), respectively. In addition the aromatic region contains broad peaks at 6.65 –



6.90 (protons labeled a, b and d) and 7.27 (proton c) assigned to the aromatic protons (Figure 3.1A).



Scheme 3.3 Synthesis of 3-aryl-3-(trifluoromethyl)diazirine dodecanethiol (**9**)

Comparison of the  $^1\text{H}$  NMR spectrum of **9** (Figure 3.1B) to that of **2-C<sub>12</sub>AuNP**, particularly the excellent agreement of the signals due to a, b, c, d and e protons that are assignable to the 3-aryl-3-(trifluoromethyl)diazirine moiety in each, illustrates the successful exchange reaction and incorporation of **9** onto **1-C<sub>12</sub>AuNP** (Figure 3.1). The presence of any free, non-bound **9** would appear as sharp signals in the  $^1\text{H}$  NMR spectrum of **2-C<sub>12</sub>AuNP**, while bound **9** (on **2-C<sub>12</sub>AuNP**) appear at the same chemical shift, however the signals become more broad.<sup>31</sup> The purity of **2-C<sub>12</sub>AuNP** from the non

bound ligands after exchange reaction and work up can thus be confirmed by the lack of sharp signals in the  $^1\text{H}$  NMR spectrum of **2**- $\text{C}_{12}\text{AuNP}$  (Figure 3.1). The integrated areas of the methylene protons alpha to oxygen, proton labeled e, (due to **9** attached to **2**- $\text{C}_{12}\text{AuNPs}$ ) and the terminal methyl group of dodecanethiolate at 0.87 ppm (nonexchanged ligands) in the  $^1\text{H}$  NMR spectrum revealed that the ratio of ligands in **2**- $\text{C}_{12}\text{AuNPs}$  is *ca.* 1:1.3, thiol **9** : dodecanethiolate. This ratio shows that  $\sim 45\%$  of dodecanethiolate of the **1**- $\text{C}_{12}\text{AuNPs}$  has been replaced by **9** through the exchange reaction and can be verified by degradation of the particles and analyzing the  $^1\text{H}$  NMR spectrum of the ligands that are cleaved.<sup>13c, d, 17a - 17c</sup> Further characterization can be accomplished using  $^{19}\text{F}$  NMR where the spectrum of **2**- $\text{C}_{12}\text{AuNP}$  shows a single peak at  $-65.7$  ppm assigned to the fluorine of the  $\text{CF}_3$  group, confirming the incorporation of **9** on the **2**- $\text{C}_{12}\text{AuNPs}$  (see inset Figure 3.1).<sup>25</sup>

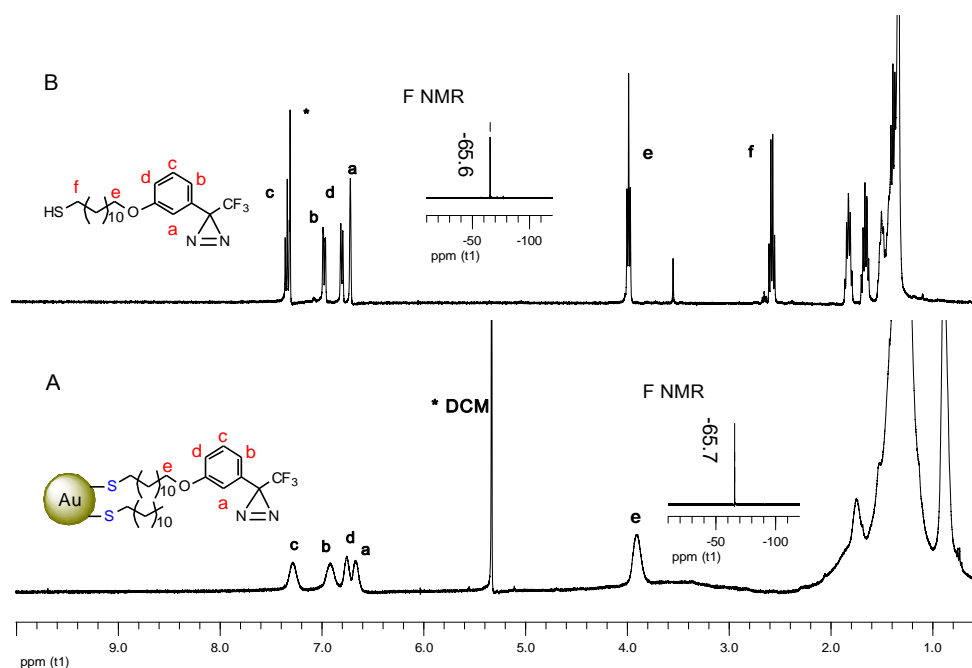
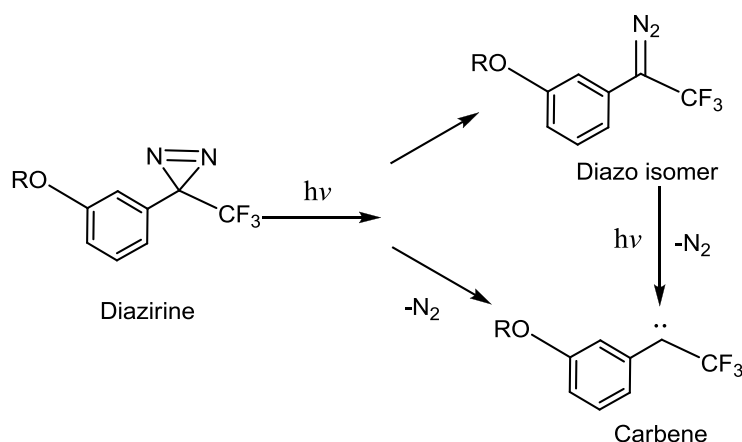


Figure 3.1  $^1\text{H}$  NMR spectra of A) **2**- $\text{C}_{12}\text{AuNP}$  and B) thiol **9**, \* denotes the signal due to residual protons in the solvent, which are  $\text{CD}_2\text{Cl}_2$  in A and  $\text{CDCl}_3$  in B.

The diazirine moiety has major absorptions at 280 and 350 nm (Supporting Information). Photolysis of **2-C<sub>12</sub>AuNP** with wavelengths above 300 nm utilizing a medium pressure Hg lamp results in photochemical nitrogen extrusion to yield the reactive carbene, which subsequently can be trapped by a variety of reagents via X–H (X : O, N) insertion or addition to alkenes.<sup>23</sup> In the present case, progress of the reaction (Scheme 3.1) can be followed using <sup>19</sup>F NMR and IR spectroscopy. As previously mentioned, the CF<sub>3</sub> moiety alpha to the diazirine group of **2-C<sub>12</sub>AuNPs** shows a sharp peak at – 65.7 ppm in the <sup>19</sup>F NMR spectrum.<sup>25</sup> Disappearance of this peak and the emergence of the new signals in <sup>19</sup>F NMR spectrum can be used to reliably follow the reaction progress. Photolysis of the diazirine can also lead to the corresponding diazo intermediate via intramolecular rearrangement, which upon further irradiation generates the carbene (Scheme 3.4).<sup>32</sup> The diazo isomer generated from **2-C<sub>12</sub>AuNP** can be detected using IR spectroscopy by the appearance of the strong N=N=C stretch centered at 2090 cm<sup>-1</sup>. The diazo stretch appears after irradiation of **2-C<sub>12</sub>AuNPs** indicating at least partial conversion of diazirine to the diazo group; therefore, complete disappearance of the diazo peak in the IR reveals that all of the carbenes generated by either diazirine or diazo isomer has undergone insertion reaction. Conversion to the diazo-derivative is also evident in the <sup>19</sup>F NMR spectrum as described below. As an initial proof of concept of using the reactive carbene to serve as a template to modify the AuNP, the irradiation of an argon-saturated solution of **2-C<sub>12</sub>AuNP** was studied in presence of CH<sub>3</sub>COOH in deuterated benzene (1:10-15 molar ratio, diazirine group on the **2-C<sub>12</sub>AuNP** : CH<sub>3</sub>COOH). To monitor the course of the reaction, <sup>19</sup>F NMR and IR spectroscopies were recorded at various times throughout the reaction. Three distinctive peaks were observed



Scheme 3.4 Photoinduced reaction pathways of diazirine in carbene formation.

in the  $^{19}\text{F}$  NMR spectra during the course of the reaction; a peak due to the unreacted diazirine at  $-65.3$  ppm that decreases in intensity on irradiation that is concomitant with a peak that appears at  $-75.9$  ppm as a result of the product of the carbene insertion into the O–H of acetic acid, and another at  $-57.5$  ppm that we assign to the diazo intermediate.<sup>25</sup> The peak at  $-57.5$  initially grows in and then diminishes on continued photolysis with continued increase in the peak at  $-75.9$  ppm (Figure 3.2). The reaction was deemed complete as determined by the disappearance of the peaks at  $-65.3$  and  $-57.5$  in  $^{19}\text{F}$  NMR spectrum. After complete reaction the  $^{19}\text{F}$  NMR spectrum showed only one peak at  $-75.9$  ppm corresponding to the  $\text{CF}_3$  group of **3a**- $\text{C}_{12}\text{AuNPs}$  (Table 3.1). In addition, the IR analysis revealed the formation and consumption of diazo isomer during the reaction; the characteristic peak at  $2090\text{ cm}^{-1}$  appeared upon irradiation and disappeared by the end of the reaction (Figure S3.13, Supporting Information). Under our irradiation conditions the reaction reached completion within 14 h at room temperature and only products from O–H insertion were obtained. A significant point to be mentioned

is that the AuNP core of **2**-C<sub>12</sub>AuNP are stable under UV irradiation in benzene and TEM taken after reaction showed no change in the Au core size.

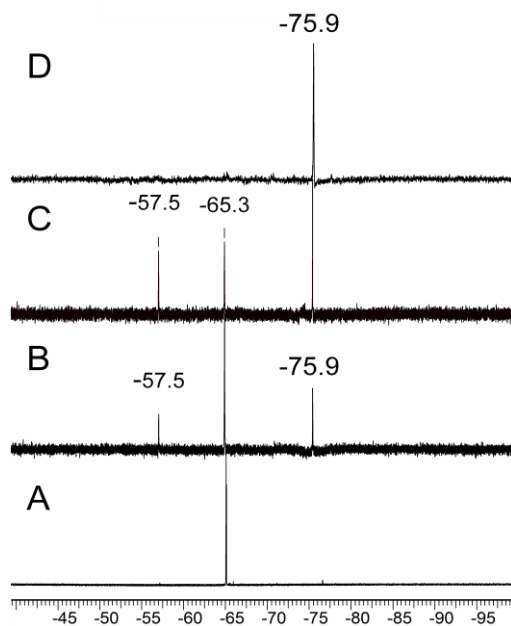


Figure 3.2 <sup>19</sup>F NMR of A) **2**-C<sub>12</sub>AuNP; B) 3 h and C) 7 h after irradiation of **2**-C<sub>12</sub>AuNP in the presence of CH<sub>3</sub>COOH, D) product **3a**-**2**-C<sub>12</sub>AuNP after 14 h irradiation.

Figure 3.3A shows the <sup>1</sup>H NMR spectrum of **3a**-C<sub>12</sub>AuNP. Evidence of the carbene insertion was the emergence of new peaks (g) and (f) which are attributed to the methyl and proton alpha to the CF<sub>3</sub> group of the product, respectively. The broadness of the peaks often makes the <sup>1</sup>H NMR assignments of functionalized AuNPs a difficult task. However, comparing the <sup>1</sup>H NMR peaks of functionalized AuNPs with those of the model compound allows for a more confident assignment. To this end, we used compound **6** as a model diazirine and it was irradiated in the presence of the same reagents, in this case CH<sub>3</sub>COOH to yield compound **11a** (Scheme 3.5, Table 3.1). The

model products **11** can be fully characterized via  $^1\text{H}$ ,  $^{13}\text{C}$ , and  $^{19}\text{F}$  NMR, and IR, as well as by mass spectroscopy. Comparing the NMR data obtained from **11** to that of the **3-C** $_{12}$ AuNP allows the validation of the product of the interfacial reactions performed on **2-C** $_{12}$ AuNP. In the  $^1\text{H}$  NMR spectra (Figure 3.3) the spectral alignment between **3a-C** $_{12}$ AuNPs and **11a**, particularly the protons indicated, confirms the modification of **2-C** $_{12}$ AuNPs with acetic acid. Further, they both give the same single peak at  $-76$  ppm in their  $^{19}\text{F}$  NMR spectra (Figure 3.3). The only difference is that the reaction of **6** with acetic acid went to completion in 90 minutes, almost 10 times faster than the corresponding reaction of **2-C** $_{12}$ AuNP with similar optical density between 350 – 360 nm. This is likely due do to efficient quenching of the excited state of the diazirine on **2-C** $_{12}$ AuNP by the gold core.<sup>33</sup>

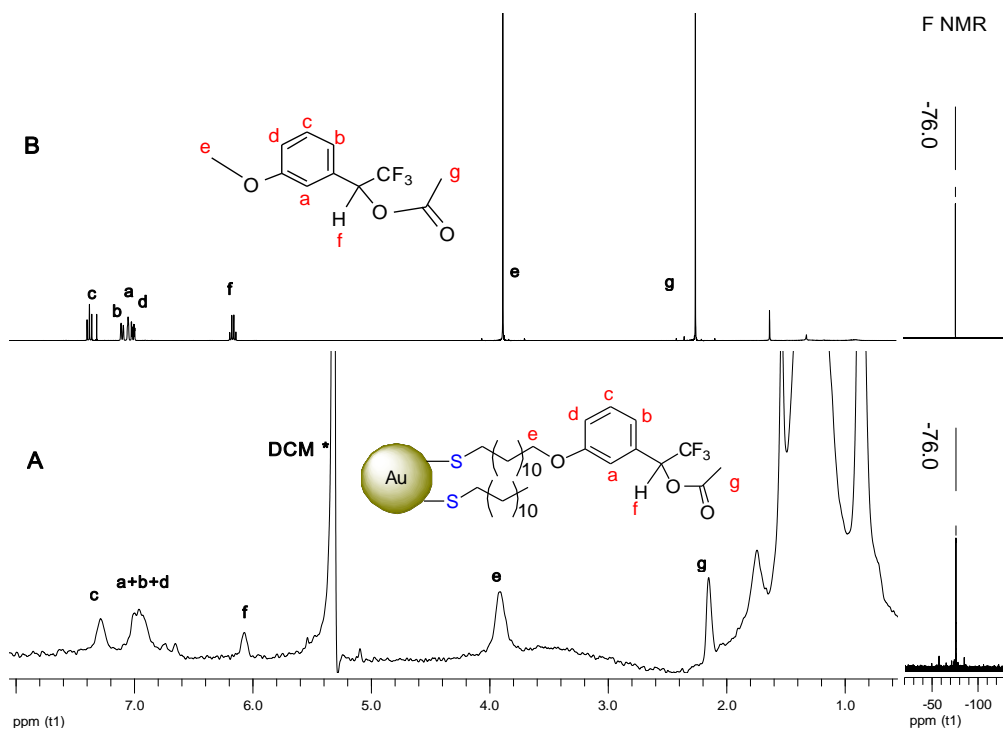
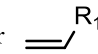
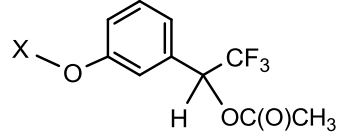
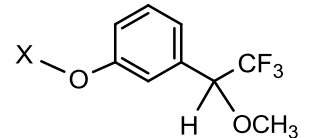
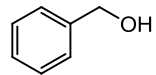
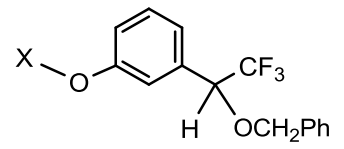
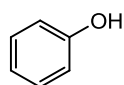
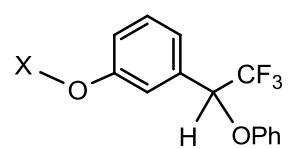
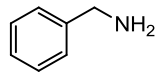
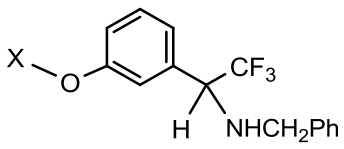
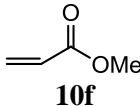
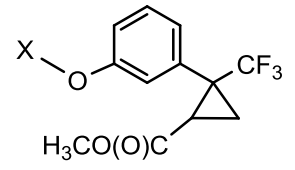
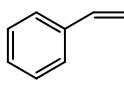
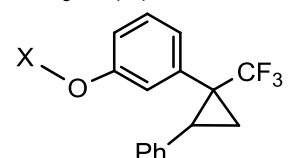
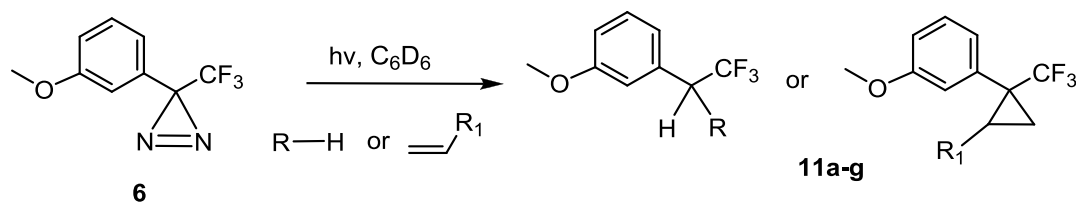


Figure 3.3  $^1\text{H}$  and  $^{19}\text{F}$  NMR spectra of A) **3a-C** $_{12}$ AuNP and B) compound **11a**, \* denotes the signal due to residual protons in the solvent  $\text{CD}_2\text{Cl}_2$ . Key assignments are indicated.

Table 3.1 Products of reaction of photolysis of the diazirines **2**-C<sub>12</sub>AuNP and **6** with a variety of carbene trapping agents to yield **3**-C<sub>12</sub>AuNP and **11**, respectively, and the <sup>19</sup>F NMR chemical shifts of the products **3**-C<sub>12</sub>AuNP

R-H or 	Product <b>3</b> -C <sub>12</sub> AuNP or <b>11</b> X = C <sub>12</sub> AuNP or CH <sub>3</sub>	Time to completion		<sup>19</sup> F NMR <sup>a</sup> ppm
		<b>3</b> -C <sub>12</sub> AuNP	<b>11</b>	
CH <sub>3</sub> COOH <b>10a</b>		14h	1.5h	-75.9
CH <sub>3</sub> OH <b>10b</b>		24h	4h	-77.4
 <b>10c</b>		14h	3.5h	-76.7
 <b>10d</b>		17h	5h	-77.4
 <b>10e</b>		26h	8h	-74.2
 <b>10f</b>		13h	2h	-65.2, -70.4
 <b>10g</b>		14h	2h	-63.6, -70.0

a) <sup>19</sup>F NMR of **3**-C<sub>12</sub>AuNPs



Scheme 3.5 Model reaction of **6** with trapping reagents to yield model **11a-g**.

To investigate the scope of using the photogenerated interfacial carbene reaction towards X–H insertion and alkene addition as a template for the modification of 2- $\text{C}_{12}\text{AuNP}$ , its photolysis was performed in the presence of a number of other reagents containing alcohol, amine and alkene moieties (**10b-g**, Table 3.1). The reagents were chosen in part in this proof of concept study to have structural features that allowed for easier identification of the products using  $^1\text{H}$  NMR spectroscopy. The photoreactions of 2- $\text{C}_{12}\text{AuNP}$  in the presence of **10b-g** were carried out under the same conditions as described for the reaction with acetic acid above, and they were monitored using  $^{19}\text{F}$  and  $^1\text{H}$  NMR and IR spectroscopies. The reactions went to completion in 13 – 26 h, depending on the substrate (Table 3.1). Figure 3.4 shows the  $^1\text{H}$  NMR spectra of **3b**, **3c**, **3e** and **3f**- $\text{C}_{12}\text{AuNP}$  as representative examples of the 3- $\text{C}_{12}\text{AuNP}$  products. The appearances of new peaks in  $^1\text{H}$  NMR spectra confirm the efficacy of the carbene insertion reactions at modifying the 2- $\text{C}_{12}\text{AuNPs}$  ( $^1\text{H}$  and  $^{19}\text{F}$  NMR as well as IR data of all 3- $\text{C}_{12}\text{AuNP}$  can be found in Supporting Information). We also performed the photoreactions with **6** in the presence of **10b-g** to prepare **11b-g** (Scheme 3.5, Table 3.1) to aid in the characterization of 3- $\text{C}_{12}\text{AuNP}$ . It is these comparisons that allowed for the characterization of the  $^1\text{H}$  NMR of 3- $\text{C}_{12}\text{AuNP}$  and the assignment of the protons identified in Figure 3.4 and the  $^{19}\text{F}$  in the products indicated in Table 3.1. In all cases the



reactions were efficient and resulted in quantitative conversion of the diazirine. For the alkene addition reactions, the two signals observed in the  $^{19}\text{F}$  NMR spectra are from the two diastereomers. Full characterization is provided in the Supporting Information.

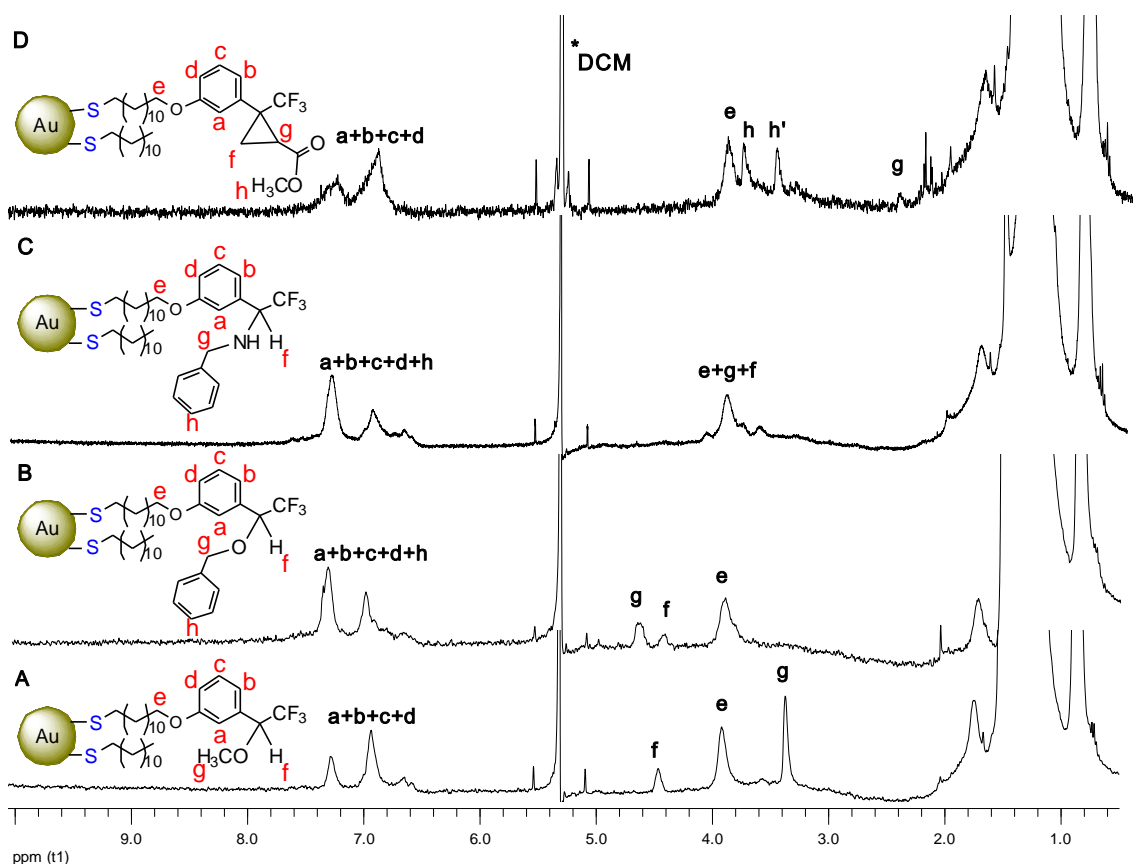


Figure 3.4  $^1\text{H}$  NMR spectra of A) **3b**- $\text{C}_{12}\text{AuNP}$  B) **3c**- $\text{C}_{12}\text{AuNP}$  C) **3e**- $\text{C}_{12}\text{AuNP}$  D) **3f**- $\text{C}_{12}\text{AuNP}$ , \* denotes the signal due to residual protons  $\text{CD}_2\text{Cl}_2$ . Key assignments are indicated.

It is important to note that in none of the reactions of **6** and **2**- $\text{C}_{12}\text{AuNPs}$  with **10a-g**, was the product of the insertion of the carbene into the deuterated benzene (solvent) detected. Only in the absence of a trapping reagent was this product observed. Following 15 h of irradiation of **2**- $\text{C}_{12}\text{AuNPs}$  in deuterated benzene two peaks were observed in the

$^{19}\text{F}$  NMR spectra: one at  $-57.5$  ppm due to the diazo isomer and another at  $-73.9$  resulting from insertion into deuterated benzene to yield cyclohepta-1,3,5-triene.<sup>25</sup> In none of the  $^{19}\text{F}$  NMR spectra of **3**- $\text{C}_{12}\text{AuNPs}$  was this latter signal observed suggesting that it was not a major competing process and that the carbene insertion into benzene- $\text{d}_6$  is much slower than X-H insertion or alkene addition.

### 3.3 Conclusion

We have prepared and characterized 3-aryl-3-(trifluoromethyl)diazirine modified gold nanoparticles (**2**- $\text{C}_{12}\text{AuNP}$ ). Further, these are efficient photo-precursors to a reactive carbene at an AuNP interface that can undergo efficient X-H insertion and alkene additions leading to the quantitative modification of the AuNP. Compound **2**- $\text{C}_{12}\text{AuNP}$  serves as a photoreactive template AuNP for the introduction of structural diversity to these particle types. In this study we utilized AuNP with a  $1.8 \pm 0.3$  nm core size, however the results are likely to be general for any similarly modified AuNP. Additionally, the ease of generation of the carbene modified AuNP and its highly reactive nature makes **2**- $\text{C}_{12}\text{AuNP}$  useful for the modification of other surface types, including carbon nanotubes, graphene, polymers, with AuNP; these studies are currently in progress.

Supporting Information:  $^1\text{H}$  and  $^{19}\text{F}$  NMR spectra of **3a-g**- $\text{C}_{12}\text{AuNP}$  and **11a-g**, TEM of **2**- $\text{C}_{12}\text{AuNP}$  and **3a**- $\text{C}_{12}\text{AuNP}$ , IR of **2**- $\text{C}_{12}\text{AuNP}$ , **3a**- $\text{C}_{12}\text{AuNP}$ , and diazo intermediate, and UV-vis spectra of **1**- $\text{C}_{12}\text{AuNP}$ , **2**- $\text{C}_{12}\text{AuNP}$ , and **3a**- $\text{C}_{12}\text{AuNP}$  are provided.

### 3.4 Experimental

#### Commercial Solvents and Reagents Used

Deuterated Benzene ( $C_6D_6$ ), deuterated chloroform ( $CDCl_3$ ) and deuterated dichloromethane ( $CD_2Cl_2$ ) (Cambridge Isotope Laboratories) were also used as received. The compounds dodecanethiol, hydrogen tetrachloroaurate(III), tetraoctylammonium bromide, 1,12-dibromododecane, 3-bromoanisole, n-butyllithium, hydroxylamine hydrochloride, (N, N-dimethylamino) pyridine, p-toluenesulfonylchloride, silver (I) nitrate, boron tribromide, potassium thioacetate, acetyl chloride, phenol, Benzyl alcohol, benzylamine, methyl acrylate and styrene were used as received from the suppliers.

#### General instrumentation

$^1H$ ,  $^{13}C$  and  $^{19}F$  NMR spectra were recorded on either a Varian Inova or Mercury 400 ( $^1H$ : 400 MHz,  $^{13}C$ : 100 MHz and  $^{19}F$ : 376 MHz) spectrometer and chemical shifts are expressed in ppm relative to internal TMS or solvent values ( $CHCl_3$ :  $\delta$  7.26 ppm for  $^1H$  NMR,  $\delta$  77.0 ppm for  $^{13}C$  NMR; and  $CFCl_3$ :  $\delta$  0 ppm for  $^{19}F$  NMR). Mass spectra and exact mass were recorded on a MAT 8200 Finnigan High resolution Mass Spectrometer. Infrared spectra were recorded on a Bruker Vector 33 FTIR spectrometer and are reported in wavenumbers ( $cm^{-1}$ ). The light source was a Hanovia medium pressure mercury lamp (PC 451050 /805221). High resolution transmission electron microscopy (HRTEM) images were collected on a JEOL 2010F HRTEM. UV-vis absorption spectra were recorded on a Cary 100Bio spectrometer in spectrometry grade benzene.

### Synthesis of Dodecanethiolate AuNP (**1-C<sub>12</sub>AuNP**)

Following the procedures of Brust and Murray,<sup>29, 13d</sup> hydrogen tetrachloroaurate (III) trihydrate (0.30 g, 0.77 mmol) was dissolved in 28 ml distilled water (resulting in a bright yellow solution) and then mixed with tetraoctylammonium bromide (2.30 g, 4.2 mmol) in 70 mL toluene. The contents were stirred for 30 minutes at room temperature in order to facilitate the phase transfer of the hydrogen tetrachloroaurate (III) trihydrate into the toluene layer, which resulted in the organic layer turning to a dark orange colour and the aqueous layer becoming clear and colorless. After phase transfer, the aqueous layer was removed and the organic layer was cooled to 0 °C in ice bath. Dodecanethiol (0.468 g, 0.57 mL, 2.31 mmol) was added to the solution via a volumetric pipette and stirred for ten minutes. The addition of dodecanethiol resulted in a colour change from brownish-orange to clear and colorless. A fresh solution of sodium borohydride (0.33 g, 8.7 mmol) in 28 ml water was then added to the rapidly stirring toluene solution over 5 seconds. The solution darkened instantly, eventually becoming dark brown. The mixture stirred overnight (~18 h) as it warmed to room temperature. After this time the aqueous layer was removed and the toluene layer was washed with 3 x 20 mL distilled water and dried over MgSO<sub>4</sub>, filtered, and evaporated to dryness. The resulting mixture of **1-C<sub>12</sub>AuNP** and tetraoctylammonium bromide was suspended in 200 ml of 95 % ethanol and placed in the freezer overnight during which time the **1-C<sub>12</sub>AuNP** precipitated from solution. When the AuNP had precipitated, the supernatant was decanted and the precipitate was dissolved in benzene and concentrated, resulting in the formation of a film in the round bottom flask. This film was washed repeatedly with 10 x 15 ml of 95% ethanol, resulting in pure AuNP as judged by <sup>1</sup>H NMR spectroscopy, which showed no signs of free dodecanethiol,

dodecylsulfide or tetraoctylammonium bromide. The resulting AuNP was dark brown in color.

### Synthesis of Diazirine-modified AuNPs (2-C<sub>12</sub>AuNP)

1-C<sub>12</sub> AuNP (200 mg) was dissolved in 25 ml of benzene and degassed with nitrogen. Diazirine thiol **9** (206 mg, 0.51 mmol) was added to AuNP solution and stirred for 20 h at room temperature. The solvent was evaporated and the resulting dark film was washed with 95% ethanol and dried.

### 2,2,2-trifluoro-1-(3-methoxyphenyl)ethanone, **2**<sup>25–27</sup>

A solution of 3-bromoanisole (1.87 g, 10.0 mmol) in dry THF (30 mL) was cooled to -78 °C under argon. n-BuLi (1.6 M in hexanes, 6.3 mL, 10.0 mmol) was added dropwise over a 5-min period. The mixture was stirred for 30 minutes at -78 °C, and N-trifluoroacetyl piperidine (1.89 g, 10.5 mmol) was added dropwise over a 10-min period with vigorous stirring. After the mixture had been stirred for 3 h, saturated aqueous NH<sub>4</sub>Cl solution (50 mL) was added and the mixture stirred for an additional 1 h at room temperature. The resulting solution was diluted with diethyl ether (150 mL) and washed with water (3 × 100 mL), dried over MgSO<sub>4</sub> and filtered. The solvent was evaporated in vacuo and the crude product was purified by flash chromatography (elution with hexane : dichloromethane, 7:3) to give 1.12 g (54%) of **2** as a pale yellow oil. <sup>1</sup>H NMR (CD<sub>3</sub>Cl, 400 MHz): δ<sub>H</sub> 3.88 (s, 3H), 7.25 (dd, J = 8.3, 2.7 Hz, 1H), 7.45 (t, J = 7.9 Hz, 1H), 7.57 (s, 1H), 7.66 (d, J = 7.8 Hz, 1H) ppm. <sup>19</sup>F NMR (CD<sub>3</sub>Cl, 376 MHz): δ<sub>F</sub> -71.3 ppm. <sup>13</sup>C

NMR (CD<sub>3</sub>Cl, 100 MHz):  $\delta_c$  55.5, 113.9 (q,  $J_{CF} = 1.7$  Hz), 116.5 (q,  $^1J_{CF} = 291.4$  Hz), 122.2, 122.7, (q,  $J_{CF} = 2.7$  Hz), 130.0, 131.0, 159.9, 180.3 ppm.

### **2,2,2-Trifluoro-1-(3-methoxyphenyl)ethanone oxime, 3**

Hydroxylamine hydrochloride (0.43 g, 6.2 mmol) and **2** (1.1 g, 5.4 mmol) were dissolved in absolute ethanol (5 mL) and pyridine (10 mL) and heated at 60 °C for 13 h. The solvent was evaporated in vacuo and the residue was partitioned between water (50 mL) and diethyl ether (50 mL). The ethereal phase was washed with 1N HCl solution and water (25 mL) and dried over MgSO<sub>4</sub> and filtered. The solvent was evaporated in vacuo and the crude product was purified by flash chromatography (elution with dichloromethane : methanol, 20:1) to afford 1.08 g (90%) of **3** as yellow crystals. <sup>1</sup>H NMR (CD<sub>3</sub>Cl, 400 MHz):  $\delta_H$  3.84 (s, 3H), 7.03-7.09 (m, 3H), 7.32-7.42 (m, 1H), 8.29 (broad, 0.3 H), 8.52 (broad, 0.7H) ppm. <sup>13</sup>C NMR of cis and trans isomers (CD<sub>3</sub>Cl, 100 MHz):  $\delta_c$  55.37, 55.39, 113.9, 114.2, 116.1, 116.2, 118.3 (q,  $^1J_{CF} = 283.1$  Hz), 120.5 (q,  $^1J_{CF} = 274.8$  Hz), 120.8, 127.1, 129.6, 129.7, 131.2, 147.8 (q,  $J_{CF} = 36.2$  Hz), 159.4 ppm.

### **2,2,2-Trifluoro-1-(3-methoxyphenyl)-N-[[4-methylphenyl]sulfonyl]oxy}ethanimine,**

#### **4**

A solution of triethylamine (1.76 g, 17.4 mmol), (N, N-dimethylamino) pyridine (50 mg, 0.4 mmol) and oxime **3** (1.3 g, 5.9 mmol) were dissolved in dry CH<sub>2</sub>Cl<sub>2</sub> and cooled to 0 °C. *p*-Toluenesulfonylchloride (1.33 g, 7 mmol) was added portionwise to the mixture. After stirring for 90 minutes, water was added to the mixture. Organic layer was washed with water (3 × 30 mL), dried over MgSO<sub>4</sub> and filtered. The solvent was

evaporated in vacuo to give **4** in quantitative yield.  $^1\text{H}$  NMR ( $\text{CD}_3\text{Cl}$ , 400 MHz):  $\delta_{\text{H}}$  2.47 (s, 3H), 3.81 (s, 3H), 6.88-7.07 (m, 3H), 7.31-7.40 (m, 3H), 7.87-7.91 (m, 2H) ppm.

### **3-(3-Methoxyphenyl)-3-(trifluoromethyl)diaziridine, 5**

Imine **4** (1.8 g, 4.82 mmol) was dissolved in dry  $\text{CH}_2\text{Cl}_2$  (10 mL) and added portionwise to liquid ammonia (*ca.* 40 mL) at  $-78\text{ }^\circ\text{C}$ . The reaction mixture was warmed up to  $-34\text{ }^\circ\text{C}$  using a dry ice condenser and stirred for 12 h. The reaction was then warmed up to room temperature. The excess ammonia evaporated and the mixture was concentrated in vacuo. The residue was partitioned between water (50 mL) and diethyl ether (50 mL). The ethereal phase was washed with water ( $3 \times 30\text{ mL}$ ), dried over  $\text{MgSO}_4$ , filtered and concentrated in vacuo. Purification of the crude product by flash chromatography (elution with chloroform: ethyl acetate 10:1) gave 0.66 g (64%) pure **5** as white solid.  $^1\text{H}$  NMR ( $\text{CD}_3\text{Cl}$ , 400 MHz):  $\delta_{\text{H}}$  2.34 (d,  $J = 8.6\text{ Hz}$ , 1H), 2.86 (d,  $J = 8.05\text{ Hz}$ , 1H), 3.87 (s, 3H), 7.03 (d,  $J = 8.3\text{ Hz}$ , 1H), 7.2 (s, 1H), 7.25 (d,  $J = 7.6\text{ Hz}$ , 1H), 7.38 (tt,  $J = 1.4, 7.6\text{ Hz}$ , 1H) ppm.  $^{19}\text{F}$  NMR ( $\text{CD}_3\text{Cl}$ , 376 MHz):  $-75.5\text{ ppm}$ .  $^{13}\text{C}$  NMR ( $\text{CD}_3\text{Cl}$ , 100 MHz):  $\delta_{\text{C}}$  55.3, 57.9 (q,  $J_{\text{CF}} = 35.9\text{ Hz}$ ), 113.5, 115.7, 120.2, 123.4 (q,  $^1J_{\text{CF}} = 278.3\text{ Hz}$ ), 129.8, 132.9, 159.6 ppm.

### **3-(3-Methoxyphenyl)-3-(trifluoromethyl)-3H-diazirine, 6**

Silver oxide was prepared as follows: Silver (I) nitrate (6.3g, 37.08 mmol) was dissolved in water (30 mL) and heated to boiling. A solution of sodium hydroxide (1.48 g, 37 mmol) in water (30 mL) was added slowly to the silver (I) nitrate solution and stirred for 5 minutes at boiling point. The brown solid was filtered and washed thoroughly with water (100 mL), acetone (200 mL), and diethyl ether (200 mL),

respectively. A mixture of diaziridine **5** (0.5 g, 2.29 mmol) and silver oxide (2.31g, 10 mmol) in dry diethyl ether (10 mL) was stirred for 12 h at room temperature. The mixture was filtered and the solvent was evaporated to give 0.42 g of **6** (83%) as a pale yellow oil.  $^1\text{H}$  NMR ( $\text{CD}_3\text{Cl}$ , 400 MHz):  $\delta_{\text{H}}$  3.81 (s, 3H), 6.69 (s, 1H), 6.77 (d,  $J = 7.8$  Hz, 1H), 6.94 (dd,  $J = 2.15, 8.3$  Hz, 1H), 7.31 (t,  $J = 7.9$  Hz, 1H), ppm.  $^{19}\text{F}$  NMR ( $\text{CD}_3\text{Cl}$ , 376 MHz): -65.6 ppm.  $^{13}\text{C}$  NMR ( $\text{CD}_3\text{Cl}$ , 100 MHz):  $\delta_{\text{C}}$  41.9, 55.3, 112.2, 115.2, 118.7, 122.0 (q,  $^1J_{\text{CF}} = 274.6$  Hz), 130.0, 130.5, 159.8 ppm.

### **3-(3-(12-bromododecyloxy)phenyl)-3-(trifluoromethyl)-3H-diazirine, 8**

A solution of diazirine **6** (0.4 g, 1.85 mmol) in dry  $\text{CH}_2\text{Cl}_2$  (10 mL) was cooled in ice bath.  $\text{BBr}_3$  (1 M in  $\text{CH}_2\text{Cl}_2$ , 3.7 mL, 3.7 mmol) was added over a 5-min period and the reaction mixture was stirred for 7 h at 0 °C. Water was added to the mixture and the organic compounds were extracted with diethyl ether. The combined organic layers were washed with aqueous  $\text{NaHCO}_3$  and water ( $2 \times 20$  mL) and the ethereal layer was dried over  $\text{MgSO}_4$ , filtered and concentrated in vacuo to give corresponding phenol **7**. Without further purification, compound **7** was used for the alkylation reaction.  $\text{K}_2\text{CO}_3$  (100 mg, 0.72 mmol) was added to a solution of **7** (130 mg, 0.64 mmol) and 1,12-dibromododecane (1.26 g, 3.8 mmol) in acetone (10 mL). The reaction mixture was refluxed overnight and then filtered. After evaporation of solvent, the residue was partitioned between water (20 mL) and  $\text{CH}_2\text{Cl}_2$  (20 mL). The organic layer was washed with water ( $3 \times 20$  mL), dried over  $\text{MgSO}_4$ , filtered and concentrated under reduced pressure. Purification of the crude product by flash chromatography (elution with hexane) gave 210 mg (73%) of **8** as pale yellow oil.  $^1\text{H}$  NMR ( $\text{CD}_3\text{Cl}$ , 400 MHz):  $\delta_{\text{H}}$  1.28-1.42



(broad, 16H), 1.77 (q,  $J = 6.7$  Hz, 2H), 1.85 (q,  $J = 7.1$  Hz, 2H), 3.41 (t,  $J = 6.9$  Hz, 2H), 3.93 (t,  $J = 6.5$  Hz, 2H), 6.67(s, 1H), 6.75 (d,  $J = 7.8$  Hz, 1H), 6.92 (dd,  $J = 2.5, 8.3$  Hz, 1H), 7.29 (t,  $J = 7.9$  Hz, 1H) ppm.  $^{19}\text{F}$  NMR ( $\text{CD}_3\text{Cl}$ , 376 MHz): -65.5 ppm.  $^{13}\text{C}$  NMR ( $\text{CD}_3\text{Cl}$ , 100 MHz):  $\delta_{\text{c}}$  25.9, 28.1, 28.7, 29.1, 29.3, 29.4, 29.5, 32.8, 34.0, 68.1, 112.8, 115.6, 118.4, 122.0 (q,  $^1J_{\text{CF}} = 276.6$  Hz), 129.9, 130.4, 159.3 ppm. FT-IR ( $\text{cm}^{-1}$ , dropcast on NaCl): 2926, 2855, 1607, 1583, 1494, 1467, 1447, 1354, 1323, 1293, 1263, 1209, 1181, 1156, 783, 732, 691, 650. HRMS: calculated  $m/z$ ; 448.1337, found: 448.1334.

**S-12-(3-(3-(trifluoromethyl)-3H-diazirine-3-yl)phenoxy)dodecyl ethanethioate, 9a**

Potassium thioacetate (53 mg, 0.46 mmol) was added to a solution of **8** (170 mg, 0.38 mmol) in acetone (10 mL). The reaction mixture was heated at reflux for overnight and then filtered. After evaporation of solvent, the residue was partitioned between water (10 mL) and  $\text{CH}_2\text{Cl}_2$  (10 mL). The organic layer was washed with water ( $3 \times 10$  mL), dried over  $\text{MgSO}_4$ , filtered and concentrated under reduced pressure to afford diazirine ethanethioate (170 mg, 100%).  $^1\text{H}$  NMR ( $\text{CD}_3\text{Cl}$ , 400 MHz):  $\delta_{\text{H}}$  1.27-1.48 (broad, 16H), 1.56 (q,  $J = 7.0$  Hz, 2H), 1.77 (q,  $J = 6.7$  Hz, 2H), 2.32 (s, 3H), 2.86 (t,  $J = 7.4$  Hz, 2H), 3.93 (t,  $J = 6.6$  Hz, 2H), 6.67(s, 1H), 6.75 (d,  $J = 7.8$  Hz, 1H), 6.92 (dd,  $J = 2.4, 8.3$  Hz, 1H), 7.29 (t,  $J = 7.9$  Hz, 1H) ppm.  $^{19}\text{F}$  NMR ( $\text{CD}_3\text{Cl}$ , 376 MHz): -65.5 ppm.  $^{13}\text{C}$  NMR ( $\text{CD}_3\text{Cl}$ , 100 MHz):  $\delta_{\text{c}}$  26.0, 28.8, 29.10, 29.13, 29.2, 29.3, 29.4, 29.50, 29.52, 30.6, 36.0, 68.1, 112.8, 115.6, 118.5, 121.97 (q,  $^1J_{\text{CF}} = 250.0$  Hz), 129.9, 130.4, 159.3, 196.0 ppm. FT-IR ( $\text{cm}^{-1}$ , dropcast on NaCl): 2930, 2856, 1694, 1607, 1584, 1495, 1464, 1447, 1353, 1293, 1263, 1208, 1178, 1157, 1110, 957, 780, 730, 691, 652, 627. HRMS: calculated  $m/z$ ; 444.2058, found: 444.2070.

### **12-(3-(3-(trifluoromethyl)-3H-diazirin-3-yl)phenoxy)dodecane-1-thiol, 9**

A solution of S-12-(3-(3-(trifluoromethyl)-3H-diazirine-3-yl)phenoxy)dodecyl ethanethioate (**9a**) (170 mg, 0.38 mmol) in dry methanol was cooled in the ice bath, then acetyl chloride was added dropwise and the solution was stirred for 6 h at room temperature. Water was added to the mixture and organic compounds was extracted with CH<sub>2</sub>Cl<sub>2</sub>. Combined extracts were washed with water (3 × 10 mL), the organic layer was dried over MgSO<sub>4</sub> and evaporated to get pure title compound **9**, 152.8 mg (100%) as pale yellow oil. <sup>1</sup>H NMR (CD<sub>3</sub>Cl, 400 MHz): δ<sub>H</sub> 1.27-1.48 (broad, 17H), 1.60 (q, J = 7.6 Hz, 2H), 1.77 (q, J = 7.2 Hz, 2H), 2.52 (q, J = 7.4 Hz, 2H), 3.93 (t, J = 6.5 Hz, 2H), 6.67(s, 1H), 6.75 (d, J = 7.8 Hz, 1H), 6.92 (dd, J = 2.0, 8.1 Hz, 1H), 7.29 (t, J = 8.1 Hz, 1H) ppm. <sup>19</sup>F NMR (CD<sub>3</sub>Cl, 376 MHz): -65.6 ppm. <sup>13</sup>C NMR (CD<sub>3</sub>Cl, 100 MHz): δ<sub>c</sub> 24.6, 26.0, 28.3, 29.0, 29.10, 29.3, 29.4, 29.50, 34.0, 68.1, 112.8, 115.6, 118.5, 122.1 (q, <sup>1</sup>J<sub>CF</sub> = 275.0 Hz), 129.9, 130.4, 159.3 ppm. FT-IR (cm<sup>-1</sup>, dropcast on NaCl): 2925, 2853, 2220, 1606, 1584, 1493, 1447, 1349, 1292, 1260, 1206, 1156, 1107, 844, 779, 729, 692. HRMS: calculated m/z; 402.1969 found: 402.1965.

### **General procedure for photolysis of diazirine-modified AuNPs, model diazirine 6 and the following carbene insertion**

#### **Synthesis of 3a-g-C<sub>12</sub>AuNPs**

**2-C<sub>12</sub>AuNP** (10 mg) was dissolved in 1 ml of deuterated benzene. The substrate **10a-g** (in a 1:10-15 molar ratio, diazirine group on the **2-C<sub>12</sub>AuNPs**: **10a-g**) was added to the solution of **2-C<sub>12</sub>AuNP**. The mixture was placed in a Pyrex NMR tube, degassed with argon for 10 minutes and irradiated using medium pressure mercury lamp (Hanovia PC

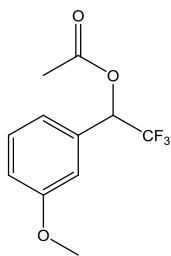
451050 /805221) at room temperature. The solvent was evaporated and the product **3a-g-C<sub>12</sub>AuNPs** were purified by washing with 95% ethanol and then CH<sub>3</sub>CN. IR and <sup>19</sup>F NMR and <sup>1</sup>H NMR spectroscopy were used to monitor the completion of the reaction and purity of the products.

### Synthesis of **11a-g** model compounds.

Compound **6** (20 mg) was dissolved in 1 ml of deuterated benzene. The substrate **10a-g** (in a 1:10-15 molar ratio, 6: of **10a-g**) was added to the solution of **6**. The mixture was placed in a Pyrex NMR tube, degassed with argon for 10 minutes and irradiated using medium pressure mercury lamp (Hanovia PC 451050 /805221) at room temperature. The solvent was evaporated and the products **11a-g** was purified by flash chromatography (elution with hexanes : dichloromethane , 3:1). IR and <sup>19</sup>F NMR spectroscopy were used to monitor the completion of the reaction and purity of the products.

### **3a-C<sub>12</sub>AuNP**

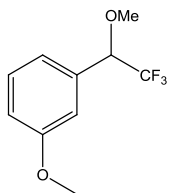
<sup>1</sup>H NMR (CD<sub>2</sub>Cl<sub>2</sub>, 400 MHz): δ<sub>H</sub> 0.84-1.76 (broad), 2.15 (broad), 3.92 (broad), 6.07 (broad), 6.93-7.28 (broad). <sup>19</sup>F NMR (CD<sub>2</sub>Cl<sub>2</sub>, 376 MHz): δ<sub>F</sub> -75.9. FT-IR (cm<sup>-1</sup>, dropcast on NaCl): 2955, 2921, 2851, 1763, 1651, 1462, 1260, 1212, 1177, 1161, 1133, 1074, 1049, 1024, 799.



**11a.** Colorless Oil,  $^1\text{H}$  NMR ( $\text{CD}_3\text{Cl}$ , 400 MHz):  $\delta_{\text{H}}$  2.20 (s, 3H), 3.83(s, 3H), 6.10 (q,  $J = 6.9$  Hz, 1H), 6.95 (ddd,  $J = 0.88, 2.6, 8.3$  Hz, 1H), 6.99 (s, 1H), 7.04 (d,  $J = 7.6$  Hz, 1H), 7.32 (t,  $J = 7.9$  Hz, 1H) ppm.  $^{19}\text{F}$  NMR ( $\text{CD}_3\text{Cl}$ , 376 MHz):  $\delta_{\text{F}}$  -76.0 ppm.  $^{13}\text{C}$  NMR ( $\text{CD}_3\text{Cl}$ , 100 MHz):  $\delta_{\text{C}}$  20.5, 55.3, 71.7 (q,  $J_{\text{CF}} = 34.7$  Hz), 113.7, 115.2, 120.3, 123.0 (q,  $^1J_{\text{CF}} = 280.7$  Hz), 129.7, 132.5, 159.6, 168.5 ppm. FT-IR ( $\text{cm}^{-1}$ , dropcast on NaCl): 2958, 2942, 2844, 1762, 1606, 1494, 1463, 1438, 1374, 1351, 1320, 1268, 1220, 1180, 1134, 1089, 1046, 926, 848, 788, 713, 690. HRMS: calculated  $m/z$ ; 248.0660, found: 248.0669.

### 3b- $\text{C}_{12}\text{AuNP}$

$^1\text{H}$  NMR ( $\text{CD}_2\text{Cl}_2$ , 400 MHz):  $\delta_{\text{H}}$  0.87-1.742 (broad), 3.37 (broad), 3.92 (broad), 4.47 (broad), 6.65-6.94 (broad), 7.29 (broad) ppm.  $^{19}\text{F}$  NMR ( $\text{CD}_2\text{Cl}_2$ , 376 MHz):  $\delta_{\text{F}}$  -77.4. FT-IR ( $\text{cm}^{-1}$ , dropcast on NaCl): 2920, 2872, 2085, 1722, 1604, 1591, 1465, 1447, 1262, 1172, 1140, 718.

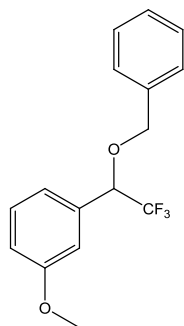


**11b.** Yellow oil,  $^1\text{H}$  NMR ( $\text{CD}_3\text{Cl}$ , 400 MHz):  $\delta_{\text{H}}$  3.42 (s, 3H), 3.83(s, 3H), 4.47 (q,  $J = 6.6$  Hz, 1H), 6.95 (dd,  $J = 2.6, 8.2$  Hz, 1H), 6.98-7.01 (m, 2H), 7.33 (t,  $J = 7.9$  Hz, 1H) ppm.  $^{19}\text{F}$  NMR ( $\text{CD}_3\text{Cl}$ , 376 MHz):  $\delta_{\text{F}}$  -76.9 ppm.  $^{13}\text{C}$  NMR ( $\text{CD}_3\text{Cl}$ , 100 MHz):

$\delta_c$  55.3, 58.1, 81.2 (q,  $J_{CF} = 31$  Hz), 113.4, 115.1, 120.6, 123.7 (q,  $^1J_{CF} = 281.7$  Hz), 129.6, 133.9, 159.4 ppm. FT-IR ( $\text{cm}^{-1}$ , dropcast on NaCl): 2933, 2875, 1725, 1606, 1588, 1492, 1456, 1372, 1344, 1265, 1175, 1138, 1112, 784, 716. HRMS: calculated m/z; 220.0711, found: 220.0718.

### 3c-C<sub>12</sub>AuNP

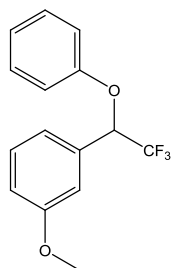
$^1\text{H}$  NMR ( $\text{CD}_3\text{Cl}$ , 400 MHz):  $\delta_{\text{H}}$  0.82-1.76 (broad), 3.89 (broad), 4.42 (broad), 4.62 (broad), 6.97-7.34 (broad) ppm.  $^{19}\text{F}$  NMR ( $\text{CD}_2\text{Cl}_2$ , 376 MHz):  $\delta_{\text{F}}$  -76.7 ppm. FT-IR ( $\text{cm}^{-1}$ , dropcast on NaCl): 2924, 2854, 1720, 1680, 1605, 1585, 1463, 1372, 1260, 1199, 1170, 1136, 1076, 1044, 1027, 795, 758, 720.



**11c.** Yellow oil,  $^1\text{H}$  NMR ( $\text{CD}_3\text{Cl}$ , 400 MHz):  $\delta_{\text{H}}$  3.80 (s, 3H), 4.46 (d,  $J = 12.0$  Hz, 1H), 4.63 (q,  $J = 6.6$  Hz, 1H), 4.69 (d,  $J = 12.0$  Hz, 1H), 6.95-7.03 (m, 3H), 7.31- 7.39 (m, 6H) ppm.  $^{19}\text{F}$  NMR ( $\text{CD}_3\text{Cl}$ , 376 MHz):  $\delta_{\text{F}}$  -76.3 ppm.  $^{13}\text{C}$  NMR ( $\text{CD}_3\text{Cl}$ , 100 MHz):  $\delta_c$  55.3, 71.4, 78.3 (q,  $J_{CF} = 31.2$  Hz), 113.7, 115.2, 120.8, 123.8 (q,  $^1J_{CF} = 274.4$  Hz), 127.9, 128.2, 128.5, 129.6, 133.0, 136.5, 159.8 ppm. FT-IR ( $\text{cm}^{-1}$ , dropcast on NaCl): 3066, 3034, 3007, 2941, 2926, 2877, 2840, 1954, 1877, 1726, 1604, 1589, 1493, 1466, 1456, 1318, 1260, 1244, 1174, 1134, 1131, 1105, 1080, 1076, 1049, 1030, 1011, 997, 859, 789, 752, 739, 715, 699. HRMS: calculated m/z; 296.1024, found: 296.1033.

**3d-C<sub>12</sub>AuNP**

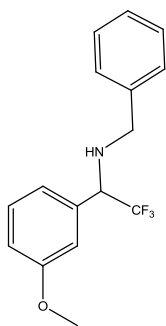
<sup>1</sup>H NMR (CD<sub>2</sub>Cl<sub>2</sub>, 400 MHz): δ<sub>H</sub> 0.90-1.78 (broad), 3.82 (broad), 5.2 (broad). <sup>19</sup>F NMR (CD<sub>2</sub>Cl<sub>2</sub>, 376 MHz): δ<sub>F</sub> -77.4 ppm. FT-IR (cm<sup>-1</sup>, dropcast on NaCl): 2922, 2851, 1602, 1587, 1491, 1462, 1348, 1258, 1194, 1163, 1116, 994, 718, 639.



**11d.** Colorless oil, <sup>1</sup>H NMR (CD<sub>2</sub>Cl<sub>2</sub>, 400 MHz): δ<sub>H</sub> 3.81 (s, 3H), 5.36 (q, J = 6.3 Hz, 1H), 6.89-6.95 (m, 3H), 6.98 (tt, J = 1, 7.4 Hz, 1H), 7.06 (s, 1H), 7.09 (d, J = 7.6 Hz, 1H), 7.21-7.25 (m, 2H), 7.32 (t, J = 7.8 Hz, 1H) ppm. <sup>19</sup>F NMR (CD<sub>3</sub>Cl, 376 MHz): δ<sub>F</sub> -77.0 ppm. <sup>13</sup>C NMR (CD<sub>3</sub>Cl, 100 MHz): δ<sub>c</sub> 55.3, 78.2 (q, J<sub>CF</sub> = 32.1 Hz), 113.4, 115.1, 116.1, 120.2, 122.4, 123.3 (q, <sup>1</sup>J<sub>CF</sub> = 281.1 Hz), 129.6, 129.8, 133.7, 156.9, 159.8 ppm. FT-IR (cm<sup>-1</sup>, dropcast on NaCl): 3064, 3041, 3009, 2941, 2839, 1610, 1549, 1492, 1461, 1437, 1363, 1318, 1266, 1232, 1179, 1136, 1082, 904, 863, 786, 755, 691, 556, 516. HRMS: calculated m/z; 282.0867, found: 282.0867.

**3e-C<sub>12</sub>AuNP**

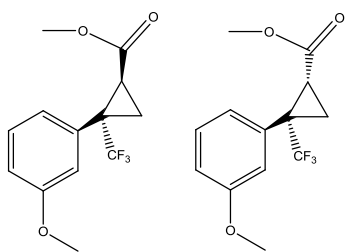
<sup>1</sup>H NMR (CD<sub>2</sub>Cl<sub>2</sub>, 400 MHz): δ<sub>H</sub> 0.85-1.76 (broad), 3.62-4.05 (broad), 6.59-7.25 (broad) ppm. <sup>19</sup>F NMR (CD<sub>2</sub>Cl<sub>2</sub>, 376 MHz): δ<sub>F</sub> -74.2 ppm. FT-IR (cm<sup>-1</sup>, dropcast on NaCl): 2923, 2852, 1697, 1652, 1559, 1540, 1506, 1498, 1458, 1437, 1360, 1259, 1162, 1124, 718, 700.



**11e.**  $^1\text{H}$  NMR ( $\text{CD}_3\text{Cl}$ , 400 MHz):  $\delta_{\text{H}}$  2.01 (broad, 1H), 3.67 (d,  $J = 13.4$  Hz, 1H), 3.83 (s, 3H), 3.84 (d,  $J = 13.4$  Hz, 1H), 4.10 (q,  $J = 7.4$  Hz, 1H), 6.92 (ddd,  $J = 0.9, 2.6, 8.3$  Hz, 1H), 6.97-6.99 (m, 2H), 7.27- 7.35 (m, 6H) ppm.  $^{19}\text{F}$  NMR ( $\text{CD}_3\text{Cl}$ , 376 MHz):  $\delta_{\text{F}}$  -73.9 ppm.  $^{13}\text{C}$  NMR ( $\text{CD}_3\text{Cl}$ , 400 MHz):  $\delta_{\text{C}}$  51.0, 55.3, 63.3 (q,  $J_{\text{CF}} = 28.7$  Hz), 114.2, 114.4, 120.9, 125.4 (q,  $^1J_{\text{CF}} = 281.4$  Hz), 127.3, 128.2, 128.5, 129.7, 135.7, 138.9, 159.8 ppm. FT-IR ( $\text{cm}^{-1}$ , dropcast on NaCl): 3348 (broad), 3063, 3030, 3006, 2957, 2937, 2922, 2840, 1701, 1607, 1591, 1492, 1458, 1437, 1346, 1316, 1259, 1162, 1121, 1083, 1046, 853, 785, 738, 701, 643. HRMS: calculated  $m/z$  295.1184, found: 295.1180.

### **3f- $\text{C}_{12}\text{AuNP}$**

$^1\text{H}$  NMR ( $\text{CD}_2\text{Cl}_2$ , 400 MHz):  $\delta_{\text{H}}$  0.85-1.78 (broad), 2.48 (broad), 3.49 (broad), 3.78 -3.92 (broad), 6.76-3.38 (broad) ppm.  $^{19}\text{F}$  NMR ( $\text{CD}_2\text{Cl}_2$ , 376 MHz):  $\delta_{\text{F}}$  -70.4, -65.2 ppm. FT-IR ( $\text{cm}^{-1}$ , dropcast on NaCl): 2957, 2920, 2850, 1744, 1725, 1603, 1587, 1462, 1412, 1374, 1351, 1294, 1260, 1204, 1161, 1091, 1020, 799, 750, 718.



**11f.** Major product (ratio 3:1):  $^1\text{H}$  NMR ( $\text{CD}_3\text{Cl}$ , 400 MHz):

$\delta_{\text{H}}$  1.71 (dd,  $J = 5.5, 8.7$  Hz, 1H), 1.84 – 1.87 (m, 1H), 2.49 (dd,  $J = 6.3, 8.7$  Hz, 1H), 3.53 (s, 3H), 3.79 (s, 3H), 6.87- 6.95 (m, 3H), 7.22- 7.30 (m, 1H) ppm.  $^{13}\text{C}$  NMR ( $\text{CD}_3\text{Cl}$ , 400 MHz):  $\delta_{\text{C}}$  14.7, 23.7, 35.9 (q,  $J_{\text{CF}} = 33.7$  Hz), 52.4, 55.4, 114.5, 117.1, 123.5, 125.3 (q,  $^1J_{\text{CF}} = 274.7$  Hz), 129.6, 133.0, 159.6, 169.4 ppm.

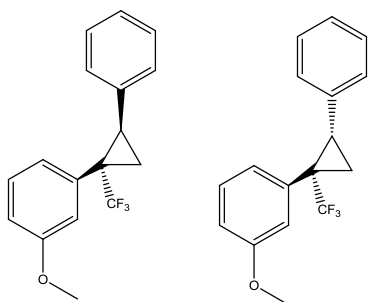
Minor Product:  $^1\text{H}$  NMR ( $\text{CD}_3\text{Cl}$ , 400 MHz):  $\delta_{\text{H}}$  1.49-1.55 (m, 1H), 2.03 (dd,  $J = 5.8, 7.3$  Hz, 1H), 2.26 (t,  $J = 7.5$  Hz, 1H), 3.79 (s, 3H), 3.82 (s, 3H), 6.87- 6.95 (m, 1H), 7.02 (s, 1H), 7.07 (d,  $J = 7.7$  Hz, 1H), 7.22- 7.30 (m, 1H) ppm.  $^{13}\text{C}$  NMR ( $\text{CD}_3\text{Cl}$ , 400 MHz):  $\delta_{\text{C}}$  14.4, 23.5, 35.9 (q,  $J_{\text{CF}} = 33.7$  Hz), 52.8, 55.7, 114.4, 116.8, 123.2, 125.5 (q,  $^1J_{\text{CF}} = 273.4$  Hz), 129.8, 133.0, 159.7, 169.4 ppm.

$^{19}\text{F}$  NMR of mixture ( $\text{CD}_3\text{Cl}$ , 376 MHz):  $\delta_{\text{F}}$  -70.5, -65.4 ppm. FT-IR of mixture ( $\text{cm}^{-1}$ , dropcast on NaCl): 3004, 2954, 2925, 2843, 1743, 1605, 1586, 1492, 1455, 1437, 1397, 1347, 1299, 1236, 1205, 1158, 1145, 1111, 1071, 1045, 997, 977, 940, 863, 818, 786, 700, 637. HRMS: calculated  $m/z$ ; 274.0816, found: 274.0810.

### **3g-C<sub>12</sub>AuNP**

$^1\text{H}$  NMR ( $\text{CD}_2\text{Cl}_2$ , 400 MHz):  $\delta_{\text{H}}$  0.86-2.21 (broad), 2.68-2.8 (broad), 3.62-3.92 (broad), 6.46-7.39 (broad) ppm.  $^{19}\text{F}$  NMR ( $\text{CD}_3\text{Cl}$ , 376 MHz):  $\delta_{\text{F}}$  -63.7, -70.0 ppm. FT-IR ( $\text{cm}^{-1}$ , dropcast on NaCl): 3060, 3026, 2921, 2851, 1602, 1492, 1450, 1350, 1288, 1233, 1211, 1147, 754, 698.





**11g.** Spectroscopic data for the mixture of major and minor

isomers (ratio 1.4:1).  $^1\text{H}$  NMR ( $\text{CD}_3\text{Cl}$ , 400 MHz):  $\delta_{\text{H}}$  1.60 (m, 0.7H), 1.68 (t,  $J = 7.3$  Hz, 1H), 1.86 (dd,  $J = 5.9, 9.6$  Hz, 1H), 1.94 (dd,  $J = 5.6, 7.4$  Hz, 0.7H), 2.73 (t,  $J = 8.2$  Hz, 0.7H), 2.83 (dd,  $J = 6.9, 9.6$  Hz, 1H), 3.61 (s, 3H), 3.86 (s, 2.1 H), 6.62 (s, 1H), 6.73-6.81 (m, 4H), 6.90 (dd,  $J = 3.3, 8.3$  Hz, 0.7H), 7.06-7.14 (m, 5H), 7.19 (d,  $J = 7.9, 0.7\text{H}$ ), 7.28-7.44 (m, 3H) ppm.  $^{19}\text{F}$  NMR ( $\text{CD}_3\text{Cl}$ , 376 MHz):  $\delta_{\text{F}}$  -63.7, -69.8 ppm.  $^{13}\text{C}$  NMR ( $\text{CD}_3\text{Cl}$ , 400 MHz):  $\delta_{\text{C}}$  14.7, 25.6, 35.9, 55.1, 55.3, 113.5, 114.1, 117.2, 117.9, 123.4, 124.0 (q,  $^1J_{\text{CF}} = 272.2$  Hz), 124.9, 125.6 (q,  $^1J_{\text{CF}} = 271.2$  Hz), 126.5, 127.8, 127.9, 128.2, 128.8, 129.3, 129.5, 131.2, 134.4, 155.8 ppm. FT-IR of mixture ( $\text{cm}^{-1}$ , dropcast on NaCl): 3061, 3031, 3005, 2953, 2925, 2851, 2843, 1727, 1604, 1585, 1492, 1459, 1431, 1351, 1316, 1287, 1235, 1217, 1139, 1084, 1041, 781, 697. HRMS: calculated  $m/z$ ; 292.1075, found: 292.1073.

## References

- 1) (a) Corma, A.; Garcia, H. *Chem. Soc. Rev.* **2008**, *37*, 2096, and references therein. (b) Juárez, R.; Corma, A.; García, H. *Green Chem.* **2009**, *11*, 949. (c) Conte, M.; Miyamura, H.; Kobayashi, S.; Chechik, V. *J. Am. Chem. Soc.* **2009**, *131*, 7189. (d) Raptis, C., Garcia, H., Stratakis, M. *Angew. Chem. Int. Ed.* **2009**, *48*, 3133.

- 2) (a) Wang, Z.; Ma, L. *Coord. Chem. Rev.* **2009**, *253*, 1607, and references therein. (b) Sperling, R. A.; Rivera, P. G.; Zhang, F.; Zanella, M.; Parak, W. J. *Chem. Soc. Rev.* **2008**, *37*, 1896, and references therein.
- 3) (a) Ghosh, P.; Han, G.; De, M.; Kim, C. K.; Rotello, V. M. *Adv. Drug Deliver. Rev.* **2008**, *60*, 1307, and references therein. (b) Nakanishi, J.; Nakayama, H.; Shimizu, T.; Ishida, H.; Kikuchi, Y.; Yamaguchi, K.; Horiike, Y. *J. Am. Chem. Soc.* **2009**, *131*, 3822. (c) Elbakry, A.; Zaky, A.; Liebl, R.; Rachel, R.; Goepferich, A.; Breunig, M. *Nano Lett.* **2009**, *9*, 2059. (d) Prabakaran, M.; Grailer, J. J.; Pilla, S.; Steeber, D. A.; Gong, S. *Biomaterials* **2009**, *30*, 6065.
- 4) (a) Chen, P. C.; Mwakwari, S. C.; Oyelere, A. K. *Nanotechnol., Sci. Appl.* **2008**, *1*, 45, and references therein. (b) Boisselier, E.; Astruc, D. *Chem. Soc. Rev.* **2009**, *38*, 1759.
- 5) (a) Daniel, M. C.; Astruc, D. *Chem. Rev.* **2004**, *104*, 293. (b) Shon, Y. S.; Choo, H. C. *R. Chimie* **2003**, *6*, 1009.
- 6) Brust, M.; Fink, J.; Bethella, D.; Schiffrina, D. J.; Kiely, C. *J. Chem. Soc., Chem. Commun.* **1995**, 1655.
- 7) Buining, P. A.; Humbel, B. M.; Philipse, A. P.; Verkleij, A. J. *Langmuir* **1997**, *13*, 3921.
- 8) Templeton, A. C.; Hostetler, M. J.; Kraft, C. T.; Murray, R. W. *J. Am. Chem. Soc.* **1998**, *120*, 1906.
- 9) Watson, K. J.; Zhu, J.; Nguyen, S. T.; Mirkin, C. A. *J. Am. Chem. Soc.* **1999**, *121*, 462.
- 10) (a) Friggeri, A.; Van Manen, H. J.; Auletta, T.; Li, X. M.; Zapotoczny, S.; Schönherr, H.; Vancso, G. J.; Huskens, J.; Van Veggel, F. C. J. M.; Reinhoudt, D. N. *J. Am.*

- Chem. Soc.* **2001**, *123*, 6388. (b) Fan, J.; Chen, S.; Gao, Y. *Colloids Surf. B* **2003**, *28*, 199.
- 11) Otsuka, H.; Akiyama, Y.; Nagasaki, Y.; Kataoka, K. *J. Am. Chem. Soc.* **2001**, *123*, 8226.
- 12) Koenig, S.; Chechik, V. *Langmuir* **2003**, *19*, 9511.
- 13) (a) Fleming, D. A.; Thode, C. J.; Williams, M. E. *Chem. Mater.* **2006**, *18*, 2327. (b) Sommer, W. J.; Weck, M. *Langmuir* **2007**, *23*, 11991. (c) Zhu, J.; Lines, B. M.; Ganton, M. D.; Kerr, M. A.; Workentin, M. S. *J. Org. Chem.* **2008**, *73*, 1099. (d) Ismaili, H.; Alizadeh, A.; Snell, K. E.; Workentin, M. S. *Can. J. Chem.* **2009**, *87*, 1708.
- 14) Zhu, J.; Ganton, M.; Kerr, M. A.; Workentin, M. S. *J. Am. Chem. Soc.* **2007**, *129*, 4904.
- 15) Thode, C. J.; Williams, M. E. *Langmuir* **2008**, *24*, 5988.
- 16) Ornelas, C.; Méry, D.; Cloutet, E.; Aranzaes, J. R.; Astruc, D. *J. Am. Chem. Soc.* **2008**, *130*, 1495.
- 17) (a) Kell, A. J.; Stringle, D. L. B.; Workentin, M. S. *Org. Lett.* **2000**, *2*, 3381. (b) Kell, A. J.; Workentin, M. S. *Langmuir* **2001**, *17*, 7355. (c) Kell, A. J.; Montcalm, C. C.; Workentin, M. S. *Can. J. Chem.* **2003**, *81*, 484. (d) Kondo, T.; Uosaki, K. *J. Photochem. Photobio. C* **2007**, *8*, 1. (e) Nakanishi, J.; Nakayama, H.; Shimizu, T.; Ishida, H.; Kikuchi, Y.; Yamaguchi, K.; Horiike, Y. *J. Am. Chem. Soc.* **2009**, *131*, 3822.

- 18) (a) Jonkheijm, P.; Weinrich, D.; Schröder, H.; Niemeyer, C. M.; Waldmann, H. *Angew. Chem. Int. Ed.* **2008**, *47*, 9618. (b) Browne, W. R. *Coord. Chem. Rev.* **2008**, *252*, 2470.
- 19) Wollman, E. W.; Kang, D.; Frisbie, C. D.; Lorkovic, I. M.; Wrighton, M. S. *J. Am. Chem. Soc.* **1994**, *116*, 4395.
- 20) Blencowe, A.; Cosstick, K.; Hayes, W. *New J. Chem.* **2006**, *30*, 53.
- 21) Sawoo, S.; Dutta, P.; Chakraborty, A.; Mukhopadhyay, R.; Bouloussa, O.; Sarkar, A. *Chem. Commun.* **2008**, 5957.
- 22) Kanoh, N.; Kumashiro, S.; Simizu, S.; Kondoh, Y.; Hatakeyama, S.; Tashiro, H.; Osada, H. *Angew. Chem. Int. Ed.* **2003**, *42*, 5584.
- 23) (a) Blencowe, A.; Hayes, W. *Soft Matter* **2005**, *1*, 178, and references therein. (b) Hashimoto, M.; Hatanaka, Y. *Eur. J. Org. Chem.* **2008**, 2513. (c) Hatanaka, T.; Hatanaka, Y.; Setou, M. *J. Am. Chem. Soc.* **2006**, *128*, 15092. (d) Vila-Perellö, M.; Pratt, M. R.; Tulin, F.; Muir, T. W. *J. Am. Chem. Soc.* **2007**, *129*, 8086. (e) Qiu, Z.; Lu, L.; Jian, X.; He, C. *J. Am. Chem. Soc.* **2008**, *130*, 14398. (f) Shigdel, U. K.; Zhang, J.; He, C. *Angew. Chem. Int. Ed.* **2008**, *47*, 90. (g) Admasu, A.; Gudmundsdóttir, A. D.; Platz, M. S.; Watt, D. S.; Kwiatkowski, S.; Crocker, P. J. *J. Chem. Soc., Perkin Trans. 2*, **1998**, 1093. (h) Platz, M.; Admasu, A. S.; Kwiatkowski, S.; Crocker, P. J.; Imai, N.; Watt, D. S. *Bioconjugate Chem.* **1991**, *2*, 337.
- 24) Brunner, J.; Senn, H.; Richards, F. M. *J. Biol. Chem.* **1980**, *255*, 3313.
- 25) Blencowe, A.; Caiulo, N.; Cosstick, K.; Fagour, W.; Heath, P.; Hayes, W. *Macromolecules* **2007**, *40*, 939.
- 26) Mayer, T.; Maier, M. E. *Eur. J. Org. Chem.* **2007**, 4711.

- 27) Hatanaka, Y.; Hashimoto, M.; Kurihara, H.; Nakayama, H.; Kanaoka, Y. *J. Org. Chem.* **1994**, *59*, 383.
- 28) Rothrock, A. R.; Donkers, R. L.; Schoenfisch, M. H. *J. Am. Chem. Soc.* **2005**, *127*, 9362.
- 29) Brust, M.; Walker, M.; Bethell, D.; Schiffrin, D. J.; Whyman, R. J. *J. Chem. Soc. Chem. Commun.* **1994**, 801.
- 30) Hostetler, M. J.; Templeton, A. C.; Murray, R. W. *Langmuir* **1999**, *15*, 3782.
- 31) Templeton, A. C.; Wuelfing, W. P.; Murray, R. W. *Acc. Chem. Res.* **2000**, *33*, 27.
- 32) (a) Buterbaugh, J. S.; Toscano, J. P.; Weaver, W. L.; Gord, J. R.; Hadad, C. M.; Gustafson, T. L.; Platz, M. S. *J. Am. Chem. Soc.* **1997**, *119*, 3580. (b) Kanoh, N.; Nakamura, T.; Honda, K.; Yamakoshi, H.; Iwabuchi, Y.; Osada, H. *Tetrahedron* **2008**, *64*, 5692.
- 33) (a) Thomas, K. G.; Kamat, P. V. *Acc. Chem. Res.* **2003**, *36*, 888. (b) Ghosh, S. K.; Pal, T. *Phys. Chem. Chem. Phys.* **2009**, 3831. (c) Dulkeith, E.; Klar, R. T. A.; Feldman, J.; Javier, A. M.; Parak, W. J. *Nano Lett.* **2005**, *5*, 585. (d) Jennings, T. L.; Singh, M. P.; Strouse, G. F. *J. Am. Chem. Soc.* **2006**, *128*, 5462.

**3.5 Supplementary Information For:****Chapter 3,****Diazirine-Modified Gold Nanoparticle: Template for  
Efficient Photoinduced Interfacial Carbene Insertion  
Reactions**

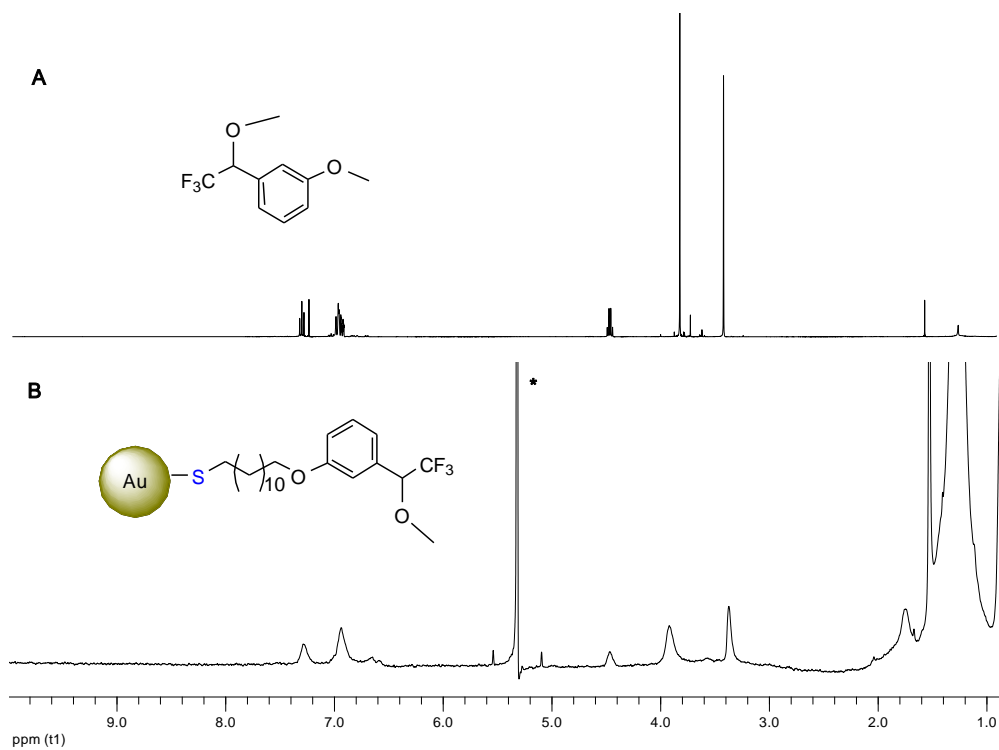


Figure S3.1  $^1\text{H}$  NMR spectra of A) **11b** in  $\text{CDCl}_3$ , B) **3b-C<sub>12</sub>AuNP** in  $\text{CD}_2\text{Cl}_2$

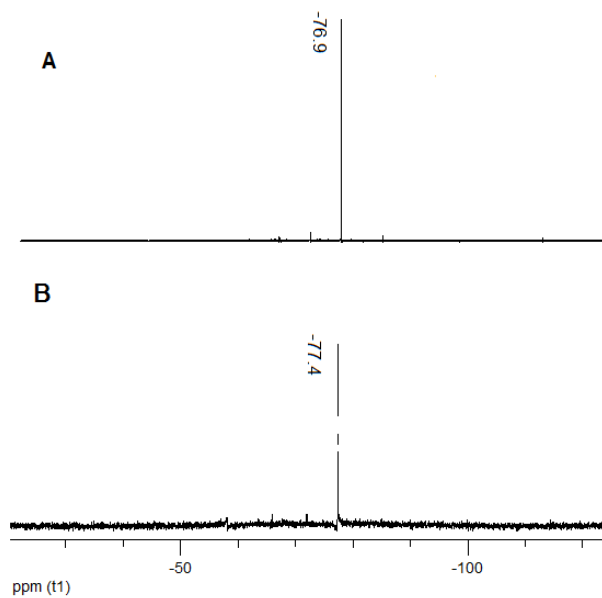


Figure S3.2  $^{19}\text{F}$  NMR spectra of A) **11b** in  $\text{CDCl}_3$ , B) **3b-C<sub>12</sub>AuNP** in  $\text{CD}_2\text{Cl}_2$

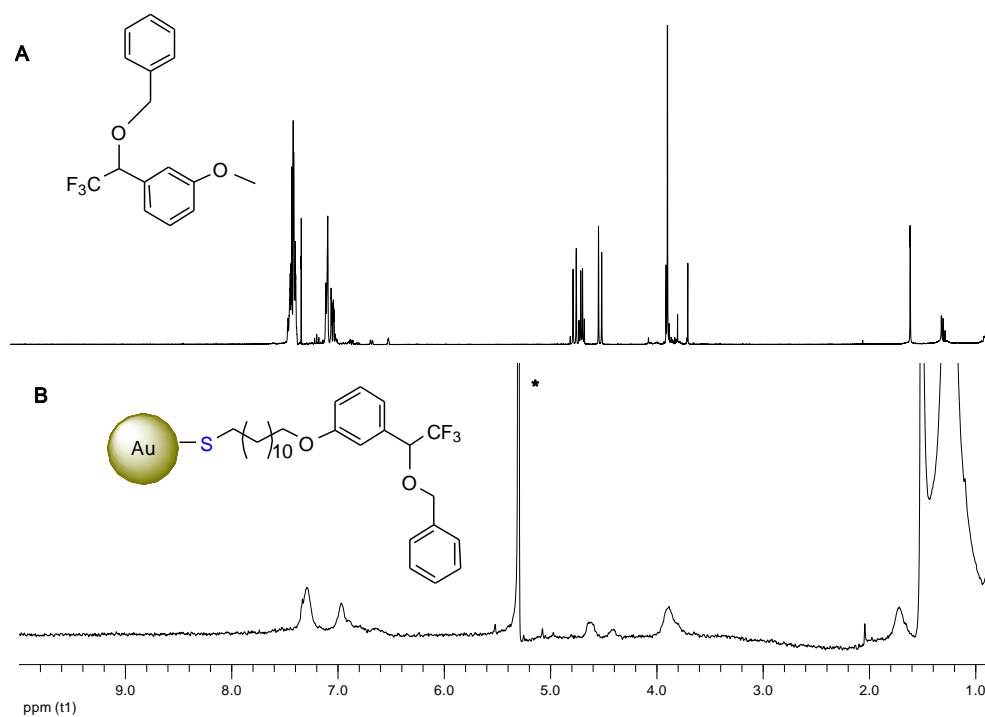


Figure S3.3  $^1\text{H}$  NMR spectra of A) **11c** in  $\text{CDCl}_3$ , B) **3c-C<sub>12</sub>AuNP** in  $\text{CD}_2\text{Cl}_2$

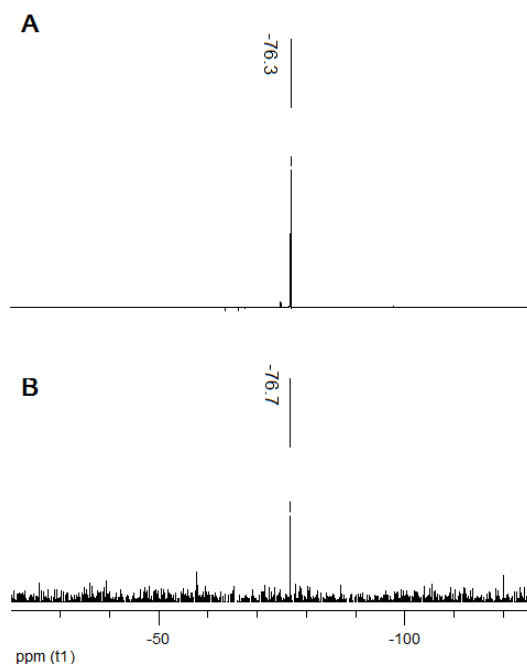


Figure S3.4  $^{19}\text{F}$  NMR spectra of A) **11c** in  $\text{CDCl}_3$ , B) **3c-C<sub>12</sub>AuNP** in  $\text{CD}_2\text{Cl}_2$



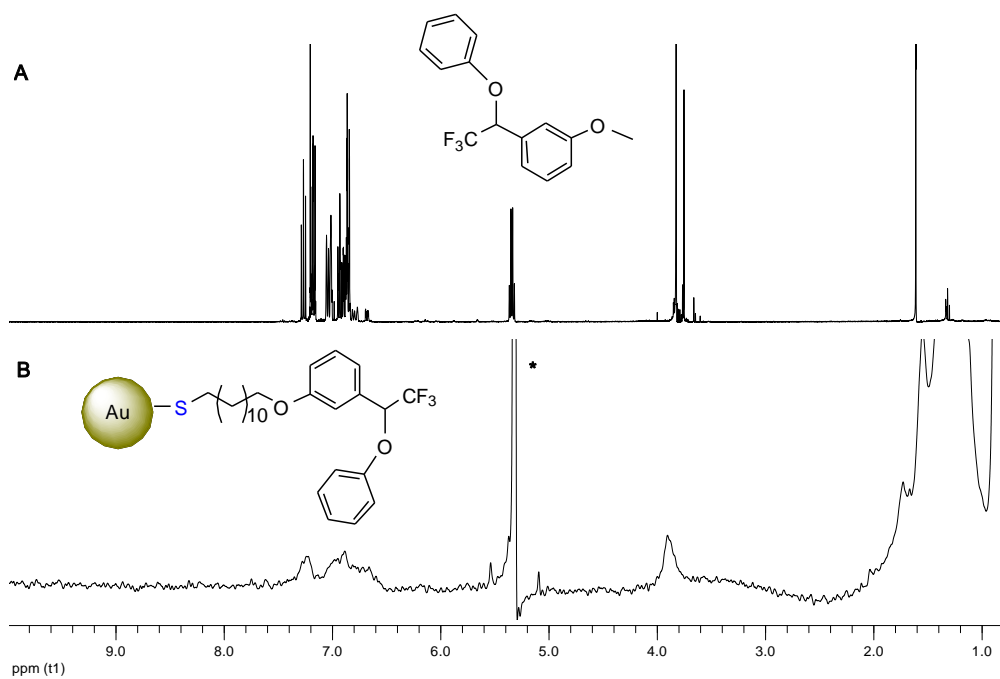


Figure S3.5  $^1\text{H}$  NMR spectra of A) **11d** in  $\text{CDCl}_3$ , B) **3d-C<sub>12</sub>AuNP** in  $\text{CD}_2\text{Cl}_2$

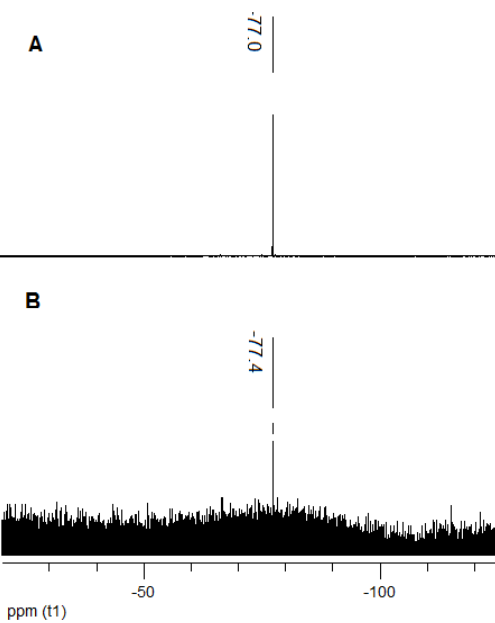


Figure S3.6  $^{19}\text{F}$  NMR spectra of A) **11d** in  $\text{CDCl}_3$ , B) **3d-C<sub>12</sub>AuNP** in  $\text{CD}_2\text{Cl}_2$

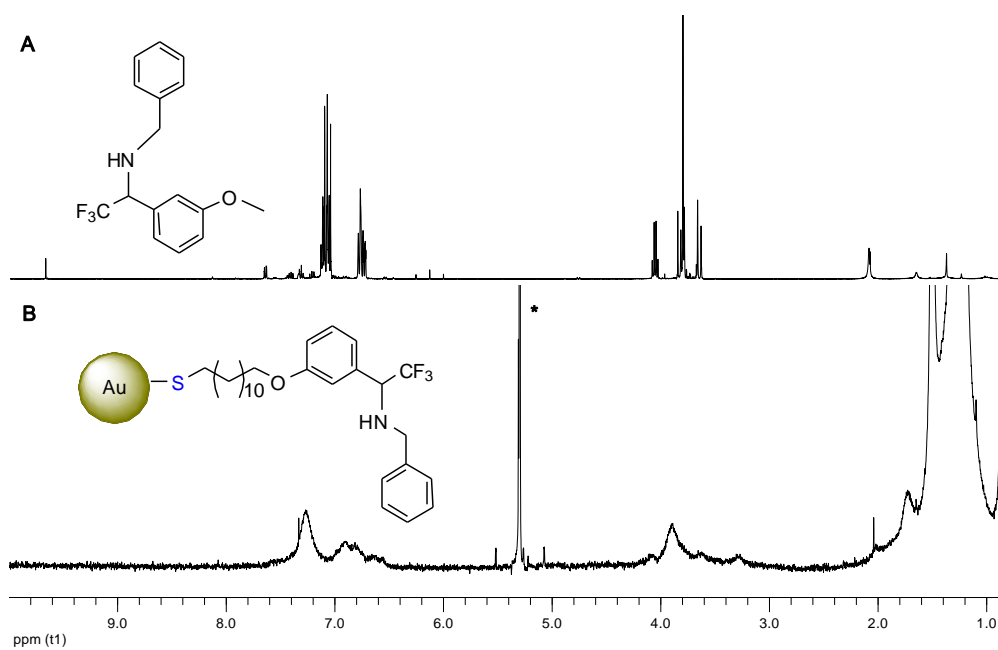


Figure S3.7  $^1\text{H}$  NMR spectra of A) **11e** in  $\text{CDCl}_3$ , B) **3e-C<sub>12</sub>AuNP** in  $\text{CD}_2\text{Cl}_2$

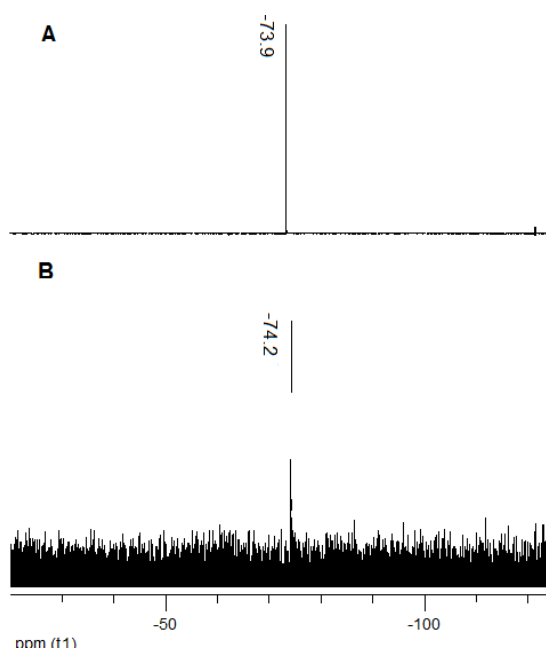


Figure S3.8  $^{19}\text{F}$  NMR spectra of A) **11e** in  $\text{CDCl}_3$ , B) **3e-C<sub>12</sub>AuNP** in  $\text{CD}_2\text{Cl}_2$

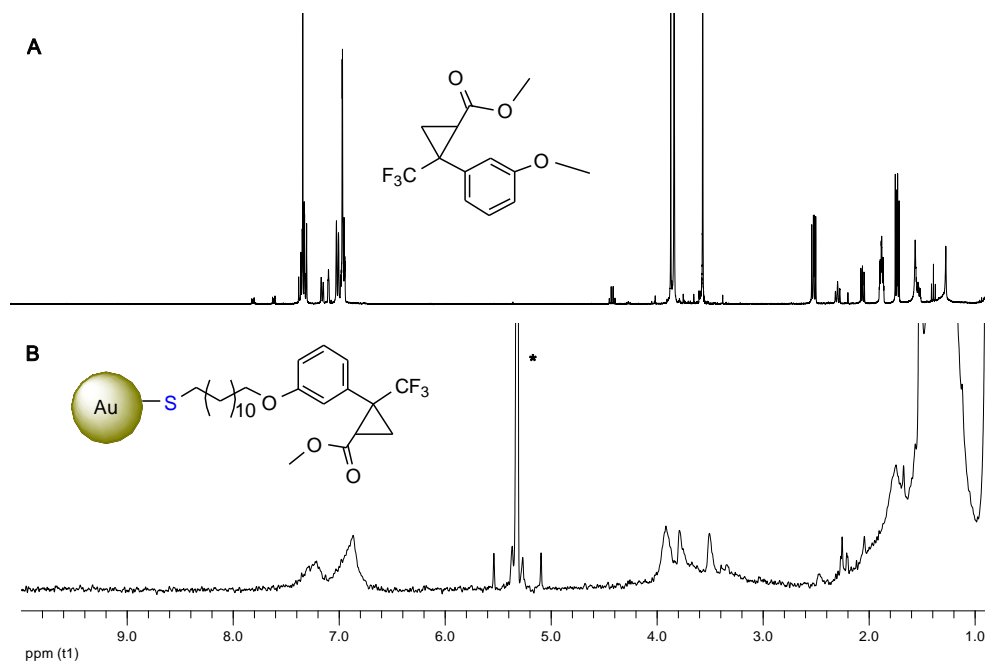


Figure S3.9  $^1\text{H}$  NMR spectra of A) **11f** in  $\text{CDCl}_3$ , B) **3f-C<sub>12</sub>AuNP** in  $\text{CD}_2\text{Cl}_2$

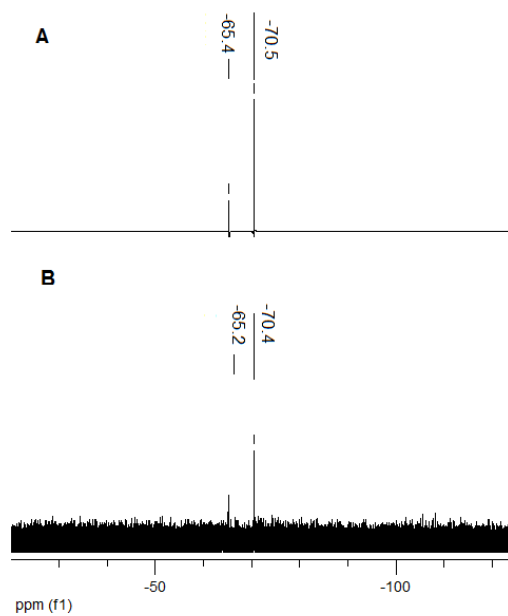


Figure S3.10  $^{19}\text{F}$  NMR spectra of A) **11f** in  $\text{CDCl}_3$ , B) **3f-C<sub>12</sub>AuNP** in  $\text{CD}_2\text{Cl}_2$

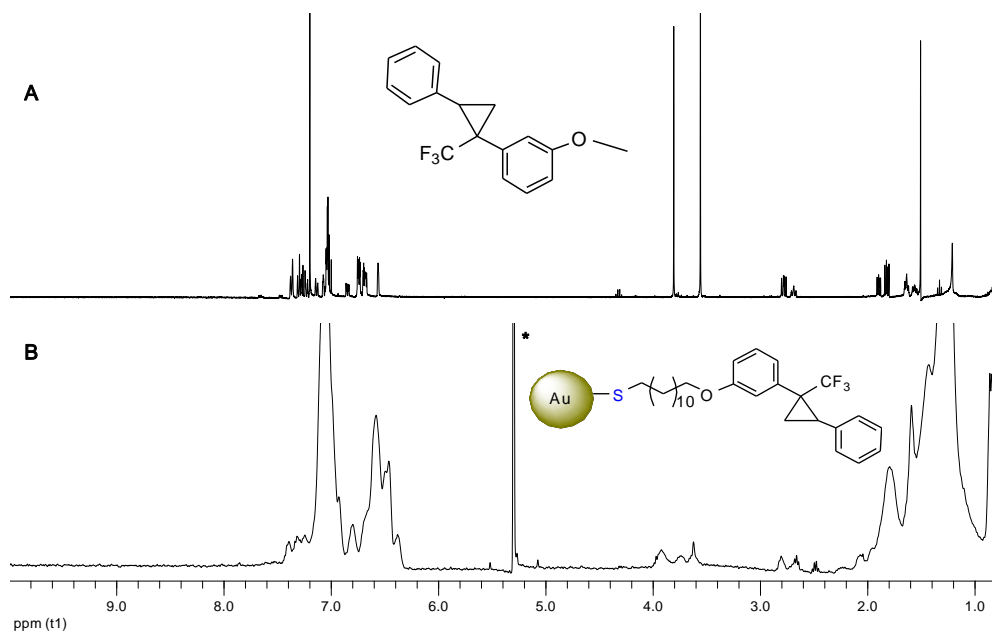


Figure S3.11  $^1\text{H}$  NMR spectra of A) **11g** in  $\text{CDCl}_3$ , B) **3g-C<sub>12</sub>AuNP** in  $\text{CD}_2\text{Cl}_2$

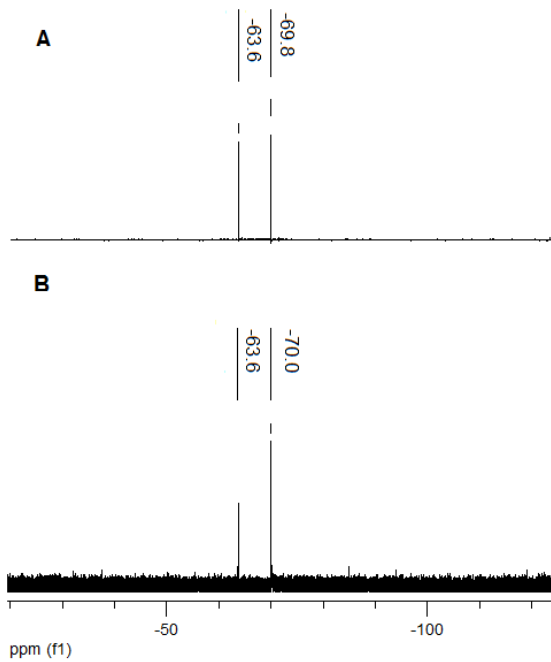


Figure S3.12  $^{19}\text{F}$  NMR spectra of A) **11g** in  $\text{CDCl}_3$ , B) **3g-C<sub>12</sub>AuNP** in  $\text{CD}_2\text{Cl}_2$

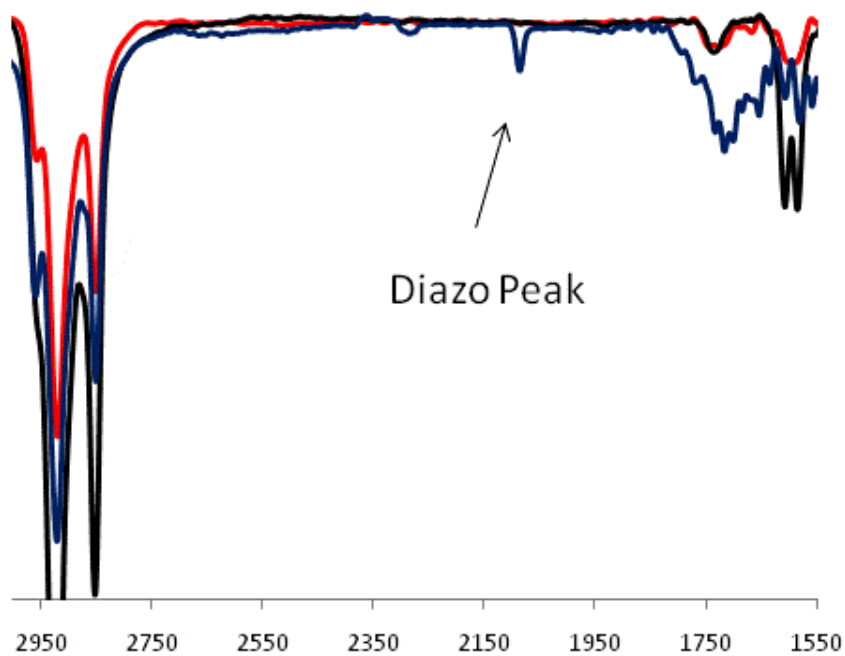
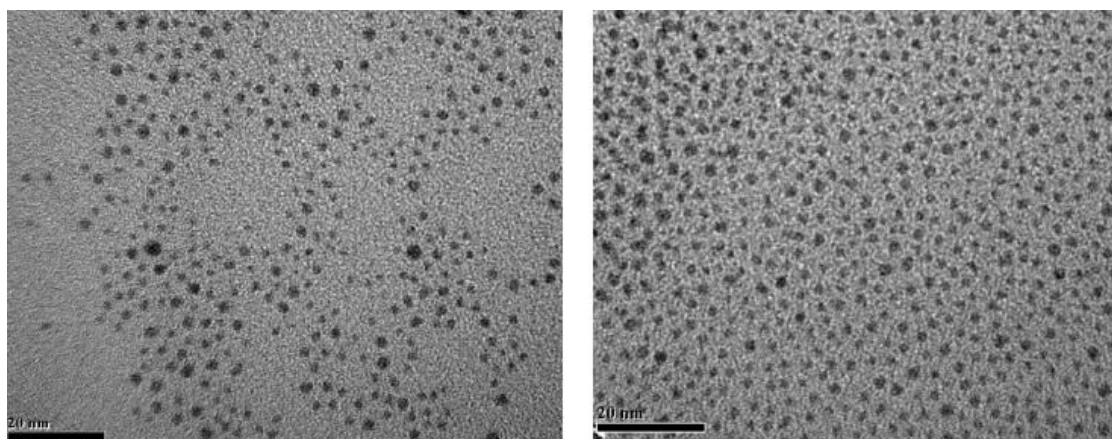


Figure S3.13 IR spectra of **2**-C<sub>12</sub>AuNP (black), **2**-C<sub>12</sub>AuNP + CH<sub>3</sub>COOH after 1 h irradiation (blue), and **3a**-C<sub>12</sub>AuNP (red) after the completion of reaction.



TEM of **2**-C<sub>12</sub>AuNPs before irradiation  
(1.8 ± 0.3 nm)

TEM of **3b**-C<sub>12</sub>AuNPs after irradiation for  
14 h (1.8 ± 0.2 nm)

Figure S3.14

## Chapter 4

# Covalently Assembled Gold Nanoparticle-Carbon Nanotube Hybrids (AuNP-CNT) via a Photoinitiated Carbene Addition Reaction

- Chapter 4 has been published as a full paper. The corresponding reference is: Hossein Ismaili, François Lagugné-Labarthet, and Mark S. Workentin\*, *Chem. Mater.* **2011**, *23*, 1519.
- Dr. Lagugné-Labarthet characterized the nanoparticle-carbon nanotube hybrids using Raman spectroscopy. Hossein Ismaili carried out the remainder of work reported in Chapter 4.
- All of the schemes, figures, and text in Chapter 4 reprinted with permission from *Chemistry of Materials*, 2011, 23, 1519, Copyright 2011 American Chemical Society.

## 4.1 Introduction

Monolayer-protected gold nanoparticles (AuNPs)<sup>1</sup> and carbon nanotubes (CNTs)<sup>2</sup> are arguably the two most common nano-sized building blocks for current materials applications. The former are one of the most stable metal nanoparticles, easy to synthesize in a variety of core sizes, there is a protocol to modify these AuNP with additional functionality and they possess attractive electrochemical and optical properties.<sup>3, 4</sup> The latter, since their discovery in 1991,<sup>5</sup> have been central to the development of hybrid nanomaterials because of their outstanding mechanical, optical, electrical, and thermal properties.<sup>6</sup> With the aim to capitalize on the features of both of these types of materials for applications in areas as diverse as chemical and biochemical catalysis,<sup>3</sup> sensors,<sup>4</sup> development of fuel cells<sup>7</sup> and transistors,<sup>8</sup> there has been much recent effort to fabricate nanohybrids where the CNT acts as a support for a variety of noble metal nanoparticles (NP), such as AgNP, PtNP and AuNP.<sup>9</sup> Applications of nanoparticle-carbon nanotube (NP-CNT) hybrids require the development of methods for their preparation that lead to robust structures without significantly compromising the integrity of the underlying CNT framework. Thus preparing covalent NP-CNT hybrids with uniform dispersion of the nanoparticles onto the CNT and tuning the size of nanoparticles remain important challenges of NP-CNT hybrids fabrication and applications.

Generally there are three main strategies that are utilized to deposit noble metal NP, specifically AuNP, onto the surface of CNT. These broadly can be classified as covalent approaches, non-covalent approaches, and direct formation of AuNPs.<sup>9</sup> In the direct formation method, AuNPs are grown on the CNTs using methods such as chemical vapor

deposition,<sup>10</sup> electrodeposition<sup>11</sup> and thermal decomposition.<sup>12</sup> This approach is limited because of the need for more complex instrumentation, the often slow deposition rate, and more importantly, the lack of control over AuNP size.<sup>6, 10 – 12</sup> Furthermore, AuNP formed in this way are also more unstable and undergo agglomeration losing control of the dispersity of the AuNP on the CNT.

Non-covalent approaches are also utilized to prepare AuNP-CNT nanohybrids. Here the preparation utilizes one or more of hydrophobic,<sup>13</sup> electrostatic,<sup>14</sup> van der Waals<sup>15</sup> as well as  $\pi$ - $\pi$  stacking<sup>16</sup> interactions between the native or treated CNT and functionality on the monolayer protected AuNPs. The advantages of these methods are that they allow for the reversible preparation of protected metal AuNP-CNT hybrids and do not lead to any destructive interactions on the integrity of the chemical structure of the CNT sidewalls. However, because the interactions are inherently weaker than covalent bonds, the AuNPs on the surface of CNTs are not robust and thus may easily disassemble, often by simple washing of the AuNP-CNT hybrids.

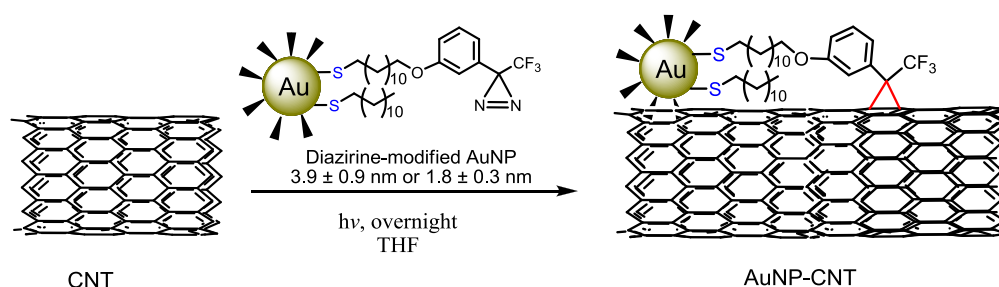
For many applications a covalent interaction between the monolayer protected AuNP and the CNT is beneficial. Covalent attachment offers several advantages: i) because the AuNPs are synthesized in advance, the size and shape of the AuNP is controlled by well-known procedures; ii) using covalent bonds leads to formation of more robust nanohybrids from which the AuNP will not easily be displaced and iii) the loading efficiency of AuNP onto the CNTs can be tailored via variation of AuNP concentration.<sup>9b, 9c, 17</sup> Most approaches to date for the preparation of covalently assembled AuNP-CNT hybrids requires the chemical pretreatment of the CNT surface to expose functionality



that can be further elaborated, for example with a functional molecule containing a terminal thiol group, which is then utilized to form the bond with the AuNP. The first step of functionalization is often the oxidation of the CNT, which usually requires aggressive acid treatment, high temperature and sonication.<sup>6a, 18</sup> The pretreatments often damage the structural integrity of the CNT and adversely affect their electrical and mechanical properties. Fracture of the CNT, formation of holes in the sidewalls, successive removal of the graphene cylinders (in the case of multi-walled CNTs), as well as functionalization of only defect sites are observed under these aggressive conditions.<sup>6a, 19</sup> Given these approaches, it remains a desirable goal to develop efficient strategies for the formation of AuNP-CNT nanohybrids through covalent assembly, while also avoiding the need to pretreat/modify the surface of CNTs and to take advantage of the ability to prepare the AuNP with known core size prior to its incorporation onto the CNT.

Carbene and nitrene addition reactions were among the first employed to modify CNTs.<sup>20</sup> Chen and coworkers reported the chemical functionalization of CNTs using nucleophilic addition of dichlorocarbene generated from different precursors, including mercury complex<sup>20a</sup> and  $\text{CHCl}_3/\text{NaOH}$ .<sup>20b</sup> In addition, photolysis and thermolysis of an azide functionality incorporated on a variety of different platforms to yield reactive nitrenes has been utilized to functionalize CNTs.<sup>20c</sup> In a recent example, McCall and coworkers took advantage of the photoreactivity of azidothymidine and the resulting nitrene chemistry to modify CNT which can be further elaborated to decorate the CNT with DNA to produce water soluble CNTs.<sup>20d</sup> Bai and co-workers used similar photoinitiated nitrene chemistry of an azide copolymer to coat the surface of CNTs.<sup>20e</sup>

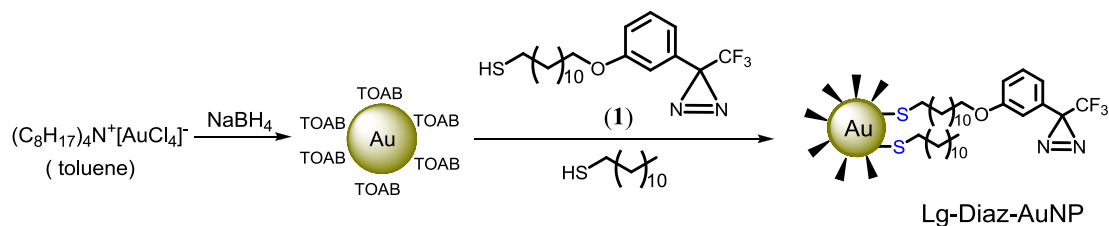
Photogenerated carbene reactivity has not been utilized like those of the nitrene reactions for the modification of CNT sidewall surfaces even though they offer many of the same advantages. In this report we utilize a photogenerated carbene to modify multi-walled CNTs with AuNPs. The carbene addition approach allows direct coupling of the carbene carrier, in our case AuNP, onto the  $\pi$ -conjugated carbon skeleton of CNT. Our strategy involves the generation of a reactive carbene intermediate directly on the monolayer of an AuNP and to utilize its subsequent addition reaction onto the  $\pi$ -backbone of CNT for covalent coupling of AuNP to the CNT, with no need for oxidizing the surface of CNTs. We recently reported the synthesis and modification of 3-aryl-3-(trifluoromethyl) diazirine-modified AuNPs (Diaz-AuNP) through photoinduced carbene insertion reactions.<sup>21</sup> We demonstrated that upon irradiation of the diazirine group tethered onto the AuNP, an intermediate carbene is generated by photoinitiated nitrogen extrusion and insertion reactions then occurred in the presence of a selection of reactants with X-H (X: O, N) and alkene functional groups. Herein, we report that the irradiation of similar Diaz-AuNP in the presence of multi-walled CNTs leads to covalent assembly of the AuNP onto the CNT by means of a carbene addition approach (scheme 4.1). We investigated this approach by using two different Au core sizes of Diaz-AuNP: Lg-Diaz-AuNP with a larger, yet more disperse core size ( $3.9 \pm 0.9$  nm) was used initially to maximize sensitivity for our characterization techniques and optimize reaction conditions and then the method was extended to a Sm-Diaz-AuNP with a smaller core size ( $1.8 \pm 0.3$  nm in diameter). The approach allows for facile formation of robust AuNP-CNT nanohybrids in a single step without the need to pre-functionalize the CNT.



Scheme 4.1 Illustration of the reaction protocol utilized for the functionalization of CNT with diazirine-modified AuNPs (Diaz-AuNPs).

## 4.2 Results and Discussion

The diazirinethiol (**1**) and Sm-Diaz-AuNPs ( $1.8 \pm 0.3$  nm) were synthesized according to a previously reported procedure.<sup>21</sup> The Lg-Diaz-AuNPs ( $3.9 \pm 0.9$  nm) were synthesized using a modified two-phase Brust-schiffrin method (scheme 4.2).<sup>22–24</sup> In this preparation procedure tetraoctylammonium bromide (TOAB)-stabilized AuNPs were made by reducing  $\text{Au}^{3+}$  with  $\text{NaBH}_4$  in the presence of TOAB. In the next step, TOABs were place-exchanged with diazirinethiol (**1**) and dodecanethiol affording Lg-Diaz-AuNPs. The product Lg-Diaz-AuNPs were characterized by  $^1\text{H}$  NMR,  $^{19}\text{F}$  NMR, and UV-vis spectroscopy and TEM. The average Au core diameter of Lg-Diaz-AuNPs prepared in this way was  $3.9 \pm 0.9$  nm with a distribution range of 2.6 – 6 nm, as determined by TEM (Figure S4.1, supporting information).



Scheme 4.2 Synthetic procedure used in the preparation of Lg-Diaz-AuNPs.

$^1\text{H}$  NMR spectroscopy is a powerful tool for characterizing and monitoring the purity of functionalized AuNPs. The  $^1\text{H}$  NMR spectra of Lg-Diaz-AuNP and Sm-Diaz-AuNP (Figure 4.1A and B, respectively) show broad peaks at 0.7 – 2.25 ppm assignable to the methylene and methyl groups of diazirinethiolate (**1**) and dodecanethiolate attached onto the AuNP core. A broad peak centered at 3.90 (e) ppm is due to the methylene alpha to the oxygen of (**1**) and broad peaks at 6.50 – 7.05 (a, b, and d) and 7.28 (c) ppm are assigned to the aromatic hydrogens of the aromatic ring. It should be noted that the  $^1\text{H}$  NMR spectrum of ligands on larger size particles is characterized by broader signals.

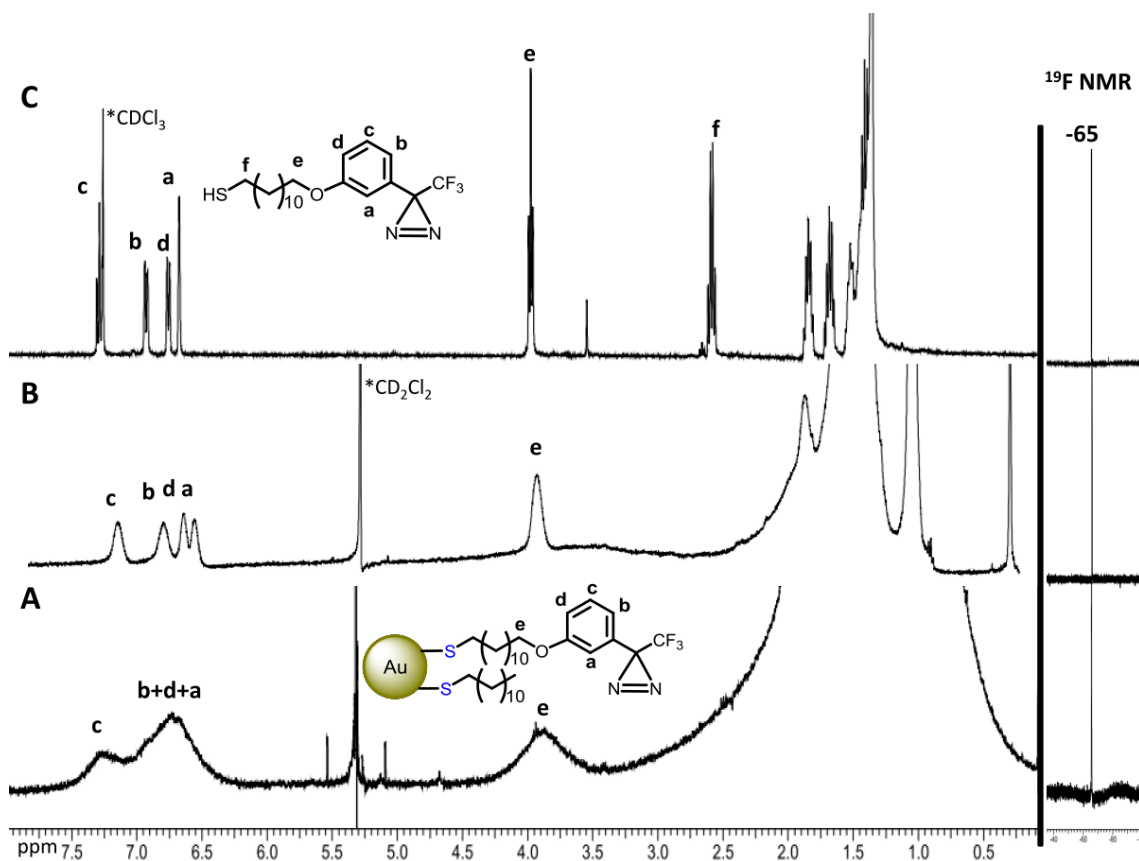


Figure 4.1  $^1\text{H}$  and  $^{19}\text{F}$  NMR spectra of A) Lg-Diaz-AuNPs; B) Sm-Diaz-AuNPs and C) diazirinethiol **1**. The  $^{19}\text{F}$  NMRs are in the far right.

Figure 4.1C shows the  $^1\text{H}$  NMR spectrum of free (**1**). As can be seen, good alignment of the chemical shifts between (**1**) and the two Diaz-AuNPs in Figure 4.1 signifies the successful exchange reaction and incorporation of (**1**) onto the AuNP. The lack of sharp signals in the  $^1\text{H}$  NMR spectra of the Diaz-AuNPs confirms the purity of product AuNPs otherwise the sharp peaks due to impurities such as unbound (**1**), dodecanethiol or TOAB would appear. In addition, we employed  $^{19}\text{F}$  NMR spectroscopy to characterize the Diaz-AuNPs. The  $^{19}\text{F}$  NMR spectrum of the two Diaz-AuNPs shows a single peak at  $-65$  ppm assignable to the fluorine of the  $\text{CF}_3$  group of (**1**), a further indication of incorporation of (**1**) onto the AuNP (Figure 4.1).<sup>21</sup>

The UV-vis spectrum of Lg-Diaz-AuNP exhibit a broadened surface plasmon band centered around 530 nm, characteristic of AuNP with a core size  $>3$  nm. The Sm-Diaz-AuNPs do not show the plasmon band. Both the Lg-Diaz and Sm-Diaz-AuNP have a stronger absorption between 270 – 350 compared to the absorption of Model-AuNP (without diazirine functionality) as expected for the incorporation of the diazirine chromophore onto the AuNP (Figure S4.2, supporting information).

Scheme 4.1 illustrates the photochemical approach utilized for the covalent attachment of the Diaz-AuNP onto the CNT. As stated, irradiation of terminal diazirine group that is attached onto the Diaz-AuNP creates a reactive carbene at the interface of the AuNP after nitrogen extrusion. The subsequent carbene then adds onto the sidewall of the CNT via a carbene nucleophilic addition. In a typical procedure, 1 mg of as-received multi-walled CNTs with 95% purity was dispersed in 10 mL of THF. A solution of Lg-Diaz-AuNP or Sm-Diaz-AuNP in THF (5 mg/1 mL) was added to the CNTs suspension

in a septum sealed Pyrex test tube and the solution was purged with argon. The system was irradiated using a medium pressure mercury lamp at room temperature for 15 h. The resulting AuNP-CNT nanohybrid was isolated by repeated centrifugation and washing using THF,  $\text{CHCl}_3$  and toluene to remove any unbound AuNPs. A drop of the obtained nanohybrid was dispersed in THF and cast onto a copper grid (300 mesh, coated with carbon film) for TEM investigations. As evident in Figure 4.2, Lg-Diaz-AuNP and Sm-Diaz-AuNP are bound to the sidewall of the CNTs with a rather even distribution. Figures 4.2A and 4.2B show the HRTEM and TEM images of Lg-Diaz-AuNP-CNT, respectively, and TEM images of Sm-Diaz-AuNP-CNT are shown in Figures 4.2C and 4.2D. It is important to note that the AuNPs were stable under UV irradiation and no noticeable change was observed in the shape or size of the Au core after irradiation.

To provide support for the role of the carbene addition in forming the AuNP-CNT nanohybrid via covalent assembly, we carried out two set of control experiments. The first was stirring a solution of Lg-Diaz-AuNP and CNTs in the absence of irradiation. The Lg-Diaz-AuNP contain alkane chains and aromatic rings, therefore non-covalent interactions including weak van der Waals and  $\pi$ - $\pi$  stacking can also engage in the assembly of a nanohybrid. Because these samples were not irradiated the diazirine groups remained intact and no carbenes were formed. In this case, only non-covalent interactions would lead to the formation of an AuNP-CNT nanohybrid. However, TEM images taken of the solid material, after the same centrifugation and washing cycle protocol (see experimental), showed just bare CNT with no AuNP attached onto the nanotubes (Figure 4.2E and 4.2F).

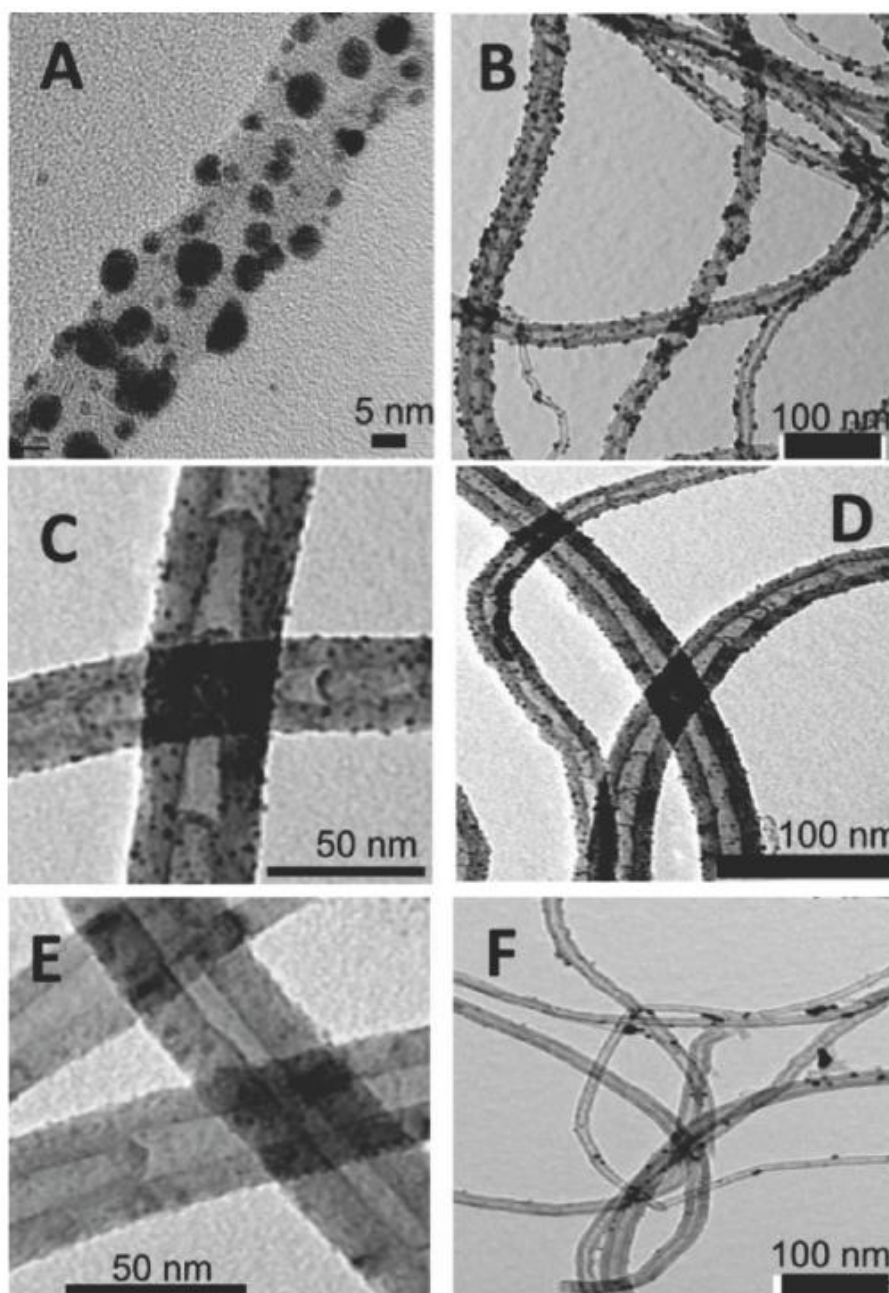


Figure 4.2 TEM images of CNTs after photoreaction and washing/purification protocol A, B) photoreaction with Lg-Diaz-AuNPs (Lg-Diaz-AuNP-CNT); C, D) photoreaction of Sm-Diaz-AuNPs (Sm-Diaz-AuNP-CNT); E, F) CNTs exposed to the same solutions as A/B but in the absence of UV irradiation and after the washing/purification protocol.

In addition, to verify the requirement for irradiation in the nanohybrid formation, a mixture of Model-AuNPs (i. e. those without incorporation of the diazirine ligand (**1**) onto the AuNP) and CNT was exposed to the same irradiation and purification protocol conditions described above. The TEM of the obtained material showed only CNT with no AuNP incorporated onto them. The conclusion of these control experiments is that UV irradiation of the diazirine moiety incorporated on the AuNP to generate the intermediate carbene and its subsequent nucleophilic addition is responsible for the covalently assembled AuNP-CNT nanohybrid.

The Diaz-AuNPs have the reactive ligand roughly equally distributed on the surface and for the formation of the nanohybrid only one (or at most a few) carbene additions are expected. One question that arises is what is the fate of the carbene intermediates generated away from the CNT surface? We suspect that carbenes that do not covalently react with the CNTs react with solvent, in this case THF, albeit at a much slower rate than addition to the CNT, an observation we made previously.<sup>21</sup> Another possible fate is for the carbenes to react with the carbenes (or ligands) on another AuNP. However, the TEM shows no real evidence for agglomeration of AuNPs due to dimerization of carbenes or reaction of a carbene ligand on one AuNP with another.

To further identify the presence of the AuNP on the surface of the CNT the AuNP-CNT nanohybrids were characterized using X-ray diffraction (XRD). The XRD of the Lg-Diaz-AuNP-CNT and Sm-AuNP-CNT nanohybrids are shown in Figure 4.3. The (111), (200), (220), (311), (222), (331) and (420) are planes of a face-centered cubic (fcc) AuNP, affirming the presence of AuNP in the nanohybrids.<sup>25</sup> The C (002) plane of carbon



nanotubes is absent in the XRD spectrum of Lg-Diaz-AuNP-CNT but is present in the XRD spectrum of Sm-Diaz-AuNP-CNT. The surface coverage of the AuNP on the Lg-Diaz-AuNP-CNT is higher than that on the Sm-Diaz-AuNP-CNT, therefore the x-ray beam does not efficiently interrogate the surface of nanotubes in the Lg-Diaz-AuNP-CNT and planes due to C (200) cannot be observed as readily in the XRD pattern of these samples.

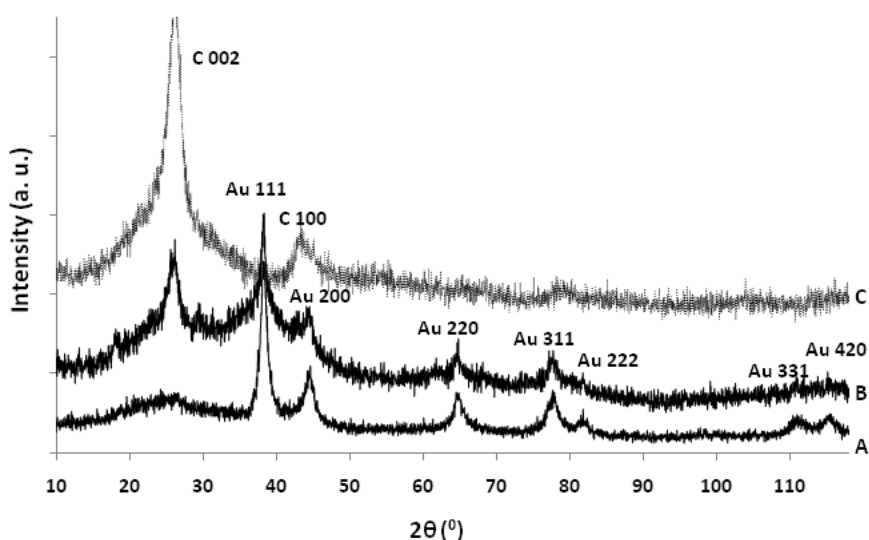


Figure 4.3 XRD patterns of A) Lg-Diaz-AuNP-CNT; B) Sm-Diaz-AuNP-CNT and C) pure CNT.

Further characterization of the AuNP-CNT nanohybrids was done using Raman spectroscopy. Raman spectra were measured using two different laser wavelengths, namely a 512 nm and a 632 nm laser. As reported previously, the D/G ratios observed for the unmodified CNT vary with the excitation wavelength,<sup>26</sup> and in the present case this ratio was 0.9 using the 512 nm laser and 1.19 using the 632 nm laser. Raman spectra of the AuNP-CNT hybrids could only be measured using the 632 nm laser, because

excitation using the 512 nm laser leads to a visible thermal decomposition of the sample. This is likely due to the thermal energy produced on excitation at the plasmon absorption band in the AuNP; we are currently investigating the practical applications of this observation further. The spectra obtained for the Lg-Diaz-AuNP-CNT and unmodified CNT measured using the 632 nm laser are shown in Figure 4.4. The peaks at 1315 and 1567  $\text{cm}^{-1}$  are the D and G bands of CNTs, respectively.<sup>16</sup> A Raman enhancement of a factor of approximately three was observed with the Lg-Diaz-AuNPs. AuNP are well known to enhance the Raman signal of these bands. It is noteworthy that the R values (intensity ratio of D/G band) of CNT ( $R = 1.21$ ) and AuNP-CNT nanohybrid ( $R = 1.19$ ) did not considerably change, suggesting that the carbene addition reaction did not significantly affect the underlying structure of the CNT. The same Raman enhancement was not observed in the case of Sm-Diaz-AuNP-CNT. The small AuNPs do not exhibit a strong surface plasmon band that is the main contribution to the surface-enhanced Raman scattering.<sup>27</sup>

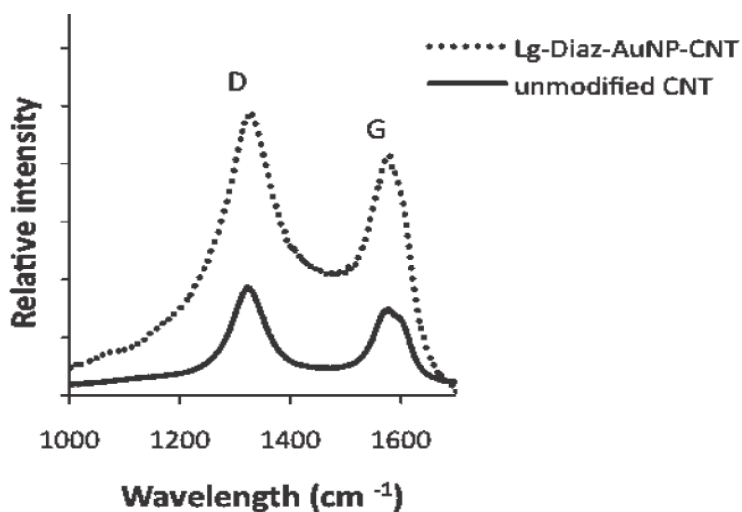


Figure 4.4 Raman spectra of Lg-Diaz-AuNP-CNT (dashed line) and unmodified CNT (solid line).

The UV-vis spectra of the CNT, Lg-Diaz-AuNP-CNT, and Sm-Diaz-AuNP-CNT provide additional support for the incorporation of the AuNP (Figure 4.5). The appearance of the surface plasmon band in the UV-vis spectrum of Lg-Diaz-AuNP-CNT implies the presence of the AuNPs onto the CNT. The surface plasmon band of AuNPs in the Lg-Diaz-AuNP-CNT nanohybrid is broader and red-shifted (from 530 nm to 555 nm) compared with that of unreacted Lg-Diaz-AuNP. It has been suggested that the red shift of the surface plasmon band is because of interparticle interactions of AuNPs attached onto the CNTs.<sup>28</sup>

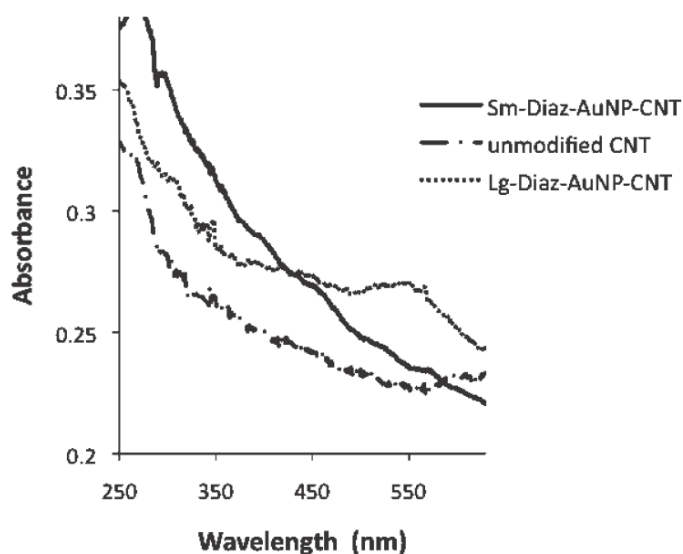


Figure 4.5 UV-vis absorption spectra of unmodified CNTs, Sm-Diaz-AuNP-CNT and Lg-Diaz-AuNP-CNT, The latter clearly exhibits the Plasmon absorption band.

### 4.3 Conclusion

The photoinitiated carbene generated from diazirine-modified AuNPs (Diaz-AuNPs) allows for the efficient covalent attachment of AuNP onto multi-walled CNT.

Presumably, this occurs via carbene addition to the C=C bonds on the surface of the CNT. The reactions proceed efficiently without the need for pretreatment of the CNT to incorporate additional surface functionality on the CNT. The monolayer ligands of the AuNP that remain exposed can, in principle, undergo place-exchange reactions with other thiols which will allow a method to tailor or adjust the solubility characteristics or other features of these AuNP-CNT nanohybrids. The high reactivity of the carbene intermediates generated towards insertion and addition reactions suggests that the approach described here can be used to incorporate suitably diazirine-derivatized AuNP (and indeed other metal NP) to other materials containing a variety of native or synthesized surface functionality. Because the mode of attachment of the AuNP is through photochemical activation the methodology can be combined with photolithographic techniques to produce patterns of the metal NP on these surfaces; we are currently investigating the breadth of materials that can be modified using the methodology described.

Supporting Information: TEM image of Lg-Diaz-AuNP and the absorption spectra of Model-AuNPs, Lg-Diaz-AuNPs, Sm-Diaz-AuNPs and diazirinethiol **1** are provided.

## 4.4 Experimental

### Commercial Solvents and Reagents Used

Deuterated chloroform ( $\text{CDCl}_3$ ) and dichloromethane ( $\text{CD}_2\text{Cl}_2$ ) (Cambridge Isotope Laboratories) were used as received. The compounds dodecanethiol, hydrogen tetrachloroaurate(III), tetraoctylammonium bromide (TOAB), 1,12-dibromododecane, 3-bromoanisole, n-butyllithium, hydroxylamine hydrochloride, (N, N-dimethylamino) pyridine, p-toluenesulfonylchloride, silver (I) nitrate, boron tribromide, potassium thioacetate, acetyl chloride and multi-walled carbon nanotubes (Alfa Aesar, 95% purity, 20 nm OD, 5-20 micron long) were used as received from the suppliers.

### General instrumentation

$^1\text{H}$ ,  $^{13}\text{C}$ , and  $^{19}\text{F}$  NMR spectra were recorded on either a Varian Inova or Mercury 400 spectrometer ( $^1\text{H}$ : 400 MHz,  $^{13}\text{C}$ : 100 MHz, and  $^{19}\text{F}$ : 376 MHz) and chemical shifts are reported in ppm relative to internal TMS (0.00 ppm) or the signals from the NMR solvent ( $\text{CHCl}_3$ :  $\delta$  7.26 ppm for  $^1\text{H}$  NMR,  $\delta$  77.0 ppm for  $^{13}\text{C}$  NMR; and  $\text{CFCl}_3$ :  $\delta$  0 ppm for  $^{19}\text{F}$  NMR). Mass spectra and exact mass were recorded on a MAT 8200 Finnigan High Resolution Mass Spectrometer. Infrared spectra were recorded on a Bruker Vector 33 FTIR spectrometer and are reported in wavenumbers ( $\text{cm}^{-1}$ ). The light source used for the photochemical reactions was a Hanovia medium pressure mercury lamp (PC 451050 /805221). Transmission electron microscopy (TEM) images were recorded on a Philips CM-10 TEM operating at 100 kV and FEI Tecnai G2 F20 operating at 200kV. UV-vis absorption spectra were recorded on a Cary 100 spectrometer in spectroscopic grade THF

and  $\text{CH}_2\text{Cl}_2$ . An Inel MPD (Multi-Purpose Diffractometer) with a curved CPS 120 detector was used to collect x-ray powder diffraction data (XRD). The pattern was taken in the range of 5 and 120 degrees  $2\theta$  with copper radiation. Raman spectra were acquired with a Horiba-Jobin-Yvon Labram HR confocal microscope with a 800 mm focal length, a 600 grooves per mm grating and a CCD detector cooled with liquid nitrogen. The excitation wavelength was set to  $\lambda=632.8$  nm and the spectrometer was calibrated against a silicon wafer reference. A 100x, 0.9 numerical aperture microscope objective was used to focus the excitation beam ( $\phi\approx 1\mu\text{m}$  at the focal point) on a bundle of carbon nanotubes. Acquisition time was set to 40 seconds for each measurement. The carbon nanotubes were deposited onto pristine fused-silica cover slips (0.2 mm thick) for the Raman experiments.

### **Synthesis of Large-diazirine-modified AuNPs (Lg-Diaz-AuNP, $3.9 \pm 0.9$ nm)**

Lg-Diaz-AuNP were prepared using a modified two phase Brust-schiffrin method (scheme 2.2).<sup>22-24</sup> Hydrogen tetrachloroaurate (III) trihydrate (88.6 mg, 0.24 mmol) was dissolved in 7.5 mL distilled water (resulting in a bright yellow solution) and then added to a solution of tetraoctylammonium bromide (TOAB) (0.574 g, 1.05 mmol) in 21 mL toluene. The contents were stirred for 20 minutes at room temperature in order to facilitate the phase transfer of the hydrogen tetrachloroaurate (III) trihydrate into the toluene layer. After phase transfer, the aqueous layer was removed and a fresh solution of sodium borohydride (90.8 mg, 2.4 mmol) in 12 mL water was slowly added to the vigorously stirring toluene solution over 10 minutes. The reaction mixture was stirred for 2 h. Dodecanethiol (93 mg, 0.46 mmol) and diazirinethiol (**1**) (93 mg, 0.23 mmol),

synthesized as previously reported,<sup>21</sup> were added to the solution and stirred overnight. The aqueous layer was removed and the wine-red toluene layer was washed with 3 x 10 mL distilled water and evaporated to reduce the volume to ~ 2 cm<sup>3</sup>. The resulting Lg-Diaz-AuNPs were suspended in 100 ml of 95 % ethanol and placed in the freezer overnight during which time they precipitated from the solution. The supernatant was decanted and the precipitate was dissolved in 100 mL of toluene/ethanol (2:3 v/v) and sonicated for 1 minute and re-precipitated. The dissolving and re-precipitation procedure was repeated five times. The Lg-Diaz-AuNP mixture was evaporated to dryness, dissolved in toluene, and stored in the freezer. The product was characterized by <sup>1</sup>H NMR, <sup>19</sup>F NMR, and UV-vis spectroscopy and TEM (Supporting information).

#### **Synthesis of Small-diazirine-modified AuNPs (Sm-Diaz-AuNPs, 1.8 ± 0.3 nm)**

Hydrogen tetrachloroaurate (III) trihydrate (0.30 g, 0.77 mmol) was dissolved in 28 ml distilled water and then mixed with tetraoctylammonium bromide (2.30 g, 4.2 mmol) in 70 mL toluene. The contents were stirred for 30 minutes at room temperature resulting in the organic layer turning to a dark orange color and the aqueous layer becoming clear and colorless. After phase transfer, the aqueous layer was removed and the organic layer was cooled to 0 °C in ice bath. Dodecanethiol (0.468 g, 0.57 mL, 2.31 mmol) was added to the solution via a volumetric pipette and stirred for 10 minutes. The addition of dodecanethiol resulted in a color change from brownish-orange to clear and colorless. A fresh solution of sodium borohydride (0.33 g, 8.7 mmol) in 28 ml water was then added to the rapidly stirring toluene solution over 5 seconds. The solution darkened instantly, eventually becoming dark brown. The mixture stirred overnight (~18 h) as it warmed to

room temperature. After this time the aqueous layer was removed and the toluene layer was washed with 3 x 20 mL distilled water and dried over  $\text{MgSO}_4$ , filtered, and evaporated to dryness. The product, small AuNPs, was suspended in 200 ml of 95 % ethanol and placed in the freezer overnight during which time the nanoparticles precipitated from solution. When the small AuNPs had precipitated, the supernatant was decanted and the precipitate was dissolved in benzene and concentrated, resulting in the formation of a film in the round bottom flask. This film was washed repeatedly with 10 x 15 ml of 95% ethanol, resulting in pure small AuNPs as judged by  $^1\text{H}$  NMR spectroscopy, which showed no signs of free dodecanethiol, dodecylsulfide or tetraoctylammonium bromide. Small AuNPs (200 mg) were dissolved in 25 ml of toluene and degassed with nitrogen. Diazirine (1) (206 mg, 0.51 mmol) was added to the small AuNP solution in toluene and stirred for 20 h at room temperature. The solvent was evaporated and the resulting dark film (Sm-Diaz-AuNP) was washed with 95% ethanol and dried.

#### **Synthesis of Dodecanethiolate-AuNP (Model-AuNP, $4.9\pm 0.9$ nm)**

Model-AuNPs (without the diazirine functionality) were prepared as described for Lg-Diaz- AuNP except that only the dodecanethiol was used as a protecting ligand.

#### **Decoration of CNTs with Lg-Diaz-AuNP (Lg-Diaz-AuNP-CNT) or Sm-Diaz-AuNP (Sm-Diaz-AuNP-CNT)**

Multi-walled CNTs (~ 1 mg) were dispersed in 10 mL of THF using sonication (5 minutes). Lg-Diaz-AuNP or Sm-Diaz-AuNP (10 mg) were dissolved in 2 mL of THF and



added to the CNTs suspension. The mixture was placed in a Pyrex test tube, degassed with argon for 15 minutes, and irradiated using a medium pressure mercury lamp (Hanovia PC 451050/805221) at room temperature for 15 h while stirring. Then the CNTs decorated with AuNPs were isolated by centrifugation. The product, Lg-Diaz-AuNP-CNT or Sm-Diaz-AuNP-CNT, was subjected to exhaustive centrifugation and washing cycles using THF, toluene and chloroform in order to remove the excess and unreacted AuNP.

Control experiments included a) stirring a solution of Lg-Diaz-AuNP and multi-walled CNTs in THF in the absence of light and subjecting the CNTs to the same work-up procedures as that the irradiated and b) irradiation of a mixture of dodecanethiol modified-AuNP (Model-AuNP, i.e., without diazirine ligand) and multi-walled CNTs in THF under the identical conditions as described above.

## References

- 1) (a) Giljohann, D. A.; Seferos, D. S.; Daniel, W. L.; Massich, M. D.; Patel, P. C.; Mirkin, C. A. *Angew. Chem. Int. Ed.* **2010**, *49*, 3280. (b) Boisselier, E.; Astruc, D. *Chem. Soc. Rev.* **2009**, *38*, 1759. (c) Wilson, R. *Chem. Soc. Rev.* **2008**, *37*, 2028. (d) Ghosh, S. K.; Pal, T. *Chem. Rev.* **2007**, *107*, 4797.
- 2) *Carbon nanotube and related structures: synthesis, characterization, functionalization, and applications*, ed. Guldi, D. M.; Martin, N. Wiley-VCH: Weinheim, 2010.

- 3) (a) Schatz, A.; Reiser, O.; Stark, W. J.; *Chem. Eur. J.* **2010**, *16*, 8950. (b) Chen, M.; Goodman, D. W. *Chem. Soc. Rev.* **2008**, *37*, 1860.
- 4) (a) Wang, Z.; Ma, L. *Coord. Chem. Rev.* **2009**, *253*, 1607. (b) Stewart, M. E.; Anderson, C. R.; Thompson, L. B.; Maria, J.; Gray, S. K.; Rogers, J. A.; Nuzzo, R. G. *Chem. Rev.* **2008**, *108*, 494.
- 5) Iijima, S. *Nature* **1991**, *354*, 56.
- 6) (a) Eder, D. *Chem. Rev.* **2010**, *110*, 1348 and references therein. (b) Wu, H. C.; Chang, X.; Liu, L.; Zhao, F.; Zhao, Y. *J. Mater. Chem.* **2010**, *20*, 1036.
- 7) Chu, H.; Wei, L.; Cui, R.; Wang, J.; Li, Y. *Coord. Chem. Rev.* **2010**, *254*, 1117.
- 8) Dong, X.; Lau, C. M.; Lohani, A.; Mhaisalkar, S. G.; Kasim, J.; Shen, Z.; Ho, X.; Rogers, J. A.; Li, L. *J. Adv. Mater.* **2008**, *20*, 2389.
- 9) (a) Singh, R.; Premkumar, T.; Shin, J. Y.; Geckeler, K. E. *Chem. Eur. J.* **2010**, *16*, 1728. (b) Peng, X.; Chen, J.; Misewich, J. A.; Wong, S. S. *Chem. Soc. Rev.* **2009**, *38*, 1076. (c) Georgakilas, V.; Gournis, D.; Tzitzios, V.; Pasquato, L.; Guldi, D. M.; Prato, M. *J. Mater. Chem.* **2007**, *17*, 2679. (d) Wildgoose, G. G.; Banks, C. E.; Compton, R. G. *Small* **2006**, *2*, 182.
- 10) Kim, K.; Lee, S. H.; Yi, W.; Kim, J.; Choi, J. W.; Park, Y.; Jin, J. I. *Adv. Mater.* **2003**, *15*, 1618.
- 11) Quinn, B. M.; Dekker, C.; Lemay, S. G. *J. Am. Chem. Soc.* **2005**, *127*, 6146.

- 12) (a) Moon, S. Y.; Kusunose, T.; Tanaka, S.; Sekino, T.; *Carbon* **2009**, *47*, 2924. (b) Xue, B.; Chen, P.; Hong, Q.; Lin, J.; Tan, K. L. *J. Mater. Chem.* **2001**, *11*, 2378.
- 13) (a) Ellis, A. V.; Vijayamohanan, K.; Goswami, R.; Chakrapani, N.; Ramanathan, L. S.; Ajayan, P. M.; Ramanath, G. *Nano Lett.* **2003**, *3*, 279. (b) Han, L.; Wu, W.; Kirk, F. L.; Luo, J.; Maye, M. M.; Kariuki, N. N.; Lin, Y.; Wang, C.; Zhong, C. J. *Langmuir* **2004**, *20*, 6019.
- 14) (a) Herrero, M. A.; Guerra, J.; Myers, V. S.; Gomez, M. V.; Crooks, R. M.; Prato, M. *ACS Nano* **2010**, *4*, 905. (b) Kim, B.; Sigmund, W. M. *Langmuir* **2004**, *20*, 8239. (c) Wang, Z.; Li, M.; Zhang, Y.; Yuan, J.; Shen, Y.; Niu, L.; Ivaska, A. *Carbon* **2007**, *45*, 2111.
- 15) Rance, G. A.; Marsh, D. H.; Bourne, S. J.; Reade, T. J.; Khlobystov, A. N. *ACS Nano* **2010**, *4*, 4920.
- 16) Liu, L.; Wang, T.; Li, J.; Guo, Z. X.; Dai, L.; Zhang, D.; Zhu, D. *Chem. Phys. Lett.* **2003**, *367*, 747.
- 17)(a) Peng, Z.; Holm, A. H.; Nielsen, L. T.; Pedersen, S. U.; Daasbjerg, K. *Chem. Mater.* **2008**, *20*, 6068. (b) Zanella, R.; Basiuk, E. V.; Santiago, P.; Basiuk, V. A.; Mireles, E.; Puente-Lee, I.; Saniger, J. M. *J. Phys. Chem. B* **2005**, *109*, 16290. (c) Coleman, K. S.; Bailey, S. R.; Fogden, S.; Green, M. L. H. *J. Am. Chem. Soc.* **2003**, *125*, 8722.
- 18) Balasubramanian, K.; Burghard, M. *Small* **2005**, *1*, 180.

- 19) (a) Chen, J.; Rao, A. M.; Lyuksyutov, S.; Itkis, M. E.; Hamon, M. A.; Hu, H.; Cohn, R. W.; Eklund, P. C.; Colbert, D. T.; Smalley, R. E.; Haddon, R. C. *J. Phys. Chem. B* **2001**, *105*, 2525. (b) Zhang, J.; Zou, H.; Qing, Q.; Yang, Y.; Li, Q.; Liu, Z.; Guo, X.; Du, Z. *J. Phys. Chem. B* **2003**, *107*, 3712. (c) Fasi, A.; Palinko, I.; Seo, J. W.; Konya, Z.; Hernadi, K.; Kiricsi, I. *Chem. Phys. Lett.* **2003**, *372*, 848. (d) Ajayan, M.; Ebbesen, T. W.; Ichihashi, T.; Iijima, S.; Tanigaki, K.; Hiura, H. *Nature* **1993**, *362*, 522. (e) Tsang, S. C.; Harris, P. J. F.; Green, M. L. H. *Nature* **1993**, *362*, 520.
- 20) (a) Chen, J.; Hamon, M. A.; Hu, H.; Chen, Y.; Rao, A. M.; Eklund, P. C.; Haddon, R. C. *Science* **1998**, *282*, 95. (b) Chen, Y.; Haddon, R. C.; Fang, S.; Rao, A. M.; Eklund, P. C.; Lee, W. H.; Dickey, E. C.; Grulke, E. A.; Pendergrass, J. C.; Chavan, A.; Haley, B. E.; Smalley, R. E. *J. Mater. Res.* **1998**, *13*, 2423. (c) Holzinger, M.; Vostrowsky, O.; Hirsch, A.; Hennrich, F.; Kappes, M.; Weiss, R.; Jellen, F. *Angew. Chem. Int. Ed.* **2001**, *40*, 4002. (d) Moghaddam, M. J.; Taylor, S.; Gao, M.; Huang, S.; Dai, L.; McCall, M. J. *Nano Lett.* **2004**, *4*, 89. (e) Li, G.; Wang, H.; Zheng, H.; Bai, R. *Langmuir* **2010**, *26*, 7529.
- 21) Ismaili, H.; Lee, S.; Workentin, M. S. *Langmuir* **2010**, *26*, 14958.
- 22) Brust, M.; Fink, J.; Bethella, D.; Schiffrin, D. J.; Kiely, C. *J. Chem. Soc., Chem. Commun.* **1995**, 1655.
- 23) Manna, A.; Chen, P. L.; Akiyama, H.; Wei, T. X.; Tamada, K.; Knol, W. *Chem. Mater.* **2003**, *15*, 20.

- 24) Kotiaho, A.; Lahtinen, R.; Efimov, A.; Metsberg, H. K.; Sariola, E.; Lehtivuori, H.; Tkachenko, N. V.; Lemmetyinen, H. *J. Phys. Chem. C* **2010**, *114*, 162.
- 25) Tzitzios, V.; Georgakilas, V.; Oikonomou, E.; Karakassides, M.; Petridis, D. *Carbon* **2006**, *44*, 848.
- 26) Behler, K.; Osswald, S.; Ye, H.; Dimovski, S.; Gogosti, Y. *J. Nanoparticle Res.* **2006**, *8*, 615.
- 27) Felidj, N.; Aubard, J.; Levi, G. *Phys. Rev. B* **2002**, *65*, 0754191.
- 28) Wang, T.; Hu, X.; Qu, X.; Dong, S. *J. Phys. Chem. B* **2006**, *110*, 6631.

**4.5 Supplementary Information For:**

**Chapter 4,**

**Covalently Assembled Gold Nanoparticle-Carbon  
Nanotube Hybrids (AuNP-CNT) via a Photoinitiated  
Carbene Addition Reaction**

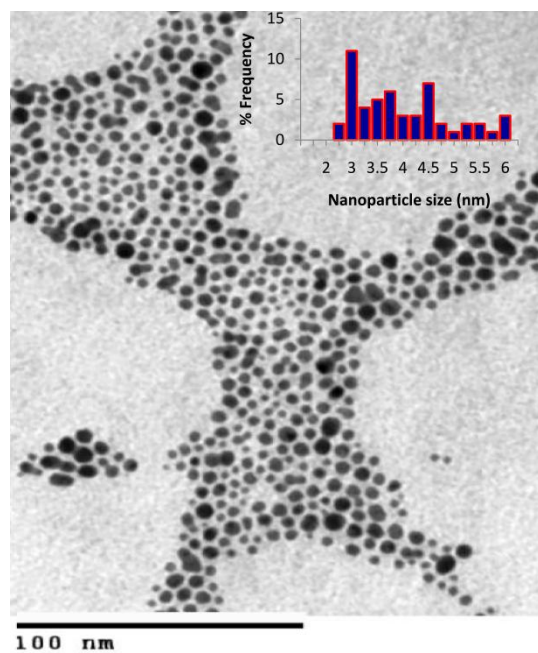


Figure S4.1 TEM image of Lg-Diaz-AuNPs (inset: statistical size distribution).

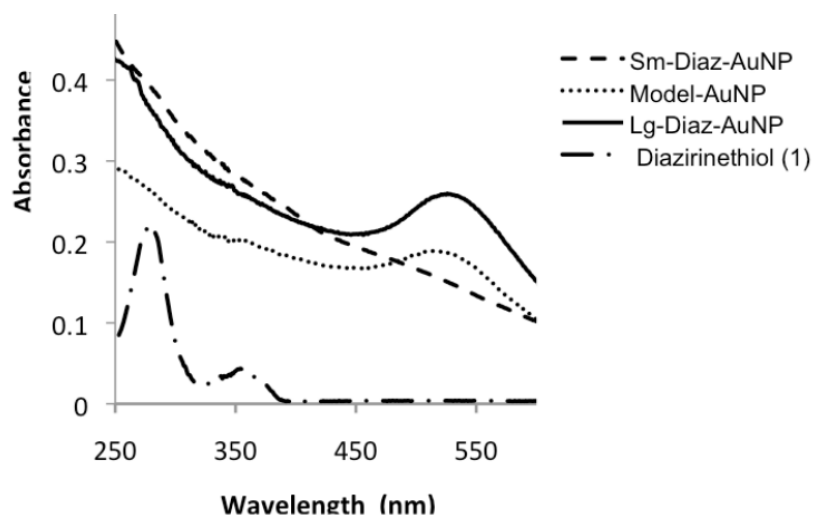


Figure S4.2 Absorption spectra of Model-AuNP, Sm-Diaz-AuNP, Lg-Diaz-AuNP and Diazirinethiol **1** in THF.

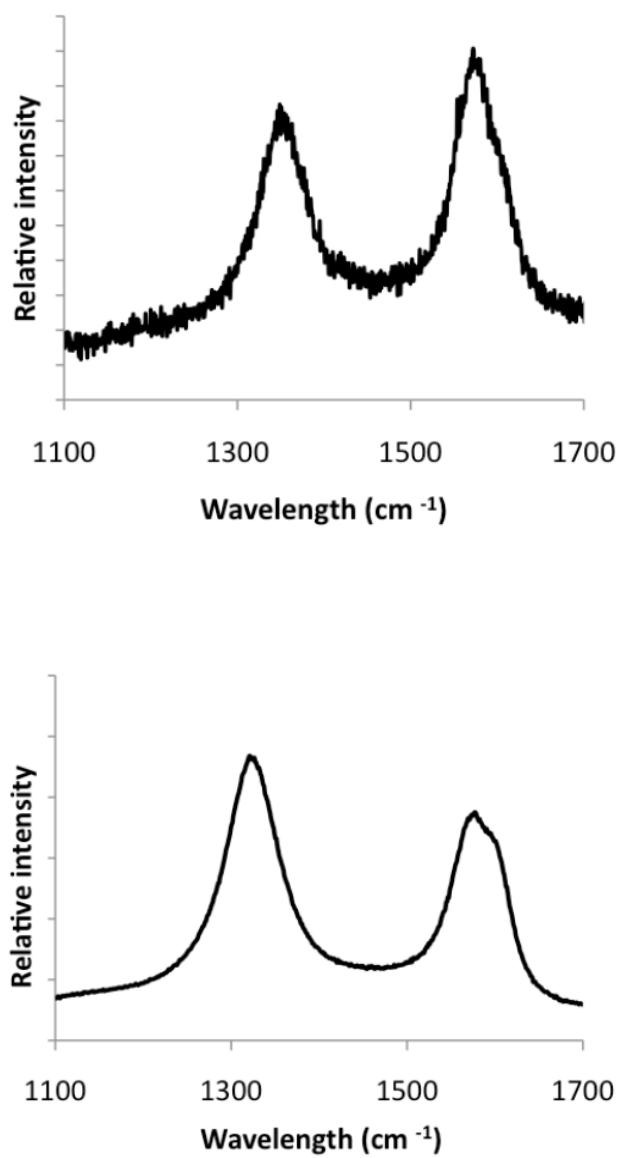


Figure S4.3 Raman spectra for as received, unmodified multi walled CNT. Top: laser wavelength is 514 nm, D/G ratio is 0.9. Bottom: Laser wavelength is 638 nm, D/G ratio is 1.19.



## Chapter 5

# Covalent Diamond-Gold Nanoparticles Hybrids via Photochemically Generated Carbenes

- Chapter 5 has been published. The corresponding reference is: Hossein Ismaili, Mark S. Workentin\*, *Chem. Commun.* **2011**, 7788.
- Hossein Ismaili carried out all of the work reported in Chapter 5.
- All of the schemes, figures, and text in Chapter 5 reproduced with permission from Chemical Communications, The Royal Society of Chemistry (RSC).

## 5.1 Introduction

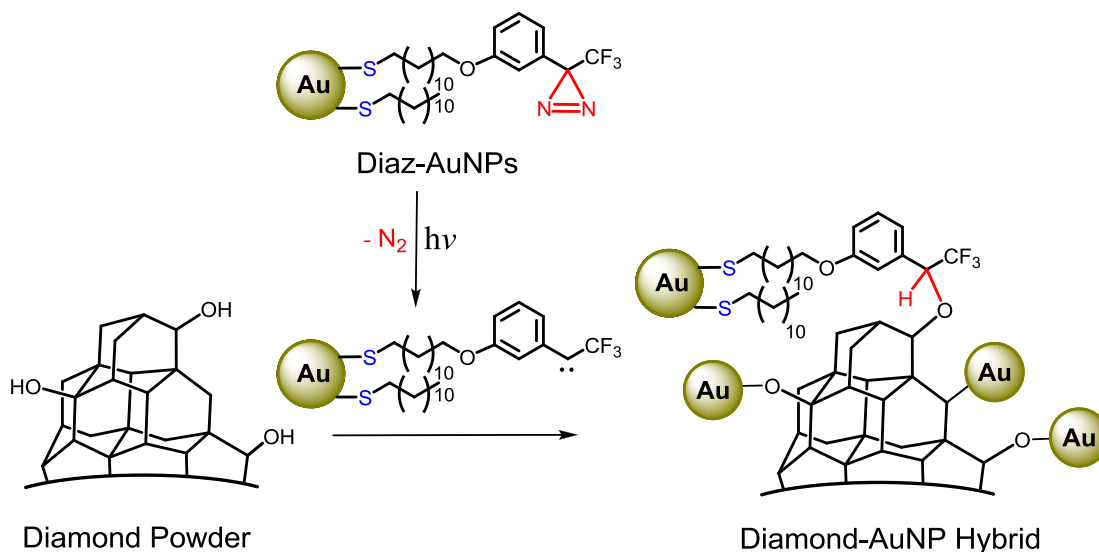
Diamond, particularly in the nano- and micro-scale size, is becoming an area of increased focus in the chemistry of carbon materials due to its extraordinary physical and chemical properties, biocompatibility, as well as the multitude of potential applications.<sup>1</sup> Diamond possesses some exceptional characteristics including high chemical inertness, optical transparency, hardness and high thermal conductivity.<sup>2</sup> It can be used as an excellent insulator because of its optical band gap of 5.47 eV or it can be doped with boron or phosphorus, giving a p-type or n-type semiconductor, respectively.<sup>3</sup>

Nano- and micro-diamonds have been extensively investigated in various fields such as gene and drug delivery,<sup>4</sup> biosensors,<sup>5</sup> photovoltaics,<sup>6</sup> electroanalysis<sup>7</sup> and solid phase extraction.<sup>8</sup> The desired application of diamonds in these fields requires chemical modification of the surface of the diamond. Several photochemical and thermal methods have been employed to modify diamond surfaces with organic compounds, including the surface graphitization of the diamond followed by radical initiated surface grafting, photolysis of elemental sulfur, covalently attachment of vinyl derivatives, carbene insertion, photolysis of perfluoroazooactane, thermolysis of peroxides, chlorination and fluorination.<sup>9</sup> Most of the methods require hydrogenation of the diamond surface because the commercially available diamond materials do not have a high concentration of suitably reactive surface functionality for efficient chemical modification using the methods described.

Gold nanoparticles (AuNPs) have also been incorporated onto diamond surfaces in an effort to enhance and complement the unique properties of each material for potential

applications. For example, it has been shown that AuNPs on diamond nanoparticles are a highly efficient Fenton catalyst<sup>10</sup> and exhibit a high antioxidant activity.<sup>11</sup> In addition, boron-doped diamond electrodes modified with AuNPs have been used for the detection of dopamine<sup>5</sup> and the reduction of oxygen.<sup>12</sup> The most common methods for the fabrication of diamond-AuNP hybrid materials involve either electrode-deposition of the gold<sup>5, 12</sup> or non-covalent adsorption of AuNPs onto the surface.<sup>10, 11, 13</sup> The lack of control over the size and instability to aggregation of the AuNP itself as well as the relatively weak interactions between the adsorbed AuNP and the diamond using these methods are key drawbacks to their usefulness in applications.

Herein we describe an efficient strategy for the preparation of covalently linked diamond-AuNP hybrid materials that allow for control of the core size and the functionality on the AuNP. Recently we reported the synthesis of 3-aryl-3-(trifluoromethyl)diazirine-modified AuNPs (Diaz-AuNPs).<sup>14</sup> We showed that irradiation of the interfacial diazirine group tethered onto the AuNP generates an intermediate carbene after nitrogen extrusion, which then undergoes insertion reactions with a wide variety of substrates leading to modification of the AuNP. To prepare diamond-AuNP hybrid materials, we utilize the photogenerated carbene on the Diaz-AuNPs to react via insertion reactions with the surface functionality of the micro-diamond powder (O–H and C–H) to yield robust covalently assembled of the diamond-AuNP hybrid (Scheme 5.1).



Scheme 5.1 Cartoon representation showing the photoreaction of the Diaz-AuNP with the OH functionality on the micro-diamond surface via a carbene insertion reaction.

## 5.2 Results and Discussion

The diazirine-modified AuNPs (Diaz-AuNPs) were synthesized using a modified two-phase Brust-Schiffrin method.<sup>14</sup> In this preparation procedure tetraoctylammonium bromide (TOAB)-stabilized AuNPs were synthesized by reducing gold (III) with NaBH<sub>4</sub> in the presence of TOAB. Next, the TOAB were place-exchanged with diazirinethiol and dodecanethiol. The product Diaz-AuNPs were characterized by <sup>1</sup>H NMR, <sup>19</sup>F NMR, UV-vis spectroscopy and TEM. The average size of Diaz-AuNPs was 3.9 ± 0.9 nm as determined by TEM (see supporting information for the characterization data).

Because the insertion reactivity of the carbene is known to be more efficient with O–H than C–H functionality,<sup>14</sup> we also desired a simple pretreatment method to increase the reactive oxygen functionality on the surface of the micro-diamond. Recently Garcia and

co-workers reported using the Fenton reaction to provide a greater surface coverage of hydroxyl groups on the surface of diamond nanoparticles.<sup>15</sup> We adapted the Fenton reaction described by Garcia, and demonstrate that it is also an effective method for the hydroxylation of commercially available micro-diamond powder. This approach avoids the need for the more difficult hydrogenation of the diamond surface while providing an increased concentration of surface active oxygen groups for our carbene insertion reaction.

The micro-diamonds before (as-received) and after Fenton treatment were characterized by IR and X-Ray photoelectron spectroscopy (XPS). Figure 5.1 shows the diffuse reflectance infrared Fourier transform spectra (DRIFT) of the micro-diamond powder before and after the Fenton treatment. It is well-known that the untreated diamond powder has an oxidized surface and contains carbonyl groups such as ketones, anhydrides and carboxylic acids. The absorptions at 1750 and 1652  $\text{cm}^{-1}$  in the spectrum of as-received diamond can be assigned to the carbonyl stretches.<sup>9e, f</sup> Fenton-treated diamond powder exhibits a decrease in the intensity of the carbonyl peaks at 1750  $\text{cm}^{-1}$  and a more diagnostic increase in the intensity of the broad peak centered at  $\sim 3300 \text{ cm}^{-1}$  and 990  $\text{cm}^{-1}$  corresponding to O–H and C–O stretches, respectively, resulting from hydroxylation of the diamond surface.

To further examine the hydroxylation of the diamond surface, the micro-diamond was analyzed by XPS before and after the Fenton treatment. The XPS analysis of as-received micro-diamond (Figure 5.2A) showed the presence of oxygen (O 1s, 8.5 %) and the carbon of diamond (C 1s, 90.3 %). The percentage of oxygen increased to 12.1% after

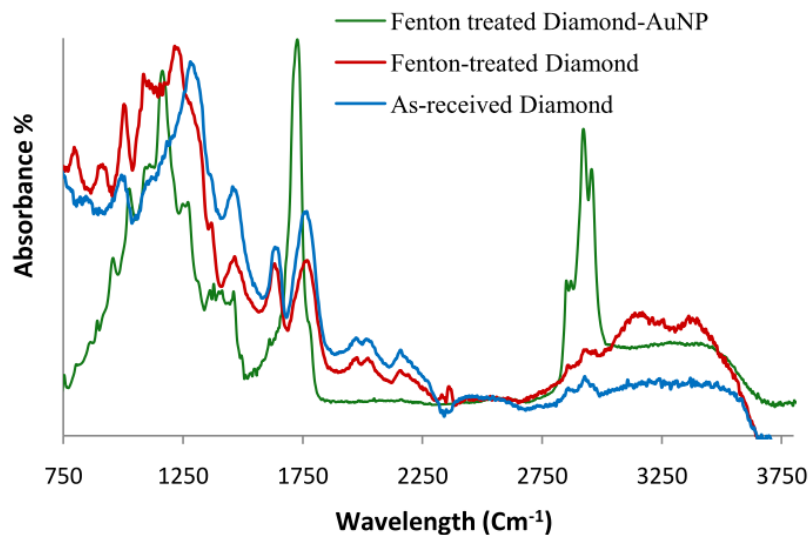


Figure 5.1 DRIFT-IR spectra of the micro-diamond powder before (blue) and after (red) the Fenton treatment. The green is the IR spectrum of the Fenton-treated diamond-AuNP hybrid material isolated after irradiation.

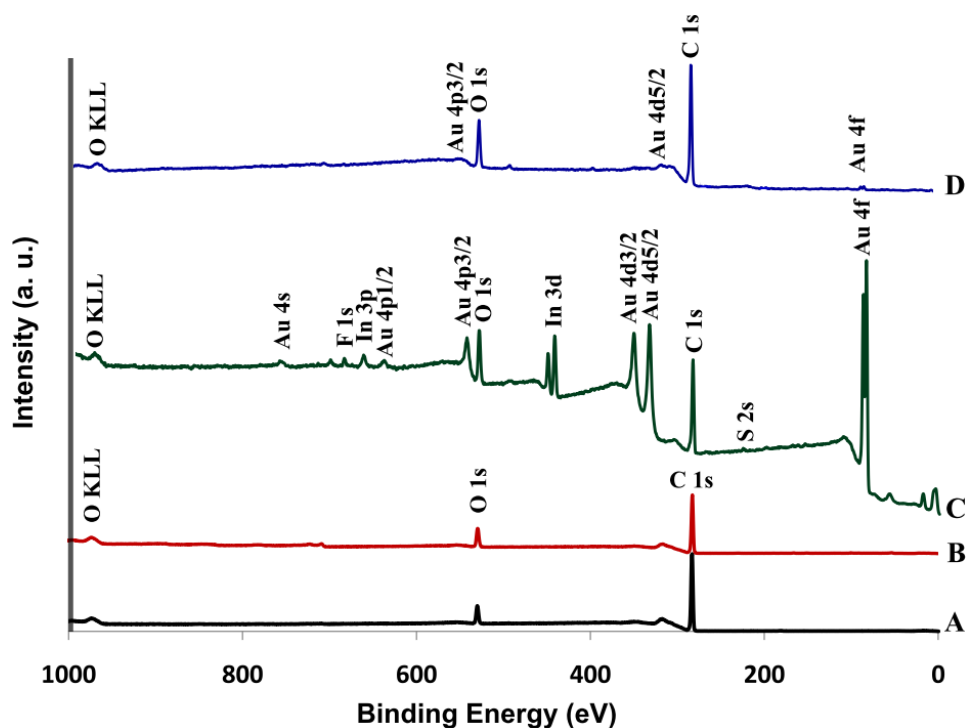


Figure 5.2 XPS spectra of A) as-received micro-diamond powder B) Fenton-treated micro-diamond powder, C) Fenton-treated diamond-AuNP hybrid pressed on an indium foil, and D) Fenton-treated micro-diamond powder subjected to the dark control experiment. Note: the indium foil is necessary as the sample with the AuNP incorporation is not a powder but greasier due to the ligands on the AuNP.

Fenton treatment while the percentage of carbon decreased to 85.7 % (Figure 5.2B). The rise of oxygen percentage in the Fenton-treated micro-diamond powder supports the hydroxylation of diamond surface via the Fenton reaction.

The Diaz-AuNPs were irradiated in the presence of both as-received and Fenton-treated micro-diamond powders. In a typical procedure, 10 mg of the relevant micro-diamond powder was dispersed in 5 mL of THF. Diaz-AuNP (15 mg) was added to the micro-diamond suspension and the solvent was evaporated. The resulting thin film was irradiated at room temperature under an argon atmosphere for 10 h using a medium pressure mercury lamp. The resulting diamond-AuNP hybrid was isolated from any excess AuNPs using a purification protocol that involved several washing and centrifugation cycles using toluene, THF, and  $\text{CHCl}_3$  consecutively. It should be noted that the Diaz-AuNPs are soluble in washing solvents utilized and any unreacted or physisorbed Diaz-AuNPs can be removed from the covalently assembled diamond-AuNP hybrid by applying washing/centrifugation cycles. Each of the irradiated samples were characterized using a number of techniques, including IR spectroscopy, powder X-ray diffraction (XRD), XPS, and SEM.

The XRD of the Fenton-treated diamond-AuNP and as-received diamond-AuNP are shown in Figure 5.3. The appearance of Au (111), (200), (220), and (311) planes of a face-centered cubic (fcc) AuNP in the spectra of the diamond-AuNP hybrids confirms the presence of AuNPs in the hybrids. It is noteworthy that the C (111), (220) and (311) planes of diamond are absent in the XRD of the Fenton-treated diamond-AuNP hybrid. This is because of high surface coverage of the AuNP on the Fenton-treated diamond-

AuNP hybrid which does not allow the X-ray beam to reach the surface of micro-diamond powder. In contrast, the diamond C planes can be observed in the XRD spectrum of as-received diamond-AuNP hybrid which is in agreement with the expected lower AuNP surface coverage (i. e. there are less O–H groups at the surface of as-received diamond, thus less Diaz-AuNPs can attach onto the surface).

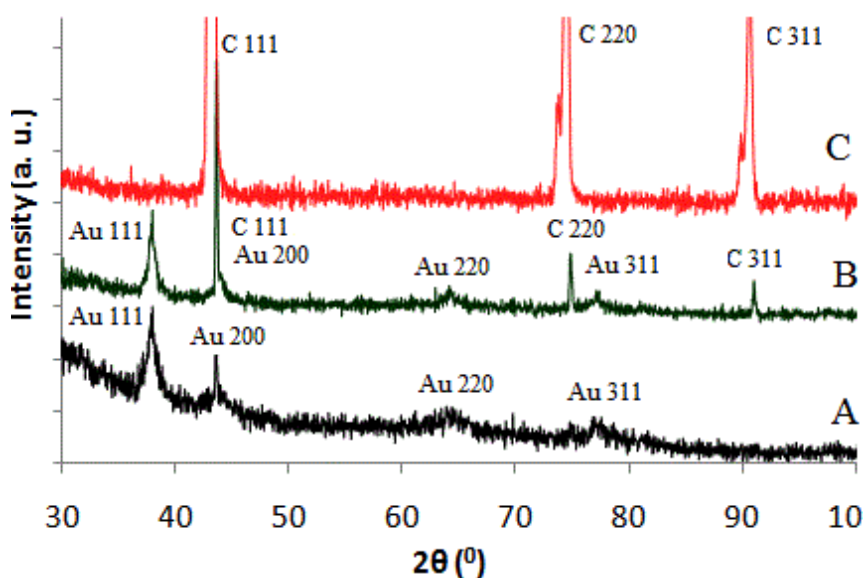


Figure 5.3 XRD of A) diamond-AuNP hybrid prepared using Fenton-treated micro-diamond, B) diamond-AuNP hybrid prepared using as-received micro-diamond, and C) Fenton-treated micro-diamond.

The IR spectrum of the Fenton-treated diamond-AuNP hybrid is shown in Figure 5.1C. While there is a decrease in the O–H stretch that would result from the carbene insertion reaction, most notable is the strong C–H stretches due to the alkyl ligands of the incorporated AuNP. The XPS obtained from the Fenton-treated diamond-AuNP hybrids prepared by irradiation is shown in Figure 5.2C. In addition to the C (1s) and O (1s) from



the diamond, the new peaks corresponding to Au (4f), (4d) and (4p), S (2s), and notably F (1s) from the CF<sub>3</sub> group are those from incorporation of the AuNPs and supports our design strategy for the modification of micro-diamond powder.

In parallel, a control experiment was also performed. The Diaz-AuNPs were mixed with the Fenton-treated micro-diamond powder and stored in the dark (no irradiation) for 10 h and then subjected to the same vigorous washing/centrifugation protocol as used for the irradiated sample. In the absence of UV irradiation no carbenes are expected to be formed and only non-covalent interactions would lead to formation of a diamond-AuNP hybrid. The XPS of the corresponding dark control experiment (Figure 5.2D) shows only trace amounts of AuNP indicating that the washing solvents could remove the majority of Diaz-AuNPs that were not covalently bound to the Fenton-treated micro-diamond. The remaining AuNPs can be due to thermal carbene formation and insertion reaction.

The presence of AuNPs on the surface of micro-diamond was also confirmed using UV-vis spectroscopy (Figure 5.4). The UV-vis of Diaz-AuNPs shows a strong surface plasmon band at 530 nm, characteristic of AuNPs with a core size >3nm. The appearance of this absorption band in the UV-vis spectrum of Fenton-treated diamond-AuNP hybrids indicates the presence of the AuNPs in these hybrids. The surface plasmon band of AuNPs in this hybrid is much broader and red-shifted (from 530 nm to 560 nm), compared with that of unreacted Diaz-AuNP. This red shift of the surface plasmon band is because of increased interparticle interactions of AuNPs attached onto the surface.<sup>16</sup>

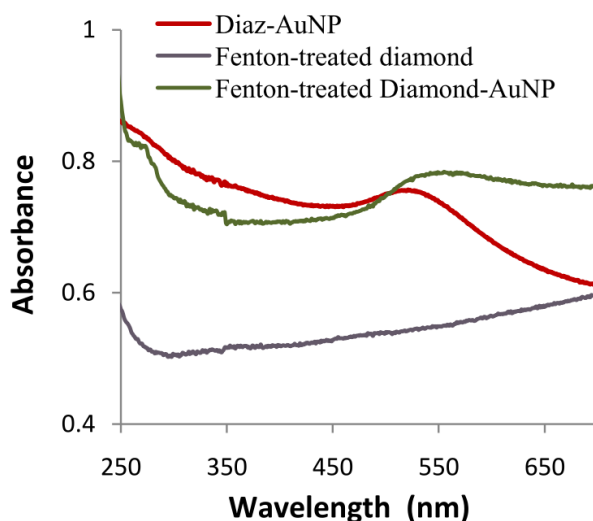


Figure 5.4 Absorption spectra of Diaz-AuNP, Fenton-treated diamond and Fenton-treated diamond-AuNP hybrid in THF.

In addition to the quantitative analysis provided by the XPS, powder XRD and the Uv-vis results, the loading of AuNPs onto the micro-diamond is observed visually by the intense color change of the samples post irradiation. The suspension of diamond-AuNP hybrid is a deep maroon color indicative of the incorporation of this size of AuNPs (Figure 5.5D), while the starting Fenton-treated micro-diamond is white/pale yellow color (Figure 5.5A). A color change of as-received micro-diamond after irradiation was also observed (Figure 5.5C), but it was much less intense, indicating a much lower incorporation of AuNPs onto the micro-diamond surface (verified by XRD and UV-vis spectra as well). Figure 5.5B shows the result of dark control experiment. The color of the diamond powder is similar to the color of original Fenton-treated micro-diamond, suggesting that photolysis is required for the covalent and robust incorporation of AuNPs onto the micro-diamond. To determine the role of UV irradiation in the diamond-AuNP

hybrid assembly a mixture of non-functionalized AuNPs (AuNPs without the diazirine functionality) and Fenton-treated diamond was exposed to the irradiation conditions and then subjected to washing/centrifugation cycles. The color of the diamond powder was unchanged compared to the original Fenton-treated micro-diamond, suggesting the lack of AuNPs on the diamond surface. This was also verified by XRD and XPS.



Figure 5.5 Photograph of the following suspensions in THF; A) Fenton- treated micro-diamond B) Fenton-treated micro-diamond after dark/control reaction C) Diamond-AuNP hybrid prepared using as-received micro-diamond post-photolysis and D) Diamond-AuNP hybrid prepared using Fenton-treated micro-diamond post-photolysis.

### 5.3 Conclusion

We described a photochemical method for the preparation of stable, robust diamond-AuNP involving the photogeneration of a reactive carbene moiety at the AuNP interface that then inserts into the surface functionality of the micro-diamond surface. Because of the high reactivity of the carbene the method requires no surface pre-treatment of the diamond. A protocol for treating the micro-diamond powder via Fenton chemistry increases the hydroxyl functionality, providing more sites of reactivity and ultimately a higher loading of AuNPs. This method should be general and could be used with

diamond nanoparticles. Because the method is photoinitiated it could be used for photopatterning of diamond surfaces. Additionally, the stabilizing ligands on the AuNP that are present after formation of the hybrid can be exchanged with other ligands, allowing additional functionality to be incorporated onto the diamond-AuNP hybrids. Supporting Information:  $^1\text{H}$  and  $^{19}\text{F}$  NMR spectra and TEM image of Diaz-AuNP as well as SEM image of Diamond-AuNP hybrid are provided.

## 5.4 Experimental

### Commercial Solvents and Reagents Used

Deuterated chloroform ( $\text{CDCl}_3$ ) and dichloromethane ( $\text{CD}_2\text{Cl}_2$ ) (Cambridge Isotope Laboratories) were used as received. The compounds dodecanethiol, hydrogen tetrachloroaurate(III), tetraoctylammonium bromide (TOAB), 1,12-dibromododecane, 3-bromoanisole, n-butyllithium, hydroxylamine hydrochloride, (N, N-dimethylamino) pyridine, p-toluenesulfonylchloride, silver (I) nitrate, boron tribromide, potassium thioacetate, acetyl chloride and Diamond powder (Aldrich, monocrystalline, *ca.* 1 micron) were used as received from the suppliers.

### General instrumentation

$^1\text{H}$ ,  $^{13}\text{C}$ , and  $^{19}\text{F}$  NMR spectra were recorded on either a Varian Inova or Mercury 400 spectrometer ( $^1\text{H}$ : 400 MHz,  $^{13}\text{C}$ : 100 MHz, and  $^{19}\text{F}$ : 376 MHz) and chemical shifts are reported in ppm relative to internal TMS (0.00 ppm) or the signals from the NMR solvent

(CHCl<sub>3</sub>:  $\delta$  7.26 ppm for <sup>1</sup>H NMR,  $\delta$  77.0 ppm for <sup>13</sup>C NMR; and CFC<sub>3</sub>:  $\delta$  0 ppm for <sup>19</sup>F NMR). Mass spectra and exact mass were recorded on a MAT 8200 Finnigan High Resolution Mass Spectrometer. Infrared spectra were recorded on a Bruker Vector 33 FTIR spectrometer and are reported in wavenumbers (cm<sup>-1</sup>). The light source used for the photochemical reactions was a Hanovia medium pressure mercury lamp (PC 451050 /805221). Transmission electron microscopy (TEM) images were recorded on a Philips CM-10 TEM operating at 100 kV. Scanning electron microscopy images were recorded on a LEO (Zeiss) 1540XB FIB/SEM. UV-Visible absorption spectra were recorded on a Cary 100 spectrometer in spectroscopic grade THF and CH<sub>2</sub>Cl<sub>2</sub>. An Inel MPD (Multi-Purpose Diffractometer) with a curved CPS 120 detector was used to collect x-ray powder diffraction data (XRD). The pattern was taken in the range of 5 and 120 degrees 2theta with copper radiation. DRIFT analysis was performed using a Bruker IFS 55 infrared spectrometer equipped with an MCT detector. A Spectra Tech Baseline™ Diffuse Reflectance attachment with a micro sampling cup was used in the main box. A mirror was used to collect the background. The powder was analysed without any further sample preparation. The XPS analyses were carried out with a Kratos Axis Ultra spectrometer using a monochromatic Al K(alpha) source (15mA, 14kV). XPS can detect all elements except hydrogen and helium, probes the surface of the sample to a depth of 5-7 nanometres, and has detection limits ranging from 0.1 to 0.5 atomic percent depending on the element. The instrument work function was calibrated to give a binding energy (BE) of 83.96 eV for the Au 4f7/2 line for metallic gold and the spectrometer dispersion was adjusted to give a BE of 932.62 eV for the Cu 2p3/2 line of metallic copper. The Kratos charge neutralizer system was used on all specimens. Survey scan

analyses were carried out with an analysis area of 300 x 700 microns and a pass energy of 160 eV. High resolution analyses were carried out with an analysis area of 300 x 700 microns and a pass energy of 20 eV. Spectra have been charge corrected to the main line of the carbon 1s spectrum (adventitious carbon) set to 284.8 eV. Spectra were analysed using CasaXPS software (version 2.3.14).

### **Synthesis of diazirine-modified AuNPs (Diaz-AuNP, $3.9 \pm 0.9$ nm)**

Hydrogen tetrachloroaurate (III) trihydrate (88.6 mg, 0.24 mmol) was dissolved in 7.5 mL distilled water (resulting in a bright yellow solution) and then added to a solution of tetraoctylammonium bromide (TOAB) (0.574 g, 1.05 mmol) in 21 mL toluene. The contents were stirred for 20 minutes at room temperature in order to facilitate the phase transfer of the hydrogen tetrachloroaurate (III) trihydrate into the toluene layer. After phase transfer, the aqueous layer was removed and a fresh solution of sodium borohydride (90.8 mg, 2.4 mmol) in 12 mL water was slowly added to the vigorously stirring toluene solution over 10 minutes. The reaction mixture was stirred for 2 h. The aqueous layer was removed and dodecanethiol (93 mg, 0.46 mmol) and diazirinethiol (93 mg, 0.23 mmol) were added to the organic layer and stirred overnight. The aqueous layer was removed and the wine-red toluene layer was washed with 3 x 10 mL distilled water and evaporated to reduce the volume to  $\sim 2$  cm<sup>3</sup>. The resulting Diaz- AuNPs were suspended in 100 ml of 95 % ethanol and placed in the refrigerator overnight during which time they precipitated from the solution. The supernatant was decanted and the precipitate was dissolved in 100 mL of toluene/ethanol (2:3 v/v) and sonicated for 1 minutes and re-precipitated. The dissolving and re-precipitation procedure was repeated

five times. The Diaz-AuNP mixture was evaporated to dryness, dissolved in toluene, and stored in the refrigerator.

### **Synthesis of Non-functionalized AuNP**

Non-functionalized AuNPs (AuNPs without diazirinethiol) were prepared as described for Diaz- AuNP except that only the dodecanethiol was used as a protecting ligand.

### **Fenton Treatment of Micro-Diamond**

Ferrous sulfate (15 g) was added to the suspension of micro-diamond (300 mg) in 50 mL of distilled water. The mixture was stirred for 30 minutes to dissolve ferrous sulfate. Concentrated sulfuric acid (15 mL) was added and the mixture was cooled in an ice-bath. Hydrogen peroxide (15 mL, 30 v/v %) was slowly dropped while observing evolution of CO<sub>2</sub>. The slurry was sonicated in an ice-bath for 2 h. Additional amounts of concentrated sulfuric acid (10 mL) and hydrogen peroxide (10 mL) were added to the mixture and sonication was continued for 2 more hours. The contents were stirred for overnight at room temperature. The excess of ferrous sulfate, acid, and hydrogen peroxide were removed by several consecutive centrifugation-dispersion cycles with Milli-Q water. The diamond powder was dried in an oven at 120 °C for 4 h.

## References

- 1) (a) J. Fan and P. K. Chu, *Small* **2010**, *6*, 2080. (b) A. Qureshi, W. P. Kang, J. L. Davidson and Y. Gurbuz, *Diamond Relat. Mater.* **2009**, *18*, 1401. (c) A. Krueger, *Chem. Eur. J.* **2008**, *14*, 1382. (d) A. Krueger, *J. Mater. Chem.* **2008**, *18*, 1485.
- 2) J. Wei and J. T. Yates Jr., *Crit. Rev. Surf. Chem.* **1995**, *5*, 1.
- 3) R. Jackman, *Semiconductor Science and Technology*, Institute of Physics Publishing, Oxford, **2003**, vol. 18.
- 4) (a) R. Martin, M. Alvaro, J. R. Herance and H. Garcia, *ACS Nano* **2010**, *4*, 65. (b) K. Liu, W. W. Zheng, C. C. Wang, Y. C. Chiu, C. L. Cheng, Y. S. Lo, C. Chen and J. I. Chao, *Nanotechnology* **2010**, *21*, 315106/1.
- 5) J. Weng, J. Xue, J. S. Ye, H. Cui, F. S. Sheu and Q. Zhang, *Adv. Funct. Mater.* **2005**, *15*, 639.
- 6) C. H. Y. X. Lim, Y. L. Zhong, S. Janssens, M. Nesladek and K. P. Loh, *Adv. Funct. Mater.* **2010**, *20*, 1313.
- 7) K. E. Toghill and R. G. Compton, *Electroanalysis* **2010**, *22*, 1947.
- 8) (a) L. Yang, M. A. Vail, A. Dadson, M. L. Lee, M. C. Asplund and M. R. Linford, *Chem. Mater.* **2009**, *21*, 4359. (b) G. Saini, L. Yang, M. L. Lee, A. Dadson, M. A. Vail and M. R. Linford, *Anal. Chem.* **2008**, *80*, 6253.



- 9) (a) I. P. Chang, K. C. Hwang, J. A. Ho, C. C. Lin, R. J. R. Hwu and J. C. Horng, *Langmuir* **2010**, *26*, 3685. (b) T. Nakamura, T. Ohana, Y. Hagiwara and T. Tsubota, *Phys. Chem. Chem. Phys.* **2009**, *11*, 730. (c) T. Kondo, H. Hoshi, K. Honda, Y. Einaga, A. Fujishima and T. Kawai, *J. Phys. Chem. C* **2008**, *112*, 11887. (d) H. Wang, J. P. Griffiths, R. G. Egdell, M. G. Moloney and J. S. Foord, *Langmuir* **2008**, *24*, 862. (e) T. Nakamura, M. Ishihara, T. Ohana and Y. Koga, *Chem. Commun.* **2003**, 900. (f) J. B. Miller and D. W. Brown, *Langmuir* **1996**, *12*, 5809.
- 10) S. Navalon, R. Martin, M. Alvaro and H. Garcia, *Angew. Chem. Int. Ed.* **2010**, *49*, 8403.
- 11) R. Martin, C. Menchon, N. Apostolova, V. M. Victor, M. Alvaro, J. R. Herance and H. Garcia, *ACS Nano* **2010**, *4*, 6957.
- 12) Y. Zhang, S. Asahina, S. Yoshihara and T. Shirakashi, *Electrochim. Acta* **2003**, *48*, 741.
- 13) (a) T. Kondo, S. Aoshima, K. Hirata, K. Honda, Y. Einaga, A. Fujishima and T. Kawai, *Langmuir* **2008**, *24*, 7545. (b) R. H. Tian, T. N. Rao, Y. Einaga and J. Zhi, *Chem. Mater.* **2006**, *18*, 939.
- 14) (a) H. Ismaili, S. Lee and M. S. Workentin, *Langmuir* **2010**, *26*, 14958. (b) H. Ismaili, F. Lagugné-Labarthe and M. S. Workentin, *Chem. Mater.* **2011**, *23*, 1519.
- 15) R. Martin, P. C. Heydorn, M. Alvaro and H. Garcia, *Chem. Mater.* **2009**, *21*, 4505.
- 16) T. Wang, X. Hu, X. Qu and S. Dong, *J. Phys. Chem. B* **2006**, *110*, 6631.

**5.5 Supplementary Information For:**

**Chapter 5,**

**Covalent Diamond-Gold Nanoparticles Hybrids via  
Photochemically Generated Carbenes**

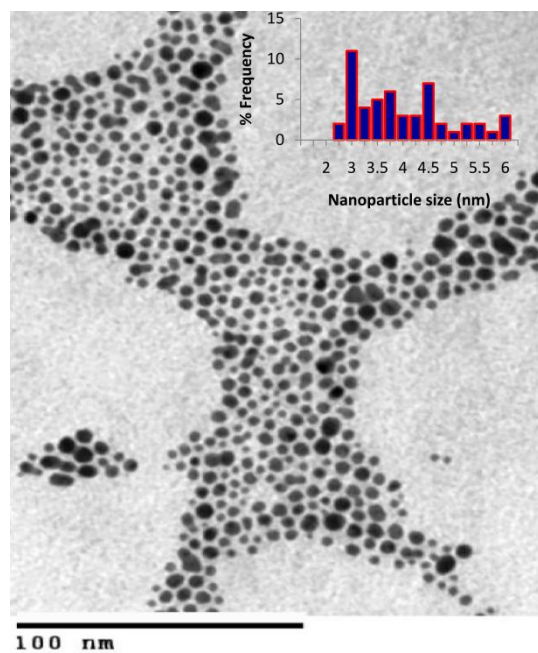


Figure S5.1 TEM image of Lg-Diaz-AuNPs (inset: statistical size distribution)

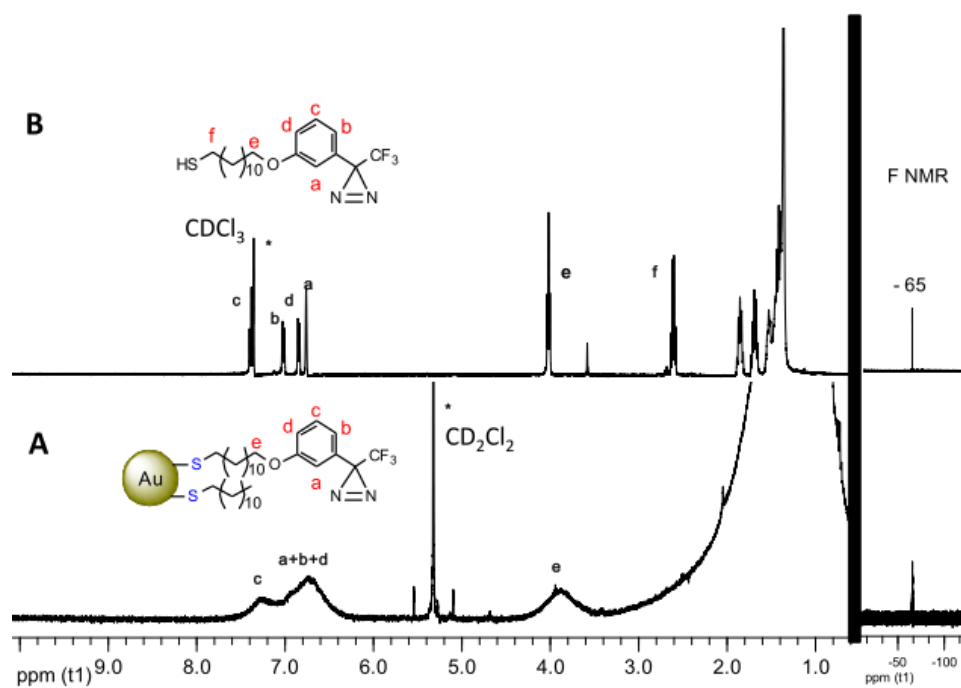


Figure S5.2  $^1\text{H}$  and  $^{19}\text{F}$  NMR spectra of A) Diaz-AuNPs and B) Diazirinethiol

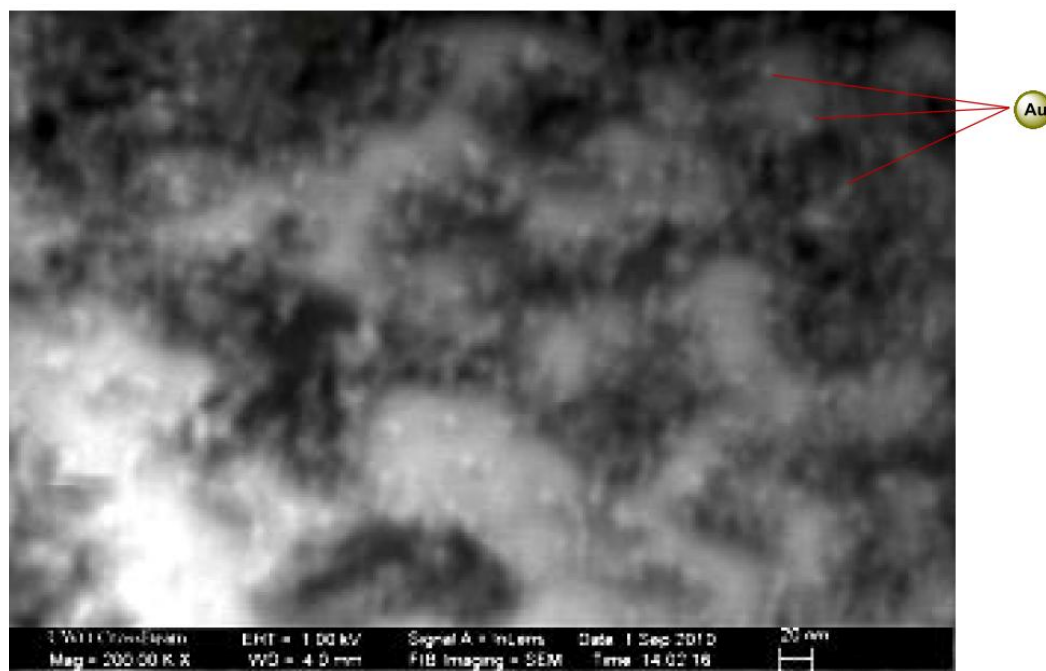


Figure S5.3 SEM of Diamond-AuNP hybrid

## Chapter 6

# Covalent Immobilization of Gold Nanoparticles (AuNP) onto Graphene and Glass Surfaces

- Chapter 6 has been submitted as a full paper. The corresponding reference is: Hossein Ismaili, Dongsheng Geng, Xueliang Sun and Mark S. Workentin\*, *Langmuir* **2011**.
- Dongsheng Geng under the supervision of Dr. Sun prepared the graphene utilized. Hossein Ismaili carried out the remainder of work reported in Chapter 6.

## 6.1 Introduction

The assembly and immobilization of metal nanoparticles onto material surfaces is a primary step in engineering interparticle properties and in the development of new hybrid materials and sensing platforms.<sup>1</sup> When nanoparticles are organized in 2D or 3D networks, new collective properties such as optical, electronic, and magnetic are displayed by the ensembles of nanoparticles that are different compared with those of the isolated counterparts. These collective properties are because of interactions between surface plasmons and/or magnetic moments of individual nanoparticles and have potential applications in biological and chemical sensing as well as in electronic, optoelectronic, and high-density information storage devices.<sup>2</sup>

Most recently, interest has centered on hybrid materials based on gold nanoparticles (AuNPs) and deposition of AuNPs onto material surfaces has been extensively investigated for the following reasons: interparticle properties of AuNPs have potential applications in catalysis, sensing, as well as electronic and optoelectronic devices; incorporation of AuNPs can improve the physical and mechanical properties of materials; the combination of AuNPs with a host nanomaterial extends the possible uses of both by prosperous integration of the properties of the two components; defined patterned structures can be obtained by assembling AuNPs on a surface; and AuNPs are an ideal candidates to study the interaction of material and biomaterial surfaces with metallic nanoparticles because there are conventional procedures to synthesize AuNPs with an organic monolayer bearing functional groups.<sup>1-3</sup>

Decoration of various materials including silicon oxide,<sup>4</sup> carbon nanotubes (CNTs),<sup>5</sup> graphene<sup>6</sup> and diamond<sup>7</sup> with AuNPs have been demonstrated. The existing approaches for this decoration include covalent, non-covalent, and direct deposition of AuNPs.<sup>4-7</sup> In the latter approach, AuNPs are formed directly on the surfaces usually via electrodeposition or in situ reduction of a gold salt. This approach has been used successfully however it requires more complex instrumentation for the deposition and control over AuNP size is difficult. In term of non-covalent approaches, electrostatic, van der Waals forces, and  $\pi$ - $\pi$  stacking interactions between functionalities on the material surface and on the monolayer of AuNPs drive the formation of the hybrid structure. However, because of the relatively weak nature of these intermolecular (intermaterial) interactions, the resulting hybrid assemblies are not mechanically robust and the AuNPs can be removed from the surface often by simple washing. Covalent attachment of AuNPs offers a method to prepare more robust hybrid structures with a designed pre-prepared AuNP core size. A typical strategy for covalent bonding the AuNPs onto the surface is to carry out a chemical reaction between terminal functional groups exposed on the monolayer of AuNPs with the functional groups accessible at the surface of the other material.

We recently reported an efficient protocol for the synthesis of covalently assembled AuNP hybrid materials that utilize a photoinitiated carbene insertion reaction between a carbene carrier, in this case the AuNP, and surfaces with any X-H (X: O, N), C-H or C=C functionality.<sup>8</sup> Specifically, we designed and prepared 3-aryl-3-(trifluoromethyl) diazirine-modified AuNPs (Diaz-AuNP) which when were irradiated, yielded a reactive

carbene AuNP that were shown to react with the surface functionality of CNTs<sup>8b</sup> and diamond,<sup>8c</sup> leading to the production of desired AuNP-nanohybrids (CNT-AuNP and diamond-AuNP). Because of the inherent reactivity of the carbene modified AuNP we proposed in the initial communication that the protocol would be general for the modification of a host of material substrates. Herein, we follow-up our suggestion and demonstrate that the protocol can be used for the fabrication of AuNP-based hybrid materials with graphene and glass.

Graphene is well known closely packed 2D nanomaterial composed of  $sp^2$ -bonded carbon atoms which has enormous potential for various applications as a promising building block of new hybrid materials.<sup>9</sup> Owing to its unique physical, thermal, electrical, and mechanical properties, graphene has been investigated in many technological fields including nano-electronics,<sup>10</sup> sensors,<sup>11</sup> biodevices,<sup>12</sup> batteries,<sup>13</sup> and drug delivery.<sup>14</sup> To further development and exploration of advanced applications of graphene, synthesis of graphene-based hybrid materials is a key requirement. Among graphene-based hybrid materials, graphene-AuNP hybrids<sup>6</sup> (graphene loaded with AuNPs) are the most studied and their application in biosensors,<sup>15</sup> catalysis,<sup>16</sup> memory devices,<sup>17</sup> and photocatalytic degradation of organic compounds<sup>18</sup> have been demonstrated. Typically, in situ reduction of a gold salt on graphene oxide or a non-covalent assembly has been employed to obtain graphene-AuNP hybrids. However, besides the need for using only graphene oxide (not reduced graphene) and small extent of AuNP loading, as previously stated, the lack of control over the AuNP size and the weak interactions between AuNPs and graphene limit the efficiency of these methods.



Because of the high reactivity of carbenes for insertion into C=C frameworks, we demonstrate that our protocol (photoinitiated carbene insertion) is efficient to produce robust covalently assembled graphene-AuNP hybrids with a high AuNP loading.

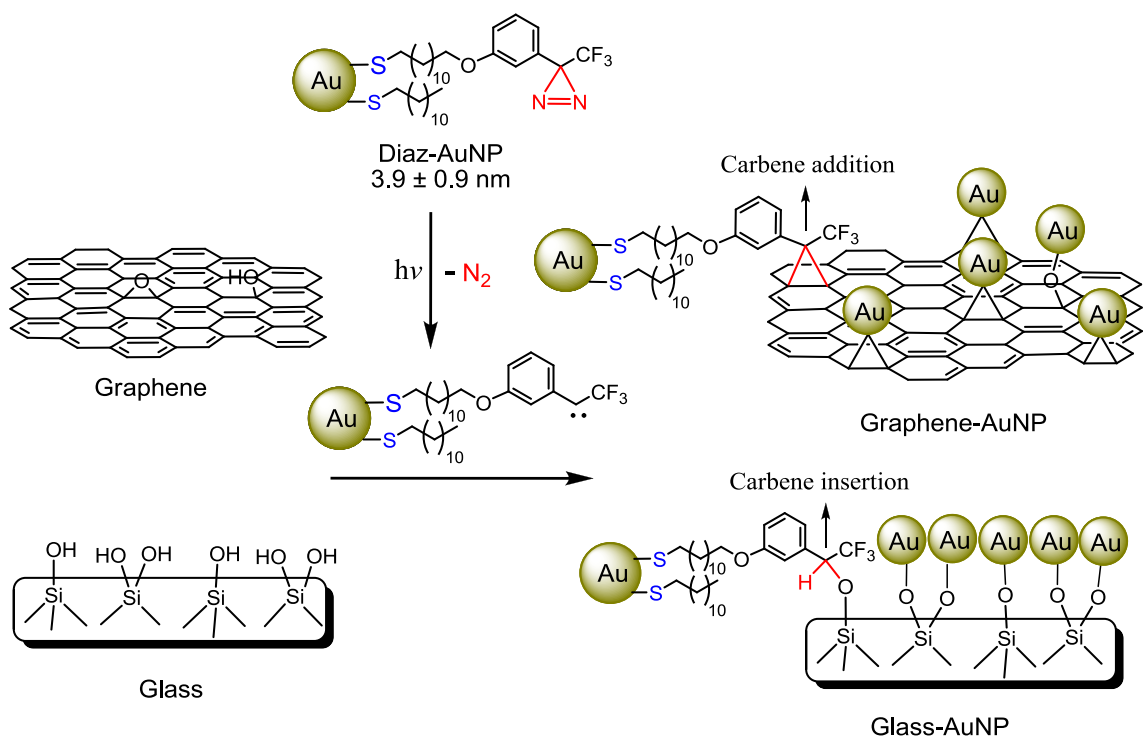
Glass slides have been widely used in plasmonic nanoparticle-based sensors<sup>19</sup> and biochips, particularly DNA and protein biochips.<sup>20</sup> This is because of their low cost, transparency, and having a flat surface with functionalization capability. As a plasmonic nanoparticle, AuNPs have also been immobilized on glass slides to make a glass-AuNP hybrid. Detection of DNA hybridization,<sup>21</sup> label-free biosensing by surface plasmon resonance<sup>19d</sup> and patterning<sup>22</sup> are examples of applications of such a glass-AuNP hybrid. Deposition of metal nanoparticles with designed size or biological substrates onto glass slides requires functionalization of the surface with suitable chemical groups. Often silanization of the surface hydroxyl groups is the initial step of functionalization of a glass surface. However, usually silanization is a sensitive reaction with a low yield and excessive polymerization often happens.<sup>20b</sup> For the AuNP case, avoiding silanization can be achieved by generating reactive groups like carbene on the monolayer of AuNPs which can then undergo reaction with hydroxyl groups at the surface of glass slides. In this paper we demonstrate the ubiquitousness of the carbene-AuNP protocol for the fabrication of covalently assembled AuNP-hybrids by extending our earlier work to the production of very different graphene-AuNP and glass-AuNP hybrids.

## 6.2 Results and Discussion

Diazirine-modified AuNPs (Diaz-AuNPs),  $3.9 \pm 0.9$  nm, were prepared according to a reported procedure.<sup>8b</sup> Briefly, tetraoctylammonium bromide (TOAB)-stabilized AuNPs were synthesized by reducing  $\text{Au}^{3+}$  with  $\text{NaBH}_4$  in the presence of TOAB. Then the following place-exchange of TOABs with diazirinethiol and dodecanethiol afforded Diaz-AuNPs. Graphene was prepared by the oxidation and exfoliation of graphite powder using the modified Hummers' method.<sup>23 - 25</sup> The SEM and TEM images (Supporting information, Figures S6.1 and S6.2) revealed the wrinkled structure of graphene. The wrinkles are composed of several graphene layers. The XRD spectrum of graphene shows very broad diffraction (002) peak at  $2\theta = 26.8^\circ$ , indicating the ordered crystal structure of graphene with the extensive conjugated  $\text{sp}^2$  carbon networks, while the XRD spectra of natural graphite powder and graphite oxide exhibit the intense peaks at  $2\theta = 12^\circ$  (001 plane) and  $26.8^\circ$  (002 plane), respectively (SI Figure S6.3). The peak shift in the latter two is due to the oxidation of natural graphite and increase in the interlayer distance of graphite oxide, respectively. Furthermore, a FTIR study was utilized to monitor the synthesis of graphene (Supporting information, Figure S6.4). The FTIR spectrum of natural graphite powder exhibits peaks characteristic of hydroxyl ( $-\text{OH}$ ) and  $\text{C}=\text{C}$  groups. In addition to these peaks, the FTIR spectrum of graphite oxide shows the peaks corresponding to  $\text{C}=\text{O}$  and  $\text{C}-\text{O}$  groups (epoxide and ether), confirming the oxidation of natural graphite. In contrast, only stretching vibrations related to the hydroxyl and  $\text{C}=\text{C}$  groups can be observed in the FTIR of graphene. The disappearance of  $\text{C}=\text{O}$  stretching and weaker intensity of the hydroxyl stretching in the FTIR spectrum of graphene reveals

that the greater part of functional groups containing oxygen have been removed (reduced) by heat treatment.<sup>25</sup>

The photochemical approach employed for the covalent decoration of graphene and the glass surface is shown in Scheme 6.1. As pointed out, upon irradiation (>300 nm) of the diazine moiety attached to the Diaz-AuNP, a carbene is generated either directly or via a diazo-intermediate.<sup>8a</sup> Because of the high reactivity of carbene, the carbene nucleophilic addition to C=C bonds of graphene and/or a carbene insertion reaction with hydroxyl groups exposed on the surface of graphene or glass is expected to occur based on our extensive preliminary studies using model OH, COOH, and C=C substrates.<sup>8a</sup>



Scheme 6.1 Illustration of carbene insertion/addition approach utilized for the covalent attachment of AuNPs onto graphene and glass.

To investigate the decoration of graphene with AuNPs, 1 mg of graphene was dispersed in 10 mL of THF. Then, a solution of Diaz-AuNPs in THF (5 mg/1 mL) was added to the graphene suspension. The mixture was purged with argon and irradiated using a medium pressure mercury lamp at room temperature for 15 h. The product, a graphene-AuNP hybrid, was isolated by centrifugation. Repeated washing/centrifugation cycles using THF,  $\text{CHCl}_3$ , and toluene were applied to remove any unbound Diaz-AuNPs.

Figures 6.1A and 6.1B show the TEM and HRTEM images of the graphene-AuNP hybrid, respectively, and the TEM image of graphene is shown in Figure 6.1D. The presence of AuNPs on graphene can be seen in Figures 6.1A and B and distribution of AuNPs is fairly even. The successful fabrication of graphene-AuNP hybrids was further confirmed by X-ray diffraction (XRD) analysis. The XRD pattern of graphene-AuNP is shown in Figure 6.2. The (111), (200), (220), (311), and (222) are planes of a face-centered cubic (fcc) AuNP, confirming the presence of AuNPs in the hybrids. It should be noted that the broad peak centered at  $2\theta = 22.8^\circ$  in the XRD of graphene-AuNP hybrids is due to the sample holder (glass) used for XRD measurement.

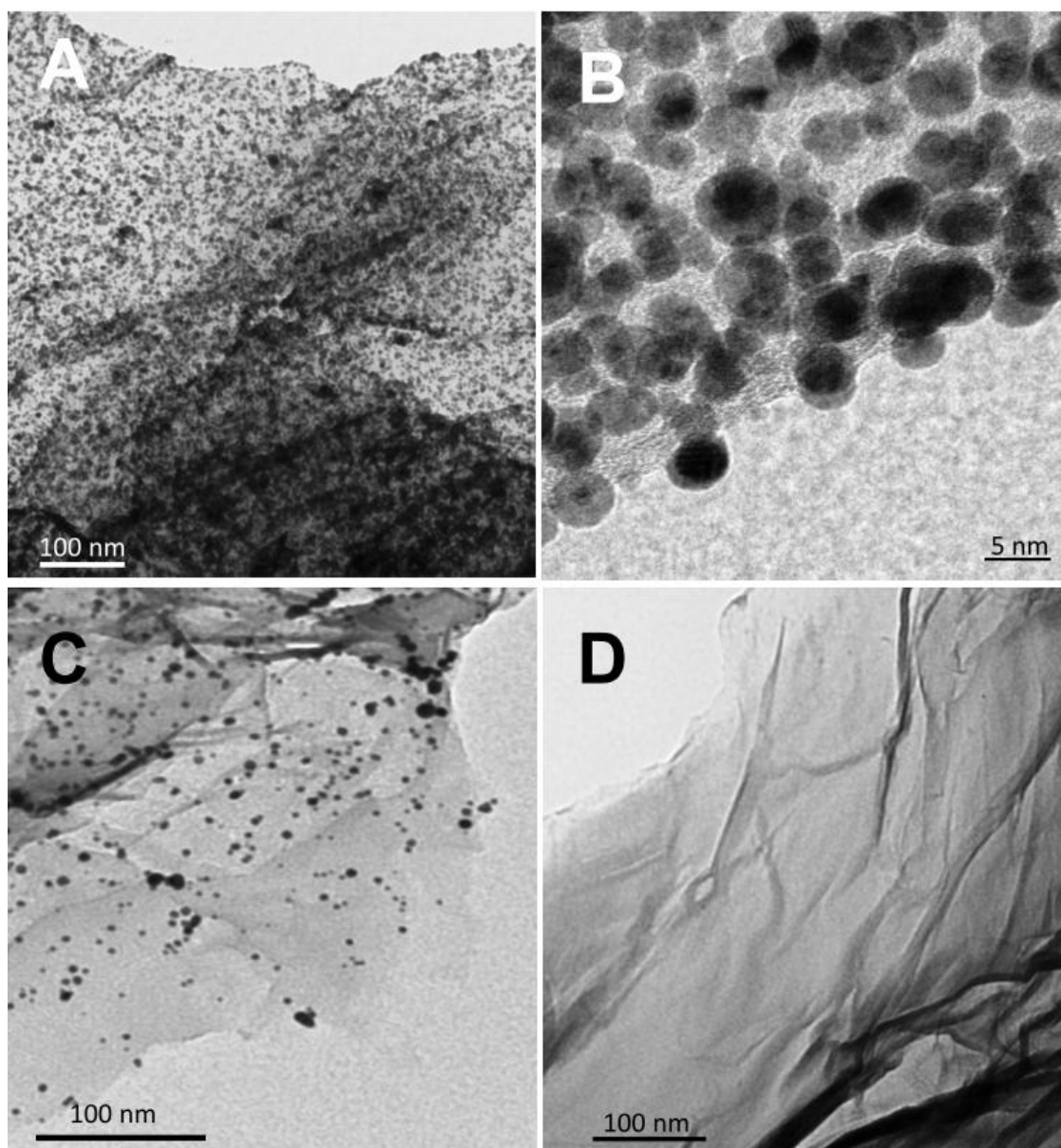


Figure 6.1 TEM images of A, B) graphene-AuNP hybrid after washing/purification protocol, C) graphene after dark/control experiment (in the absence of UV irradiation and after the washing/ purification protocol), D) unmodified graphene.

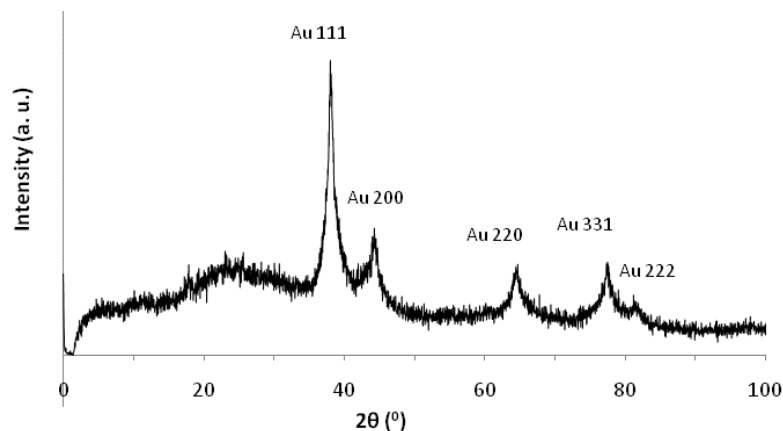


Figure 6.2 XRD patterns of graphene-AuNP.

Further characterization of the graphene-AuNP hybrids was done using UV-vis spectroscopy (Figure 6.3). The UV-vis absorption spectrum of Diaz-AuNPs exhibits a weak shoulder at around 275 nm, corresponding to transitions of the incorporated diazine chromophore onto the AuNP, and a surface plasmon resonance band (SPR) centered at 535 nm, characteristic of AuNPs with a core size > 3nm. As can be observed, the UV-vis absorption of graphene-AuNP hybrids shows the weak shoulder at 270 nm and a very broad growing peak at ~ 500 nm. The former absorption peak can be assigned to the diazine groups bound to the AuNPs in the obtained hybrids and the latter broad peak is due to the SPR of AuNPs, indicating the presence of the AuNPs in the graphene-AuNP hybrids. It is noteworthy that the decrease in the interparticle distance of AuNPs induces the red shift and broadness in the SPR, and observed SPR of AuNPs in the hybrids is roughly similar to that of aggregated nanoparticles.<sup>26, 27</sup>

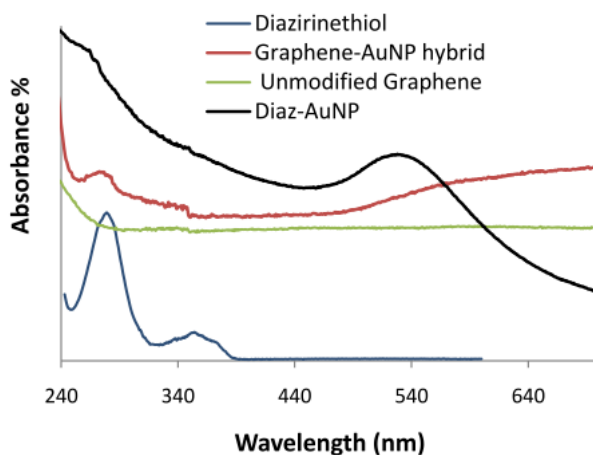


Figure 6.3 UV-vis absorption spectra of Diaz-AuNPs, graphene-AuNP hybrid (SPR peak growing at  $\sim 500$  nm), unmodified graphene, and Diazirinethiol ( $\lambda$  max at 275 nm).

When the Diaz-AuNP/graphene mixture is not irradiated, the diazine groups incorporated to the AuNPs do not generate any carbene, and therefore no covalent attachment would happen between graphene and Diaz-AuNPs. In this case if any graphene-AuNP hybrids were formed, only non-covalent interactions between graphene and Diaz-AuNPs would be responsible for them. However, due to weak nature of non-covalent interactions, AuNPs can be removed from the graphene surface simply by washing with solvent. To test the effect of carbene formation owing to irradiation, and subsequent carbene addition onto graphene in forming covalently assembled graphene-AuNP hybrids, a control experiment was carried out. Graphene was dispersed in THF and added to a solution of Diaz-AuNPs in THF and stored in the dark. Then, the mixture was subjected to the same washing/centrifugation protocol to remove the Diaz-AuNPs from the graphene. As can be seen in Figure 6.1C, the amount of AuNPs on the graphene is considerably less than that of the irradiated sample (Figures 6.1A and 6.1B). This test confirms that AuNPs in the graphene-AuNP hybrids obtained after irradiation are indeed

covalently bound to the  $\pi$ -conjugated skeleton and hydroxyl groups of graphene. The AuNPs remaining on the graphene in the non-irradiated sample may be trapped in defect sites of graphene, making them more difficult to remove with washing or due to some unintentional carbene activation and reactivity with the surface during the lengthy washing procedure, some AuNPs were bound to graphene covalently. The TEM images of irradiated and non-irradiated samples provided in Figure 6.1 were taken after extensive and repeated washing/centrifugation cycles.

In a silicate glass surface, Si–O and Si–Si bonds readily react with atmospheric water to form silanol groups (Si–OH); thus the glass surface is usually hydroxylated. However, to generate more reactive silanol groups on the surface, glass can be treated with piranha solution ( $\text{H}_2\text{SO}_4/\text{H}_2\text{O}_2$ ). We employed both piranha-treated and intact glass slides for depositing AuNPs on. The glass slides were immersed in a solution of Diaz-AuNPs in THF and irradiated. Characterizations were made after thoroughly rinsing the glass slides with several solvents to discard physisorbed AuNPs. The UV-vis absorption spectra of glass-AuNPs are shown in Figure 6.4. The emergence of the SPR band in the spectra of piranha-treated and intact glass slides verifies the deposition of AuNPs onto the glass surfaces through carbene insertion of Diaz-AuNPs into silanol groups exposed on the glass surface. The SPRs of AuNPs are red-shifted, from 535 nm of unreacted Diaz-AuNPs to 545 and 550 nm of AuNPs on the intact glass-AuNP and piranha-treated glass-AuNP, respectively. Again, these red-shifts are because of interparticle interactions of AuNPs attached onto the glass surfaces. However, the greater red-shift observed in the case of piranha-treated glass-AuNP suggests that the AuNPs are situated closer to each



other compared with those attached to the intact glass surface. Piranha-treated glass has more silanol groups, thus more Diaz-AuNPs can react with and become attached to the surface.

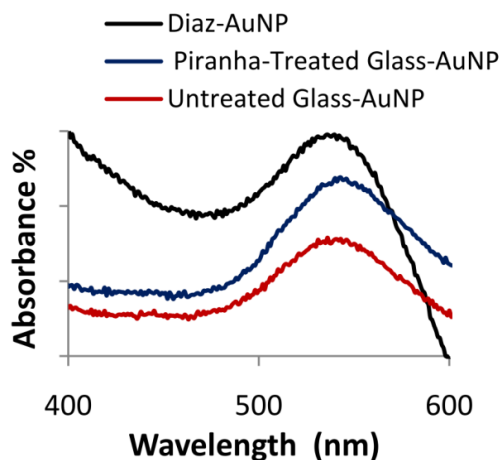


Figure 6.4 UV-vis absorption spectra of Diaz-AuNPs (SPR peak at 535 nm), untreated glass-AuNP (SPR peak at 545 nm) and piranha-treated glass-AuNP (SPR peak at 550 nm).

A control experiment including immersing the piranha-treated glass slide in a Diaz-AuNP solution and storing it in the dark was carried out as well, to ensure the need for irradiation and to determine the role of carbene insertion in the covalent attachment of AuNPs onto the glass surface. After removing the glass slide and rinsing with solvent, no SPR was observed in the UV-vis spectrum of the glass slide, indicating the absence of AuNPs on the glass surface. Further characterization of the glass-AuNP was done using X-ray photoelectron spectroscopy (XPS). In addition to the typical peaks of glass, peaks corresponding to Au (4f), Au (4d) and Au (4p), S (2s), and F (1s) are those from the bound AuNPs and confirm the deposition of AuNPs onto the glass (Figure 6.5).

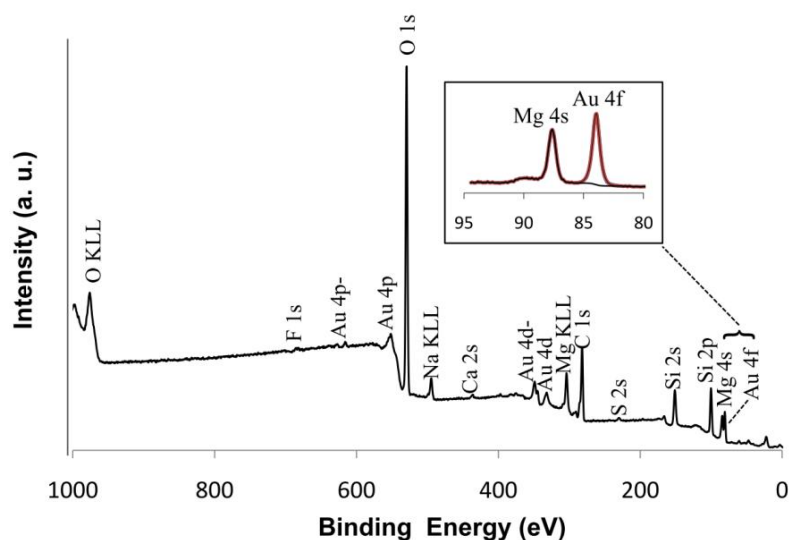


Figure 6.5 XPS spectrum of piranha-treated glass-AuNP (The inset is Au 4f and Mg 4s peaks).

Atomic force microscopy (AFM) revealed more detail about the glass-AuNP structure. Figure 6.6A displays the AFM image of piranha-treated glass-AuNP hybrid. The AuNPs are rather closely packed and retained their spherical character. Based on line scan and height profile (Figure 6.6B), the average height of the AuNPs is  $\sim 6 \pm 0.5$  nm, indicating deposition of a monolayer of AuNPs on the glass surface. It should be noted that the TEM analysis gives only the average Au core size of AuNPs and not the actual entire size of AuNPs which consists of both the size of the Au core and that of the protecting alkane monolayer. The length of the protecting monolayer is approximately 1 nm. By assuming a protecting monolayer between the glass surface and the Au core and another one between the Au core and the AFM tip, the average size of  $\sim 6 \pm 0.5$  nm measured by AFM is in accord with the average Au core size of Diaz-AuNPs ( $3.9 \pm 0.9$  nm) measured using TEM. Figures 6.6C and 6D show the AFM and height profile, respectively, of a piranha-treated glass slide.

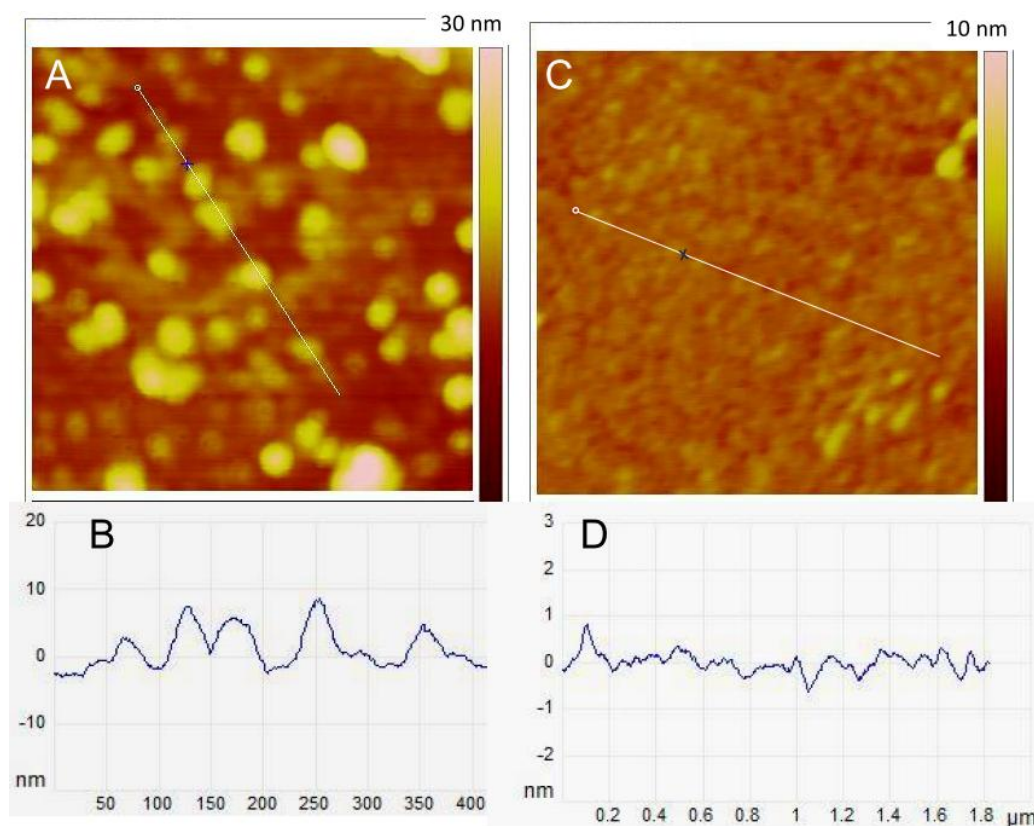


Figure 6.6 A) Tapping mode AFM image showing AuNPs covalently deposited onto piranha-treated glass surface, B) cross section analysis of AuNPs attached onto the surface, c) AFM image of piranha-treated glass slide, and D) cross section analysis of piranha-treated glass slide.

Lastly, we investigated a crude proof of concept patterning of Diaz-AuNPs onto the glass slide. Due to the chemical inertness and transparency of glass slides, they offer an ideal surface for the fabrication of patterned structures; in particular by utilizing UV-driven approaches. Figure 6.7 displays the assembly of AuNPs on a glass slide in a star shape. First, a star shape film on the glass surface was formed by applying the solution of Diaz-AuNPs dropwise. Next, the glass slide was irradiated under argon atmosphere at room temperature. The glass slide was rinsed thoroughly with several solvents and then sonicated in THF for 30 s to remove any unreacted Diaz-AuNPs from the glass surface.



Figure 6.7 AuNPs patterned on a piranha-treated glass slide utilizing photoinitiated carbene insertion method.

### 6.3 Conclusion

We have shown the ubiquitousness of the carbene-modified AuNP protocol for the fabrication of covalently assembled AuNP-hybrid materials by extending our previous works to the fabrication of graphene-AuNP and glass-AuNP hybrids. Because of the high reactivity of carbenes generated at the monolayer of nanoparticles, insertion/addition reactions with virtually any inherent surface functionality (or that which can be added/enhanced) cause the formation of AuNP-based hybrids. While we used AuNP of *ca.* 4 nm, smaller and much larger particles modified with our carbene moiety can also be utilized to deposit nanoparticles onto the surface of various materials. TEM, XRD, XPS, and UV-vis spectroscopy, as well as AFM analysis, verified the incorporation of AuNPs onto graphene and glass surfaces.

Supporting Information: TEM and SEM images of graphene, IR and XRD spectra of graphite, graphene oxide and graphene are provided.

## 6.4 Experimental

### Commercial Solvents and Reagents Used

Deuterated chloroform ( $\text{CDCl}_3$ ) and dichloromethane ( $\text{CD}_2\text{Cl}_2$ ) (Cambridge Isotope Laboratories) were used as received. The compounds dodecanethiol, hydrogen tetrachloroaurate(III), tetraoctylammonium bromide (TOAB), 1,12-dibromododecane, 3-bromoanisole, n-butyllithium, hydroxylamine hydrochloride, (N, N-dimethylamino) pyridine, p-toluenesulfonylchloride, silver (I) nitrate, boron tribromide, potassium thioacetate, and acetyl chloride were used as received from the suppliers.

### General instrumentation

$^1\text{H}$ ,  $^{13}\text{C}$ , and  $^{19}\text{F}$  NMR spectra were recorded on either a Varian Inova or Mercury 400 spectrometer ( $^1\text{H}$ : 400 MHz,  $^{13}\text{C}$ : 100 MHz, and  $^{19}\text{F}$ : 376 MHz) and chemical shifts are reported in ppm relative to internal TMS (0.00 ppm) or the signals from the NMR solvent ( $\text{CHCl}_3$ :  $\delta$  7.26 ppm for  $^1\text{H}$  NMR,  $\delta$  77.0 ppm for  $^{13}\text{C}$  NMR; and  $\text{CFCl}_3$ :  $\delta$  0 ppm for  $^{19}\text{F}$  NMR). Mass spectra and exact mass were recorded on a MAT 8200 Finnigan High Resolution Mass Spectrometer. Fourier transform infrared spectra were recorded on a Bruker spectrometer (FTIR, Bruker Tensor 27) and are reported in wavenumbers ( $\text{cm}^{-1}$ ). The light source used for the photochemical reactions was a Hanovia medium pressure mercury lamp (PC 451050 /805221). Transmission electron microscopy (TEM) images were recorded on a Philips CM-10 TEM operating at 100 kV and FEI Tecnai G2 F20 operating at 200kV. UV-vis absorption spectra were recorded on a Cary 100 spectrometer in spectroscopic grade THF and  $\text{CH}_2\text{Cl}_2$ . An Inel MPD (Multi-Purpose Diffractometer)

with a curved CPS 120 detector was used to collect X-ray powder diffraction data (XRD). The pattern was taken in the range of 5 and 120 degrees 2theta with copper radiation. The XPS analyses were carried out with a Kratos Axis Ultra spectrometer using a monochromatic Al K(alpha) source (15mA, 14kV). XPS can detect all elements except hydrogen and helium, probes the surface of the sample to a depth of 5-7 nanometres, and has detection limits ranging from 0.1 to 0.5 atomic percent depending on the element. The instrument work function was calibrated to give a binding energy (BE) of 83.96 eV for the Au 4f<sub>7/2</sub> line for metallic gold and the spectrometer dispersion was adjusted to give a BE of 932.62 eV for the Cu 2p<sub>3/2</sub> line of metallic copper. The Kratos charge neutralizer system was used on all specimens. Survey scan analyses were carried out with an analysis area of 300 x 700 microns and a pass energy of 160 eV. High resolution analyses were carried out with an analysis area of 300 x 700 microns and a pass energy of 20 eV. Spectra have been charge corrected to the main line of the carbon 1s spectrum (adventitious carbon) set to 284.8 eV. Spectra were analysed using CasaXPS software (version 2.3.14). The atomic force microscopy (AFM) images were obtained using tapping mode in ambient conditions with a Multimode AFM (Veeco Metrology) equipped with a Nanoscope V controller (Veeco). Si probes (VISTA probes, force constant 40 N/m, resonant frequency 300 kHz) were used. Before the imaging, the gold nanoparticle samples were allowed to dry under ambient conditions for 3 days.

### **Synthesis of Graphene**

Natural graphite was used as the starting material. Graphene was prepared by the oxidation of natural graphite powder using the modified Hummers' method. <sup>23 - 25</sup>

Typically, graphite powder (1 g) and sodium nitrate (0.75 g) were first stirred in concentrated sulphuric acid (37.5 mL) while being cooled in an ice bath. Then potassium permanganate (4.5 g) was gradually added to form a new mixture. After two hours in an ice bath, the mixture was allowed to stand for five days at room temperature with gentle stirring. Thereafter, 100 mL of 5 wt% sulphuric acid aqueous solution was added into the above mixture over 1h with stirring. Then, 3 g of hydrogen peroxide (30 wt% aqueous solution) was added to the above mixture and was stirred for 2h. After that, the suspension was filtered and washed until the pH value of the filtrate was neutral. The as-received slurry, so-called graphite oxide, was dried in a vacuum oven at 60 °C. Then, the graphite oxide was heated at 1050 °C for 30s under argon to get graphene. The graphene was characterized using SEM, TEM, XRD and FTIR.

### **Piranha Treatment of Glass Slides**

Standard microscope slides (VWR) were immersed in a piranha solution (70/30 (v/v) H<sub>2</sub>SO<sub>4</sub>/30% H<sub>2</sub>O<sub>2</sub>) overnight at room temperature. (CAUTION: piranha solution is an extremely strong oxidant and the handling of piranha solutions requires special protection equipment including: a full face shield, heavy duty rubber gloves). The slides were then rinsed extensively with Milli-Q water and kept in distilled water until use.

### **Decoration of Graphene with AuNPs to yield Graphene-AuNP Hybrids**

Graphene (~ 1 mg) was dispersed in 10 mL of THF using sonication (2 minutes). A solution of Diaz-AuNP (10 mg in 2 mL of THF) was added to the graphene suspension. The mixture was placed in a Pyrex test tube, degassed with argon for 15 minutes, and

irradiated at wavelengths above 300 nm using a Pyrex filtered medium pressure mercury lamp (Hanovia PC 451050 /805221) at room temperature for 15 h while stirring. Graphene decorated with AuNPs was isolated by centrifugation. The product, the graphene-AuNP hybrid, was then subjected to exhaustive centrifugation and washing cycles using THF, toluene, and chloroform for 3 weeks in order to remove the excess and unreacted Diaz-AuNPs.

A control experiment was carried out which involved stirring dispersed graphene and Diaz-AuNP in THF and keeping the mixture in the absence of light for 15 h, then subjecting the graphene to the same work-up procedures as that of the irradiated sample.

#### **Attachment of AuNPs onto Glass Slides**

Piranha-treated glass slides were dried by centrifugation. Untreated glass slides were cleaned with Aqua regia solution and dried prior to use. The glass slides were immersed in a solution of Diaz-AuNPs (5 mg) in THF (20 mL). After saturating the solution with argon for 15 minutes, the solution was irradiated using a medium pressure mercury lamp at room temperature for 3 h while stirring. The glass slides were removed and rinsed thoroughly with THF, toluene, and chloroform in order to remove the unreacted Diaz-AuNPs. A control experiment was performed and included immersing piranha-treated and untreated glass slides in a solution of Diaz-AuNPs in THF, storing in the dark (no irradiation) for 3h and then thoroughly rinsing with THF, toluene, and chloroform.

#### **Crude Patterning of AuNPs on Glass Slide**

One side of piranha-treated glass slide was covered with transparent tape, and then a



star shape was engraved. A film of Diaz-AuNPs was formed in the star shaped region by applying the solution of Diaz-AuNPs dropwise. The glass slide was irradiated under argon at room temperature for 3h. After removing the transparent tape, the glass slide was rinsed thoroughly with several solvents and then sonicated in THF for 30 s.

## References

- 1) (a) Z. Nie, A. Petukhova and E. Kumacheva, *Nature Nanotech.* **2010**, *5*, 15. (b) M. L. Curri, R. Comparelli, M. Striccoli and A. Agostiano, *Phys. Chem. Chem. Phys.* **2010**, *12*, 11197. (c) L. Wang, J. Luo, M. J. Schadt and C. J. Zhong, *Langmuir* **2009**, *26*, 618.
- 2) (a) T. K. Sau, A. L. Rogach, F. Jackel, T. A. Klar and J. Feldmann, *Adv. Mater.* **2010**, *22*, 1805. (b) S. I. Lim and C. J. Zhong, *Accounts Chem. Res.* **2009**, *42*, 798. (c) S. Kinge, M. Crego-Calama and D. N. Reinhoudt, *Chem. Phys. Chem.* **2008**, *9*, 20. (d) M. E. Stewart, C. R. Anderson, L. B. Thompson, J. Maria, S. K. Gray, J. A. Rogers and R. Nuzzo, *Chem. Rev.* **2008**, *108*, 494.
- 3) (a) R. Singh, T. Premkumar, J. Y. Shin and K. E. Geckeler, *Chem. Eur. J.* **2010**, *16*, 1728. (b) S. Navalon, R. Martin, M. Alvaro and H. Garcia, *Angew. Chem. Int. Ed.* **2010**, *49*, 8403. (c) A. S. Urban, A. A. Lutich, F. D. Stefani and J. Feldmann, *Nano Lett.* **2010**, *10*, 4794. (d) Z. Wang and L. Ma, *Coord. Chem. Rev.* **2009**, *253*, 1607. (e) C. M. Copley, J. Chen, E. C. Cho, L. V. Wang and Y. Xia, *Chem. Soc. Rev.* **2011**, *40*, 44.

- 4) (a) D. Aureau, Y. Varin, K. Roodenko, O. Seitz, O. Pluchery and Y. J. Chabal, *J. Phys. Chem. C* **2010**, *114*, 14180. (b) S. Hsieh and C. W. Hsieh, *Chem. Commun.* **2010**, *46*, 7355.
- 6) (a) B. M. Quinn, C. Dekker and S. G. Lemay, *J. Am. Chem. Soc.* **2005**, *127*, 6146. (b) G. A. Rance, D. H. Marsh, S. J. Bourne, T. J. Reade and A. N. Khlobystov, *ACS Nano* **2010**, *4*, 4920. (c) Z. Peng, A. H. Holm, L. T. Nielsen, S. U. Pedersen and K. Daasbjerg, *Chem. Mater.* **2008**, *20*, 6068.
- 7) (a) X. W. Liu, J. J. Mao, P. D. Liu and X. W. Wei, *Carbon* **2011**, *477*. (b) Z. Liu, L. Jiang, F. Galli, I. Nederlof, R. C. L. Olsthoorn, G. E. M. Lamers, T. H. Oosterkamp and J. P. Abrahams, *Adv. Funct. Mater.* **2010**, *20*, 2857. (c) J. Huang, L. Zhang, B. Chen, N. Ji, F. Chen, Y. Zhang and Z. Zhang, *Nanoscale* **2010**, *2*, 2733. (d) R. Muszynski, B. Seger and P. V. Kamat, *J. Phys. Chem. C* **2008**, *112*, 5263.
- 8) (a) T. Kondo, S. Aoshima, K. Hirata, K. Honda, Y. Einaga, A. Fujishima and T. Kawai, *Langmuir* **2008**, *24*, 7545. (b) J. Weng, J. Xue, J. S. Ye, H. Cui, F. S. Sheu and Q. Zhang, *Adv. Funct. Mater.* **2005**, *15*, 639.
- 9) (a) H. Ismaili, S. Lee and M. S. Workentin, *Langmuir* **2010**, *26*, 14958. (b) H. Ismaili, F. Lagugne-Labarthet, and M. S. Workentin, *Chem. Mater.* **2011**, *23*, 1519. (c) H. Ismaili and M. S. Workentin, *Chem. Commun.* **2011**, DOI: 10.1039/C1CC12125A.

- 10) (a) H. Bai, C. Li and G. Shi, *Adv. Mater.* **2011**, *23*, 1089. (b) R. Verdejo, M. M. Bernal, L. J. Romasanta and M. A. Lopez-Manchado, *J. Mater. Chem.* **2011**, *21*, 3301. (c) M. Pumera, *Chem. Soc. Rev.* **2010**, *39*, 4146. (d) C. N. R., Rao, A. K., Sood, K. S., Subrahmanyam, A. Govindaraj, *Angew. Chem. Int. Ed.* **2009**, *48*, 7752.
- 11) P. Avouris, *Nano Lett.* **2010**, *10*, 4285.
- 12) (a) W. Yang, K. R. Ratinac, S. P. Ringer, P. Thordarson, J. J. Gooding and F. Braet, *Angew. Chem. Int. Ed.* **2010**, *49*, 2114. (b) D. R. Kauffman and A. Star, *Analyst* **2010**, *135*, 2790.
- 13) N. Mohanty and V. Berry, *Nano Lett.* **2008**, *8*, 4469.
- 14) (a) X. Zhou, F. Wang, Y. Zhu and Z. Liu, *J. Mater. Chem.* **2011**, *21*, 3353. (b) Z. S. Wu, W. Ren, L. Wen, L. Gao, J. Zhao, Z. Chen, G. Zhou, F. Li and H. M. Cheng, *ACS Nano* **2010**, *4*, 3187.
- 15) L. Zhang, J. Xia, Q. Zhao, L. liu and Z. Zhang, *Small* **2010**, *6*, 537.
- 16) (a) W. Hong, H. Bai, Y. Xu, Z. Yao, Z. Gu and G. Shi, *J. Phys. Chem. C* **2010**, *114*, 1822. (b) J. H. Jung, D. S. Cheon, F. Liu, K. B. Lee and T. S. Seo, *Angew. Chem. Int. Ed.* **2010**, *49*, 5708.
- 17) J. Huang, L. Zhang, B. Chen, N. Ji, F. Chen, Y. Zhang and Z. Zhang, *Nanoscale* **2010**, *2*, 2733.
- 18) S. Myung, J. Park, H. Lee, K. S. Kim and S. Hong, *Adv. Mater.* **2010**, *22*, 2045.

- 19) Z. Xiong, L. L. Zhang, J. Ma and X. S. Zhao, *Chem. Commun.* **2010**, 46, 6099.
- 20) (a) O. Kedem, A. B. Tesler, A. Vaskevich and I. Rubinstein, *ACS Nano* **2011**, 5, 748.  
(b) C. Y. Hsu, J. W. Huang and K. J. Lin, *Chem. Commun.* **2011**, 47, 872. (c) T. Karakouz, M. Goomanovsky, A. Vaskevich and I. Rubinstein, *Chem. Mater.* **2009**, **21**, 5875. (d) N. Nath and A. Chilkoti, *Anal. Chem.* **2004**, 76, 5370.
- 21) (a) P. Jonkheijm, D. Weinrich, H. Schroder, C. M. Niemeyer and H. Waldmann, *Angew. Chem. Int. Ed.* **2008**, 47, 9618. (b) S. Onclin, B. J. Ravoo and D. N. Reinhoudt, *Angew. Chem. Int. Ed.* **2005**, 44, 6282. (c) S. D. Conzone and C. G. Pantano, *Mater. Today* **2004**, 20.
- 22) E. Hutter and M. P. Pileni, *J. Phys. Chem. B* **2003**, 107, 6497.
- 23) M. T. Demko, J. C. Cheng and A. P. Pisano, *Langmuir* **2010**, 26, 16710.
- 24) W. S. Hummers and R. E. Offeman, *J. Am. Chem. Soc.* **1958**, 80, 1339.
- 25) M. Hirata, T. Gotou, S. Horiuchi, M. Fujiwara and M. Ohba, *Carbon* **2004**, 42, 2929.
- 26) H. C. Schniepp, J. L. Li, M. J. McAllister, H. Sai, M. Herrera-Alonso, D. H. Adamson, R. K. Prud'homme, R. Car, D. A. Saville and I. A. Aksay, *J. Phys. Chem. B* **2006**, 110, 8535.
- 27) J. Tan, R. Liu, W. Wang, W. Liu, Y. Tian, M. Wu and Y. Huang, *Langmuir* **2010**, 26, 2093.
- 28) T. Wang, X. Hu, X. Qu and S. Dong, *J. Phys. Chem. B* **2006**, 110, 6631.

**Supporting Information for:**

**Chapter 6,**

**Covalent Immobilization of Gold Nanoparticles (AuNP)  
onto Graphene and Glass Surfaces**

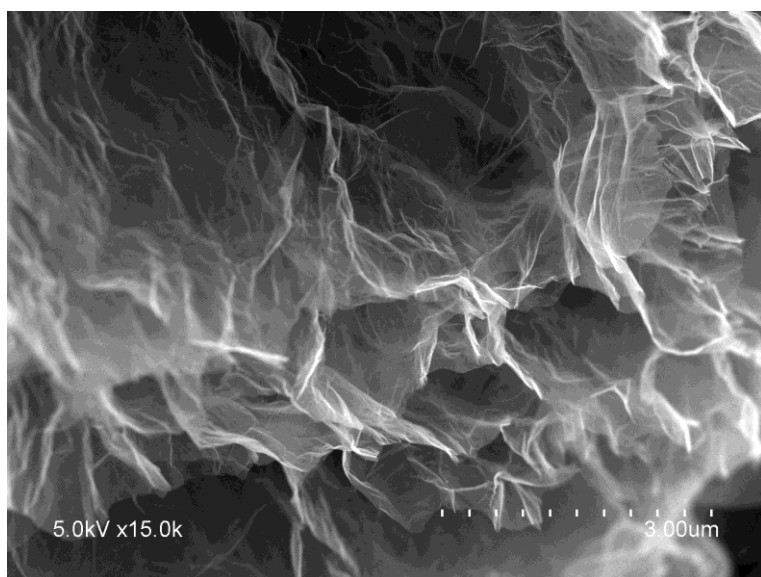


Figure S6.1 SEM image of graphene

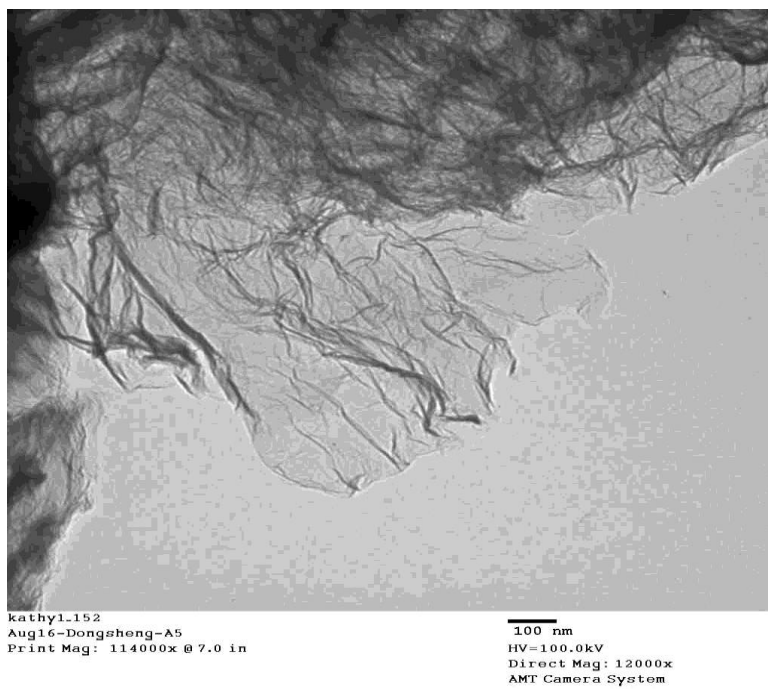


Figure S6.2 TEM image of graphene

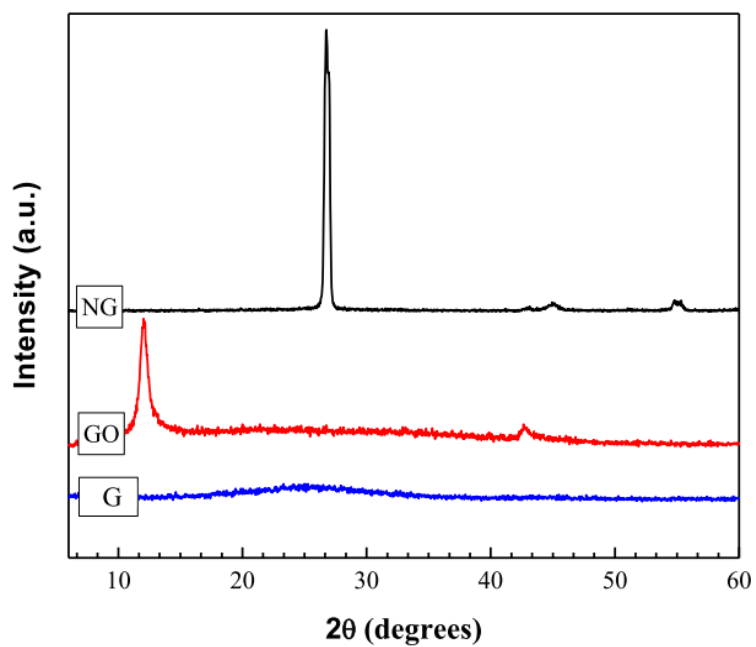


Figure S6.3 XRD patterns of natural graphite powder (NG), graphite oxide (GO), and graphene (G).

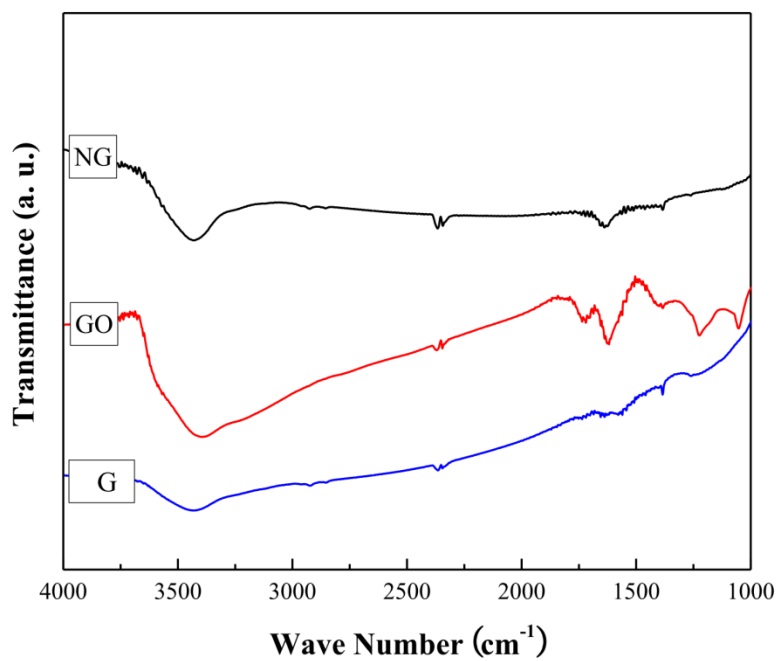


Figure S6.4 FTIR of natural graphite powder (NG), graphite oxide (GO), and graphene (G).

## Chapter 7

# Contributions of the Studies

Monolayer protected gold nanoparticles (AuNPs) continue to be an active area of discovery because of their unique chemical and physical properties as well as potential applications in catalysis, sensors, drug delivery, and nanomedicine, to name a few. These applications require the AuNPs surface to be protected by a monolayer of ligands (thiolate) with an appropriate functionality specific for the desired interaction or reactions required for the function envisioned. Therefore, developing techniques to prepare nanoparticles with specific moieties or functionalities, directly or by carrying out chemical reactions on the protecting shells, is a key component necessary in all AuNP applications. Among the exciting approaches for the synthesis of AuNPs with the desired functionality, interfacial reactions of AuNPs have attracted research interest due to their effectiveness and simplicity. It has been shown that utilizing an AuNP as a macromolecular-type reagent and carrying out organic reactions on the surface monolayer containing suitable functional groups is a promising strategy to introduce new functionality. However, often reactions of the monolayer moieties on the AuNPs are slowed or impeded relative to similar reactions in the solution phase because of the unique environment afforded by the former or by the reaction conditions that must be



used to maintain their stability to decomposition or aggregation. More specifically, the low stability of the AuNPs to both high temperature and several catalysts limits the ability for chemical modification of these particles through interfacial reactions. Our group showed that high pressure conditions can be used as an efficient tool for the chemical modification of the gold nanoparticles through interfacial Diels-Alder, nitrene 1,3-dipolar cycloadditions, and Michael addition reactions. At ambient conditions these reactions would be extremely time consuming and impractical, while hyperbaric conditions (11 000 atm) decreases reaction time to minutes without affecting the core size of the nanoparticles.

Chapter Two of this thesis reviewed my efforts toward the modification of monolayer protected gold nanoparticles using the Huisgen 1,3-dipolar cycloaddition of azides with terminal alkynes under high pressure conditions. I showed that in contrast to the identical reaction at ambient conditions, this reaction proceeds to high yield under hyperbaric conditions. The reactions on the AuNPs were characterized by IR,  $^1\text{H}$  NMR and UV-vis spectroscopy. Under high pressure conditions the click-type reactions of the azide-terminated AuNPs with activated alkynes were essentially quantitative in the absence of a copper catalyst. Reactions that were completed up to 95% of conversion in 15 h under hyperbaric conditions proceeded slowly (60 h) with an extremely poor yield (less than 13%) at ambient conditions. The results of our study show that the sluggish and inefficient uncatalyzed click-type reaction at ambient conditions can be remarkably improved in terms of conversion and reaction time by applying pressure. Furthermore due to the stability of AuNPs under high pressure conditions coupled with the

acceleration of the reaction rate, the hyperbaric click-type reaction can be used as a preparative tool for the modification of AuNPs where high chemical conversion is desirable and the use of the copper as a catalyst is problematic (purification or toxicity).

The need to perform reactions on AuNPs under relatively mild and low temperature conditions limits the types of thermal reactions that can be done efficiently and quantitatively in these systems. However, photochemical approaches provide a versatile tool for synthesizing functionalized AuNPs, recall that, photo-induced reactions can be performed under mild conditions and are generally harmless to nanoparticles. In Chapter Three, in the continuation of our studies on exploring new methods for the modification of AuNPs through interfacial reactions, I reported on carbene generation on the monolayer of AuNPs using photochemistry and demonstrated that carbene insertion/addition into the selection of trapping agents such as alcohols, amines, and alkenes is a feasible strategy to chemically modify the surface monolayer of AuNPs. 3-aryl-3-(trifluoromethyl)diazirine-modified AuNPs were prepared and characterized. Upon irradiation of tethered diazirines with 350 – 360 nm light, intermediate carbene-modified AuNPs were formed via photoinitiated nitrogen extrusion and subsequent insertion reaction/addition reactions with trapping reagents yielded in AuNPs with new functionalities. Under our irradiation conditions, depending on the trapping reagent, the reactions went to completion in 13 – 26 h. An important point to be mentioned is that the Au core of diazirine-modified AuNPs was stable under UV irradiation and TEM taken after reaction showed no change in the Au core size. Additionally, the ease of generation of the carbene-modified AuNP and its highly reactive nature makes it useful for the

incorporation of AuNP onto material surface, including carbon nanotubes, diamond, graphene, and glass.

As demonstrated in section 1.4, covalent assembly of AuNPs onto the surface of host material is an efficient means of fabrication of robust AuNP-based hybrid materials and for many applications a covalent interaction is beneficial. In Chapter Four I described formation of nanohybrid consisting of AuNPs covalently attached to multi-walled carbon nanotubes (CNT), prepared using a photoinitiated carbene addition approach. Photolysis of 3-aryl-3-(trifluoromethyl)diazirine-modified gold nanoparticles of two core sizes ( $3.9 \pm 0.9$  nm and  $1.8 \pm 0.3$  nm in diameter) resulted in the generation of reactive carbene intermediates on the monolayer of the AuNPs. In the presence of untreated CNT, the reactive carbenes underwent an addition reaction with the  $\pi$ -conjugated carbon skeleton. The AuNPs were well dispersed on the sidewall of the CNT and were robust enough to survive vigorous washing of the hybrids in a variety of solvents. In the absence of photolysis no covalent attachment occurred with the same AuNP. The nanohybrid AuNP-CNTs were characterized using TEM, XRD, Raman and UV-vis spectroscopy.

In Chapter Five I described an efficient strategy for the preparation of covalently linked diamond-AuNP hybrid materials that allow for control of the core size and the functionality on the AuNP. As the insertion reactions of carbenes with O–H bonds are known to be more efficient, I further showed that pretreatment of the micro-diamonds to increase the concentration of hydroxyl functionality leads to a higher loading of the AuNP onto the diamond than obtained with as-received micro-diamond powder. Photochemical generation of a reactive carbene-modified gold nanoparticle (AuNP,  $3.9 \pm$

0.9 nm) in the presence of micro-diamond (monocrystalline) powder resulted in a robust covalent diamond-AuNP hybrid material. Fenton chemistry increased the hydroxyl functionality of micro-diamond, providing more sites of reactivity toward carbene insertion, therefore, the coverage of the AuNP on the micro-diamond was enhanced when micro-diamond was treated by Fenton chemistry. The nanohybrid AuNP-diamond was characterized using IR, XRD, XPS, and UV-vis spectroscopy.

Finally, in Chapter Six I demonstrated the ubiquitousness of the carbene-AuNP protocol for the fabrication of covalently assembled AuNP-hybrids by extending our earlier works to the production of graphene-AuNP and glass-AuNP hybrids. As pointed out, upon irradiation (>300 nm) of the diazirine-modified AuNP, a carbene is generated either directly or via a diazo-intermediate and because of the high reactivity of carbene, the carbene nucleophilic addition to C=C bonds of graphene and/or a carbene insertion reaction with hydroxyl groups exposed on the surface of graphene or glass occurred are expected, affording graphene and glass decorated with AuNPs. TEM, XRD, XPS, UV-vis spectroscopy as well as AFM analysis verified the incorporation of AuNPs onto graphene and glass surfaces.

Overall throughout this thesis, new thermal and photochemical reactions were described which can be utilized to efficiently and quantitatively functionalize AuNPs under mild conditions. Thermal reactions included Huisgen 1,3-dipolar cycloadditions of azide-modified AuNPs under high pressure conditions; carbene generation on the monolayer of AuNPs using irradiation of diazirine modified-AuNPs was our photochemical approach. Additionally in this thesis, a novel strategy for the fabrication of

robust AuNP hybrid materials was introduced and it was shown that photogeneration of a carbene on the monolayer of AuNPs in the presence of host materials leads to the formation of covalently assembled AuNP-based hybrid materials via carbene insertion/addition reactions. Using this strategy, hybrids including AuNP-CNT, AuNP-Diamond, AuNP-Graphene, and AuNP-Glass were prepared and characterized.

## Appendix

# Copyright & Permission

### License Details

This is a License Agreement between Hossein Ismaili ("You") and NRC Research Press ("NRC Research Press"). The license consists of your order details, the terms and conditions provided by NRC Research Press, and the payment terms and conditions.

**License Number:** 2652580538145

**License date:** Apr 19, 2011

**Licensed content publisher:** NRC Research Press

**Licensed content publication:** Canadian Journal of Chemistry

**Licensed content title:** Remarkable high-yielding chemical modification of gold nanoparticles using uncatalyzed click-type 1,3-dipolar cycloaddition chemistry and hyperbaric conditions

**Licensed content author:** Hossein Ismaili et al.

**Type of Use:** reuse in a thesis/dissertation

**Licensed content date:** Dec 1, 2009

**Volume number:** 87

**Issue number:** 12

**Requestor type:** Author (original work)

**Format:** Print and electronic

**Portion:** Full article

**Title of your thesis/dissertation:** Strategies for the Thermal and Photochemical Modification of Gold Nanoparticles (AuNPs) and the Fabrication of AuNP Hybrid Materials

**Expected completion date:** August 2011

**Estimated size (number of pages):** 250

**Total:** 0.00 USD

---

## **License Details**

This is a License Agreement between Hossein Ismaili ("You") and American Chemical Society ("American Chemical Society"). The license consists of your order details, the terms and conditions provided by American Chemical Society, and the payment terms and conditions.

**License Number:** 2652580028533

**License date:** Apr 19, 2011

**Licensed content publisher:** American Chemical Society

**Licensed content publication:** Langmuir

**Licensed content title:** Diazirine-Modified Gold Nanoparticle: Template for Efficient Photoinduced Interfacial Carbene Insertion Reactions

**Licensed content author:** Hossein Ismaili et al.

**Licensed content date:** Sep 1, 2010

**Volume number:** 26

**Issue number:** 18

**Type of Use:** Thesis/Dissertation

**Requester Type:** Author (original work)

**Are you the Author of original article?** Yes

**Format:** Print and electronic

**Portion:** Full article

**Title of the thesis / dissertation :** Strategies for the Thermal and Photochemical Modification of Gold Nanoparticles (AuNPs) and the Fabrication of AuNP Hybrid Materials

**Expected completion date:** August 2011

**Estimated size (number of pages):** 250

**Billing Type:** Invoice

**Permissions price:** 0.00 USD

---

### **License Details**

This is a License Agreement between Hossein Ismaili ("You") and American Chemical Society ("American Chemical Society"). The license consists of your order details, the terms and conditions provided by American Chemical Society, and the payment terms and conditions.

**License Number:** 2652570706824

**License date:** Apr 19, 2011

**Licensed content publisher:** American Chemical Society

**Licensed content publication:** Chemistry of Materials

**Licensed content title:** Covalently Assembled Gold Nanoparticle-Carbon Nanotube Hybrids via a Photoinitiated Carbene Addition Reaction

**Licensed content author:** Hossein Ismaili et al.

**Licensed content date:** Mar 1, 2011

**Volume number:** 23

**Issue number:** 6

**Type of Use:** Thesis/Dissertation

**Requester Type:** Not specified



**Are you the Author of original article?** Yes

**Format:** Print and electronic

**Portion:** Full article

**Title of the thesis / dissertation:** Strategies for the Thermal and Photochemical Modification of Gold Nanoparticles (AuNPs) and the Fabrication of AuNP Hybrid Materials

**Expected completion date:** August 2011

**Estimated size (number of pages):** 250

**Billing Type:** Invoice

**Permissions price:** 0.00 USD

---

### **Permission for Paper Reused in Chapter Five**

The Royal Society of Chemistry (RSC) hereby grants permission for the use of your paper(s) specified below in the printed and microfilm version of your thesis. You may also make available the PDF version of your paper(s) that the RSC sent to the corresponding author(s) of your paper(s) upon publication of the paper(s) in the following ways: in your thesis via any website that your university may have for the deposition of theses, via your university's Intranet or via your own personal website. We are however unable to grant you permission to include the PDF version of the paper(s) on its own in your institutional repository. The Royal Society of Chemistry is a signatory to the STM Guidelines on Permissions (available on request). Please note that if the material specified below or any part of it appears with credit or acknowledgement to a third party then you must also secure permission from that third party before reproducing that material. Please ensure that the thesis states the following:

Reproduced by permission of The Royal Society of Chemistry and include a link to the paper on the Royal Society of Chemistry's website. Please ensure that your co-authors are aware that you are including the paper in your thesis.

Regards

Gill Cockhead

Contracts & Copyright Executive

Gill Cockhead (Mrs), Contracts & Copyright Executive

Royal Society of Chemistry, Thomas Graham House

-----Original Message-----

To: CONTRACTS-COPYRIGHT (shared)

**Subject:** Permission Request Form: Hossein Ismaili

**Name:** Hossein Ismaili

I am preparing the following work for publication:

**Thesis title:** Strategies for the Thermal and Photochemical Modification of Gold Nanoparticles (AuNPs) and the Fabrication of AuNP Hybrid Materials

**Publisher:** University of Western Ontario

I would very much appreciate your permission to use the following material:

**Journal/Book Title:** Chemical Communications

**Editor/Author(s):** Hossein Ismaili, Mark S. Workentin

**Year of Publication:** 2011

**Description of Material:** Full Communication, DOI: 10.1039/C1CC12125A

---

## License Details

This is a License Agreement between Hossein Ismaili ("You") and American Chemical Society ("American Chemical Society"). The license consists of your order details, the terms and conditions provided by American Chemical Society, and the payment terms and conditions.

**License Number:** 2670410723417

**License date:** May 15, 2011

**Licensed content publisher:** American Chemical Society

**Licensed content publication:** Chemistry of Materials

**Licensed content title:** One Step Synthesis of Multi-walled Carbon Nanotube/Gold Nanocomposites for Enhancing Electrochemical Response

**Licensed content author:** Renyun Zhang et al.

**Licensed content date:** Mar 1, 2007

**Volume number:** 19

**Issue number:** 5

**Type of Use:** Thesis/Dissertation

**Requester Type:** Not specified

**Are you the Author of original article?** No

**Format:** Print and electronic

**Portion:** Table/Figure/Micrograph

**Number of Tables/Figures/Micrographs:** 1

**Title of the thesis / dissertation:** Strategies for the Thermal and Photochemical Modification of Gold Nanoparticles (AuNPs) and the Fabrication of AuNP Hybrid Materials

**Expected completion date:** August 2011

**Estimated size (number of pages):** 250

**Billing Type:** Invoice

**Permissions price:** 0.00 USD

---

## **License Details**

This is a License Agreement between Hossein Ismaili ("You") and Elsevier ("Elsevier"). The license consists of your order details, the terms and conditions provided by Elsevier, and the payment terms and conditions.

**License Number:** 2671070276187

**License date:** May 16, 2011

**Licensed content publisher:** Elsevier

**Licensed content publication:** Applied Surface Science

**Licensed content title:** A simple approach for immobilization of gold nanoparticles on graphene oxide sheets by covalent bonding

**Licensed content author:** Tuan Anh Pham, Byung Choon Choi, Kwon Taek Lim, Yeon Tae Jeong

**Licensed content date:** 1 February 2011

**Licensed content volume number:** 257

**Licensed content issue number:** 8

**Number of pages:** 8

**Type of Use:** reuse in a thesis/dissertation

**Portion:** figures/tables/illustrations

**Number of figures/tables/illustrations:** 1

**Format:** both print and electronic

**Are you the author of this Elsevier article?** No

**Will you be translating?** No

**Title of your thesis/dissertation:** Strategies for the Thermal and Photochemical Modification of Gold Nanoparticles (AuNPs) and the Fabrication of AuNP Hybrid Materials

**Expected completion date:** August 2011

**Estimated size (number of pages):** 250

**Elsevier VAT number:** GB 494 6272 12

**Permissions price:** 0.00 USD

**VAT/Local Sales Tax:** 0.0 USD / 0.0 GBP

**Total:** 0.00 USD

---

## License Details

This is a License Agreement between Hossein Ismaili ("You") and Elsevier ("Elsevier"). The license consists of your order details, the terms and conditions provided by Elsevier, and the payment terms and conditions.

**License Number:** 2671070669210

**License date:** May 16, 2011

**Licensed content publisher:** Elsevier

**Licensed content publication:** Chemical Physics Letters

**Licensed content title:** Self-assembly of gold nanoparticles to carbon nanotubes using a thiol-terminated pyrene as interlinker

**Licensed content author:** Luqi Liu, Tongxin Wang, Junxin Li, Zhi-Xin Guo, Liming Dai, Deqing Zhang, Daoben Zhu

**Licensed content date:** 10 January 2003

**Licensed content volume number:** 367

**Licensed content issue number:** 5-6

**Number of pages:** 6

**Type of Use:** reuse in a thesis/dissertation

**Portion:** figures/tables/illustrations

**Number of figures/tables/illustrations:** 1

**Format:** both print and electronic

**Are you the author of this Elsevier article?** No

**Will you be translating?** No

**Title of your thesis/dissertation:** Strategies for the Thermal and Photochemical Modification of Gold Nanoparticles (AuNPs) and the Fabrication of AuNP Hybrid Materials

**Expected completion date:** August 2011

**Estimated size (number of pages):** 250

**Elsevier VAT number:** GB 494 6272 12

**Permissions price:** 0.00 USD

**VAT/Local Sales Tax:** 0.0 USD / 0.0 GBP

**Total:** 0.00 USD

---

### **Permission from RSC**

The Royal Society of Chemistry hereby grants permission for the use of the material specified below in the work described and in all subsequent editions of the work for distribution throughout the world, in all media including electronic and microfilm. You may use the material in conjunction with computer-based electronic and information

retrieval systems, grant permissions for photocopying, reproductions and reprints, translate the material and to publish the translation, and authorize document delivery and abstracting and indexing services. The Royal Society of Chemistry is a signatory to the STM Guidelines on Permissions (available on request).

Please note that if the material specified below or any part of it appears with credit or acknowledgement to a third party then you must also secure permission from that third party before reproducing that material.

Please ensure that the published article carries a credit to The Royal Society of Chemistry in the following format:

*[Original citation] – Reproduced by permission of The Royal Society of Chemistry*

and that any electronic version of the work includes a hyperlink to the article on the Royal Society of Chemistry website. The recommended form for the hyperlink is [http://dx.doi.org/10.1039/DOI suffix](http://dx.doi.org/10.1039/DOI_suffix), for example in the link <http://dx.doi.org/10.1039/b110420a> the DOI suffix is 'b110420a'. To find the relevant DOI suffix for the RSC paper in question, go to the Journals section of the website and locate your paper in the list of papers for the volume and issue of your specific journal. You will find the DOI suffix quoted there.

Regards

Gill Cockhead

Contracts & Copyright Executive

Gill Cockhead (Mrs), Contracts & Copyright Executive

Royal Society of Chemistry, Thomas Graham House

-----Original Message-----

To: CONTRACTS-COPYRIGHT (shared)

**Subject:** Permission Request Form: Hossein Ismaili

**Name:** Hossein Ismaili

I am preparing the following work for publication:

**Thesis title:** Strategies for the Thermal and Photochemical Modification of Gold Nanoparticles (AuNPs) and the Fabrication of AuNP Hybrid Materials

**Publisher:** University of Western Ontario

I would very much appreciate your permission to use the following material:

**Journal/Book Title:** Journal of Material Chemistry

**Editor/Author(s):** Fenghua Li, Huafeng Yang, Changsheng Shan, Qixian Zhang, Dongxue Han, Ari Ivaska and Li Niu

**Volume Number:** 19

**Year of Publication:** 2009

**Description of Material:** Figure 1

**Pages:** 4022-4025

---

**Permission from Wiley-VCH Verlag GmbH & Co. KGaA**

Dear Customer,

Thank you for your email.

We hereby grant permission for the requested use expected that due credit is given to the original source. If material appears within our work with credit to another source, authorization from that source must be obtained.

**From:** Hossein Ismaili

**Sent:** Tuesday, May 17, 2011 6:07 PM

**To:** Permissions - US

**Subject:** NON-RIGHTSLINK (reuse a figure in thesis)



Hello,

I would like to reuse below in my Thesis. I would appreciate if you send the permission.

1) *Angew. Chem. Int. Ed.* **2009**, 48, 4166, Figure 1a.

2) *Angew., Chem., Int., Ed.*, **2007**, 46, 5480, Figure 7.

3) *Small* **2010**, 6, No. 4, 513–516, Figure 2a, 3.

Thanks

Hossein Ismaili

---

## Curriculum Vitae

### Hossein Ismaili

Department of Chemistry  
The University of Western Ontario

#### Education

<b>Dates</b>	<b>University</b>	<b>Degree</b>
Jan. 1999 - Jun. 2004	Tabriz University, Iran	BSc, Chemistry
Sep. 2004 - Sep. 2006	Sharif University of Technology, Iran	MSc, Chemistry
Jan. 2007-Current	The University of Western Ontario	PhD, Chemistry

#### TA and Research Experience

Laboratory Research and Teaching Assistant at the University of Western Ontario (Chemistry Department) Since Jan. 2007.

Research Supervisor: Prof. Mark S. Workentin

Courses TAed: Chemistry 2213a, Chemistry 2223b, Chemistry 2273a, Chemistry 2283g.

#### Conferences

- 1) H. Ismaili, J. Zhu, M. S. Workentin, Chemical modification of monolayer protected gold nanoparticles using ultra high-pressure. 90<sup>th</sup> Canadian Chemistry Conference and Exhibition, Winnipeg, Manitoba, **2007**, Poster presentation.
- 2) H. Ismaili, H. Alizadeh, M. S. Workentin, High yielding chemical modification of monolayer protected gold nanoparticles using click-type chemistry and hyperbaric conditions. 91<sup>st</sup> Canadian Chemistry Conference and Exhibition, Edmonton, Alberta, **2008**, Oral.
- 3) H. Ismaili, M. S. Workentin, Diazirine monolayer protected gold nanoparticles (MPGNs): Precursor to photoaffinity labeling of MPGNs via interfacial carbene chemistry. 92<sup>nd</sup> Canadian Chemistry Conference and Exhibition, Hamilton, Ontario, **2009**, Oral.
- 4) H. Ismaili, M. S. Workentin, Fabrication of hybrid materials based on gold nanoparticles: interaction of carbene-modified gold nanoparticles with carbon nanotubes & functionalized polymers. 93<sup>rd</sup> Canadian Chemistry Conference and Exhibition, Toronto, Ontario, **2010**, Oral.

- 5) H. Ismaili, M. S. Workentin, S. Kostina, R. Guterman, W. J. Leigh, Laser flash photolysis of chromophore-functionalized gold nanoparticles: size-dependant transient behavior of triplet excited state. 93<sup>rd</sup> Canadian Chemistry Conference and Exhibition, Toronto, Ontario, **2010**, Poster presentation.
- 6) H. Ismaili, M. S. Workentin, Diazirine photochemistry to prepare gold nanoparticle-based hybrid materials (submitted). 94<sup>th</sup> Canadian Chemistry Conference and Exhibition, **2011**, Montreal, Oral.

### **Publications**

- 13) H. Ismaili, S. Kostina, R. Guterman, W. J. Leigh, M. S. Workentin, Laser flash photolysis of acetophenone-functionalized gold nanoparticles: size-dependant transient behavior of triplet excited state (In preparation).
- 12) H. Ismaili, X. A. Sun, M. S. Workentin, Covalent immobilization of gold nanoparticles onto graphene and glass, **2011**, *Journal of Materials Chemistry*, submitted.
- 11) K. D. Hartlen, H. Ismaili, M. S. Workentin, Modification of maleimide-functionalized gold nanoparticles via Michael addition at hyperbaric conditions. *Journal of Organic Chemistry*, **2011**, to be submitted.
- 10) H. Ismaili, M. S. Workentin, Physical organic chemistry of functionalized-gold nanoparticles: photochemical and thermal probe reactions. *Langmuir* (Invited Article), **2011**, to be submitted.
- 9) H. Ismaili, M. S. Workentin, Covalent diamond-gold nanojewel hybrids via a photochemically generated Carbenes. *Chemical Communications*, **2011**, Accepted.
- 8) H. Ismaili, F. Lagugné-Labarthet, M. S. Workentin, Covalently assembled gold nanoparticle-carbon nanotube hybrids (AuNP-CNT) via a photoinitiated carbene addition reaction. *Chemistry of Materials*, **2011**, 23, 1519.
- 7) H. Ismaili, S. Lee, M. S. Workentin, Diazirine-modified gold nanoparticles: template for efficient photoinduced interfacial carbene insertion reactions. *Langmuir*, **2010**, 26, 14958.
- 6) H. Ismaili, A. Alizadeh, K. E. Snell, M. S. Workentin, Remarkable high-yielding chemical modification of gold nanoparticles using uncatalyzed click-type 1,3-dipolar cycloaddition chemistry and hyperbaric conditions. *Canadian Journal of Chemistry*, **2009**, 87, 1708.

- 5) F. M. Moghaddam, G. R. Bardajee, H. Ismaili, Synthesis of bis(indolyl)methanes in presence of anhydrous copper(II) sulfate. *Asian Journal of Chemistry*, **2008**, 20, 1063.
- 4) F. M. Moghaddam, G. R. Bardajee, H. Ismaili, Microwave-assisted one-pot synthesis of symmetrical 4H-pyran-4-ones. *Journal of the Brazilian Chemical Society*, **2007**, 18, 1024.
- 3) F. M. Moghaddam, S. M. Dokht Taimoory, H. Ismaili, G. R. Bardajee, KF/Al<sub>2</sub>O<sub>3</sub>-mediated N-alkylation of amines and nitrogen heterocycles and S-alkylation of thiols. *Synthetic Communications*, **2006**, 36, 3599.
- 2) F. M. Moghaddam, G. R. Bardajee, H. Ismaili, S. M. Dokht Taimoory, Efficient one-pot protocol for the synthesis of benzoxazole and benzothiazole derivatives using molecular iodine as catalyst. *Synthetic Communications*, **2006**, 36, 2543.
- 1) F. M. Moghaddam, H. Ismaili, G. R. Bardajee, Zirconium (IV) oxide chloride and anhydrous copper (II) sulfate mediated synthesis of 2-substituted benzothiazoles. *Heteroatom Chemistry*, **2006**, 17, 136.